REPORT NO.
UCB/EERC-95/01
AUGUST 1995

EARTHQUAKE ENGINEERING RESEARCH CENTER

GEOTECHNICAL RECONNAISSANCE OF THE EFFECTS OF THE JANUARY 17, 1995, HYOGOKEN-NANBU EARTHQUAKE, JAPAN

A report based on the results of observations
of the geotechnical reconnaissance team
funded by the Siting and Geotechnical Systems
Earthquake Hazard Mitigation Program
of the Engineering Directorate of the
National Science Foundation Award No. CMS-9520204

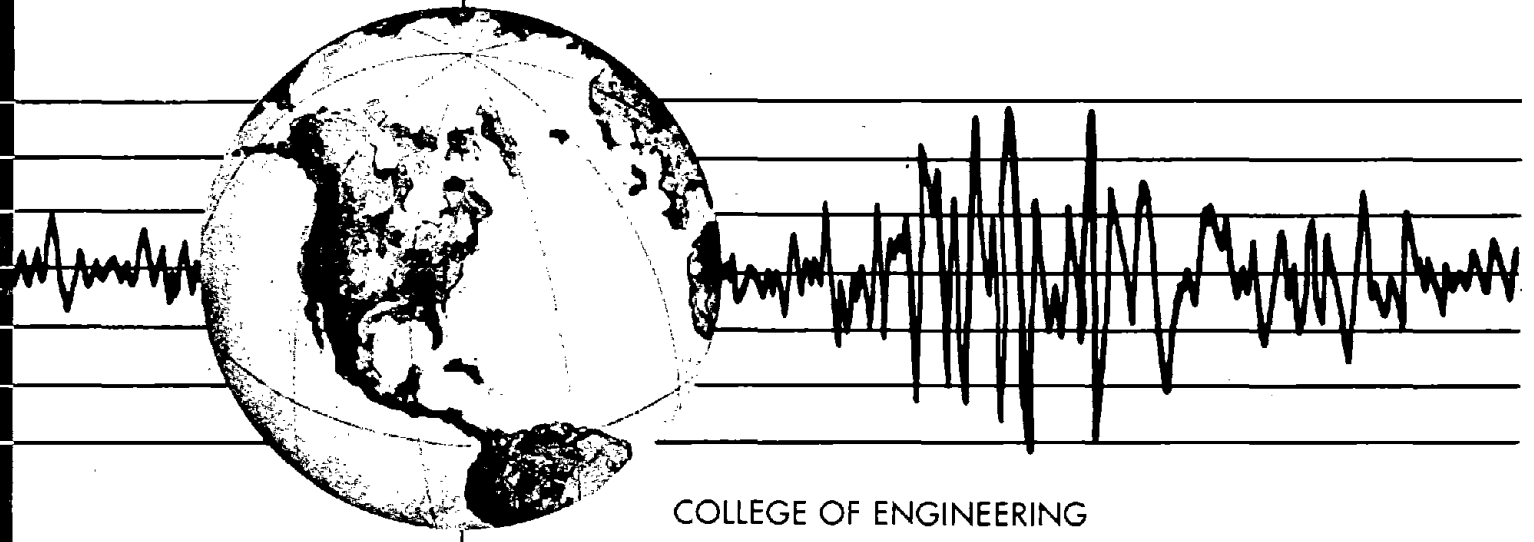

COLLEGE OF ENGINEERING

UNIVERSITY OF CALIFORNIA AT BERKELEY

For sale by the National Technical Information Service, U.S. Department of Commerce, Springfield, Virginia 22161

See back of report for up to date listing of EERC reports.

GENERAL DISCLAIMER

This document may be affected by one or more of the following statements

- **This document has been reproduced from the best copy furnished by the sponsoring agency. It is being released in the interest of making available as much information as possible.**

- **This document may contain data which exceeds the sheet parameters. It was furnished in this condition by the sponsoring agency and is the best copy available.**

- **This document may contain tone-on-tone or color graphs, charts and/or pictures which have been reproduced in black and white.**

- **This document is paginated as submitted by the original source.**

- **Portions of this document are not fully legible due to the historical nature of some of the material. However, it is the best reproduction available from the original submission.**

GEOTECHNICAL RECONNAISSANCE OF THE EFFECTS OF THE JANUARY 17, 1995, HYOGOKEN-NANBU EARTHQUAKE JAPAN

Principal Authors and Contributors:

Koichi Akai - Kyoto University; Geo-Research Institute, Osaka
Jonathan D. Bray - University of California, Berkeley
Ross W. Boulanger - University of California, Davis
John T. Christian - Consulting Engineer, Boston, MA
W.D. Liam Finn - University of British Columbia
Leslie F. Harder, Jr. - Calif. Dept. of Water Resources, Sacramento, CA
Izzat M. Idriss - University of California, Davis
Kenji Ishihara - University of Tokyo; Science University of Tokyo
Yoshinori T. Iwasaki - Geo-Research Institute, Osaka
James K. Mitchell - Virginia Polytechnic Institute and State University
Yoshiharu Moriwaki - Woodward-Clyde Consultants, Inc., Santa Ana, CA
Koichi Nakagawa - Osaka City University
Thomas D. O'Rourke - Cornell University
Raymond B. Seed - University of California, Berkeley
Nicholas Sitar (editor) - University of California, Berkeley
Kenichi Soga - Cambridge University, U.K.
Paul Somerville - Woodward-Clyde Federal Services, Pasadena, CA
Ikuo Towhata - University of Tokyo
T. Leslie Youd - Brigham Young University

A report based on the results of observations of the geotechnical reconnaissance team funded by the Siting and Geotechnical Systems Earthquake Hazard Mitigation Program of the Engineering Directorate of the National Science Foundation
Award No. CMS-9520204

Report No. UCB/EERC-95/01

Earthquake Engineering Research Center
College of Engineering
University of California at Berkeley

July 1995

PREFACE

The January 17, 1995, Hyogoken-Nanbu Earthquake was one of the worst disasters to hit Japan in almost a half a century, and it has been compared in its impact to the great Kanto (Tokyo) Earthquake of 1923 (AIJ, 1995). Immediately following the earthquake it became apparent that the Kobe-Osaka region held many similarities in its geologic and tectonic setting to many areas along the West Coast and, possibly, other areas of the United States. Therefore, a geotechnical reconnaissance to identify the relevant problems and issues was organized under the auspices of the Siting and Geotechnical Systems Earthquake Hazard Mitigation Program of the Engineering Directorate of the National Science Foundation. The mission of the reconnaissance team was to provide a timely, first-hand overview of the type and extent of the geotechnical aspects of the damage, and to provide the necessary background information for future research and for US-Japan cooperation in geotechnical earthquake engineering. The assembled team consisted of the following individuals:

Jonathan D. Bray - University of California, Berkeley
Ross W. Boulanger - University of California, Davis
John T. Christian - Consulting Engineer, Boston, MA
W.D. Liam Finn - University of British Columbia (also on the Canadian team)
Leslie F. Harder, Jr. - Calif. Dept. of Water Resources, Sacramento, CA
Izzat M. Idriss - University of California, Davis
James K. Mitchell - Virginia Polytechnic Institute
Yoshiharu Moriwaki - Woodward-Clyde Consultants, Inc., Santa Ana, CA
Thomas D. O'Rourke - Cornell University
Raymond B. Seed - University of California, Berkeley
Nicholas Sitar - University of California, Berkeley
Kenichi Soga - Cambridge University, U.K.
T. Leslie Youd - Brigham Young University

The reconnaissance team's visit was officially sponsored by the Japanese Society of Soil Mechanics and Foundation Engineering, and the Japanese hosts were led by Professor Koichi Akai, Professor Emeritus of the Kyoto University, Professor Kenji Ishihara of the University of Tokyo, Professor Koichi Nakagawa of the Osaka City University, and Dr. Yoshinori T. Iwasaki, Director of the Geo-Research Institute in Kobe.

Due to the extensive disruption to the transportation network, the investigation within Kobe was performed principally on foot, the port facilities were inspected by boat and on foot, and a couple of helicopter overflights were made. Thus, while effort has been made to provide a balanced overview, the limited ground time, on the order of less than a week for the U.S. members of the team, necessarily limits the scope and substance of this report. Consequently, the observations and opinions presented here are intended to serve as a guidance to further in depth assessment and not as a final, definitive evaluation of the specific events and phenomena.

A combination of several factors contributed significantly to the severity of much of the damage: the area had been previously considered to have relatively low seismic risk, the projected location of the release of energy along the earthquake fault was almost immediately below a densely developed urban area, and the geologic setting of the region, on the shores of a large embayment, provided for a substantial thickness and areal distribution of soft and liquefiable sediments. The principal geotechnical aspects of the Hyogoken-Nanbu Earthquake include the following:

- Extensive liquefaction of natural and artificial fill deposits occurred along much of the shoreline on the north side of the Osaka Bay. Probably the most notable were the liquefaction failures of relatively modern fills on the Rokko and Port Islands. On the Kobe mainland, evidence of liquefaction extended along the entire length of the waterfront, east and west of Kobe, for a distance of about 20 km. Overall, liquefaction was a principal factor in the extensive damage experienced by the port facilities in the affected region.

- Liquefaction caused disruption of underground utilities, including gas, water, and sewer systems. In fact, the pervasive damage to the underground utilities throughout the region affected by liquefaction may yet prove to be a major, and as yet not fully appreciated, aspect of the earthquake damage.

- Notably, areas of fills that have been densified using fairly conventional techniques performed satisfactorily. Similarly, mechanically stabilized soil walls also performed very well.

- While numerous pile foundations for various types of structures apparently performed very well, there were several failures of large pile-supported bridge piers. These cases provide a unique opportunity for further studies of lateral pile capacity and of the overall seismic performance of piles.

- Shallow foundations for most modern buildings consisting of reinforced mats or, more commonly for houses, reinforced perimeter and wall footings that are strongly tied together performed quite well. These types of foundations acted as diaphragms, holding structures together and preventing differential ground movements from fracturing the foundations and superstructures.

- Although the region immediately north of downtown Kobe is relatively hilly, landsliding was minimal, mostly limited to shallow sliding and raveling of boulders. However, one large flow slide occurred in decomposed granite in a residential area in the Nigawa district, northeast of Kobe. This slide destroyed several houses and killed 34 people.

- Movement of fills and retaining walls was evident in many parts of the residential area in the hills northeast of Kobe. In some locations, the displacement of side-hill and valley bottom fills was sufficiently large to cause structural damage, and to damage the utilities and disrupt service. This type of damage was also observed in the 1994 Northridge Earthquake.

- While underground structures are generally considered relatively safe from seismically induced damage, a failure of a cut-and-cover underground metro station did occur.

- A number of relatively modern dams of various types within the region of intense shaking seemed to survive the earthquake with little or no damage. However, three small embankment dams, the Niteko Dams, more than 100 years old, failed by lateral spreading and liquefaction. The damage, as a result of these failures, appeared to be minimal because of the initially low water level and low overall height of the dams ($\leq$12 m).

- So far, the ground rupture due to right lateral strike slip faulting has been reported only on the Awaji Island, to the southwest of the epicenter. However, the north and south towers of the Akashi Kaikyo Bridge, currently under construction, are known to have been displaced relative to each other laterally and vertically. This is the first time that a structure of this size has been known to be offset by a fault rupture.

Overall, the area affected by the 1995 Hyogoken-Nanbu Earthquake has many similarities, in terms of geologic setting and the level of development to other locations around the world, the San Francisco Bay area and the Los Angeles basin, for example. Therefore, much can be learned about the type and the extent of damage that can occur when a major fault ruptures through an urban environment. In this context, the collective body of information gathered following the October 17, 1989, Loma Prieta Earthquake, the January 17, 1994, Northridge Earthquake, and now the Hyogoken-Nanbu Earthquake should serve to provide

important lessons for engineering professionals, researchers, government officials, and the public, alike. More importantly, we hope that this, and other reports which will follow, will help in providing the inspiration and guidance in developing strategies to minimize the extent of avoidable damage in future earthquakes, at least in the well-known seismically active regions.

ACKNOWLEDGMENTS

This report would not have been possible without the generous help and guidance from many of our Japanese friends and colleagues, who selflessly acted as guides and interpreters, and provided much needed assistance with the logistics of the site visits. Dr. Yashimi, President of the Japanese Geotechnical Society, and the Japanese Geotechnical Society generously hosted and sponsored the reconnaissance visit. Prof. Akai, Prof. Ishihara, Prof. Nakagawa, Dr. Iwasaki, and Prof. Towhata were instrumental in making most of the arrangements for accommodations and in coordinating the site visits. Prof. Ohnishi led the ground reconnaissance of slopes and structural fills, and he and his family graciously opened their home to provide a lunch stop for the members of the reconnaissance team.

While much of the information contained in the report is based on site visits by the reconnaissance team members, important observations and background information was obtained and corroborated from many sources, including: M. Ando, K. Irikura, M. Kikuchi, K. Koketsu, T. Nakata, K. Toki, and Y. Yoshimi; and participants in the Fourth Japan-U.S. Workshop on Urban Earthquake Hazard Mitigation, led by H. Kameda and S. Tubessing, which coincidentally began in Osaka on the day of the earthquake.

The Kansai Electric Power Co. and the Toyo Construction Co. donated boat transportation, and the Konoike Corp. provided bus transportation for visits of the Port of Kobe, and to Port and Rokko Islands. Messrs. Matsumoto and Akiyama of the Kansai Electric Power Co., Dr. Konoike and Dr. Ono of the Konoike Corp., the representatives of the Fudo Construction Company, especially Messrs. Kanda, Takahashi, and Tsuboi, Mr. Yamamoto of the Ministry of Transportation, Mr. Tsutui of the Toyo Construction Co., Mr. Nakaya of the Kuraray Co. Ltd., Dr. Yoshida of the Sato Kogyo Co., Ltd., and Mr. Nitta of the Kobe Kosoku Railway Co. helped as tour guides and provided technical information about foundation conditions in the inspected localities.

Dr. Iwasaki provided the CEORKA seismic array data for Port Island. He also obtained background information about the GRS-RW wall systems and arranged a meeting with Japanese Railroad (JR) personnel. Mr. Nagato of JR provided technical details and guided a tour of the sites.

Prof. Tatsuoka generously provided information on the design and construction of geosynthetically reinforced slopes and walls, and shared his observations of earthquake performance. Prof. Matsui provided much of the background information on the soil conditions and properties in the region.

The funding for most of the reconnaissance team and the report was provided by a grant from the Siting and Geotechnical Systems Earthquake Hazard Mitigation Program of the Engineering Directorate of the National Science Foundation Award No. CMS-9520204. Dr. C. Astill of the National Science Foundation was instrumental in providing timely support for this effort. Dr. L. Weber of the National Science Foundation, Tokyo, helped in obtaining essential information on the situation and conditions for travel immediately following the earthquake.

In addition, L.F. Harder, Jr., received funding from the Department of Water Resources, State of California, for the reconnaissance of dams and levees, and W.D.L. Finn's visit was funded by the National Sciences and Engineering Council of Canada. The financial support from these organizations is gratefully acknowledged. K. Soga would like to acknowledge support from the Engineering and Physical Sciences Research Council of the U.K., Dr. S. Steedman of Sir Alexander Gibb & Partners, Ltd., and Sir Alexander Gibb & Partners, Ltd.

Finally, we would like to acknowledge and thank the people of the Kobe area. Despite having to deal with the catastrophic impact of a large natural disaster, the people we encountered went out of their way to provide assistance and welcome, so we could learn from their experience.

TABLE OF CONTENTS

CHAPTER ONE: INTRODUCTION

The January 17, 1995, Hyogoken-Nanbu Earthquake is the most damaging earthquake to have struck Japan since the great Kanto earthquake destroyed large areas of Tokyo and Yokohama and killed approximately 140,000 people (mostly by fire) in 1923. Part of the reason for the great devastation was the location of the epicenter of the earthquake, at the tip of Awaji Island, within 20 km of the city of Kobe in the Hyogo prefecture (see Figure 1.1). The city of Kobe houses about 1.5 million people, and it is a part of a continuous, densely developed urban area which extends from west of Kobe eastward to Osaka and has a population of more than 4 million inhabitants (AIJ, 1995; Figure 1.2). As of March 31, 1995, the toll from the earthquake in Kobe has reached over 5,500 dead and over 26,000 injured. More than 200,000 houses, about 10% of all houses in the Hyogo prefecture, were damaged, including more than 80,000 collapsed, 70,000 severely damaged, and 7,000 consumed by fire (AIJ, 1995). Current estimates of losses in Kobe are about 20 trillion yen (200 billion dollars), one order of magnitude larger than that from the January 17, 1994, Northridge Earthquake.

The strategic location of Kobe, at a point where the proximity of the mountains and the sea constricts the transportation corridor, also meant that the damage to the transportation network, as exemplified by the now famous picture of the collapsed section of the Hanshin Expressway (Figure 1.3), had a large economic impact extending well beyond the immediately affected area. Before the earthquake, Kobe was Japan's busiest and the second largest port after Yokohama. It was also the largest Japanese port for foreign trade cargo, mostly containerized, with over 53 million metric tons of foreign trade in 1990. It was the fourth largest container cargo port in the world. About 39% of the city's gross industrial product was derived from port related industries, accounting for more than 17% of the city work force. The earthquake damage caused essentially total shutdown of all facilities in the port area for several weeks following the earthquake.

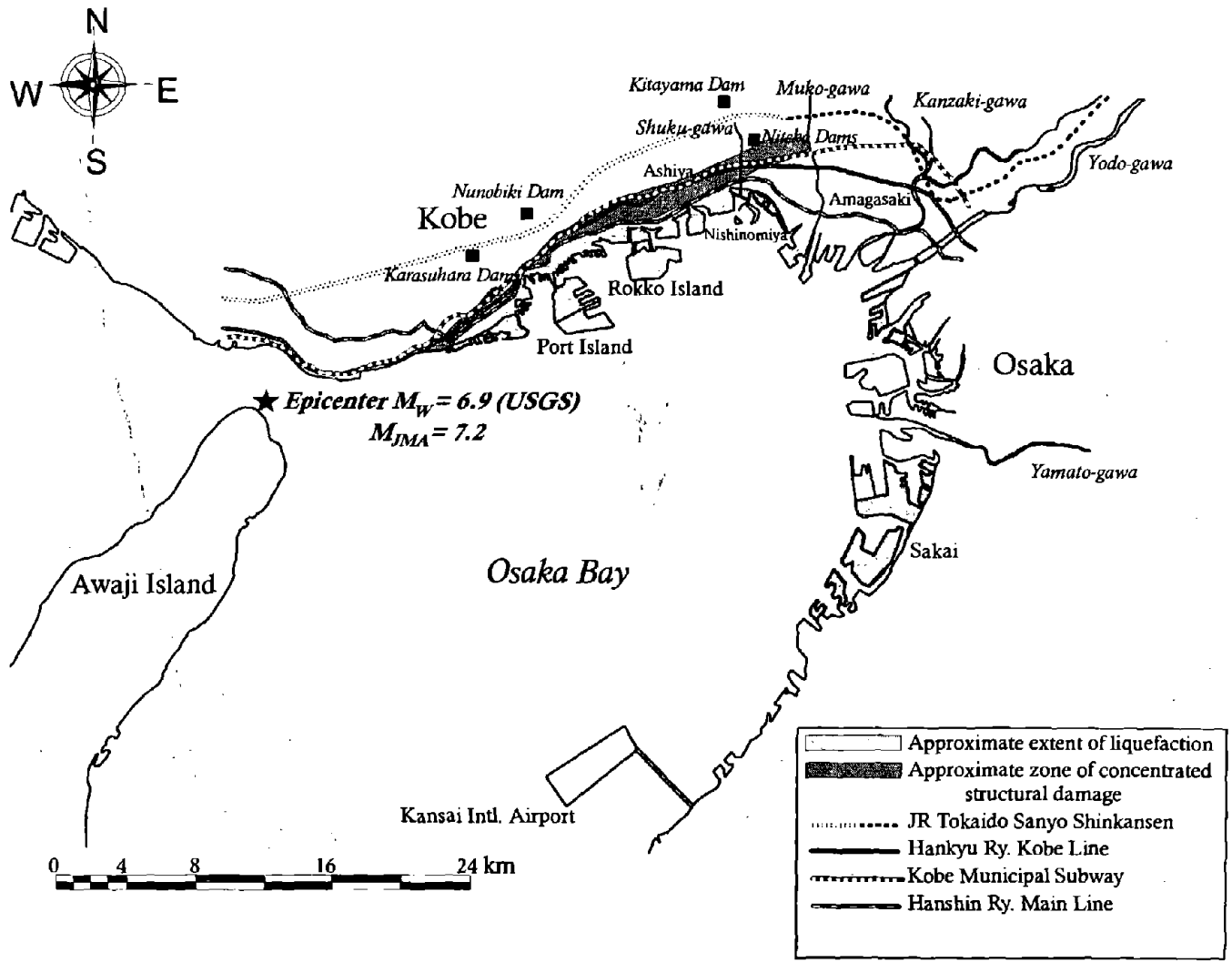

Figure 1.1. Schematic map of the Kobe-Osaka region, showing the location of the epicenter of the Hyogoken-Nanbu earthquake and major points of interest, including the approximate extent of the areas of severe structural damage and liquefaction.

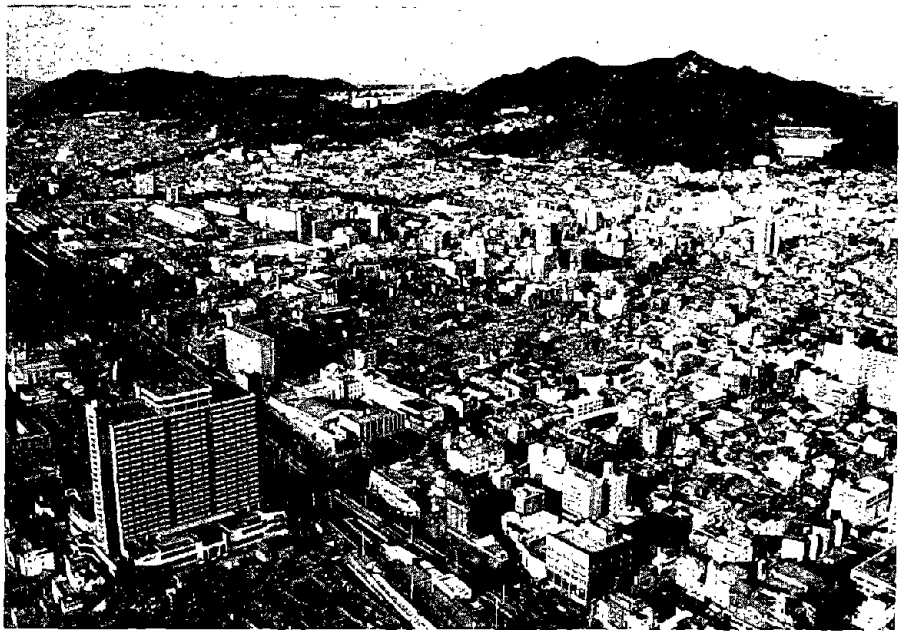

Figure 1.2: Aerial view of the Kobe metropolitan region showing the density of urban and commercial development.

Figure 1.3: Collapsed section of the Hanshin Expressway (reproduce from Asahigraph, 1995)

The purpose of this report is to provide an overview of the principal geotechnical aspects of the earthquake. To this end, the seismological aspects of the Kobe earthquake are presented in Chapter 2. The regional seismicity and tectonics, including local geology, are reviewed first, followed by a discussion of the source characteristics of the earthquake. Observations of surface rupture are presented, and recorded strong ground motions and site response issues are examined. The recorded strong motions are compared with empirical attenuation relationships based on primarily California data, and important implications for US practice are drawn.

Liquefaction and liquefaction related effects are described in Chapter 3. The extent of liquefaction provided a unique opportunity to asses the performance of various types of foundations under conditions of loss of bearing capacity and lateral support, and subjected to lateral spreading. The performance of improved ground is reviewed in Chapter 4. The observation of the behavior of dams and levees are presented in Chapter 5. The damage to lifeline systems is described in Chapter 6, and other geotechnical aspects of the earthquake damage, including the performance of slopes, structural fills, mechanically stabilized slopes, and landfills, are presented in Chapter 7.

CHAPTER TWO: GEOSCIENCE AND STRONG MOTIONS

2.1 Introduction

The January 17, 1995, Hyogoken-Nanbu (Kobe) Earthquake was assigned a JMA magnitude of 7.2 by the Japan Meteorological Agency (JMA). Seismological analyses indicate a seismic moment of 2.5×10^{26} dyne-cm, corresponding to a moment magnitude of 6.9, with a source duration of 6 to 10 seconds (Kikuchi, 1995). The hypocenter of the earthquake (34.60° N and 135.00° E, focal depth of 14 km, origin time 05:46:53.9, 1/17/1995 JST; JMA) was located about 20 km southwest of downtown Kobe between the northeast tip of Awaji Island and the mainland (Figure 2.1). The rupture length of this shallow, primarily strike-slip earthquake is inferred from the aftershock distribution and the waveform modeling of teleseismic and strong motion seismograms to have been about 30 km to 50 km long and 15 km wide, produced by bilateral rupture from the hypocenter (Pitarka et al., 1995; Kikuchi, 1995). The rupture of this earthquake directly into downtown Kobe appears to have contributed to the high level of destruction that occurred.

2.2 Geologic Setting

The geology in the Kobe area is fairly complex and is dominated by a number of northeast/southwest trending strike-slip faults. Basement bedrock of Late Cretaceous and Miocene age form the mountainous region to the north and west of downtown Kobe. The dominant rock type northwest of Kobe is a biotite granite known as the Rokko granite. Other basement rock types include sandstone, conglomerate, mudstone, and tuff. Pleistocene gravel, sand, and clay terrace deposits lie to the southeast of the basement rock outcrops that are terminated by a system of right-lateral faults (Rokko fault zone), which include, from southwest to northeast, the Suma, Egeyama, Suwayama, Ashiya, Koyo, and Arima-Takatsuki faults. The Pleistocene deposits are overlain by Holocene alluvium (sand, gravel, and clays) that form the relatively level, narrow corridor of land which contains most of the development in the Kobe area. A map depicting contours of the base

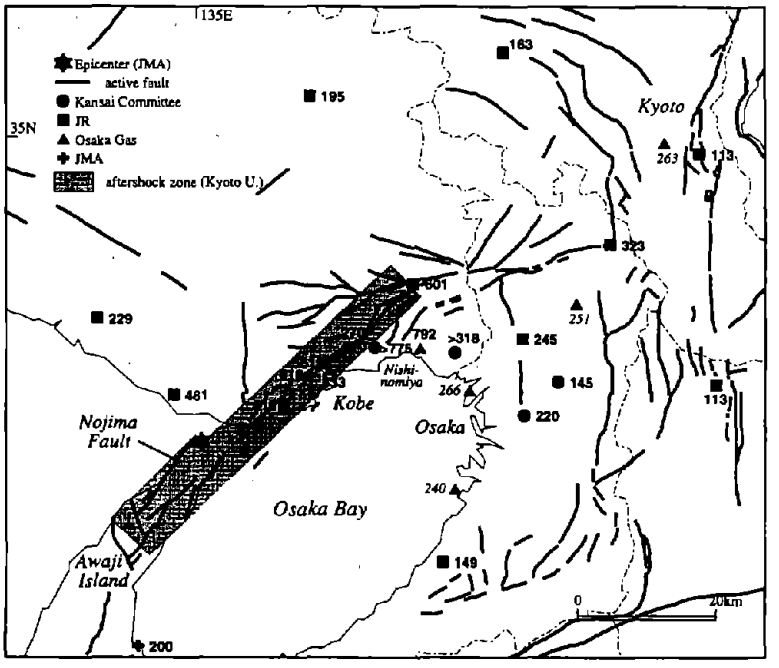

Figure 2.1: Mainshock epicenter (JMA), aftershock zone, and peak ground motions of the 1995 Kobe earthquake, superimposed on a map of active faults. The aftershock zone is based on locations by the Disaster Prevention Research Institute, Kyoto University, using data from the micro-earthquake networks of Kyoto, Tokyo, and Nagoya Universities. The strong motion data are from the Committee of Earthquake Observation and Research in the Kansai Area, JR, Osaka Gas, and JMA, and represent different measures of ground motion. The active faults are from Research Group for Active Faults (1980). Modified from K. Kohketsu, Earthquake Research Institute, University of Tokyo.

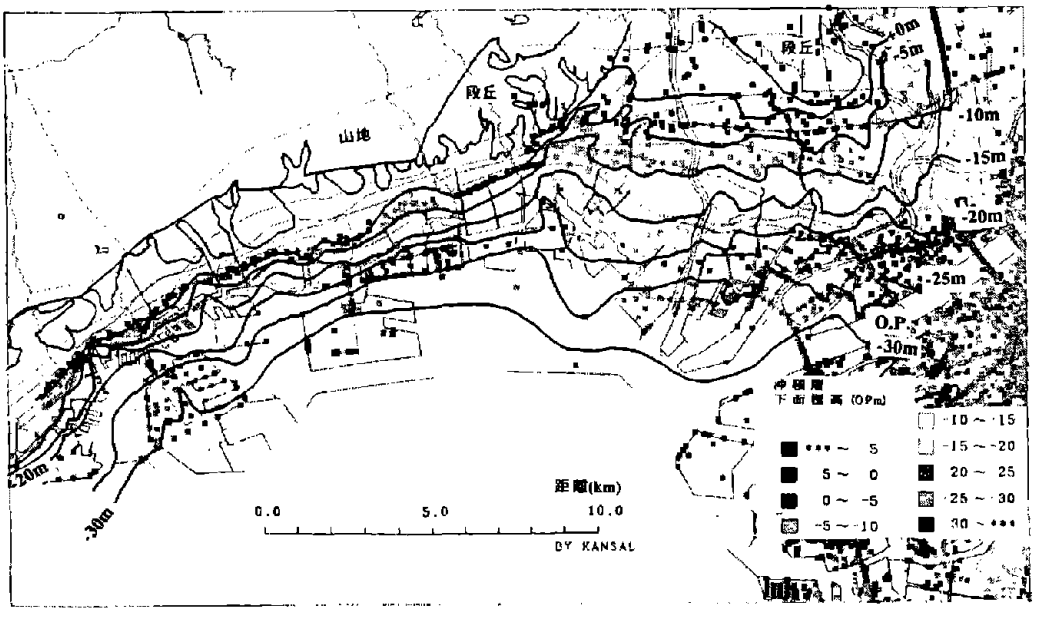

Figure 2.2: Holocene base elevation contours. Source: Iwasaki (1995).

elevation of the Holocene deposits in the Kobe area is presented in Figure 2.2. The Holocene alluvium thickness generally increases to the southeast from roughly 20 m under downtown Kobe to as much as 40 m under the Port Island. Much of the exposed land near the Kobe waterfront, including the islands, is reclaimed land that was constructed by loosely dumping granular material generally borrowed from the decomposed Rokko granite. To the east of the Kobe area, alluvial deposits brought down by rivers such as the Yodo River dominate the surficial geology; whereas, to the west on Awaji Island, outcropping basement rock bordered by narrow shorelines consisting of Pliocene alluvium with some Holocene alluvium at the shore comprises the surficial geology. The basement rock is terminated along the northwestern flank of Awaji Island by the Nojima fault and along the southeastern flank of the island by a parallel fault system. The basement rock under central Osaka Bay is at depths on the order of 2 km, and it rises to depths between 0.5 to 1.5 km below central Kobe. A recent assessment of the subsurface geology by Iwasaki (1995) has located basement rock at depths between 1.7 and 2.0 km at Port Island and at a depth of about 2.5 km at Rokko Island.

2.3 Regional Seismicity and Tectonics

The earthquake occurred in a region where a complex system of active faults had been previously mapped (Research Group for Active Faults in Japan, 1980; Figure 2.1). The focal mechanism of the earthquake indicates right-lateral strike-slip faulting on a nearly vertical fault striking slightly east of northeast, parallel to the strike of the mapped faults (Pitarka et al., 1995). The earthquake mechanism is compatible with the tectonic environment of western Japan as revealed by historical seismicity. This seismicity contains a sequence of earthquakes between 1891 and 1948 which includes the magnitude 8 Nobi earthquake of 1891, the magnitude 7.3 Tango earthquake of 1927, the magnitude 7.2 Tottori earthquake of 1943, and the magnitude 7.1 Fukui earthquake of 1948 (Kanamori, 1973). All of these earthquakes, as well as the 1995 earthquake, had strike-slip mechanisms that accommodated east-west shortening of the Eurasian plate due to its collision with the North American plate along the Izu-Itoigawa line to the east in central Honshu (Huzita, 1980), as illustrated in Figure 2.3. The last major earthquake (M>7) in the near vicinity of

Kobe occurred in 868; it is believed to have been generated on the Yamasaki fault, which is located about 50 km northwest of the epicenter of the Kobe earthquake (Kanamori, 1995). Kobe was probably also affected by a magnitude 7 earthquake in 1596 whose effects were most strongly felt in the region between Kyoto and Osaka. A smaller magnitude earthquake (M=6.1) occurred near the epicenter of the 1995 Kobe Earthquake in 1916. In summary, the 1995 Kobe earthquake occurred on a mapped system of active faults, and had a mechanism that is compatible with the tectonics of western Japan as inferred from similar earthquakes that occurred during the past century. Currently available evidence does not suggest any difference between the source characteristics of the Kobe earthquake and those of crustal earthquakes that occur in California.

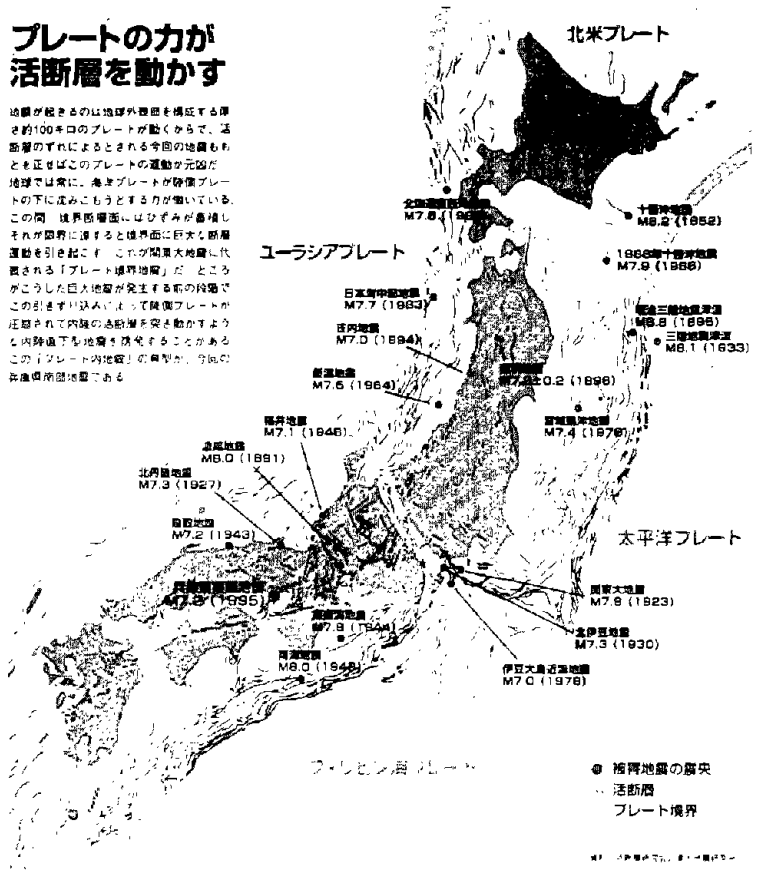

Figure 2.3: Collision of the North American plate with the Eurasian plate in central Japan. Plate boundary faults and active crustal faults in Japan. Epicenters of large earthquakes during the past century are shown. Source: Newsweek, February 1, 1995, Japan edition.

2.4 Source Characteristics

The distribution of aftershocks is shown in Figure 2.4. The aftershock pattern is aligned with the roughly northeast-southwest orientation of the Rokko fault zone and extends over a distance of about 45 km. The time sequence and orientation of faulting during the Kobe earthquake has been inferred from the analysis of strong motion data by Pitarka et al. (1995) and teleseismic data by Kikuchi (1995). The focal mechanism and fit of recorded and synthetic strong motion waveforms in the Pitarka et al (1995) model is shown in Figure 2.5, and the focal mechanism developed by Kikuchi (1995) is shown in Figure 2.6. Southwest of the epicenter, away from Kobe, the earthquake produced 11 km of surface rupture with an average horizontal displacement of 1 to 1.5 m on the Nojima fault, which runs along the northwest shore of Awaji Island. The surface faulting is described in further detail in the next section. The strike-slip motion was accompanied by a component of thrust motion, producing a fault scarp dipping to the southeast, with the northwest side down. This dip direction is consistent with the offset of the surface rupture by a few kilometers to the northwest from the epicenter, and with the focal mechanism of the first event as inferred by Kikuchi (1995) and Pitarka et al. (1995). The dip direction and the dip-slip motion is reversed on the part of the rupture that extends to the northeast from the epicenter, toward Kobe. A releveling survey after the earthquake found a decrease in elevation of 26 cm between Tarumi and Suma Wards in western Kobe. This change in elevation is inferred to mark the location of subsurface faulting. The dip-slip displacement to the southeast on a fault plane dipping northwest is seen in the focal mechanisms of later subevents in the rupture model of Pitarka et al. (1995) shown in Figure 2.5. Both the Kikuchi and Pitarka et al. rupture models indicate that the propagation of the rupture toward Kobe involved several subevents distributed along the fault at depths of 6 to 8 km. Pitarka's model has uniform strike but variations in dip and rake among four subevents, while Kikuchi's model has variations in strike as well as variations in rake of three subevents. From the fault geometry (30-50 km long x 15 km wide), the average slip is 1.1 to 1.9 m and the stress drop is 14 to 24 bars (Kanamori, 1995).

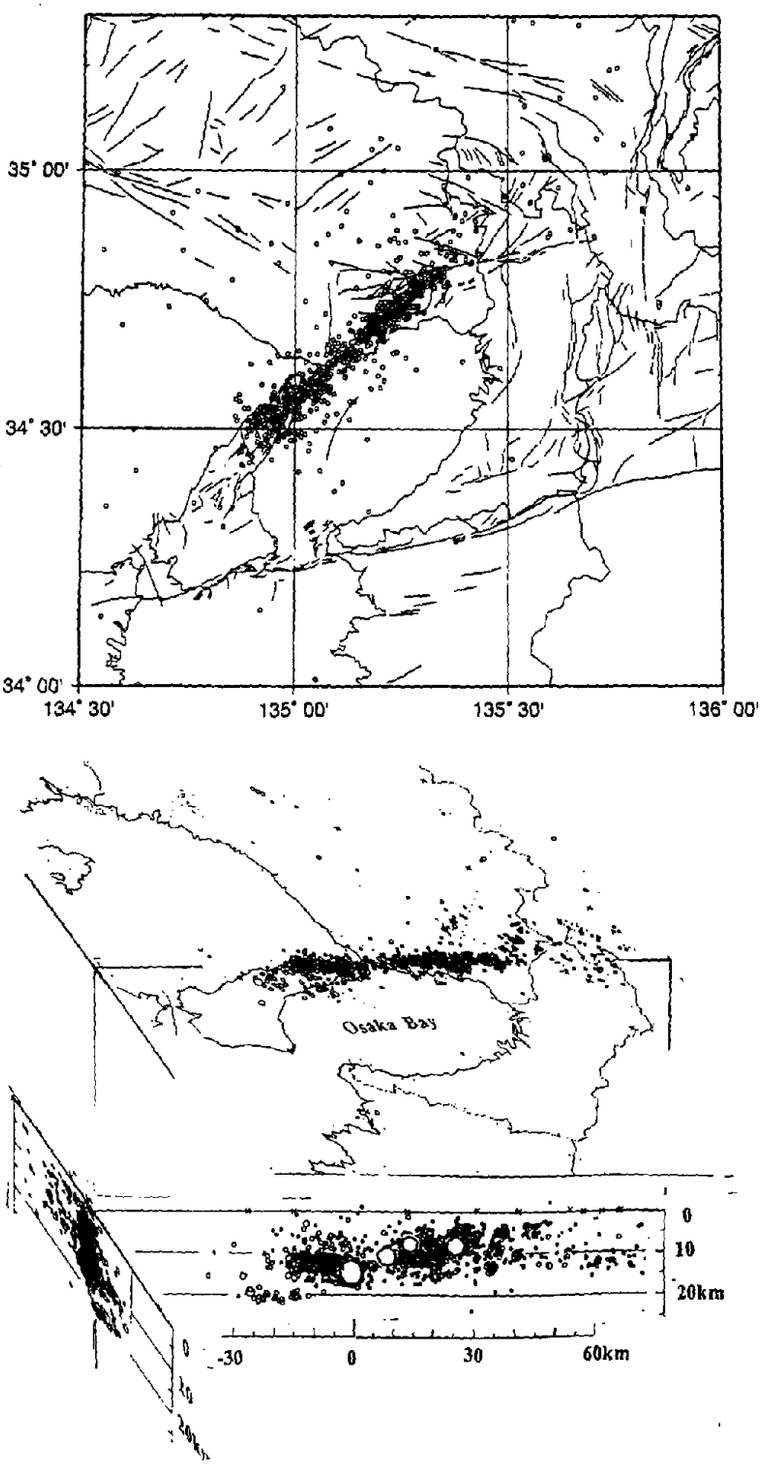

Figure 2.4: Locations of aftershocks for the period from January 17 to January 20, 1995 (JST) located using the data from the micro-earthquake network of Kyoto, Tokyo and Nagoya universities. Source: Disaster Prevention Research Institute, Kyoto University.

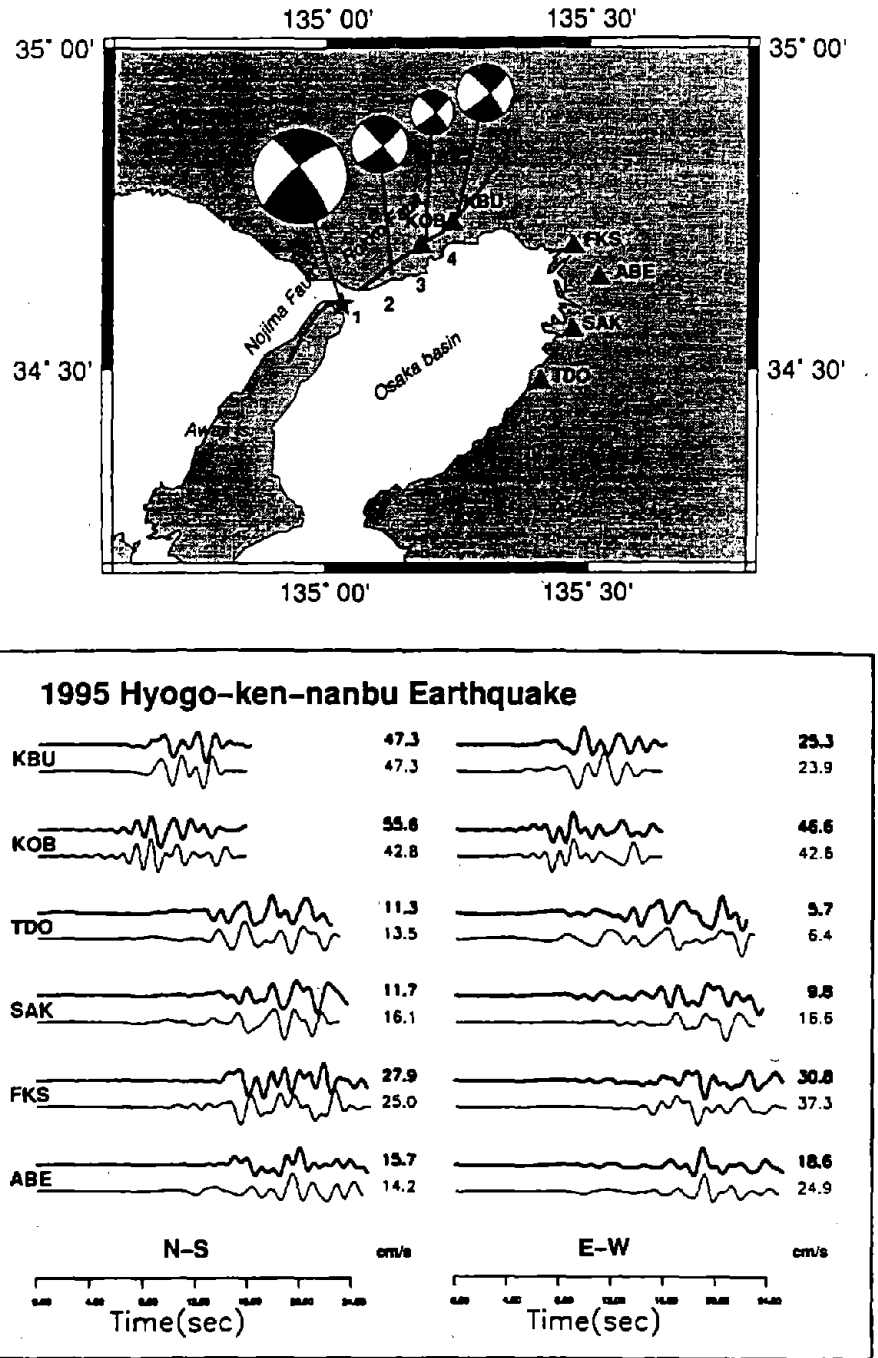

Figure 2.5: Focal mechanism and source process of the Kobe earthquake by Pitarka et al. (1995). The earthquake consisted of four subevents, whose locations and focal mechanisms are shown at the top. Recorded (heavy lines) and synthetic (light lines) waveforms are compared at the bottom. Source: Pitarka et al. (1995).

2.5 Surface Rupture

The earthquake produced surface rupture with an average horizontal displacement of 1 to 1.5 m and a maximum recorded horizontal displacement of 1.7 m on the Nojima fault, which runs along the northwest shore of Awaji Island (Nakata, personal communication, 1995). Figure 2.7 illustrates the general characteristics of the topography along the Nojima fault and the surface expression of the predominantly strike-slip faulting. A close-up view of a scarp of the Nojima fault, which showed both vertical and horizontal offsets (at one spot, these offsets were measured to be approximately 1.2 m right-lateral and 15 cm dip-slip (east side up), respectively) is shown in Figure 2.8. The house shown in the background in Figure 2.8 was nearly offset by the surface fault rupture, but it appeared to be only slightly damaged by the ground shaking. Just to the north of this area, the Nojima fault cut across a number of wet rice paddies before continuing along the base of the hills formed from the uplift of Pre-Miocene bedrock. It was more difficult to see the surface expression of the faulting in the wet rice paddies, and in areas the faulting was expressed as en echelon shears with minor offsets across them. At numerous locations the observed surface expression of the fault was fairly narrow (<5 m wide), and this is consistent with the style of faulting (fairly linear strike slip faulting through shallow soil deposits overlying the bedrock). However at a few locations, the ground breakage zone was noticeably wider. For example, at the northern end of the surface expression of the Nojima fault where it travels offshore of Awaji Island, about 1 m of horizontal displacement was spread across a zone roughly 50 m wide, which contained several ground cracks. Most of the offset was concentrated on three or four cracks within the middle of this zone. Vertical displacement across the observed surface rupture of the Nojima fault varied considerably with an average vertical displacement of 0.5 to 1 m (east side up) and a maximum vertical displacement of 1.3 m (east side up). At the southern end of the exposed ground rupture, the observed vertical displacement decreased and was actually in the opposite sense with the west side moving up slightly (<0.2 m) with respect to the east side.

Marine seismic surveys have found a 300 meter long offshore extension of this rupture (Japan Maritime Safety Agency). This segment of the fault ran between the main towers of the Akashi Kaikyo suspension bridge, which is under construction, offsetting the southern tower 1.1 m

in a right lateral sense with respect to the northern tower (Fig. 2.9). The surveys also found two fault rupture segments that span a length of about 7 km in the region offshore from the northeast tip of Awaji island, parallel to the Nojima fault but offset from it by about 5 km. Near the onshore projection of these underwater rupture segments, a releveling survey after the earthquake found a change in elevation of 26 cm over a distance of 6 km between Tarumi and Suma Wards in western Kobe. Ground surface deformations, which are possibly associated with surface ruptures, have been identified east of Kobe in the Takarazuka area on a number of active fault strands just south of the Arima-Takatsuki fault zone (see Figure 2.10, M. Seo and Y. Yoshimi, personal communication, 1995). Aerial reconnaissance identified possible right lateral surface rupture expressions to the southwest of this area across the Muko River along the general trend of the strike of identified active faults in the area. A close-up view of a tennis court which shows ground cracks with noticeable right lateral offsets is shown in Figure 2.11. This feature has not been field-checked, and there are numerous fills and buried stream deposits in the area, so ground cracking may have resulted from phenomena other than faulting. However, field data provided by M. Seo and general observations of damage in the Takarazuka area suggest that there may be a correlation between some concentrations of heavily damaged areas (both buildings and transportation systems) and active fault segments that expressed some ground movement during the Kobe Earthquake. Additional study is warranted to confirm these preliminary observations.

2.6 Strong Ground Motions

Strong ground motions were recorded by several organizations, including the Committee on Earthquake Observation and Research in the Kansai Area, Japan Rail, Osaka Gas, JMA, Hankyu Railroads, Japan Highways, Building Research Institute, and Port and Harbor Research Institute. The ground motions varied significantly in the epicentral region, indicating a complex interaction of important effects such as directivity, local site conditions, and topography. Peak ground accelerations as large as 0.8 g were recorded in the near-fault region on alluvial sites in Kobe and Nishinomiya. The recordings at near-field rock sites typically had significantly lower

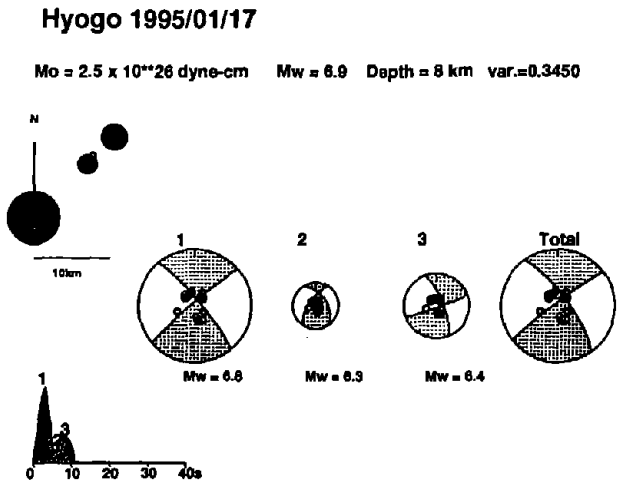

Figure 2.6: Focal mechanism and source process of the earthquake by Kikuchi (1995). The earthquake consisted of three subevents, whose relative locations are shown in the upper left, time functions in the lower left, and focal mechanisms and moment magnitudes to the right. The largest subevent was located at the hypocenter. Source: Kikuchi (1995).

Figure 2.8: Scarp of the Nojima fault on Awaji Island showing both vertical and horizontal offset. Source: Newsweek, February 1, 1995, Japan edition.

Figure 2.7: Aerial view of northwest shore of Awaji Island showing the surface rupture of the faulting. Note the surface rupture that cuts across the middle of the picture.

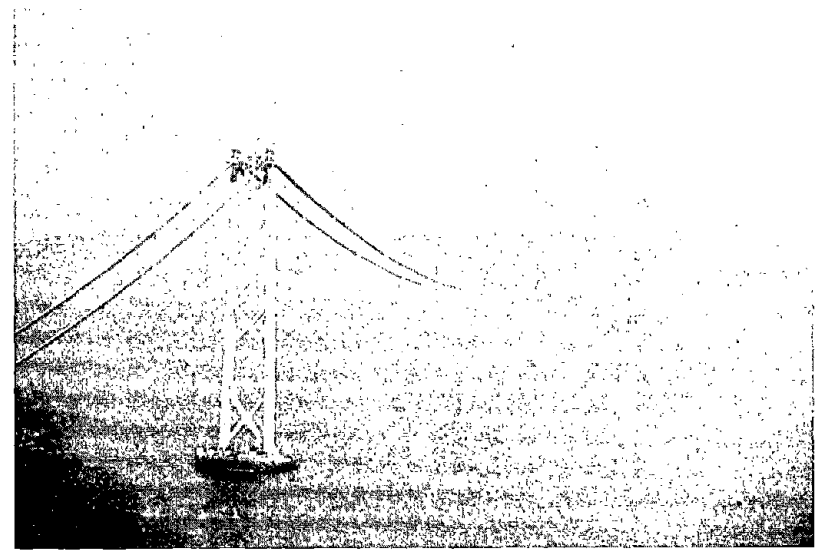

Figure 2.9: Akashi Kaikyo suspension bridge. The tower in the foreground was offset 1.1m RL with respect to the tower to the north. The distance between the towers is 2000 m.

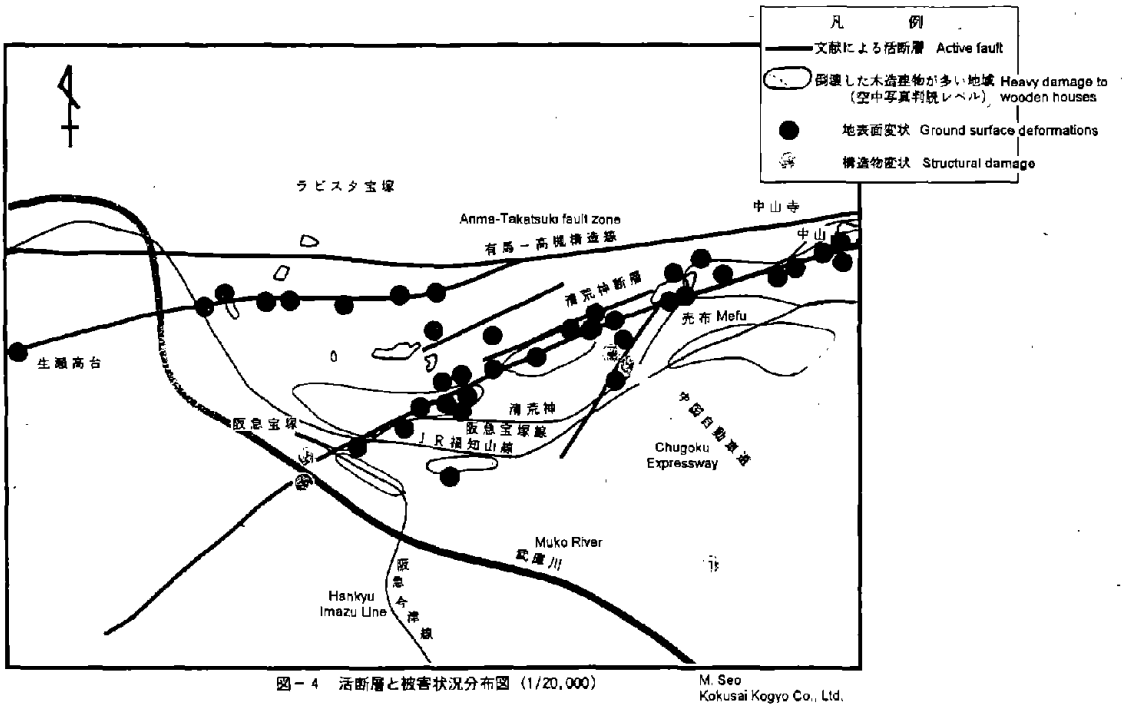

Figure 2.10: Map of the Takarazuka area showing locations of ground surface deformations, active faults, and associated damage. Source: M. Seo of Kokusai Kogyo Co., Ltd.

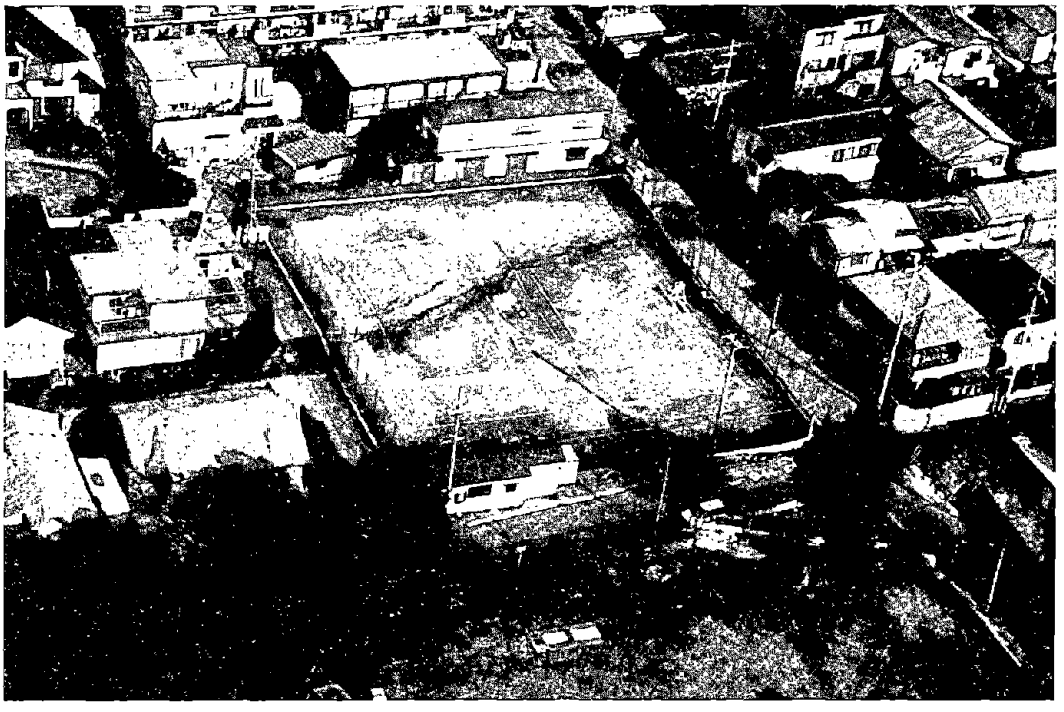

Figure 2.11: Aerial view of possible right lateral surface rupture in tennis court in area just southwest of Takarazuka.

magnitudes of peak ground acceleration (i.e. around 0.3 g). The vertical peak ground accelerations were generally about two-thirds as large as the horizontal accelerations in the near-field, and significantly lower than this at more distant alluvial sites. Velocity waveforms recorded at a number of strong motion stations in the Osaka Bay area are shown in Figure 2.12 along with their respective locations. Note the difference in the motions recorded in the near-field (i.e. at KMO (Kobe) and KBU (Kobe University)) from those recorded at more distant stations (e.g. FKS (Fukushima) and YAE). The near-field motions contain brief, intense pulses; whereas, the more distant records have significantly longer duration of strong shaking with dominant low frequency periodic motions resulting from surface waves or site resonance.

The rupture of this strike-slip earthquake directly into downtown Kobe (Figures 2.1 and 2.4) caused near-fault rupture directivity effects which appear to have contributed to the high level of damage. As stated previously, the near-fault ground velocity time histories have large, brief pulses of ground motion (Figure 2.12) which are indicative of rupture directivity effects and are potentially damaging to multi-story buildings and other long-period structures such as bridges. The recorded peak velocities were as large as 175 cm/sec at Takatori in western Kobe, and the largest values occurred in the densely populated urban region, as shown in Figure 2.13. The near-fault horizontal peak velocities were 55 cm/sec on rock at Kobe University and went off scale at soil sites at levels of 40 cm/sec and 100 cm/sec in central Kobe. These values are similar to those recorded close to comparable earthquakes in California. Currently, buildings over 60 meters in height in Japan are designed to withstand peak velocities of 50 cm/sec in Tokyo and 40cm/sec in the Osaka-Kobe area without collapse. The horizontal motions in the fault-normal direction are about twice as large as those in the fault-parallel direction, as seen in the velocity-time histories shown in Figure 2.14 and the response spectra shown in Figure 2.15. This feature, which is caused by rupture directivity effects, has been widely observed in near fault strong motion data in California (e.g. Somerville and Graves, 1993) and quantified as a modification to empirical attenuation relationships recently proposed by Somerville and Graves (1995).

Due to near-field rupture directivity effects, the structural damage in central Kobe was noticeably influenced by the orientation of the structural system with respect to the strike of the fault. Structural damage was more severe in the fault-normal direction than in the fault-parallel

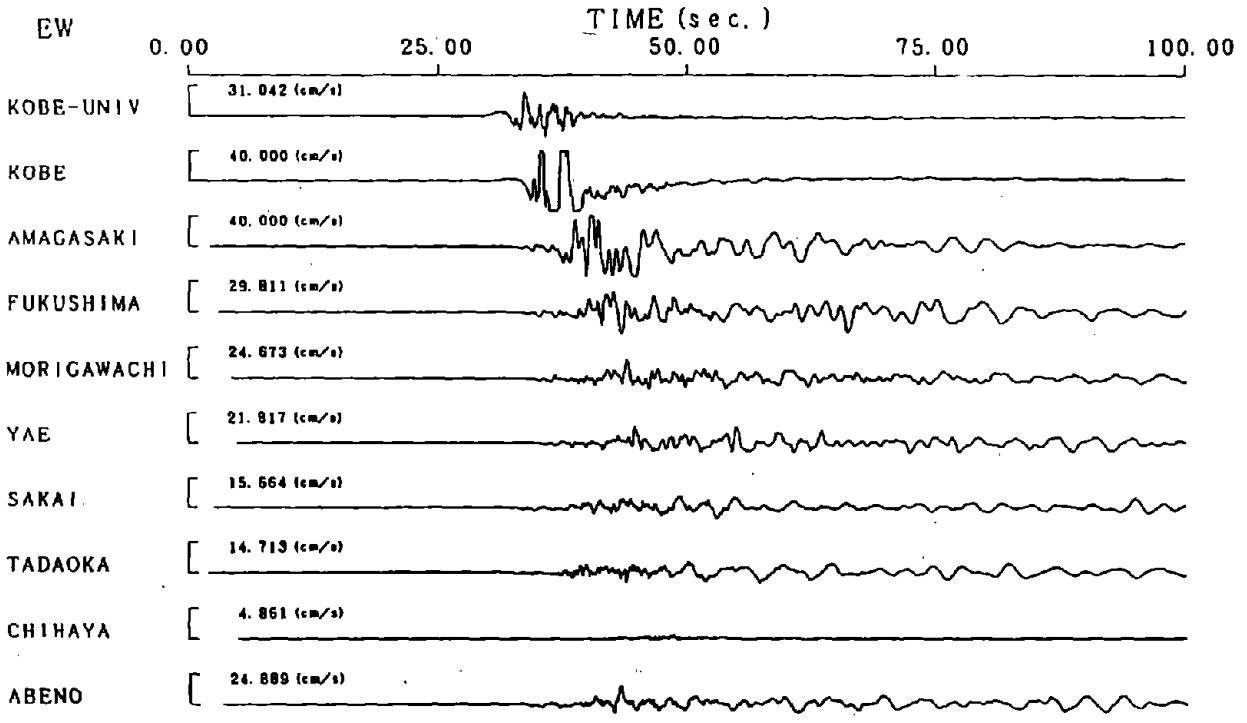

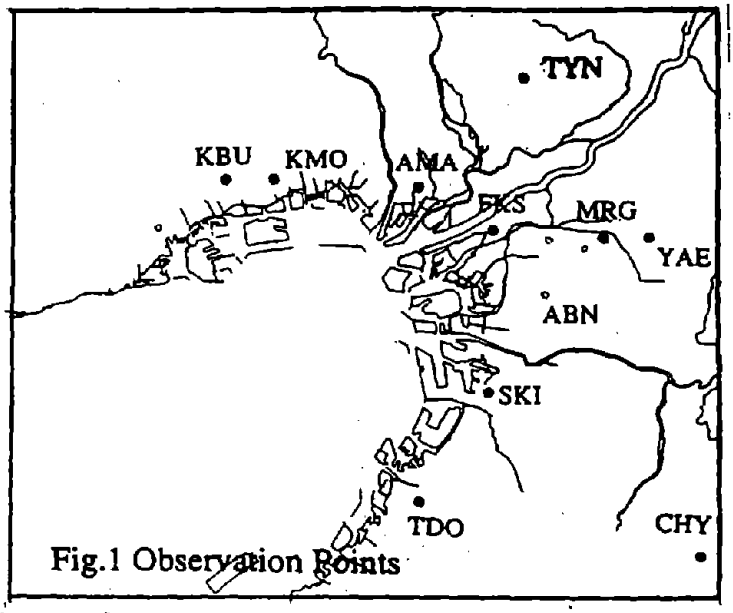

Figure 2.12: Velocity waveforms (horizontal east-west component) recorded by the Kinki Strong Motion Observation Network. Source: GeoResearch Institute, 1995.

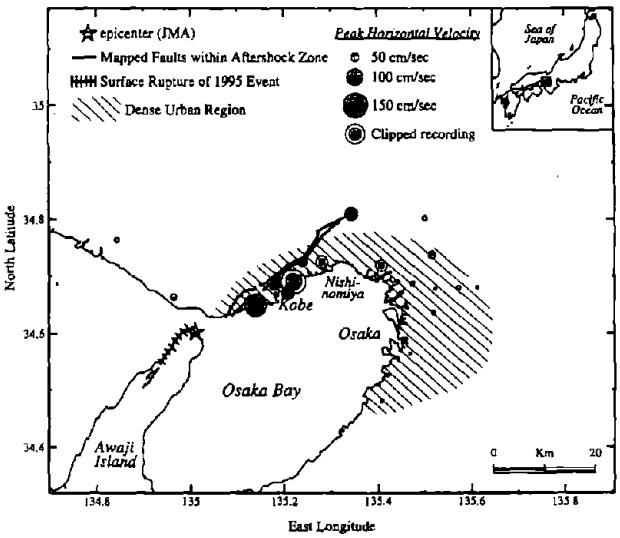

Figure 2.13: Location of the mainshock epicenter, mapped active faults within the aftershock zone (including surface rupture of the Nojima fault on Awaji Island), the dense urban region, and peak velocities recorded from the 1995 Kobe earthquake.

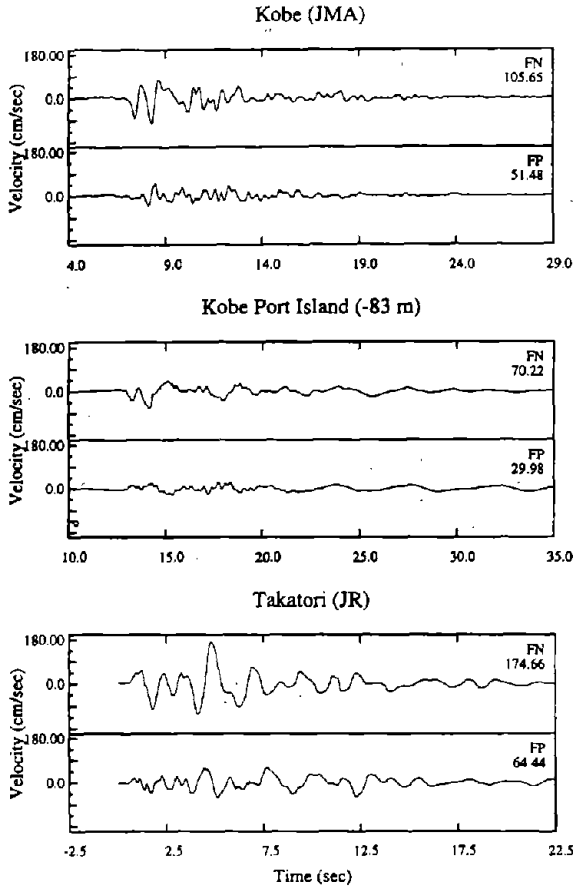

Figure 2.14: Recorded velocities at Kobe JMA, Port Island at a depth of 83 m, and Takatori rotated into fault-normal and fault-parallel components.

direction. For example, the seven story office building shown in Figure 2.16 has shear cracking of the building cladding, with extensive window damage, in the fault-normal direction and little damage in the fault-parallel direction. Buildings characteristically displayed interstory damage, such as that shown in Figure 2.17, in the fault-normal direction. Moreover, the collapse of the Hanshin elevated expressway appeared to result from strong displacement pulses in the fault-normal direction, which is perpendicular to the orientation of the highway.

The recorded peak horizontal accelerations from the Kobe earthquake are comparable to those predicted for a strike-slip earthquake using the Abrahamson and Silva (1995) empirical attenuation relation for soil based mainly on California data, as shown in Figure 2.18. The recorded peak horizontal velocities are slightly higher (about one standard deviation higher) than those predicted for a similar event using the Campbell (1990) empirical attenuation relation for soil based mainly on California data, as shown in Figure 2.19. The much larger level of damage that occurred in the Kobe earthquake compared with that of recent earthquakes in California may be attributable in part to the fact that the dense urban region of Kobe was subject to strong rupture directivity effects. As shown in Figure 2.13, the largest peak velocities recorded from the Kobe earthquake were in the dense urban region. Peak velocities as large and larger than these values were recorded during the 1994 Northridge earthquake. However, as shown in Figure 2.20, the dense urban region of the southern San Fernando Valley and the northwest Los Angeles basin were not subject to rupture directivity effects. The effects were experienced in the northern San Fernando Valley and Santa Susana Mountains, which are located away from the dense urban region. Other factors, such as quality of construction and evolution of the respective design codes, also contributed to the different levels of damage observed during the Northridge and Kobe earthquakes.

2.7 Site Response

Severe damage to buildings due to the Kobe earthquake was observed along a strip about 30 km long and 1 km wide. Figure 2.21 shows the severely damaged area, active faults, and aftershock distribution (Kohketsu, 1995). The hachured zone indicates the area where the rate of

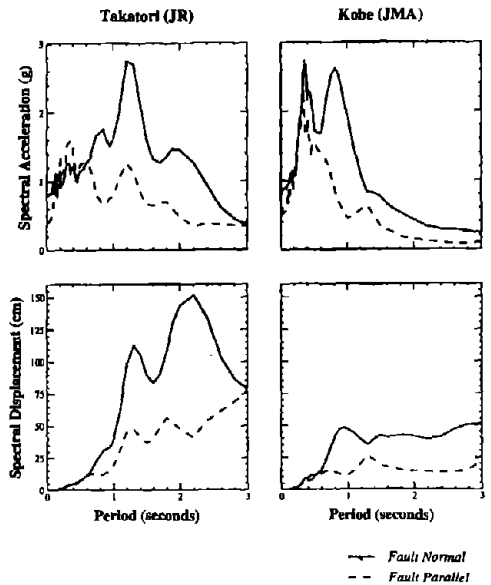

Figure 2.15: Response spectral acceleration (top) and displacement (bottom) of the fault-normal and fault-parallel components of the Kobe earthquake recorded at Kobe JMA and Takatori.

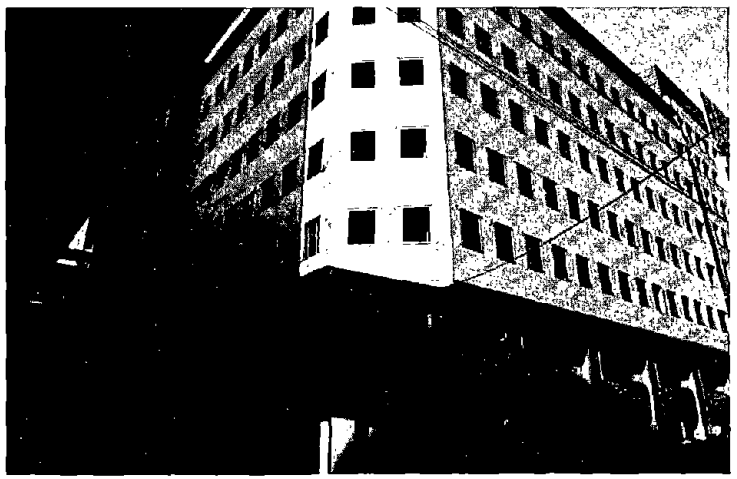

Figure 2.16: Office building in Kobe with significant cladding damage in the fault-normal direction (left side) and little damage in the fault-parallel direction. Photograph courtesy of C. Thewalt, UC Berkeley.

Figure 2.17: Building in central Kobe with mid-height story collapse in the fault-normal direction.

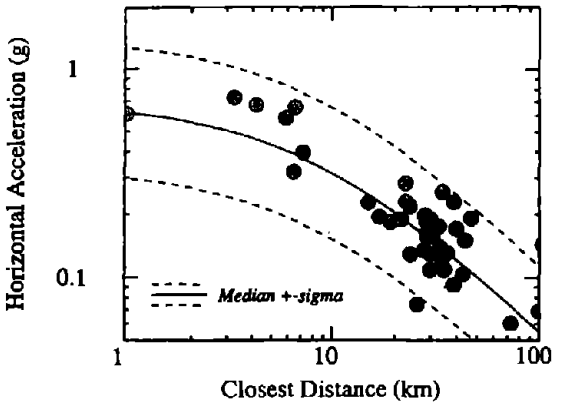

Figure 2.18: Attenuation of recorded peak horizontal acceleration at soil sites from the Kobe earthquake, compared with empirical relations for strike-slip earthquakes recorded on soil based mainly on California data (Abrahamson and Silva, 1995).

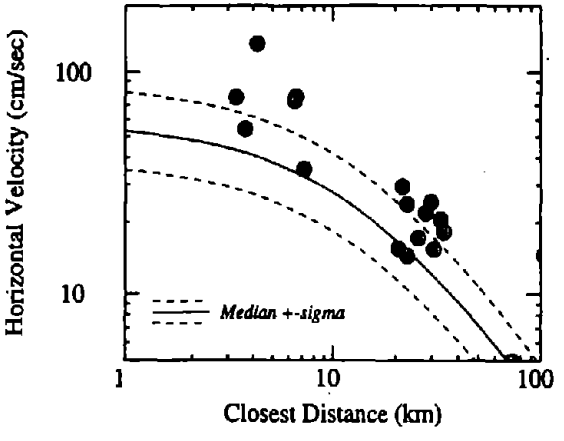

Figure 2.19: Attenuation of recorded peak velocity at soil sites from the Kobe earthquake, compared with empirical relations for strike-slip earthquakes recorded on soil based mainly on California data (Campbell, 1990).

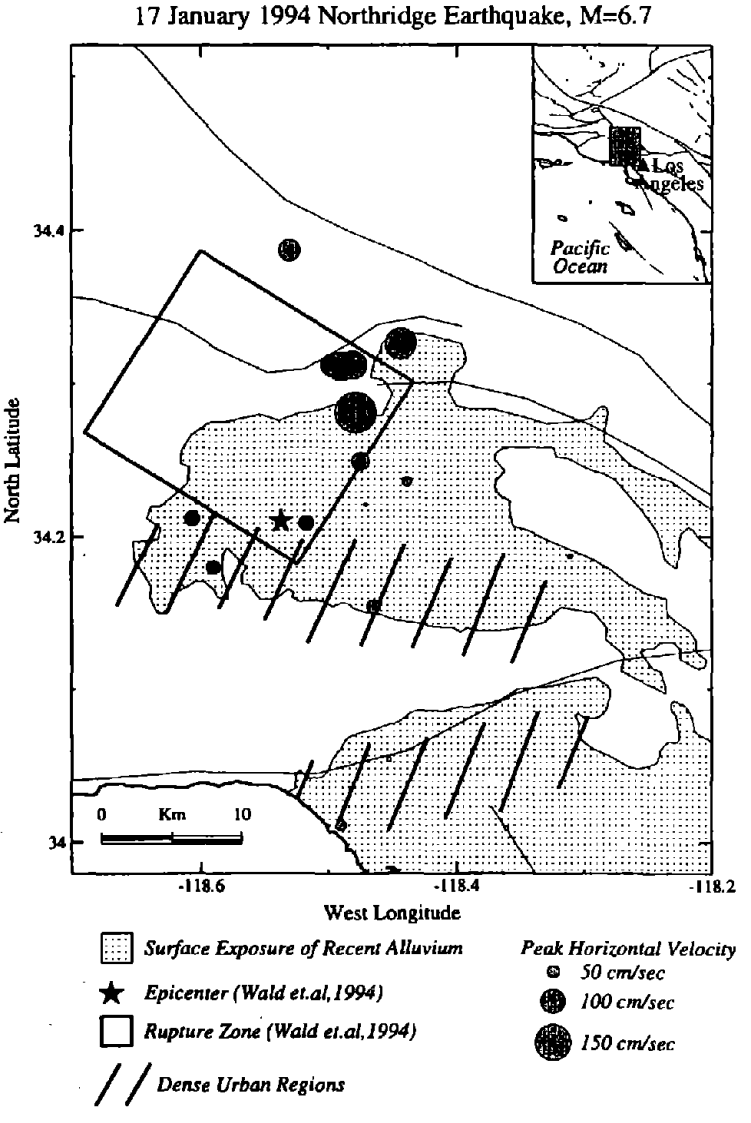

Figure 2.20: Location of the mainshock epicenter, surface projection of the fault rupture model of Wald and Heaton (1994), dense urban regions, and peak ground velocities recorded from the 1994 Northridge earthquake.

collapsed wood-frame buildings is more than 30%; this rate exceeded 70% in the central part of this area. To investigate whether these large variations in site response in the Kobe area were attributable to site effects, investigators from Ohsaki Research Institute recorded aftershocks at several sites on alluvium in the heavily damaged area as well as at rock sites on the foot of Rokko mountain in Kobe (Kawase et al, 1995). The locations of their stations are shown in Figure 2.22, and their study area is shown as an inset in Figure 2.21. They found that, for six aftershocks, horizontal peak accelerations recorded at three sites located on a thin layer of alluvium (about 10 to 15 meters thick) were about 3 to 5 times larger than those at a reference site on rock, as shown in Figure 2.22.

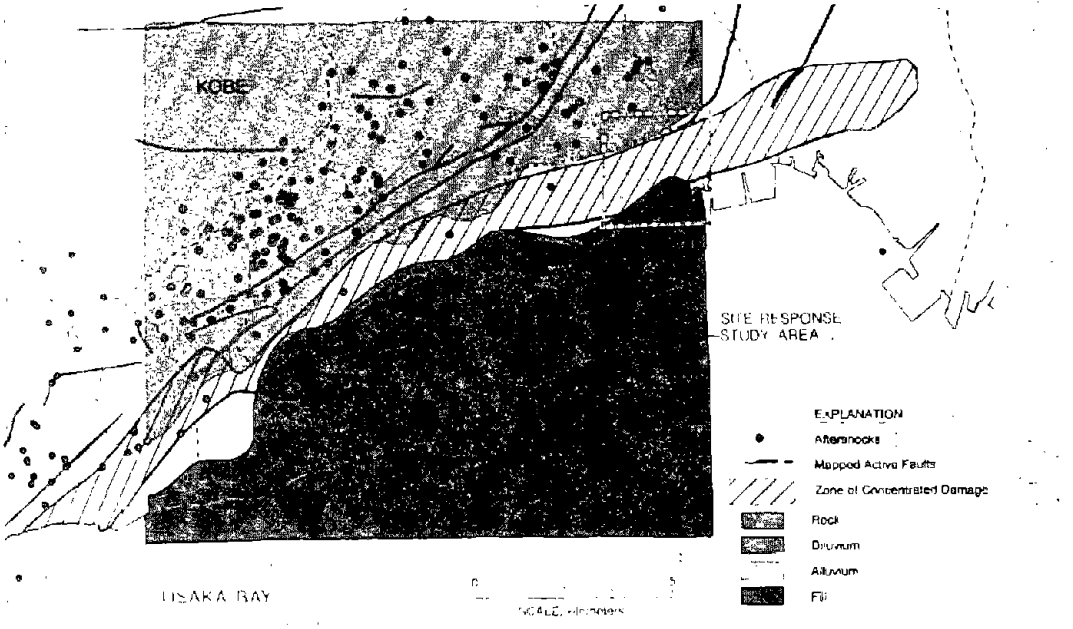

Figure 2.21: Location of zone of intense destruction in the Kobe area, and its relationship to the location of active faults, the aftershock distribution, and geological site conditions. Modified from Kohketsu (1995).

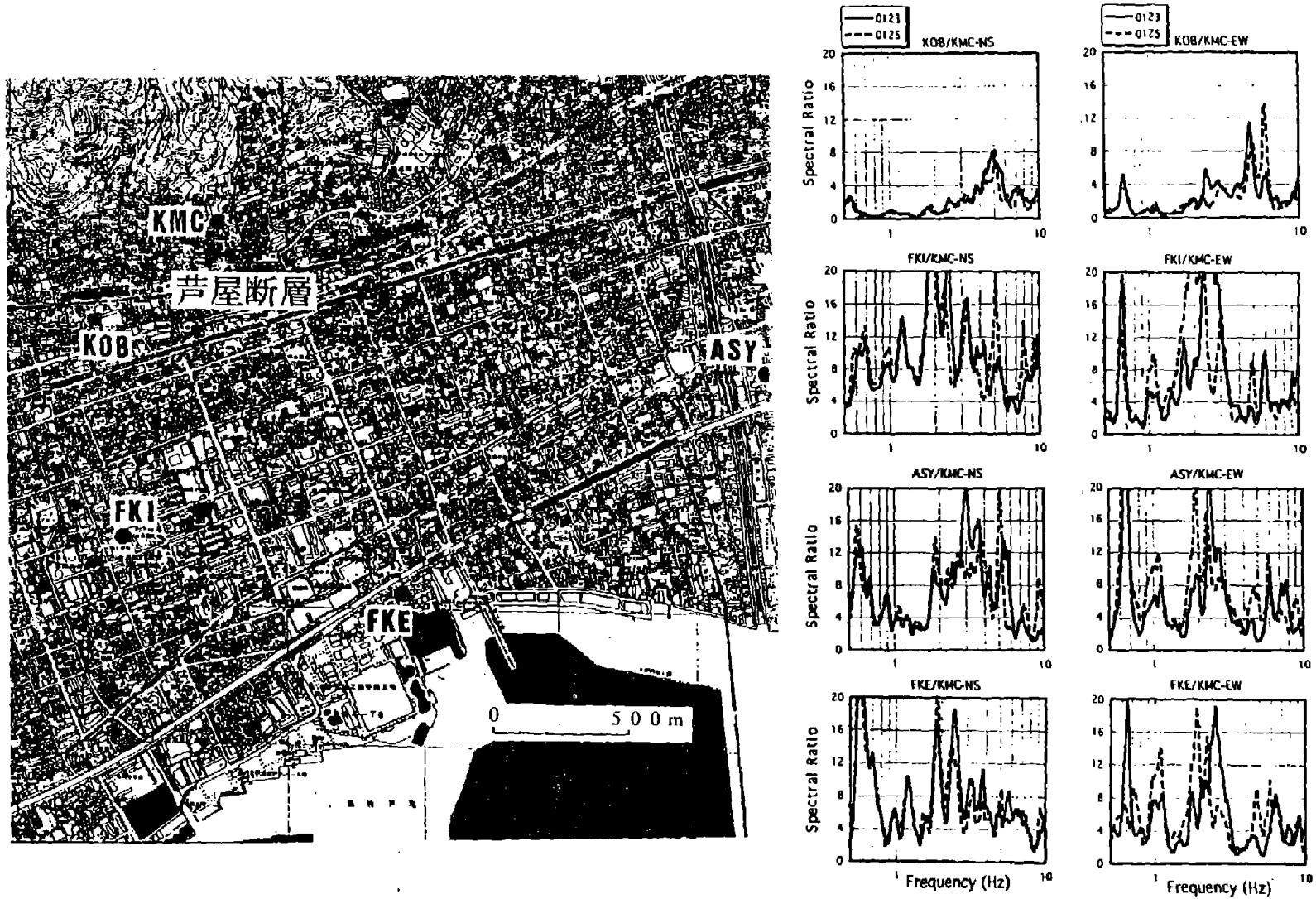

Figure 2.22: Left: Locations of aftershock recording sites used in the site response study conducted by Kawase et al. (1995). The location of the study area is shown in Figure 2.21. Right: Fourier spectral ratios, averaged over six aftershocks and referenced to rock site KMC, for diluvial site KOB, alluvial sites FKI and ASY, and fill site FKE. Source: Kawase et al. (1995).

A downhole array on the northwest corner of Port Island (see top of Figure 2.23), which is located just south of downtown Kobe, provided valuable site response data. Strong motion instruments were located at the ground level and at depths of 16 m, 32 m, and 83 m. The generalized soil profile, with shear wave velocities (Iwasaki, 1995), is shown is Figure 2.23. The thickness of Quaternary deposits at this site is on the order of 1000 m. Acceleration-time histories for each component are shown in Figures 2.24-2.26. The horizontal acceleration-time histories shown in Figures 2.24 and 2.25 clearly show the initiation of liquefaction in the loosely dumped granular fill located between a depth of 12 m and the ground level. Moreover, the instrument records show the characteristics of the near-field response (i.e. brief, intense pulses) at this deep soil site. The peak ground accelerations tended to be sustained or to increase slightly as the motions propagated to the ground surface, except through the liquefied fill deposit.

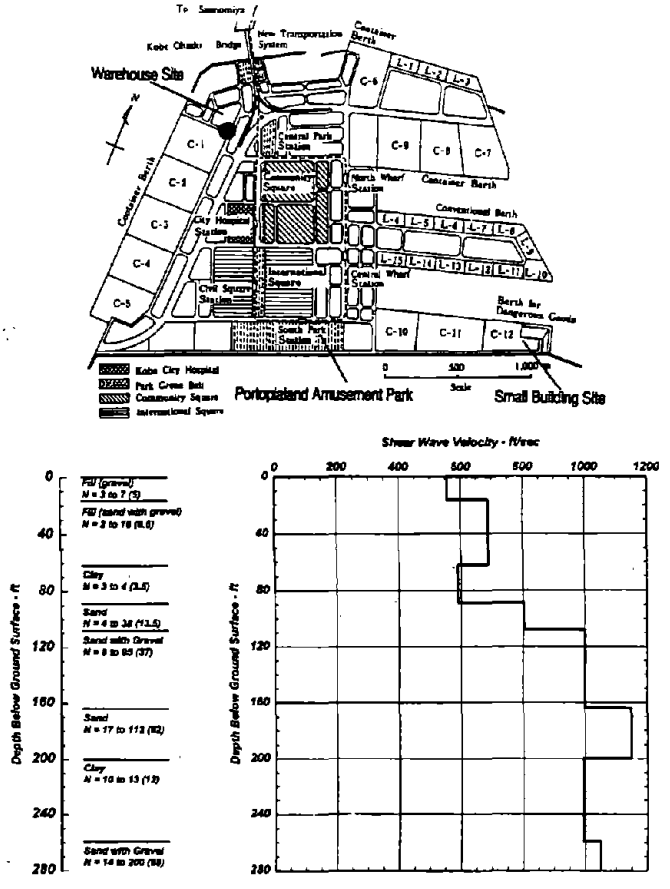

Figure 2.23: Generalized soil profile with shear wave velocity data at the downhole array site on the northwest corner of Port Island. Source: Iwasaki (1995).

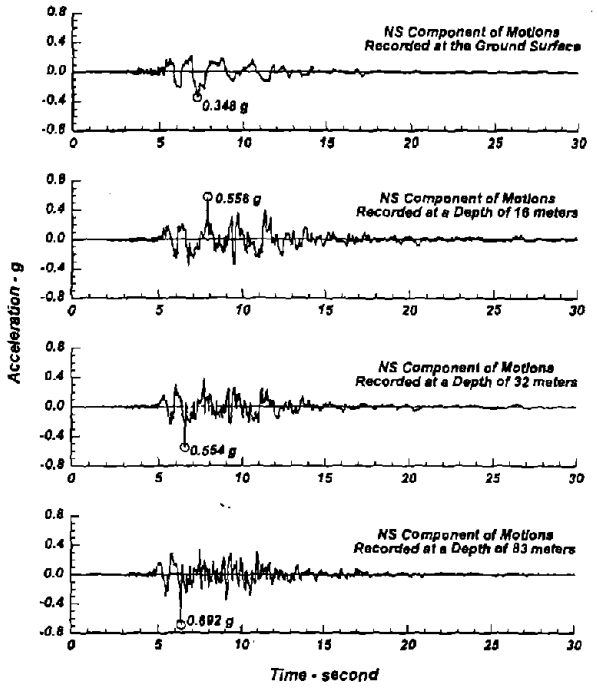

Figure 2.24: Horizontal acceleration-time histories recorded at Port Island downhole array; NS direction. Source: GeoResearch Institute, 1995.

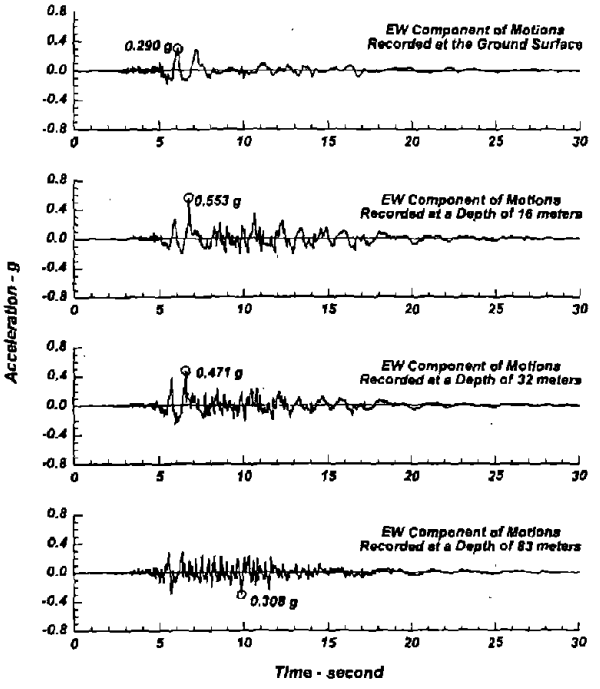

Figure 2.25: Horizontal acceleration-time histories recorded at Port Island downhole array; EW direction. Source: GeoResearch Institute, 1995.

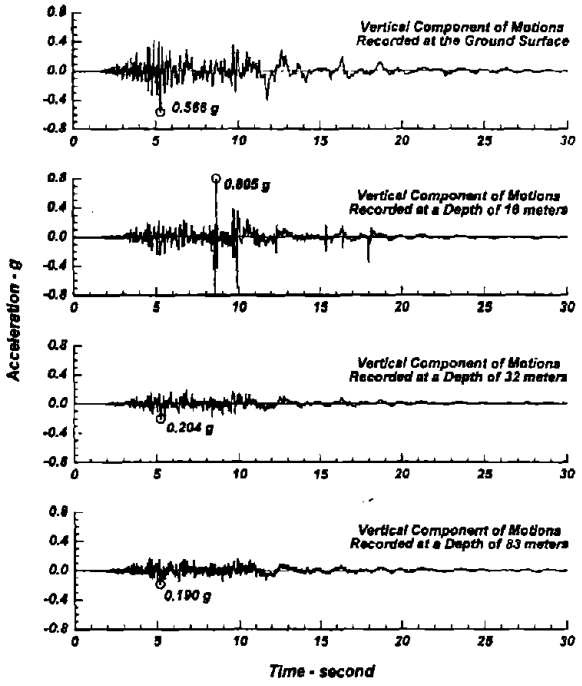

Figure 2.26: Vertical acceleration-time histories recorded at Port Island downhole array. Source: GeoReserch Institute, 1995.

The Kansai International Airport is built on reclaimed ground similar to Port Island, but it is located about 30 km from the zone of energy release, so the motions were significantly lower. Free-field instruments located at the northern and southern ends of the runway recorded ground level maximum horizontal accelerations (MHA) of 0.15 g and 0.09 g, respectively. The terminal building has strong motion instruments located at its basement, fourth floor and roof levels. The MHA recorded at the basement level was relatively low at only 0.04 g, whereas, at the fourth floor level, the recorded MHA increased to 0.10 g. One of the piers of the bridge that connects Kansai Airport Island to the mainland has instruments located at its bottom and top, and these instruments recorded MHAs of 0.13 g and 0.27 g, respectively. These data from the strong motion instrumentation array at the Kansai International Airport present a valuable opportunity for further investigation of site response and soil-structure interaction issues.

CHAPTER THREE: LIQUEFACTION AND RELATED EFFECTS

3.1 Introduction

Extensive liquefaction of filled land occurred throughout the region affected by strong ground motion. The general setting of the Kobe and Osaka metropolitan regions, on the margins of a major bay flanked by mountains, resulted in a gradual but extensive reclamation of land along the bay margins. Infilling of the bay has occurred along most of the waterfront over a long period of time, and in many places these fills are liquefiable or have been placed over liquefiable beach sand deposits. In addition, the rapid expansion of port facilities, mainly after 1963, has led to extensive construction of man-made islands. These islands were constructed using the most readily available local material: decomposed granite, which is a relatively coarse granular material that is quite susceptible to liquefaction unless well compacted.

Severe liquefaction occurred on Rokko and Port Islands (Figure 3.1), and in most of the port areas along the Kobe mainland. Some of the most damaging effects were lateral spreads around the margins of Rokko and Port Islands and mainland port areas, and ground settlement in the interior of Rokko and Port Islands. However, liquefaction effects were widespread as far as 3 km inland from the waterfront, and for several kilometers laterally along the bay. These effects caused minor disruption to residential and industrial areas of Kobe, Nishinomiya, and Ashiya within the narrow urban corridor that lies between the bay to the south and the mountains to the north. Evidence of liquefaction in areas away from the waterfront consisted of buckled and fractured curbs, walkways, and other pavements (Figure 3.2); small ground fissures; sporadic sand boils; and small amounts of ground settlement. Interestingly, liquefaction seems to have had relatively little influence on the structural damage observed in many of these areas; in fact, buildings of various types seem to have survived remarkably well in view of the liquefaction-induced ground deformations (Figure 3.3). Damage to underground utilities, however, was extensive throughout the liquefied area.

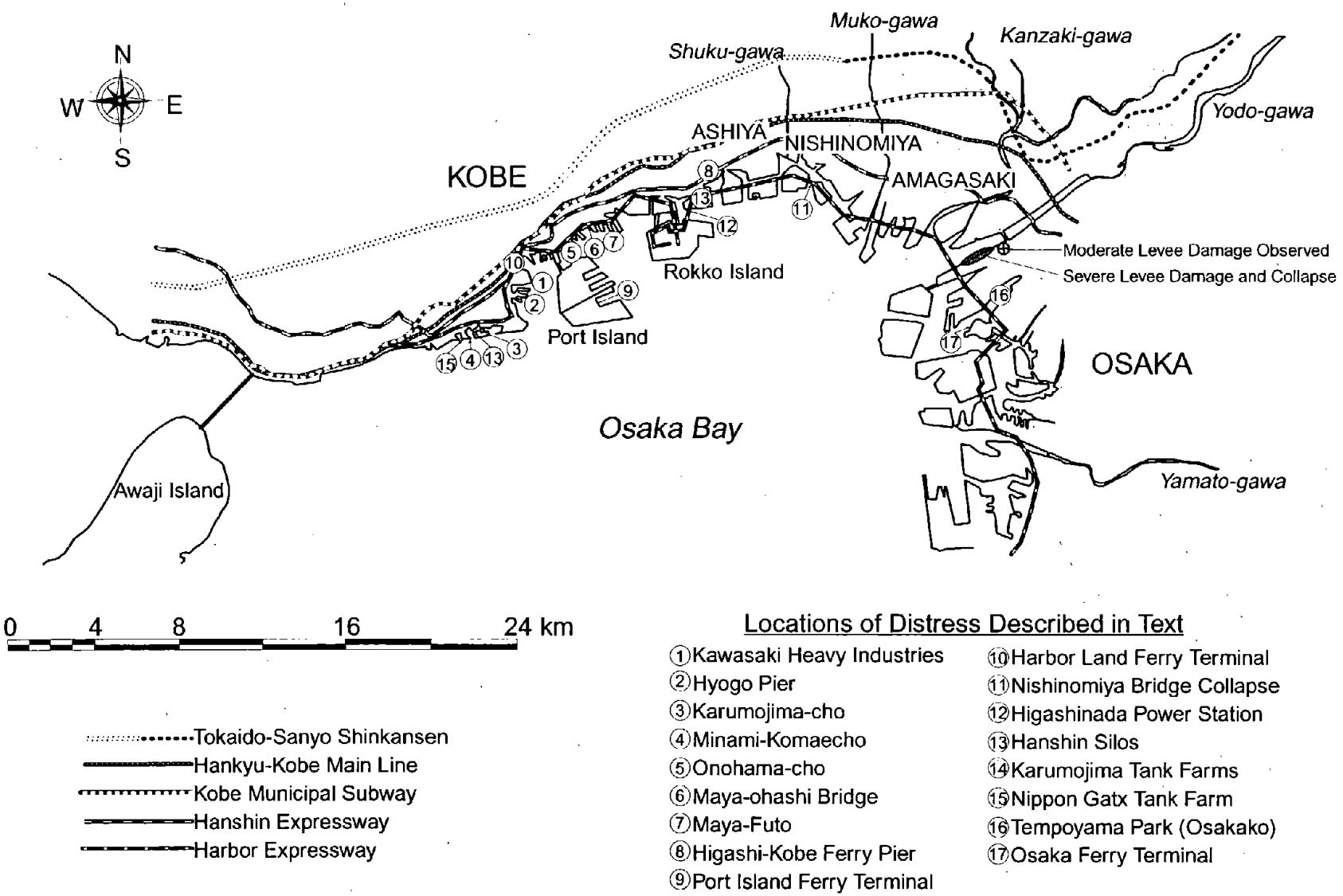

Figure 3.1 General location reference map of the Kobe waterfront.

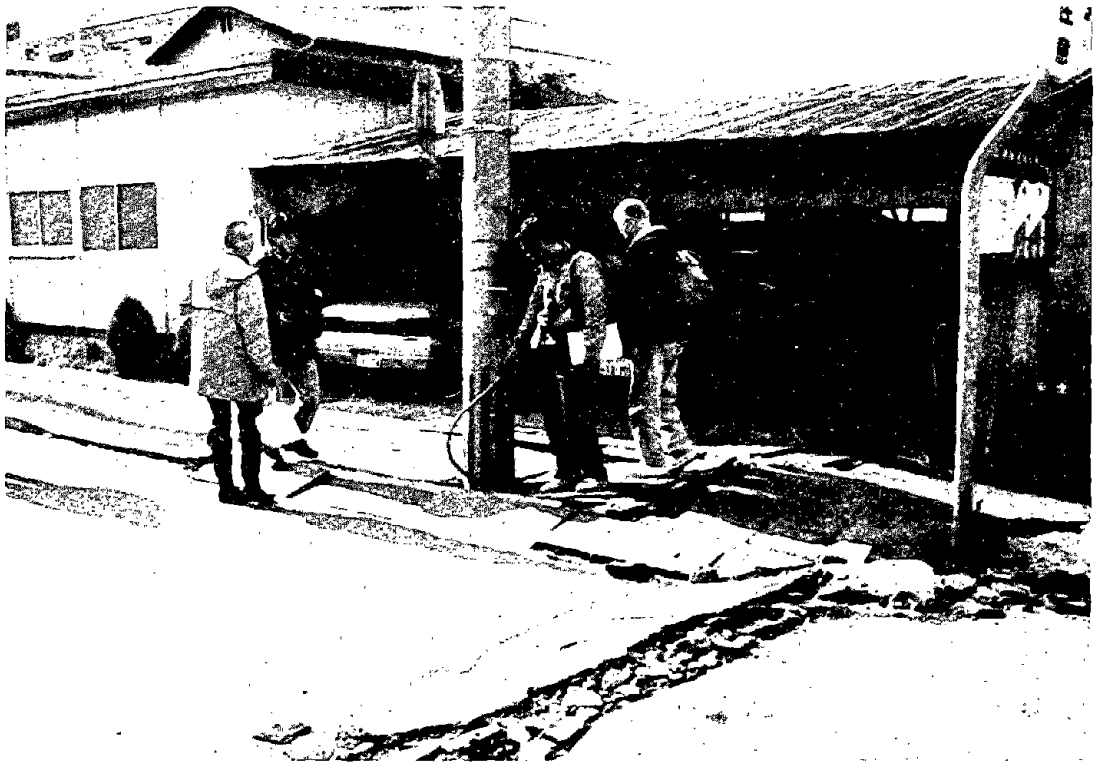

Figure 3.2: Evidence of liquefaction damage in a residential area of Nishinomiya; buckled pavement, cracked curbs, differential settlement.

Figure 3.3: Relatively undamaged houses in a residential area in Ashiya. Note the evidence of lateral spreading caused by the liquefaction of the fill.

3.2 Port Facilities and Artificial Islands

3.2.1 Setting and Soil Conditions.

The main port facilities in Kobe harbor are located primarily on reclaimed land along the coast and on two man-made islands, Port Island and Rokko Island, which are joined by bridges to the mainland (Figure 3.1). The liquefaction and lateral spread-induced damage to harbor structures on the islands disrupted nearly all of the container loading piers, and effectively shut down the Port of Kobe to international shipping. All but 6 of about 187 berths were severely damaged.

Port Island was constructed in two phases; only Phase I is shown in Figure 3.4. Phase I, consisting of 436 ha was completed in 1981 after 15 years of filling and construction operations. Located on the island are port facilities, wharves, container yards, high-rise apartments, an amusement park, warehouses, and commercial buildings. The filling for Phase II, which consists of a 390-ha area extending directly to the south of the area shown in Figure 3.4, began in 1986. Completion of construction of Phase II facilities was scheduled for 1996. Rokko Island has an area of 580 ha. Filling began in 1972, and reclamation was completed in 1992. Land use on Rokko Island is much the same as on Port Island.

The fills beneath Port and Rokko Islands were constructed using residual soil formed by weathering of granite (Masa soil), which was obtained from borrow sites in the Rokko Mountains and brought to the site through a combination of conveyor belts and barges. This soil is collapsible in its natural state and its grain size distribution varies depending on the degree of weathering. The general ranges of grain sizes reported for the decomposed granite fills beneath Port and Rokko Islands are shown in Figure 3.5. Beneath Port Island, the Phase I fill usually has a maximum grain size between 2 mm and 40 mm, a mean grain size between 0.2 mm and 6 mm, and a fines content between 5 percent and 30 percent. These grain-size characteristics indicate a material that is well graded, rather coarse, and which contains a significant fraction of gravel. Although the fines content is somewhat low, deposits from sand boils that erupted to the surface contained layers of very fine material which was slimy and difficult to walk on. The Phase II fill beneath Port Island and the fill beneath Rokko Island are generally similar to the Port Island fill, except that material from the Kobe Group, a layered Miocene sediment, was mixed with the decomposed granite.

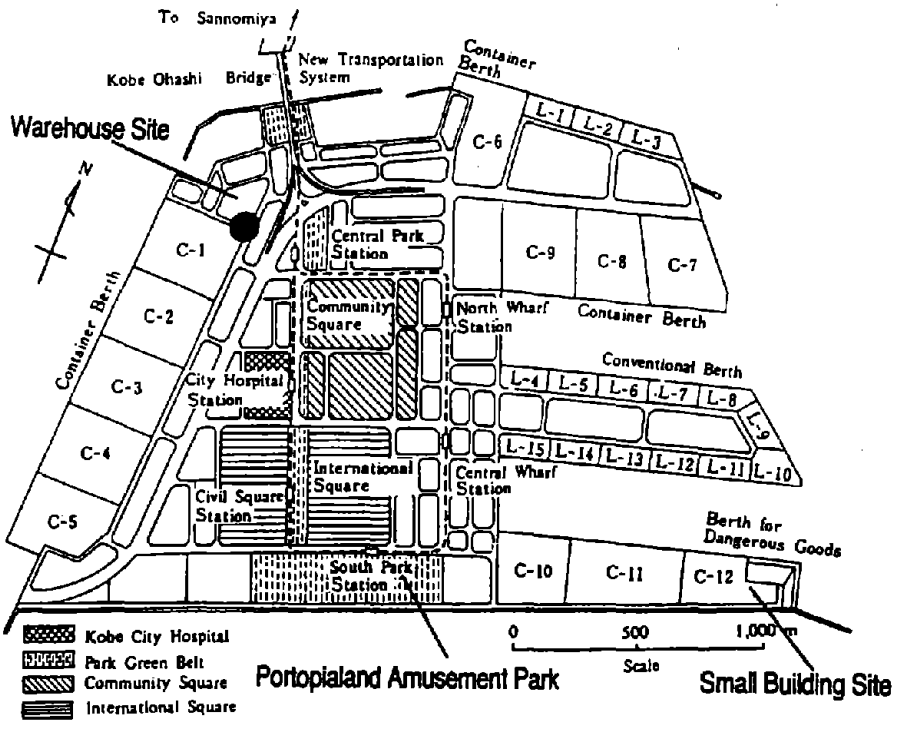

Figure 3.4: Map showing layout of facilities located on the older part of Port Island; at the time of the earthquake, an extension of the island was being developed south of the southern seawall shown on the map (Fudo Construction Corp., Ltd., 1995).

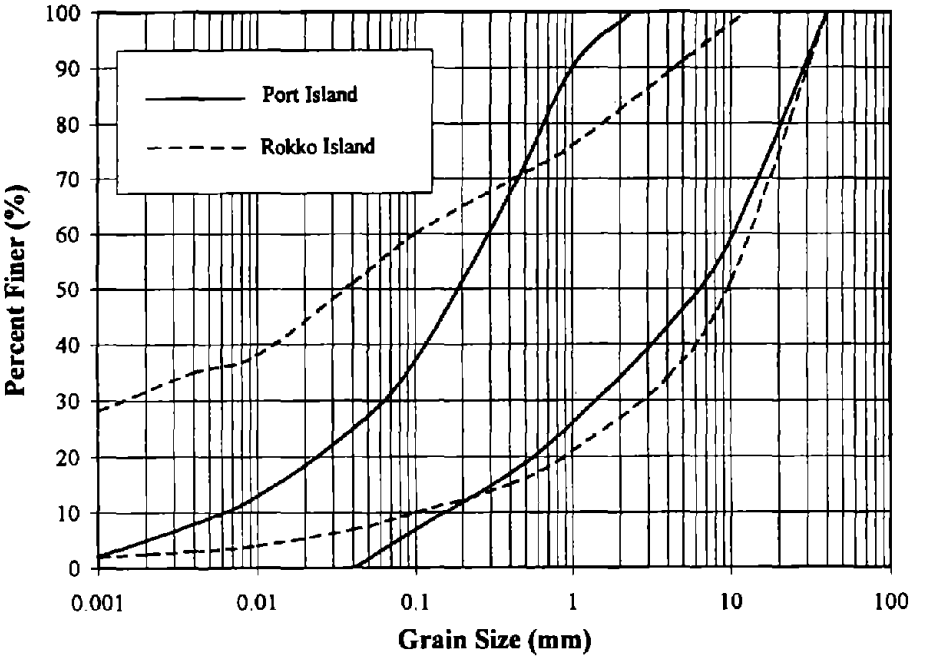

Figure 3.5: Representative ranges of grain sizes for fill materials beneath Port and Rokko Islands.

Accordingly, the latter fills are characterized by higher fines contents than the Phase I fill beneath Port Island (Matsui, 1994).

Owing to the low strength and sensitive character (sensitivity of about 8 to 10) of the soft alluvial clay on the sea bottom, a 2 to 3 m thick uniform coverage of the bottom was completed before dumping the fill in 3 to 4 m thick steps across the site. Barge dumping continued to 2 m below the water surface, above which end dumping from conveyor belts was used. Surface compaction was used for the upper few meters.

A typical soil profile for Port Island, with some relevant soil properties, as given by Nakakita and Watanabe (1981), is shown in Fig. 3.6. Some variations in thickness of the different strata exists across the islands. Borehole logs plotted on Figure 3.6 show that SPT values, N^1, range between 5-10 blows/30 cm. The soil profile beneath the Portopia Hotel, shown in Figure 3.7, is typical of Port Island sub-surface conditions. The diluvial sand and gravel layer is equivalent to the interlayered sand and clay layer shown in Figure 3.6. This is the bearing layer for pile foundations on the island. The conditions on Rokko Island are very similar (Figure 3.8), and blow counts from several boreholes are shown in Figure 3.9. These blow counts are somewhat higher than those measured beneath Port Island; nevertheless, the distributions of liquefaction effects was generally similar.

Detailed site specific liquefaction studies were conducted for some projects on Port Island prior to the earthquake. These studies applied a procedure similar to the "simplified procedure" of Seed and Idriss (1982) for estimating effective cyclic shear stress ratios, τ/σ, which were thought to be likely during anticipated earthquakes. The estimated peak ground acceleration used in these studies was 0.15 g, and the duration corresponded to that expected from a magnitude 8+ earthquake. Critical accelerations determined from cyclic triaxial tests, for durations corresponding to a magnitude 8+ earthquake, were determined to be about 0.2 g. Recent test data show somewhat smaller critical accelerations for normally consolidated fill (Figure 3.10). On the basis of the anticipated ground motions, the sites were judged to have adequate resistance to liquefaction.

[1] It is important to note that the average SPT energy used for the drill rigs in Japan is about 75 percent of nominal, whereas the US energy efficiency is about 60 percent. Thus, the N-values used in empirical correlations should be taken as about 1.2 times the measured values after correction for overburden pressure.

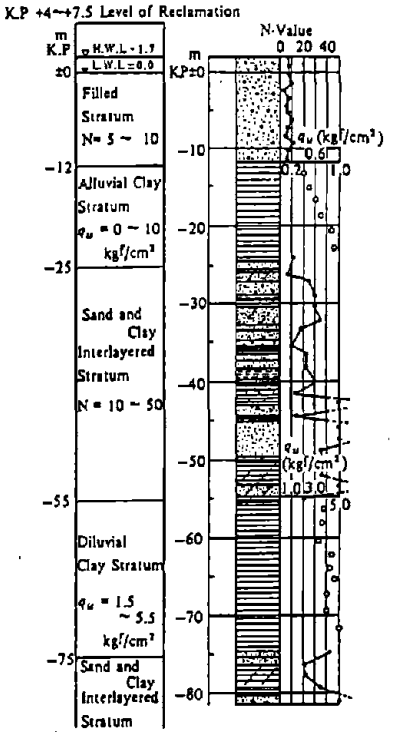

Figure 3.6: Soil condition and standard penetration test data from a site on Port Island (Nakakita and Watanabe, 1981).

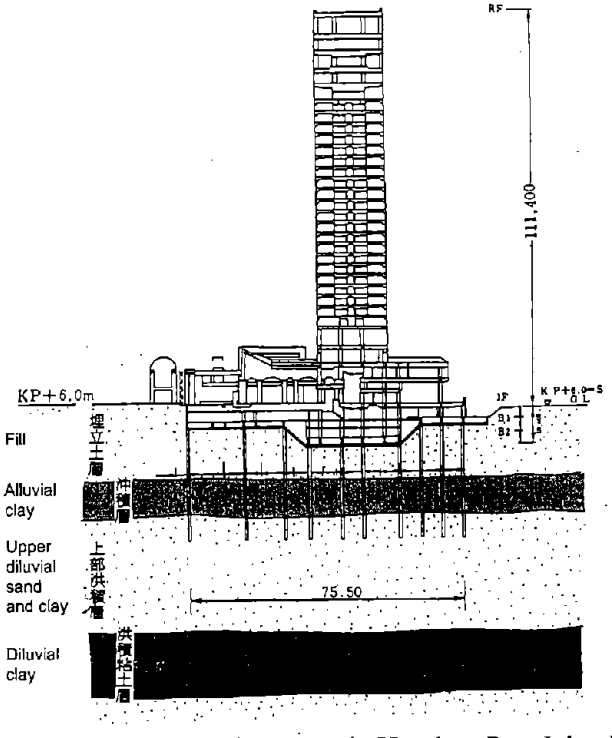

Figure 3.7: Foundation conditions under the Portopia Hotel on Port Island.

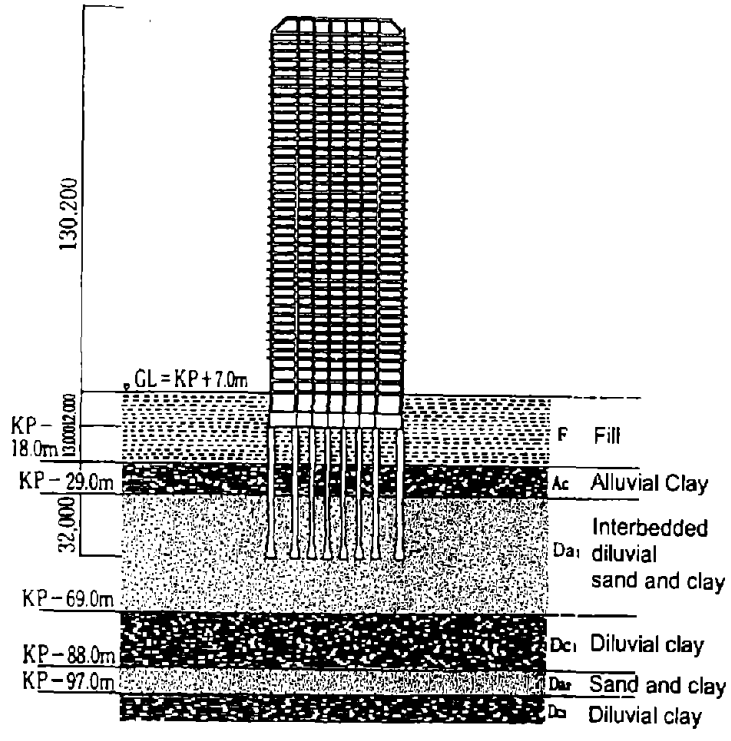

Figure 3.8: Foundation conditions under a high rise building on Rokko Island.

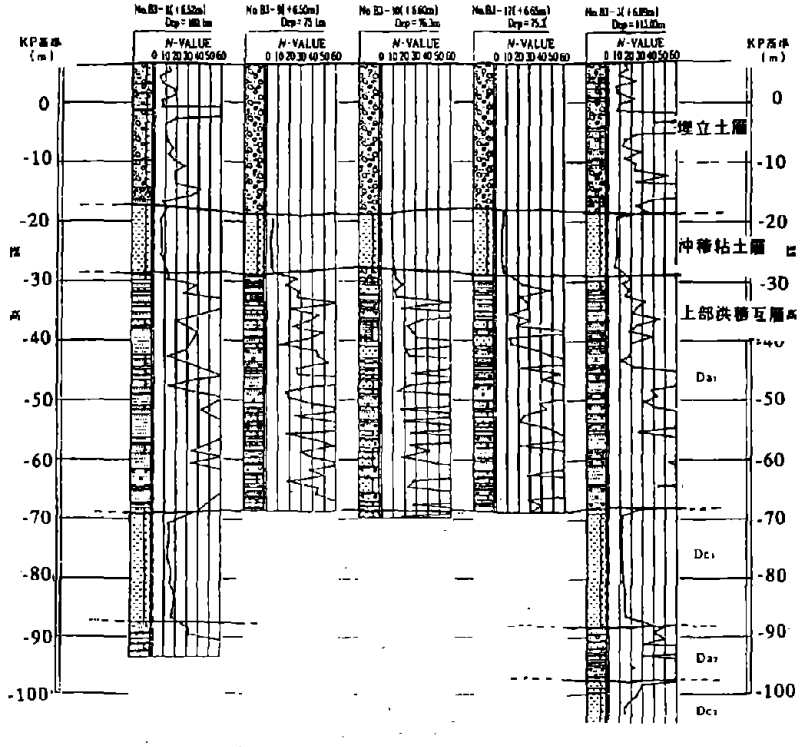

Figure 3.9: Data from site investigations on Rokko Island.

However, as noted below, accelerations measured during the earthquake were much larger than these pre-earthquake estimates.

3.2.2 Ground Motions.

Ground motions during the earthquake greatly exceeded the design motions for Port Island. Motions recorded at a site in Kita Koen Park are tabulated in Table 3.1. This locality is on Port Island, not far from the bridge to Kobe Ohashi, and is in an area disturbed by surface effects of liquefaction.

Table 3.1 Maximum Accelerations in Gals Recorded near Kita Koen Park, Port Island

Depth	Acceleration (gals)		
	NS	EW	UD
0 m	341.2	284.3	555.9
12 m	564.9	543.2	789.5
28 m	533.6	461.7	200.0
79 m	678.8	302.6	186.7

The time histories at the four depths for the N90°E component were already shown in Figure 2.24. These records indicate that the onset of strong ground shaking began about 5 seconds into the record, and the strong motions were effectively complete by 17 seconds. The records also indicate that ground motions on the fill surface were greatly modified compared to records registered at greater depths. These records indicate that as liquefaction occurred, large shear stresses could be transmitted through the liquefied zone. As a consequence, accelerations attenuated and fundamental periods lengthened at the surface compared to motions recorded below the liquefied layer. N-values in the fill at this location ranged between 5 and 10 blows/30 cm, which are typical values for liquefiable parts of the island. Thus, it was not surprising that liquefaction occurred at this and other areas of Port Island since the recorded peak accelerations below the liquefied layer were about four times the design accelerations and the surface accelerations were about two times the anticipated values, despite the effects of liquefaction.

3.2.3 Damage to Port Structures and Adjacent Facilities.

In general, the seismically induced liquefaction resulted in pervasive lateral spreading around the margins of the islands and mainland port areas, and in ground settlement within the interiors of the islands. Figure 3.11 gives a partial listing of damaged areas on Port Island and also shows areas of improved ground which are further discussed in Chapter 4. At many localities lateral spreads pushed quay walls, used for berthing of ships, outward as much as several meters, with average displacements of 2 to 3 m (Figure 3.12). A typical quay wall section consists of a caisson, concrete box structures, up to 15 m wide and 20 m deep, with two or more interior cells (Figure 3.13). These caissons were towed to the site, submerged in position to form the wall, and then the interior cells backfilled with sand to form the quay.

Depressions and grabens, as deep as 4 m and as wide as 30 m, formed pervasively behind the quay walls, and lateral spreading caused ground fissures parallel to the walls as far as 200 m inland. Unfortunately, nearly all of the major cranes used for transferring containers and other freight to and from ships were located within the graben or lateral spread zones. These structures were pulled apart at their bases by lateral ground movements and tilted by the subsidence. Supporting crane rails were also displaced and deformed (Figures 3.14 and 3.15). The extensive damage to the giant cranes was particularly evident on Rokko Island (Figure 3.16). The outward movement of the sea wall by as much as 3 m spread the crane legs off the wheel bogeys and, in a few instances, led to collapse of the cranes (Figure 3.17). In other instances, the movement led to deformation of crane legs and formation of plastic hinges above or within the horizontal brace (Figure 3.18). The consequences of the loss of the port facilities is dramatically illustrated in Figure 3.19 by the large number of vans and trucks ready for export before the earthquake, which were trapped in the flooded settled areas behind the displaced sea wall.

3.2.4 Specific Observations of Port and Quay Wall Damage.

Kawasaki Heavy Industries. A Kawasaki Heavy Industries facility is located on the mainland waterfront south of the Harbor Land ferry terminal, as shown in Figure 3.1. The quay walls around one large warehouse were displaced laterally and settled vertically enough to drop the apron slabs below the water level and to severely tilt a large crane beside the warehouse (Figure 3.20). Damage also occurred to quay walls, warehouses, and crane facilities south and north of the warehouse.

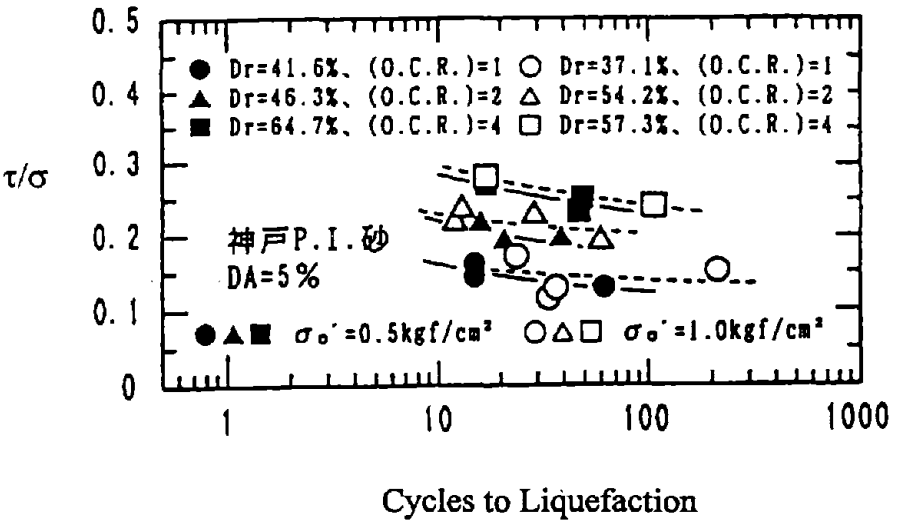

Figure 3.10: Liquefaction resistance of Port Island fill at various overconsolidation ratios (provided by N. Yoshida, Sato Kogyo, Ltd., Japan).

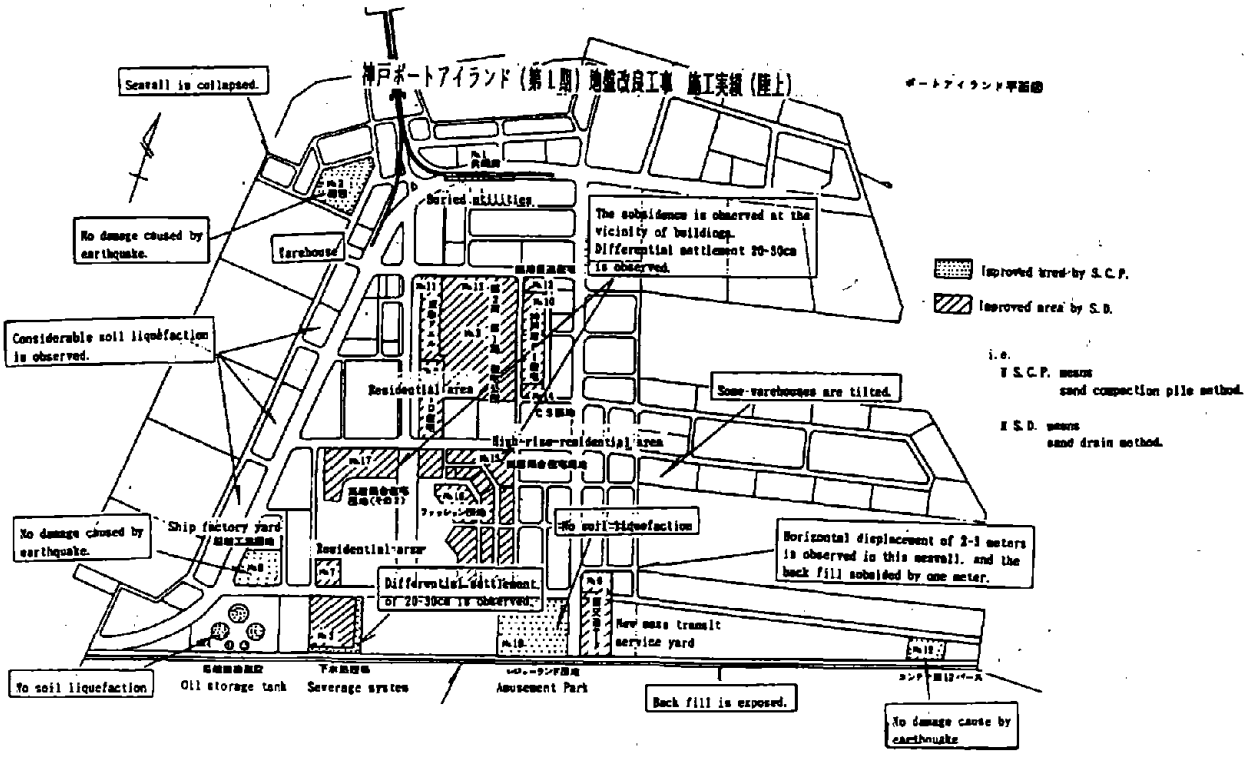

Figure 3.11: Damage assessment of Port Island (Phase 1) and zones of ground improvement by sand compaction piles.

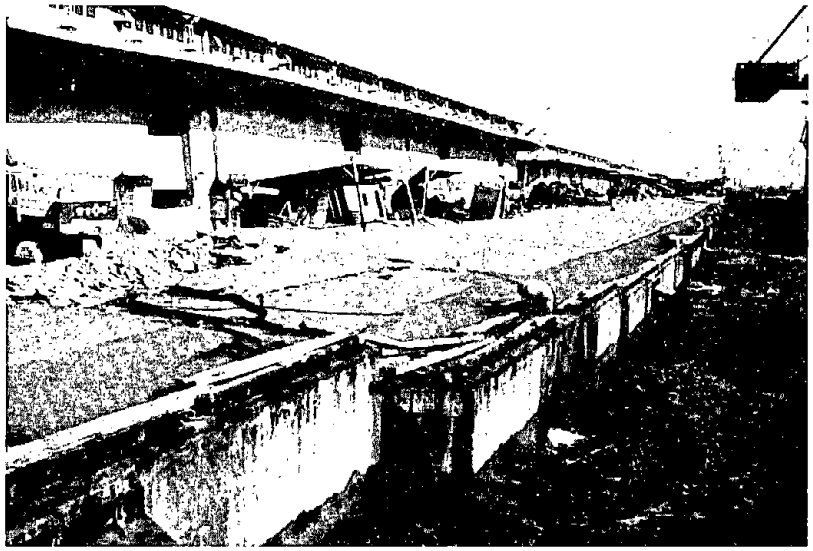

Figure 3.12: Example of lateral displacement of older quay walls on Port Island.

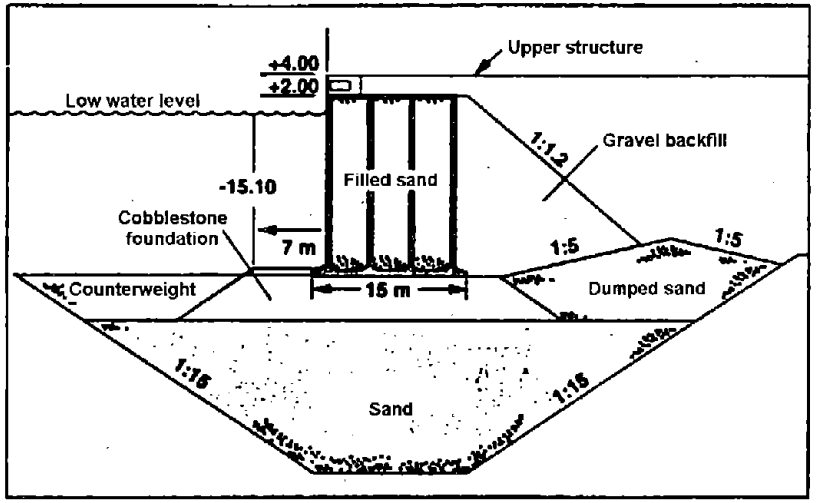

Figure 3.13: Typical cross section of a quay wall, foundation construction and backfill.

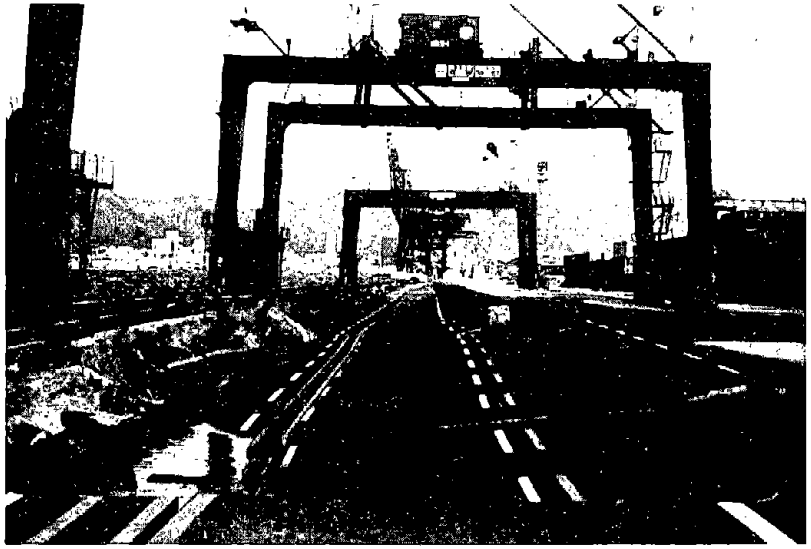

Figure 3.14: Graben caused by lateral displacement of the quay wall on Port Island. Note the cranes straddling the graben and the lateral deformation of the crane rails.

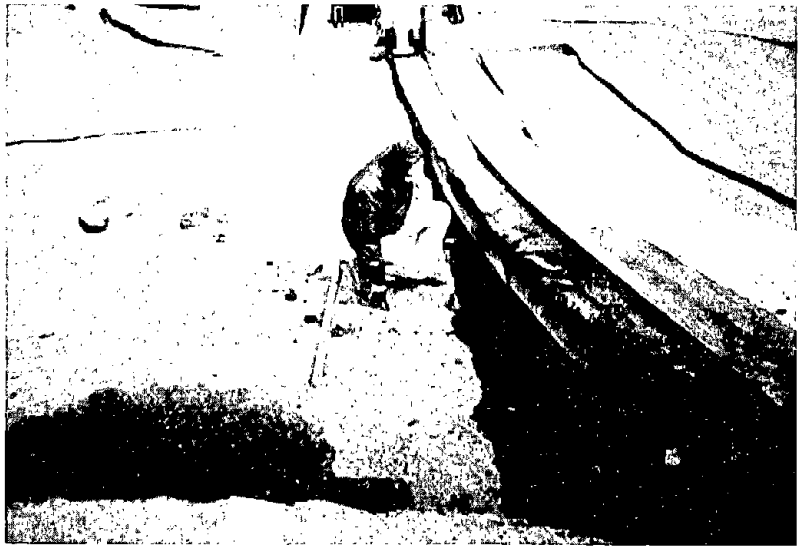

Figure 3.15: Crane rail on Port Island that settled into graben behind quay wall.

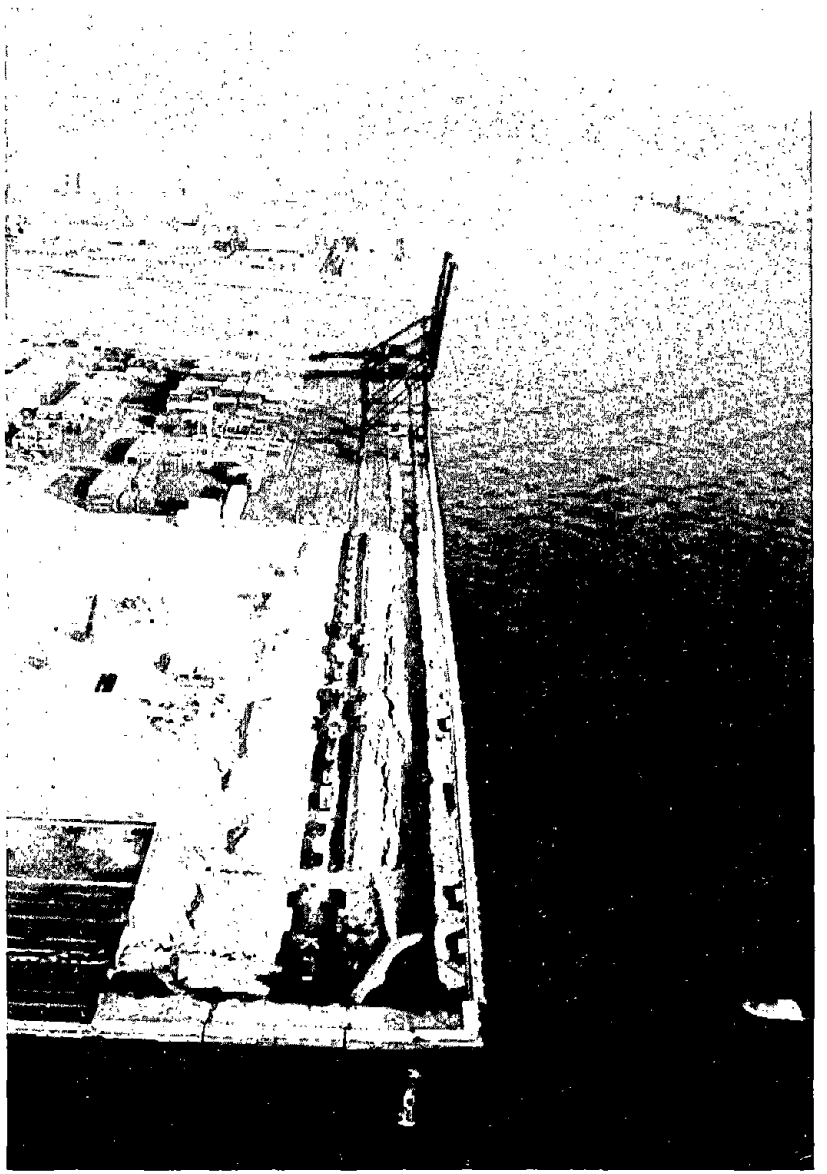

Figure 3.16: Air view of damaged quay walls and port facilities on Rokko Island. Quay walls have been pushed outward by 2 m to 3 m with depressed areas called grabens 3 m to 4 m deep forming behind the walls.

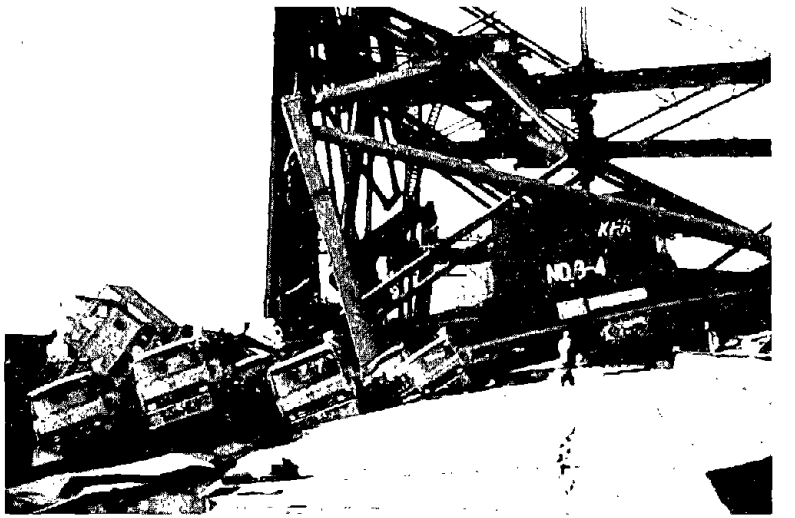

Figure 3.17: Collapse of crane due to lateral movement (~2 m) of quay wall on Rokko Island. Note settlement of 1-2 m also occurred behind wall.

Figure 3.18: Buckled or plastically yielded crane legs due to about 2 m of spreading between crane rails as a consequence of lateral caisson displacement.

Tsukiji-cho and Hyogo Pier. Tsukiji-cho and the Hyogo Pier are located on the mainland waterfront south of Kawasaki Heavy Industries and to the west of Port Island (Figure 3.1). Without exception, all quay walls around the full perimeter of the Tsukiji-cho were damaged to some degree. The most spectacular quay wall failures were at the eastern ends of Hyogo Piers No. 1 and No. 2. At these piers, the quay walls displaced sufficiently to bring the warehouses and surrounding apron slabs below water level: The end of Pier No. 1 is shown in Figures 3.21 and 3.22, and the end of Pier No. 2 is shown in Figures 3.23 and 3.24. Similar quay wall damage occurred on the west side of Tsukiji-cho, just north of the land-bridge to Nakanoshima, as shown in Figure 3.25.

Karumojima-cho. Karumojima-cho is an island located about 4 km west of Port Island (Figure 3.1). Quay walls along both sides of the channel on the north side of Karumojima-cho were extensively damaged by liquefaction-induced lateral deformations. Deformations were often sufficient to drop the walls and apron slabs below water level, as shown in Figures 3.26 and 3.27. Associated damage also occurred to structures located along the channel, such as the crane shown in Figure 3.26. Damage to a tank farm located near the northwest corner of Karumojima-cho is described in Section 3.5.

Of particular interest was the observed range of quay wall performance along the channel to the west of Karumojima-cho, which corresponds to the channelized mouths of the Karumo and Minato Rivers. The quay walls extending north and east from the southwest corner of Karumojima-cho experienced relatively small amounts of deformation. Differential lateral displacements between individual quay wall blocks were generally less than about 10 cm in this area. These sections of the quay walls were protected by buttresses of reinforced concrete rip-rap, as shown in Figure 3.28. Across the channel to the west is Minami-Komaecho, which is adjacent to the Port of Nagata. The quay walls on the southern side of Minami-Komaecho (Figure 3.29, looking west from the southeast corner), were also buttressed by reinforced concrete rip-rap and experienced differential displacements between individual quay wall blocks that were generally less than about 10 to 15 cm. The quay walls on the eastern side of Minami-Komaecho (and facing Karumojima-cho), shown in Figure 3.30 (looking north from the southeast corner), were not buttressed by rip-rap and suffered both vertical and lateral displacements of 1 to 2 m. Ground cracking and sand boils were observed in the area behind these quay walls. This performance

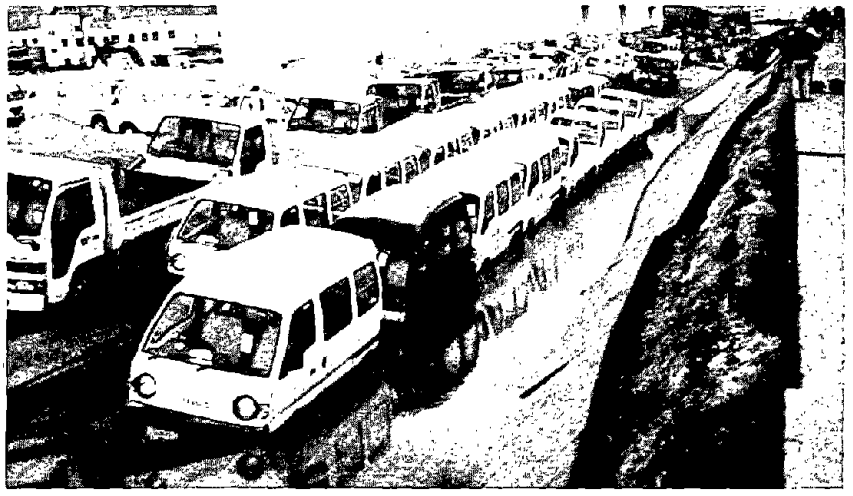

Figure 3.19: Vans and trucks ready for shipment before earthquake. Lateral spreading caused 1.5 m-2 m drop of paved surface and local flooding.

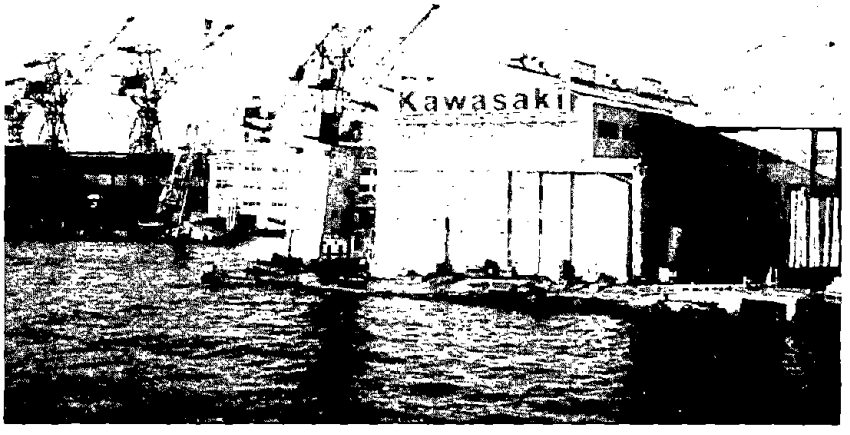

Figure 3.20: Quay walls around a large Kawasaki warehouse displaced laterally and vertically enough to drop apron slabs below the water level and tilt large cranes.

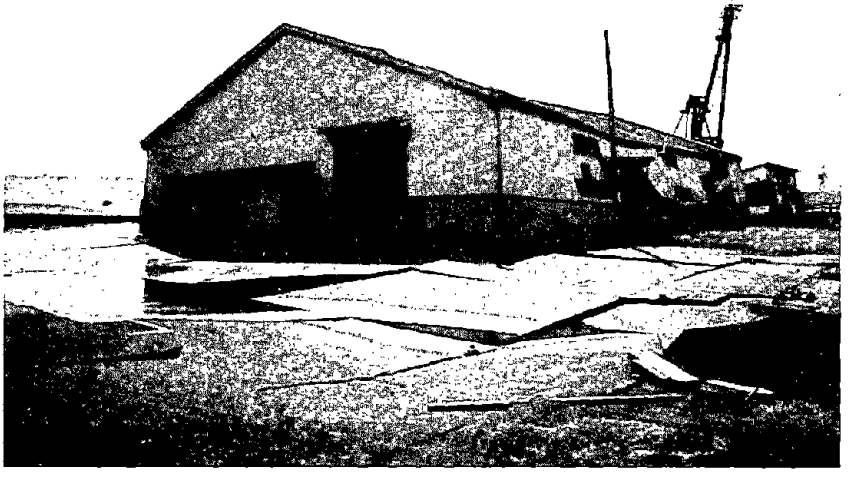

Figure 3.21: Damage to the end of Hyogo Pier No. 1

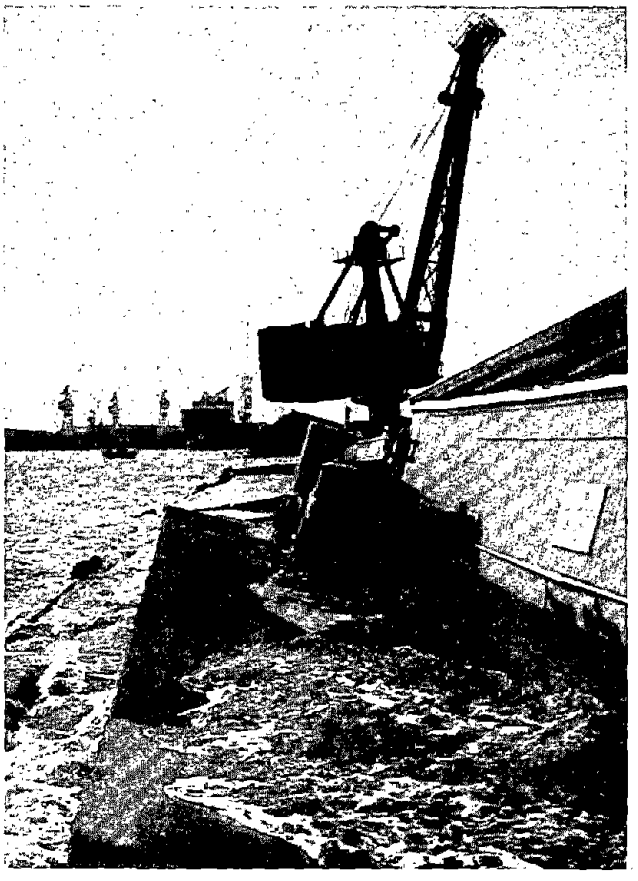

Figure 3.22: Damage to the end of Hyogo Pier No. 2.

Figure 3.23: Damage to the end of Hyogo Pier No. 2.

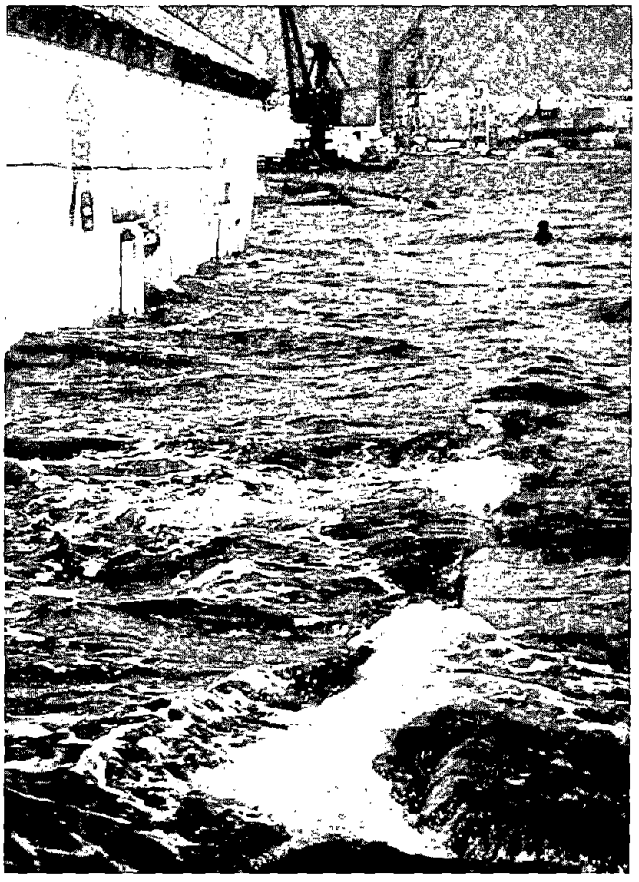

Figure 3.24: Damage to the end of Hyogo Pier No. 2.

Figure 3.25: Damaged quay wall on west side of Tsukiji-cho.

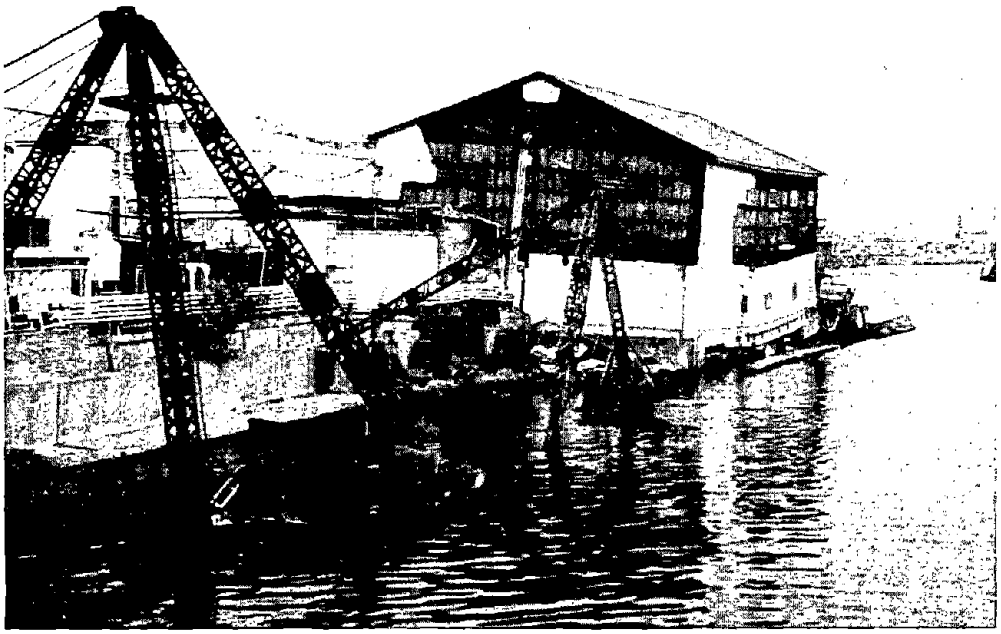

Figure 3.26: Channel on north side of Karumojima-cho (looking east).

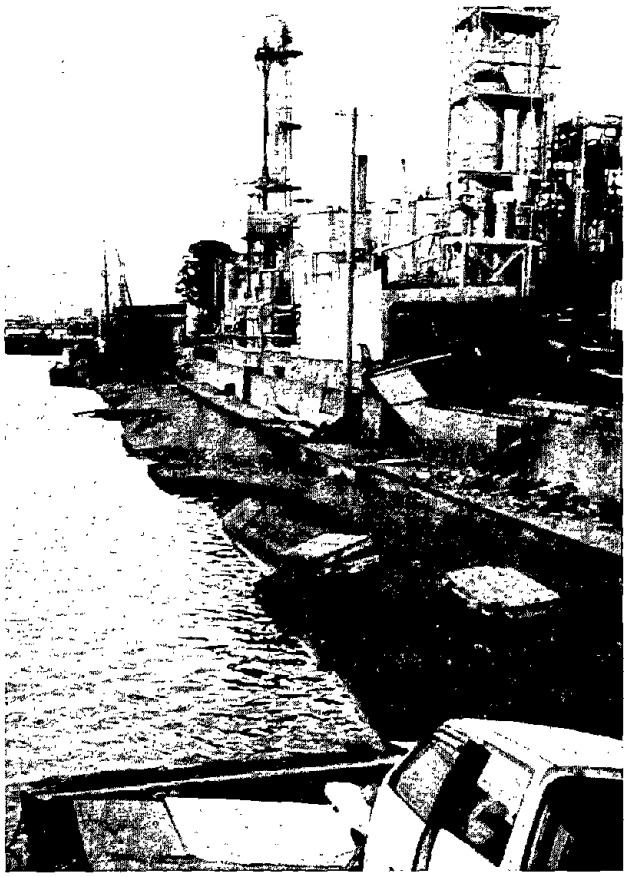

Figure 3.27: Channel on north side of Karumojima-cho (looking west).

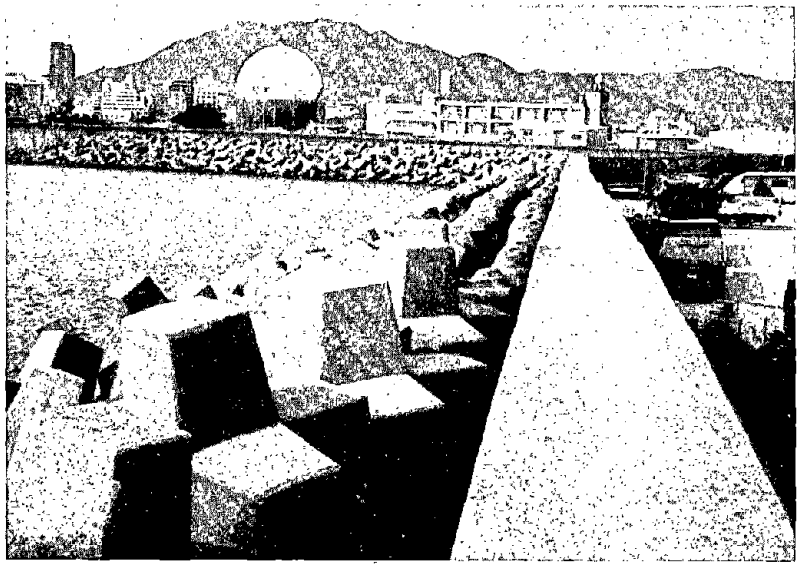

Figure 3.28: Dolos buttressed quay wall along west side of Karumojima-cho.

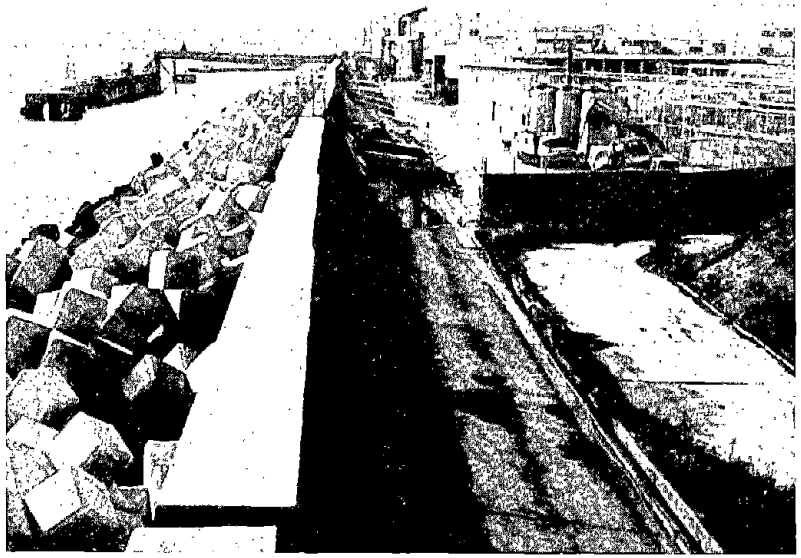

Figure 3.29: Dolos buttressed quay wall along south side of Minami Komaecho.

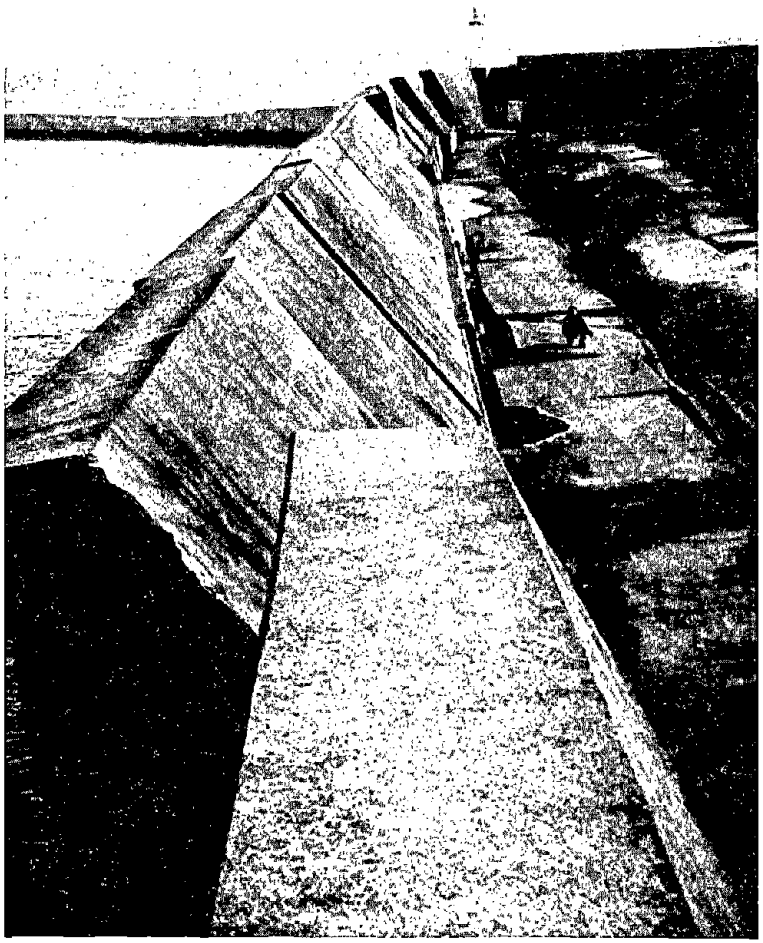

Figure 3.30: Quay wall along east side of Minami-Komaecho.

indicates that buttressing with reinforced concrete rip-rap had a beneficial restraining effect on wall movements at this location. The relatively good performance of buttressed quay walls was in sharp contrast to the large deformations of the non-buttressed quay wall. This difference in behavior warrants additional study. Similar beneficial buttressing was noted at Piers A, B, and C, at Maya-Futo (described below), except that in these instances the buttressing effect was through a pile-supported relieving platform.

Onohama-cho. Onohama-cho is located north of Port Island (Figure 3.1). The quay walls at the south end of Shinko Pier No. 5 (the largest southward-extending pier) were severely deformed, dropping the foundation for a crane and much of the surrounding apron slabs below the water level. An aerial view of this damage is shown in Figure 3.31. The channel to the north of Onohama-cho was ringed with displaced quay walls and associated damage.

East Bank of the Maya-ohashi Bridge (Harbor Expressway). The Maya-ohashi bridge on the Harbor Expressway spans a channel between Onohama-cho and Maya-Futo north of Port Island. The eastern end of this bridge is elevated above a spit of land extending off Maya-Futo. Severe lateral spreading and differential settlements occurred on both the north and south sides of this spit beneath the Maya-ohashi bridge. On the north side of this spit, the outward displacement of a quay wall created a large graben and dropped a large truck halfway into the water (Figure 3.32). Differential settlements of roughly 1 m occurred around the piers of the elevated highway in the middle of this spit, as illustrated in Figures 3.33 and 3.34. These photographs also show the severe damage to the reinforced concrete bridge piers.

Maya-Futo. Maya-Futo is located to the north of Port Island, east of Onohama-cho (Figure 3.1). The quay walls for the four piers extending southward from the mainland were designed with strong pile foundations to resist seismic loading. An aerial view of the western-most pier (Figure 3.35) shows extensive cracking in the asphalt pavement and sand ejected by liquefaction across the entire pier. Quay walls at the southeast corner of this western-most pier were the most significantly deformed, with large gaps between quay wall blocks. Elsewhere, however, the quay walls experienced relatively little deformation.

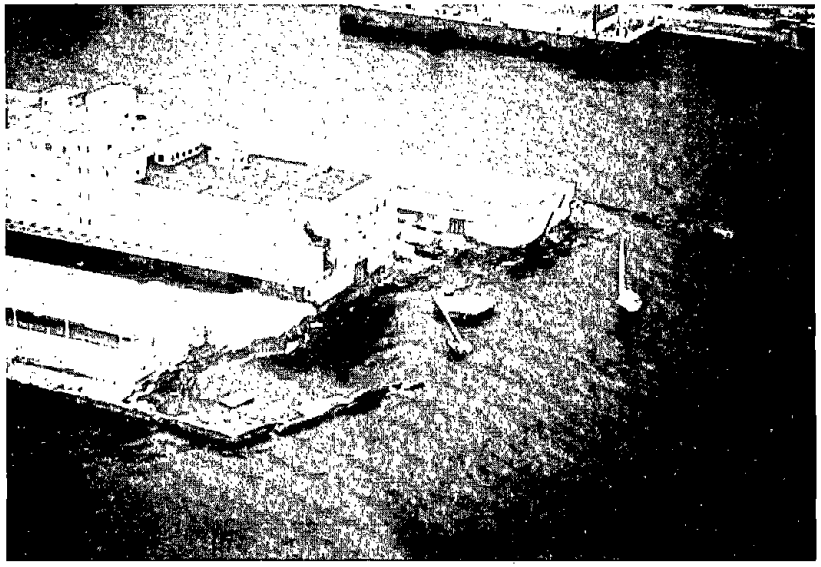

Figure 3.31: Pier No. 5 on Onohama-cho.

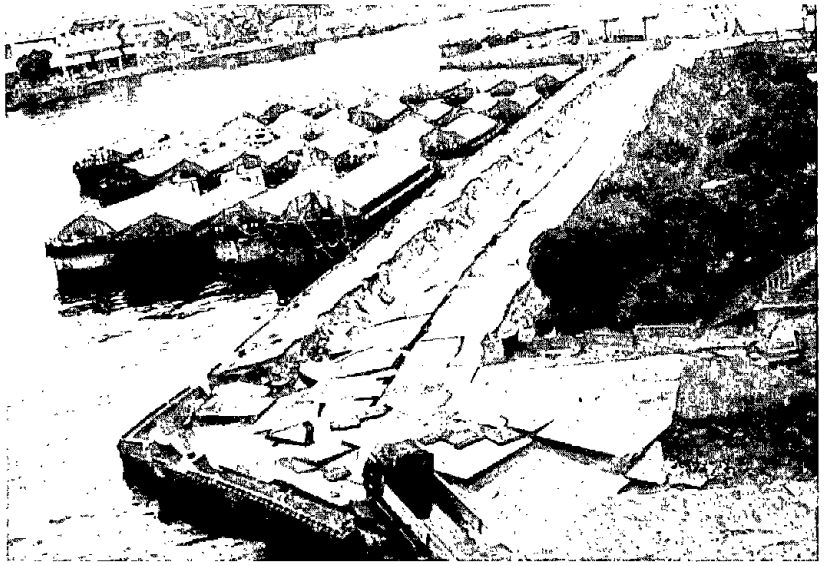

Figure 3.32: East bank of Maya-ohashi bridge: north side.

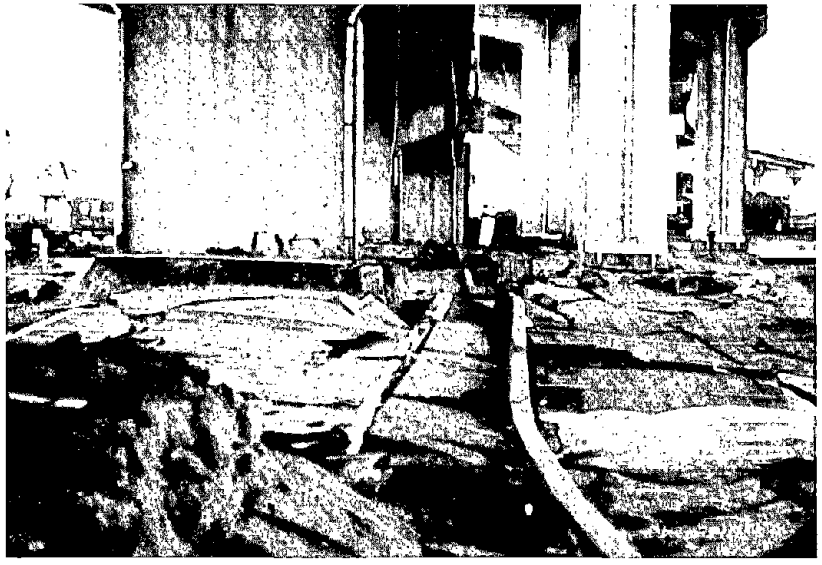

Figure 3.33: East bank of Maya-ohashi bridge: beneath elevated roadway.

Figure 3.34: East bank of Maya-ohashi bridge: south side.

One of the piers at Maya-Futo was rebuilt in the late 1980s. The reconstruction was in three sections: A, B, and C in order from the seaward end of the pier to the landward end. These sections were designed to a nominal 0.25 g horizontal acceleration, which was unusually high for the port of Kobe. There was no observable damage at either sections B or C of this new pier complex and, at the time of the site visit, a container ship was tied up at section C and clearly handling cargo (Figure 3.36).

Section A is a pile-supported structure built in front of the old seawall, leaving the old wall in place. The new berth is 10 m wide. The harbor bottom is at -10.3 m. The harbor bottom was excavated and backfilled with gravel to an elevation of -13.0 m; the excavated area extended about 12 m in front of the new wall. A single row of very tightly spaced vertical piles were driven 1 m back from the front of the new wall, terminating in the harbor bottom sand at elevation -21.5 m, or slightly more than 10 m below the mudline. A distance of 3.5 m behind this row of piles another row of vertical piles was driven. These were spaced 3.0 m on center and driven to approximated elevation -19 m. A further 3.5 m behind this row, another row of vertical piles was driven, again 3.0 m on center but terminating at approximately elevation -20 m. Immediately next to each of the latter piles a batter pile was driven at an inclination so that the tips of the batter piles terminated at about an elevation of -20 m at points and very near to the tips of the second row of vertical piles. The space behind the new wall and between the piles was filled with gravel up to elevation -1.5 m. The old quay wall, its sand backfill, and the piles supporting the old relieving platform were left in place. The pavement over the old section was heavily damaged during the earthquake, but the new platform and pavement showed no distress.

Sections B and C were constructed as concrete caisson structures. Both sections have four cells. At section B, each cell is 3.25 m in width and filled with gravel. The width of the foundation slab, at the base of the caisson, is 17.4 m. The caissons are founded on a gravel backfill that was placed in a trench excavated into the harbor bottom sands. Trench depths varied from -13 m to -14 m, but the top of the gravel fill was consistently at elevation -10.3 m. Because the harbor bottom at this section is a little deeper than elevation -10.3 m, the backfill rises slightly above the sea bottom. The crest of the backfill extended some 5.5 m in front of the new wall.

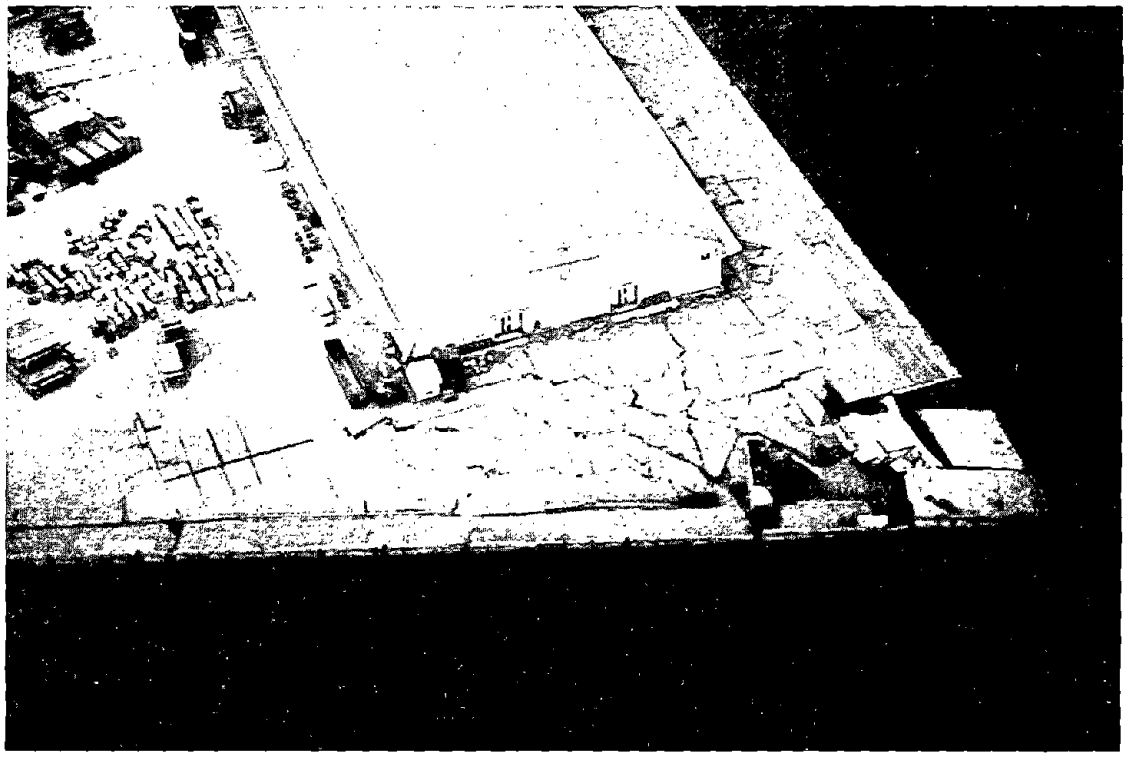

Figure 3.35: Aerial view of western piers on Maya-Futo.

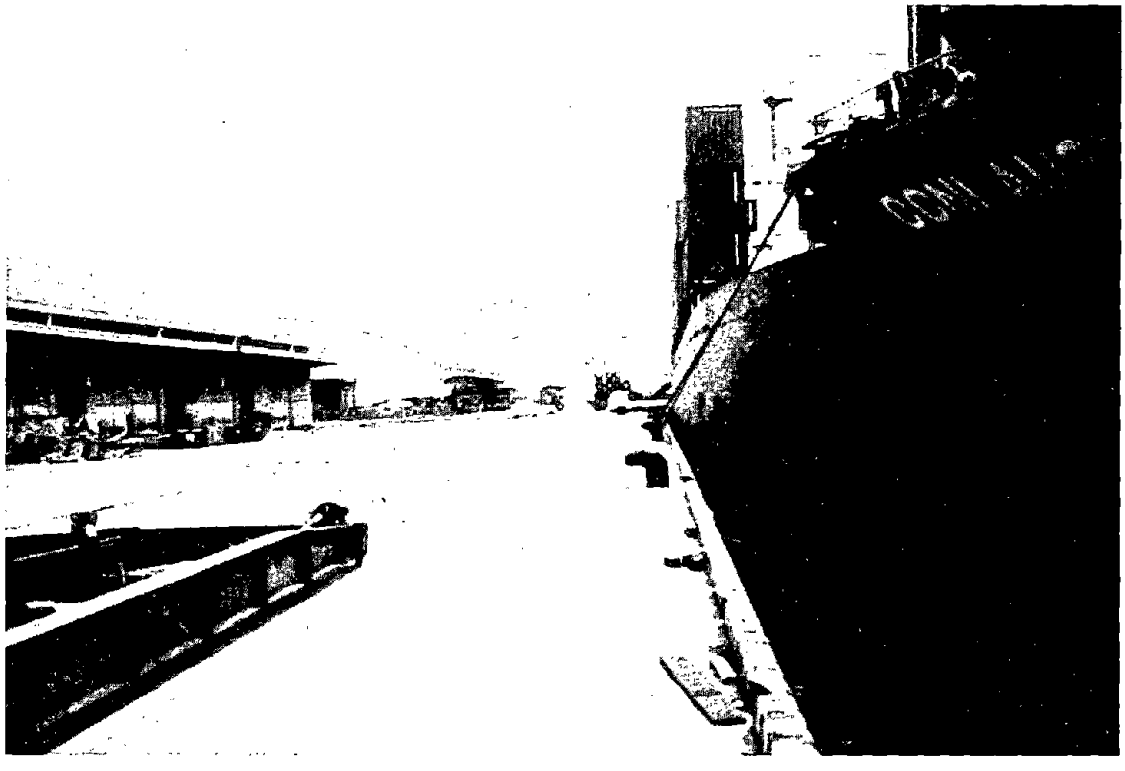

Figure 3.36: Undamaged Section C pier at Maya-Futo.

The widths of the caisson cells in Section C are 3.825 m each, and the bottom mat is 19.70 m wide. The foundation trench for this caisson was excavated to elevation of -14.3 m and backfilled with gravel to an elevation of -12.8 m, which is just below the natural harbor bottom. The backfill extended about 3 m in front of the new wall.

Higashi-Kobe Ferry Pier. The Higashi-Kobe Ferry Pier is located on the mainland to the north of Uozaki-Hamacho, as shown in Figure 3.1. This ferry pier includes four different berths with loading ramps for automobiles and passengers. The eastern two berths were inspected and, at both berths, the quay walls were displaced outward and large grabens formed that were 6 to 10 m wide and 2 to 3 m deep. The ramps for the east-end berth straddled the graben, were torn apart, and had collapsed (Figure 3.37). The columns supporting the inboard side of these ramp structures were apparently supported by groups of one to four piles. The exposed piles were approximately 30-cm-diameter steel pipe piles. Pile caps were dislodged from the supporting piles in several locations, as shown in Figures 3.38 and 3.39. The exposed piles were generally hollow, although some were partially filled with concrete. Embedment of piles into the pile cap appeared limited, with no apparent connecting steel ties, dowels, or other strengthening details.

The inboard columns of the damaged ramp structures and the graben behind the displaced quay wall east of the terminal building were apparently supported by piles, in groups of four. These piles were approximately 35-cm-diameter steel pipe piles filled with concrete with some vertical reinforcing steel connecting the pile to the cap. The damage to the pile-to-pile-cap connection in the exposed piles at this location is shown in Figure 3.40. Overall, the damage to the pile foundations of the loading ramps at the Higashi-Kobe Ferry Pier was clearly a consequence of severe lateral displacement of the surrounding ground. This poor behavior contrasts with the good performance of pile-supported structures where liquefaction led to ground settlement, but not to large lateral ground deformations. This better behavior is described following section.

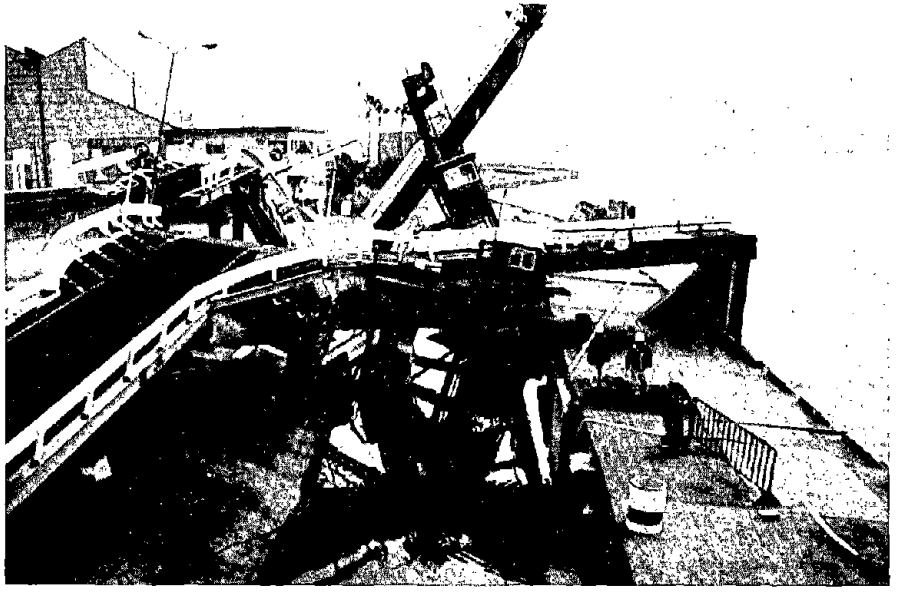

Figure 3.37: Ramp structure at Higashi-Kobe ferry pier.

Figure 3.38: Pile caps for ramp structure at Higashi-Kobe ferry pier.

Figure 3.39: Pile caps for ramp structure at Higashi-Kobe ferry pier.

3.3 Building Foundations

The interiors of the Rokko and Port islands settled as much as one meter with an average of about 0.5 m. This settlement was accompanied by pervasive eruption of large sand boils that flooded many areas and covered much of the island with sand boil deposits as thick 0.5 m (Figure 3.41). Ground settlements were relatively uniform, with most roadways and other open areas showing little evidence of differential ground deformation. Many fissures, however, opened in these areas and formed conduits through which sand boils erupted. Most of the structures on these islands, including many low- and high-rise buildings and a monorail system on Port Island, are founded on deep foundations, presumably piles and piers, that extend to competent material below the fill. These deep foundations generally performed well, remaining in place and providing uninterrupted support for the overlying structures. In nearly all instances, the ground subsided around the buildings, with the foundations remaining at the constructed elevation and providing a reference for estimating ground settlement (Figure 3.42). A common consequence of settlement was the protrusion of pile-supported structures above ground surface. For example, the ground around piers supporting the monorail on Port Island settled as much as 0.5 m relative to the pier caps (Figure 3.43).

Many buildings on piles near the piers suffered little damage (Figure 3.44). However, inspection of foundation elements that were exposed to ground displacements beneath some buildings, revealed severe damage to piles due to lateral ground displacement. For example, Figure 3.45 shows a badly cracked pile with buckled reinforcing steel; this pile supported the corner of a low-rise building. This pile evidently was cast with nominal reinforcement and had been designed to resist vertical loads only. Another hollow concrete tube pile with nominal reinforcement under the same building fractured completely and was displaced about 20 cm (Figure 3.46).

Some imprints showing relative displacements between piles and surrounding soil were provided by ground and pile movements under an inner crane rail on Rokko Island. The imprints of the pile circumference on the displaced soil (Figures 3.47) give an accurate measure of relative displacements. At this locality, closer examination of the piles was not possible, but the piles appeared undamaged.

Figure 3.40: Damaged pile to pile-cap connection at Higashi-Kobe ferry pier.

Figure 3.41: View of sand deposits, as deep as 0.5 m, generated by eruption of sand boils and associated ground settlement. Pile of sand in center of photo was scraped up in preparation for transport from area.

Figure 3.42: Approximately 0.3 m ground settlement around ferry terminal on Port Island.

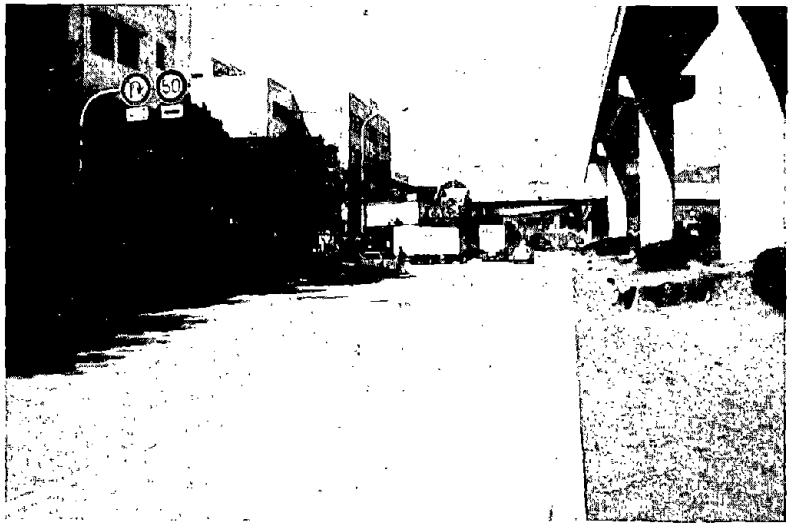

Figure 3.43: Pier supporting a section of elevated railway on Port Island rose relatively about 0.4 m as a consequence of ground settlement.

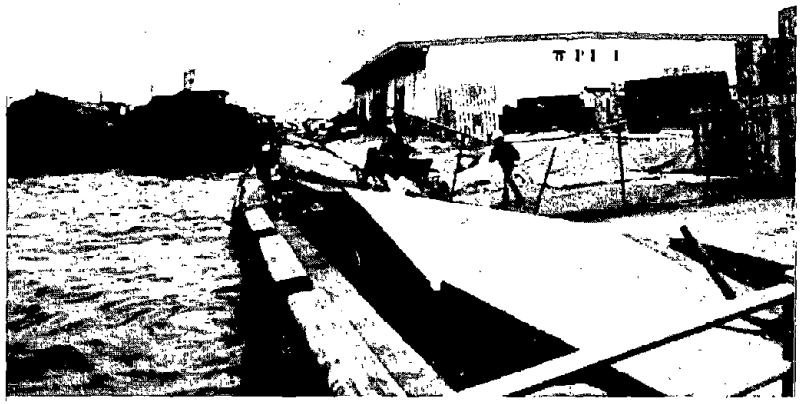

Figure 3.44: Extensive lateral spreading, ~2 m, and associated settlement exposed warehouse foundation piles on Port Island.

Figure 3.45: Cracked pile and extension of nominal vertical reinforcing. Piles not designed for lateral spreading.

Figure 3.46: Sheared and translated hollow-tube pile which had little lateral resistance. Pile had supported warehouse building shown in Figure 3.44.

Figure 3.47: Example of soil movement about pile; pile apparently stayed in place while soil oscillated back and forth leaving imprint in soil about 30 cm to left of pile. Pile supported a crane rail on Rokko Island.

Port Island Ferry Terminal. Two buildings at the newly completed ferry terminal on Port Island provide examples of generally good performance. The seaward ends of both buildings lay within a graben that formed due to liquefaction and seaward displacement of an adjacent wall (Figure 3.48). Inland from the graben, both buildings were intersected by additional open ground fissures caused by lateral spread. The larger of the two buildings, the main ferry terminal, was constructed on a pier-supported grid of perimeter walls and connected grade beams. The fill and an overlying asphalt apron were pulled away from the building in the graben area, exposing the foundation (Figure 3.49). Other than one benign horizontal crack in one pier, which may have been of pre-earthquake origin, inspection of the exposed piers revealed no damage or distress to either the piers, their connections with overlying perimeter walls, or the superstructure (Figure 3.50). The perimeter and internal foundation walls beneath the building were strongly tied together and acted as a diaphragm, effectively preventing differential horizontal movements between structural elements, including pier caps. An inspection of the interior of the building also revealed no cracks or other structural damage. In addition to the graben and lateral spread displacements, as much as 0.3 m ground settlement occurred around the perimeter of the building (Figure 3.42). In spite of these relatively severe liquefaction effects, the building and its deep foundation were apparently undamaged and the building was in operation within a few days after the earthquake, albeit without gas for heating or water for drinking and sanitation.

The second and smaller building at the ferry port was either constructed on shallow foundations or a deep foundation that did not fully penetrate the liquefiable fill. This building remained intact and generally undamaged, but tilted about 2.5 degrees downward toward the graben. The back part of the building subsided into the graben, but the structure rotated as a block, with little or no structural damage, at least as revealed by a brief inspection of the first floor. There were a few hairline fractures in the foundation a few meters inland from the edge of the graben, but these cracks did not continue upward into the superstructure. The building was also intersected by several open fissures, indicative of lateral spreading toward the graben, without fracture of the foundation.

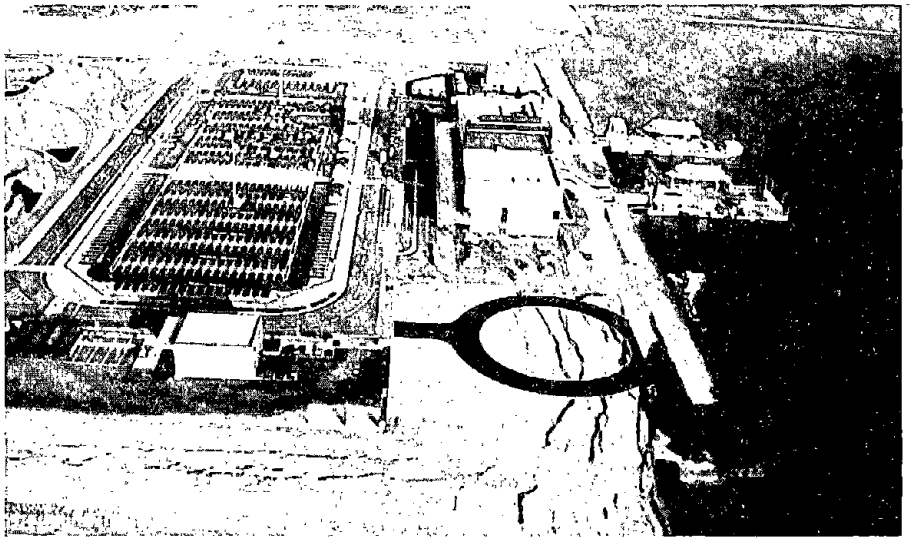

Figure 3.48: Air view of ferry terminal buildings on Port Island. Backs of buildings are in graben area. Lateral spread fissures, dark lines on top of photo, pass beneath buildings. View looking southward.

Figure 3.49: Lateral spread and graben exposed foundation walls and supporting shafts beneath the larger ferry terminal building (see Figure 3.48).

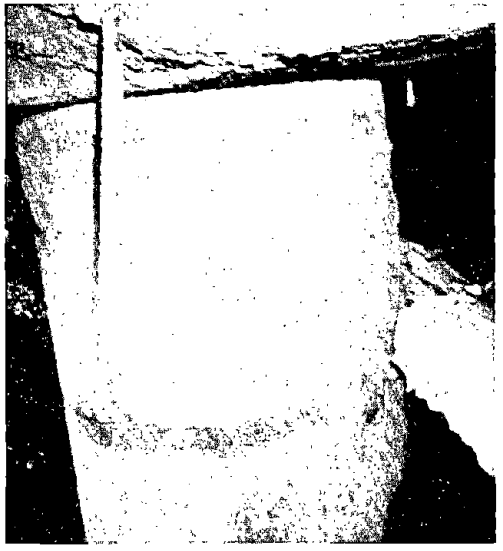

Figure 3.50: Shaft (0.5 m diameter) beneath larger ferry building was undamaged by liquefaction induced ground settlement and lateral spread.

Harbor Land Ferry Terminal. An example of poor performance in areas of lateral spreading is provided by the terminal building for the Harbor Land Ferry, located on the Kobe waterfront northwest of Port Island (Figure 3.1). Differential settlements of roughly 0.5 m occurred between the surrounding ground and the terminal building (which appears to be pile-supported). On the north side of the terminal building, the ground spread toward the waterfront which was about 10 m from the building (Figure 3.51). As a consequence, a column near the northeast corner was displaced laterally 0.5 m to 1 m, enough to tear the bolts from the first floor cross-beam connection and leave the column tilting outward at the base (Figure 3.52).

Kobe and adjacent communities. Many low-rise buildings in the Kobe area, built on reinforced-concrete shallow footings, performed well during the earthquake. These buildings were primarily 2-story houses and small commercial or industrial buildings. For example, liquefaction within or underneath a relatively recent fill in Ashiya caused the eruption of many large sand boils and the opening of many fissures (Figure 3.53). Although a few houses tilted slightly, none were seriously damaged as seen in Figures 3.2 and 3.53. The foundations consisted of reinforced concrete perimeter footings with inter-tied crossing grade beams; these foundations acted as diaphragms, preventing differential movements between foundation elements. An example of this type of foundation under construction is shown in Figure 3.54. The foundation consists of a well reinforced perimeter wall footing with interior grade-beam footings that also reinforced and tied into the perimeter walls. This type of foundation also performed well in similarly liquefiable areas during the 1993 Hokkaido Nansei Oki earthquake (Youd et al., 1995).

3.4 Bridges

Although many elevated highway and railway bridge structures collapsed or were severely damaged during the earthquake, nearly all of this destruction was due to structural rather than foundation failure. Members of the investigation team inspected bases of bridge piers in most areas where the most severe bridge damage occurred; little evidence was observed of penetration or tilting of foundation elements, except for several tilted piers in areas of lateral spreading.

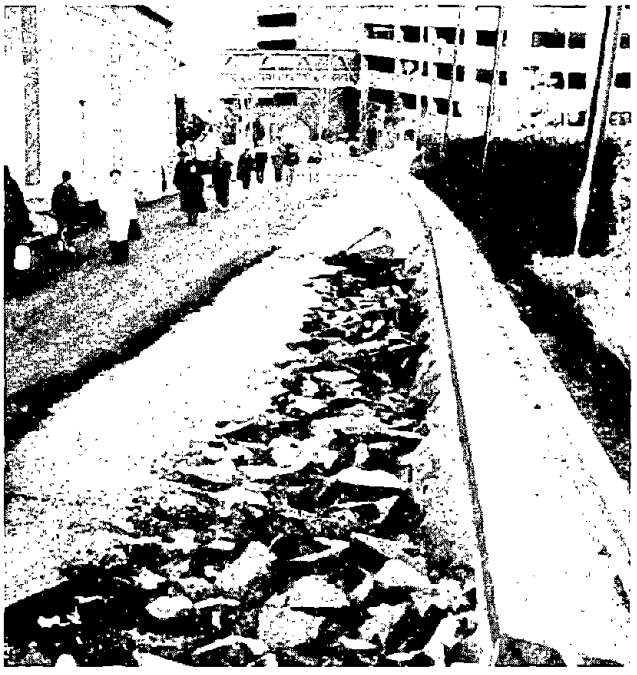

Figure 3.51: Lateral spreading on north side of Harborland ferry terminal.

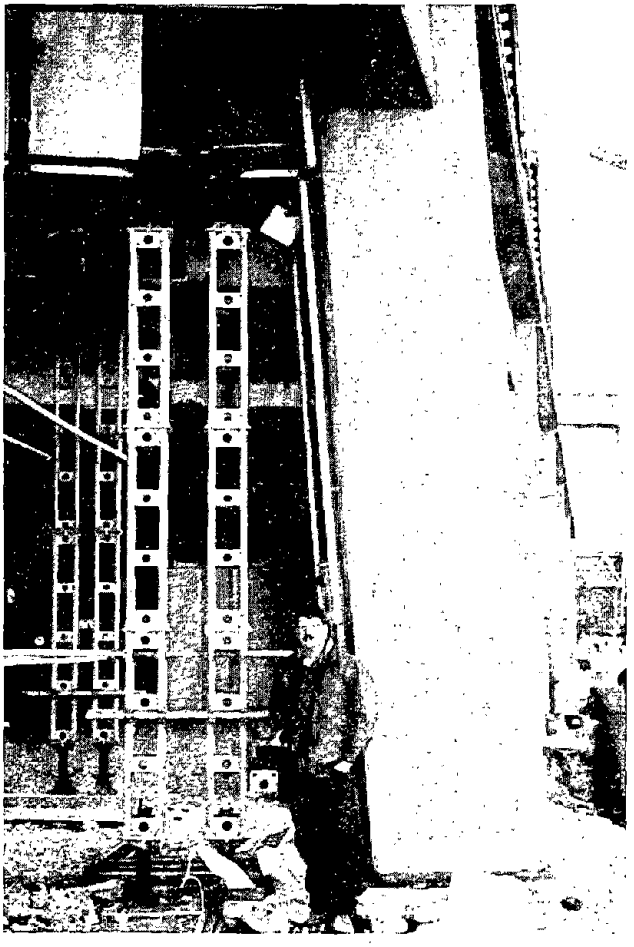

Figure 3.52: Damaged column-beam connection on north side of Harborland ferry terminal.

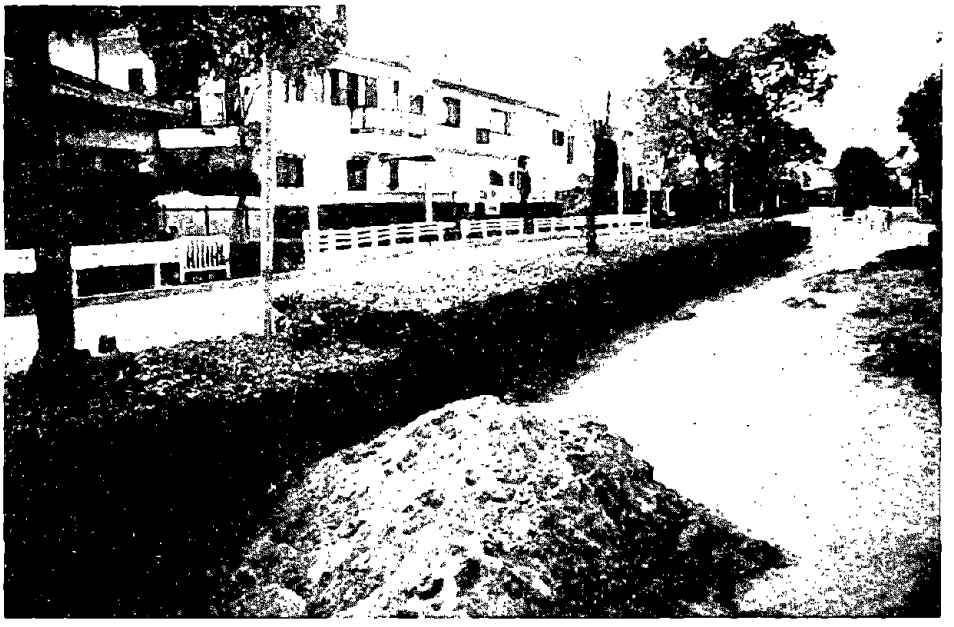

Figure 3.53: Modern Japanese houses in Ashiya constructed with wood studs and plywood sheeting similar to many U.S. single-unit houses. Liquefaction and ground oscillation occurred beneath area. Piles of sand in roadway are from residents clearing sand boil deposits from their gardens. The only damage noted in this area was slight tilting of a few houses.

Figure 3.54: Foundation under construction for house in Kobe area. Note that perimeter and interior wall footings are well reinforced and tied together. Foundations of this type allowed houses in areas affected by liquefaction to survive the earthquake with no damage except for slight tilting of a few units.

On the Kobe mainland, most of the piers supporting damaged highway and railway bridges were examined. Most of the foundation elements were hidden from direct view by overlying soils and pavements, but the bases of piers extending upward out of the soil were nearly all plumb and undamaged. Above these lower segments, however, structural damage was pervasive and commonly severe. For example, Figure 3.55 shows a spalled bridge pier supporting an elevated highway section. The fissures in the foreground are evidence of ground deformation caused by liquefaction and ground oscillation. In spite of the evident occurrence of liquefaction around the pier, no penetration or tilting of the pier was detected.

For some new bridges, especially those with tall piers, ground conditions were an important factor leading to bridge damage. Liquefaction apparently reduced resistance to lateral forces on foundation piles, while lateral spreading imposed increased lateral loads on these same elements. As a consequence, several bridge foundations shifted laterally which caused lateral displacement or tilting of the supported bridge piers. In a few instances, pier displacements were large enough to dislodge bridge girders, causing the girders and deck to fall to the ground. A example of this type of failure is shown in Figure 3.56, where a bridge pier tilted and shifted sufficiently to allow one end of the bridge deck to slip off its bridge seat and fall to the ground. That bridge formed part of a causeway from the mainland to Rokko Island.

Liquefaction and lateral spreading may have also played a part in the collapse of a section of the Nishinomiya Bridge (Figure 3.57). The entire fill beneath the approach to the failed bridge was disturbed by liquefaction and lateral spreading (Figure 3.58). The lateral ground displacements may have displaced the bridge pier leading to the collapse.

The damage to bridges with tall columns in areas of liquefaction and lateral ground displacement suggest that more attention should be devoted to making reliable estimates of displacements of bridge columns during earthquakes. Such an analysis should realistically model the response of column and the pile foundation.

Figure 3.55: Major elevated highway structure in Kobe that suffered considerable spalling of concrete and distress of reinforcing steel in single column support. No evidence of foundation penetration or tilting was detected, even though fissures in foreground and nearby sand boils indicate liquefaction and ground oscillation were pervasive beneath bridge.

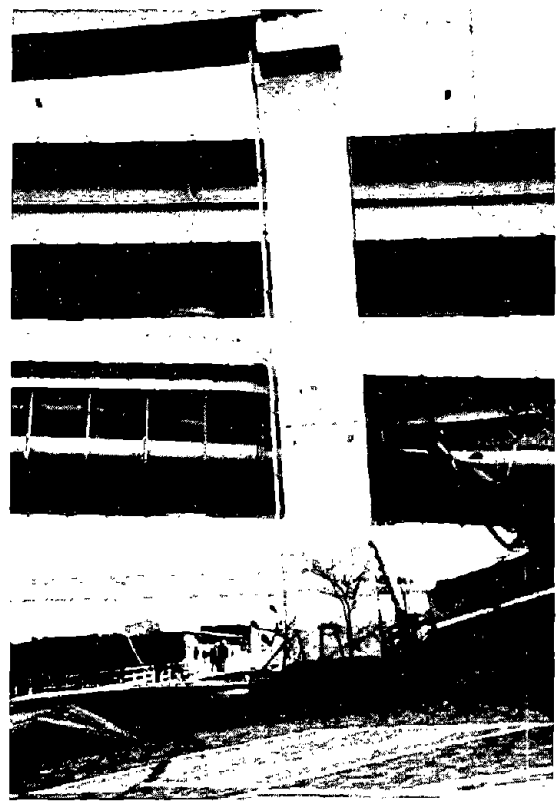

Figure 3.56: Tilting of support on Rokko Island causeway (~40 cm at top) led to drop of girder.

3.5 Tank Foundations

General observations. There are numerous tank farms in the area most severely affected by the earthquake. Some of the tank farms are associated with the port facilities, while others provide storage for refineries, fossil fuel power plants, and chemical manufacturing facilities. Most of the tanks surveyed from the air appeared to have performed well, and there were no reports of widespread damage to tanks even within port areas disturbed by severe liquefaction effects. The generally good performance of tanks may be due to the apparent practice of placing tanks on pile foundations. However, there were a few exceptions to the generally good performance; these few instances of poor performance may have been due to use of mat foundations in areas where liquefaction occurred. The following sections describe observations noted at selected tank farms visited by team members during this reconnaissance.

Higashinada Power Station Fuel Tank. The Higashinada Power Station is owned and operated by the Kansai Electric Power Company, Inc., and is located on the southwest corner of a man-made island, Uozaki-Hamacho, near the north side of Rokko Island (Figure 3.1). Figure 3.59 provides an aerial view of the facility. Estimated peak ground accelerations in this area were 0.5 g to 0.7 g. As with many of the man-made harbor fills in the Kobe area, the island experienced extensive liquefaction. Figure 3.60 shows the south quay wall of the island which displaced laterally toward the water. This lateral movement was associated with two major fissures bracketing a 5-meter-wide tension zone located approximately 10 to 15 meters behind the south quay wall. There was also movement and cracking along the quay walls on the west side of the island. Numerous sand boils erupted within the power station complex, fissures formed, pavements fractured and separated, and the ground settled differentially. A group of tanks used to store fuel and water for the power station was constructed approximately 50 to 60 meters inland from the quay walls. An excavation had been made around the perimeter of one of the tanks to expose the piles for inspection of damage (Figure 3.61). The tank, reportedly supported by 33 piles extending to depths of approximately 33 meters, was undamaged. The piles consist of reinforced-concrete sections with diameters of approximately 35 centimeters. Twelve of the 33 piles were arranged in an outer ring near the perimeter of the tank (Figure 3.62); the rest are situated closer to its center. Beneath the

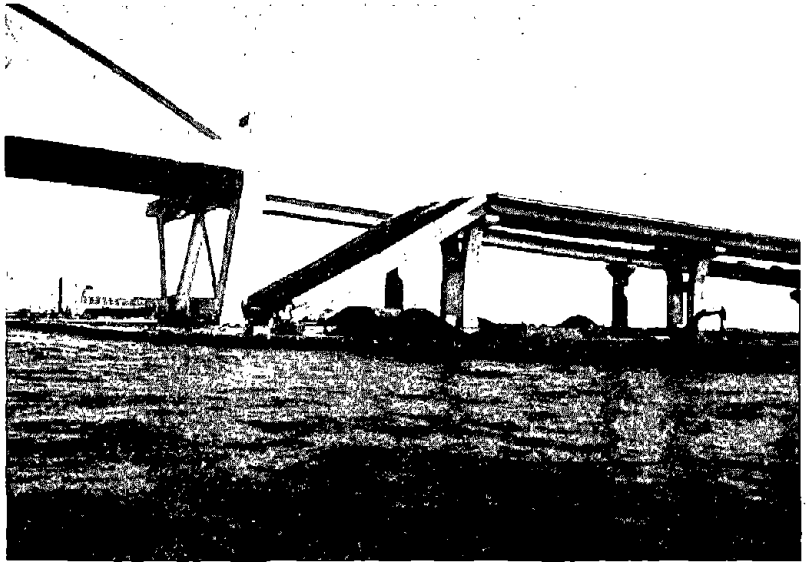

Figure 3.57: Collapse of a span of the Nishihomiya bridge on the new Harbor Expressway.

Figure 3.58: Note liquefaction induced lateral spread fissures and sporadic sand boils near pier of Nishihomiya bridge which previously supported collapsed freeway section.

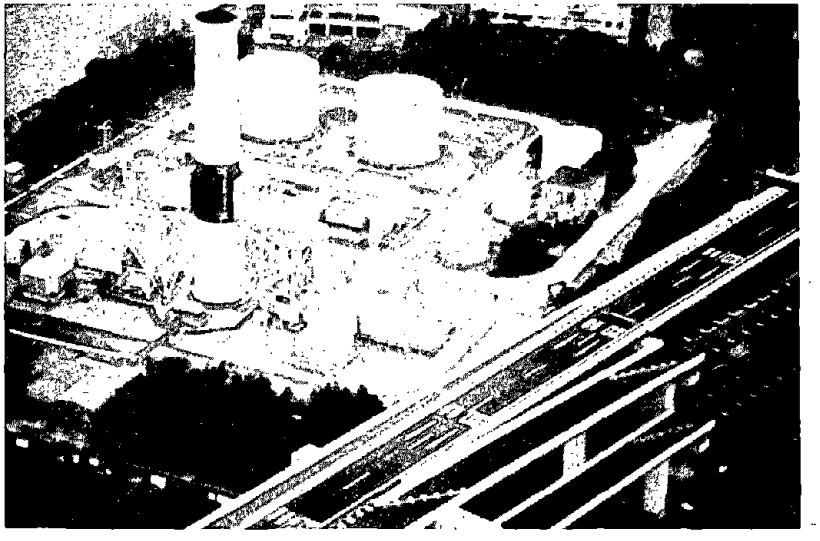

Figure 3.59: Aerial view of Higashinada power station

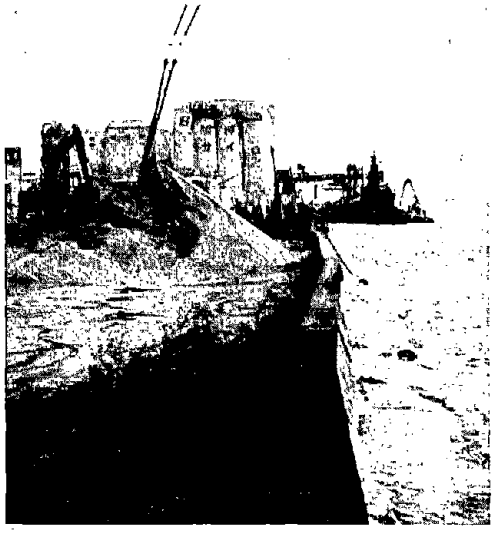

Figure 3.60: South quay wall near Higashinada Power Station.

tank, the ground had liquefied and settled 28 centimeters. Lateral spreading near the tank seemed to have been insignificant. From within the perimeter excavation, daylight was visible between the tops of the piles (Figure 3.63).

Damage to the exposed portions of the piles appeared to be relatively light. Several piles contained hairline cracks in the upper meter or two (Figures 3.64). At least one pile contained intersecting cracks that could allow large of concrete to spall out. The most seriously damaged piles were located along the northwestern part of the perimeter. The piles appeared repairable and thus were not classified as having failed.

Hanshin Silos. The Hanshin silos are located a few hundred meters to the east of the Higashinada Power Station on Uozaki-Hamacho (Figure 3.1). Some of these silos are visible in the background of Figure 3.60. Several silos, at the western end of a complex of attached silos, sustained significant structural damage. As shown in Figure 3.65, the tops of the western silos are irregular due to differential settlement, and parts of the silo skins appear to have buckled and sheared. One of the silos collapsed and damaged an adjacent wharf and crane structures. This site was not visited on the ground during this reconnaissance and no information on foundation type or cause of failure was obtained. However, due to the widespread liquefaction on the island, ground failure must be considered a potential contributor to the observed structural failure. A point worth investigating is why the majority of the silos appeared to perform well whereas those on the western end suffered distress and failure.

Karumojima Tanks. Field reconnaissance in the western Kobe area of Karumojima near the Port of Nagata identified several small tank farms. Most of this area consists of man-made fills situated around the channelized mouths of the Karumo and Minato Rivers. This area was estimated to have sustained peak ground accelerations of between 0.5 and 0.7g. Extensive liquefaction was observed in this area in the form of sand boils, differential settlements, and quay wall distress. Figure 3.66 shows a view along one of the channels affected by slumping of quay walls. In the background of the photograph are several tanks which tilted in one or more directions. The ground around these tanks contained several large fissures, presumably associated with the lateral spread, and sand boils had erupted through many of the fissures (Figures 3.67).

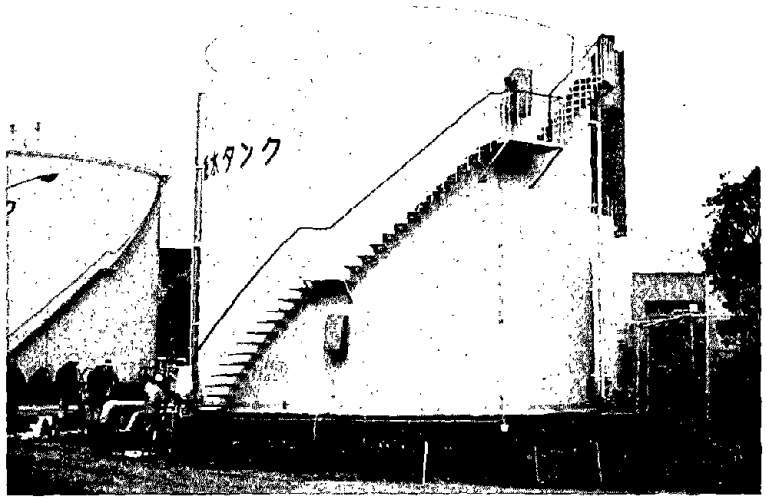

Figure 3.61: Damaged pile-supported tank at the Higashinada PowerStation.

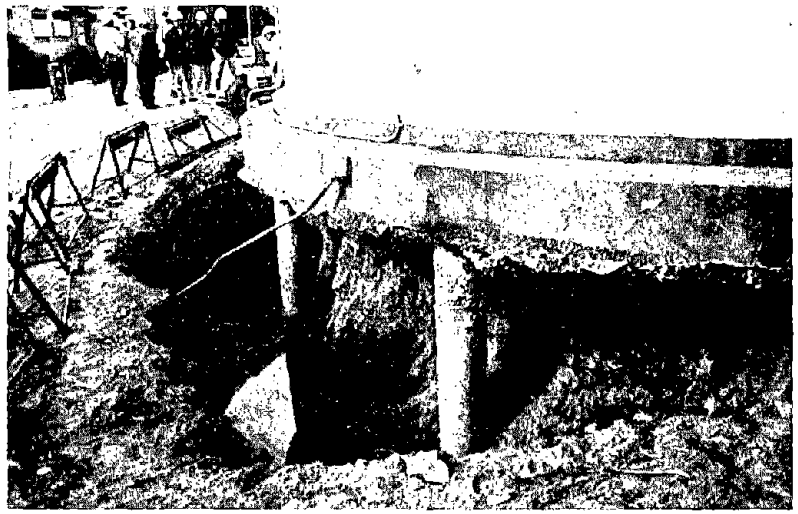

Figure 3.62: Close up view of the exposed perimeter piles supporting the tank shown in Figure 3.61.

Figure 3.63: Gap beneath the tank mat created by settlement of liquefied soil.

Figure 3.64: Excavated upper part of pile foundation beneath the tank shown in Figure 3.61.

The tilting of the smaller diameter tanks appeared to be a result of one side of the foundation mat sinking into the ground, presumably a result of liquefaction. Although there was no information available regarding foundation type and no excavation had been made at the site, the performance of the mats for the smaller tanks suggested that they were founded at shallow depth and were not supported by piles. The tilting of the large tank is thought to have occurred in a similar manner. However, the large tank had a perimeter concrete collar ring which separated from the tank as the tank settled into the ground (Figure 3.68). Although this separation led to an offset of several centimeters at the collar ring, it is not known if a structural failure of the mat was involved.

Nippon Gatx Tanks. Nippon Gatx Company, Ltd. operates a tank farm located at the Port of Nagata in the western Kobe area. Figure 3.69 is an aerial view of this tank farm. There are several dozen tanks at the facility that are used to store chemicals such as ethylene glycol, alcohol, and water. The terminal manager for the facility reported that none of the tanks were on piles and several of these tanks were observed to be tilted after the earthquake (Figure 3.70). As at the Karumojima tank farm, the cause of the distress appeared to be liquefaction of foundation soils as evidenced by several sand boils and ground fissures that developed in the area. The mats settled differentially, with one end sunken into ground and covered with ejected sand (Figures 3.71 and 3.72).

3.6 Other Observations

While most of the liquefaction damage was located in Kobe and its immediate vicinity, some recent fills failed as far away as the Osaka waterfront. The Tempoyama Park (Osakako) and the Osaka Ferry Terminal are located on a man-made island in the Port of Osaka, approximately 2 kilometers south of the mouth of the Yodo River (Figure 1.1). Peak ground accelerations in this area were estimated to have been 0.2 g to 0.3 g. Liquefaction effects were observed only within a few blocks of the Osaka Ferry Terminal. The liquefaction effects consisted of sand boils, pavement separations, differential settlements, and ground fissures generally 1 to 5 centimeters wide. The

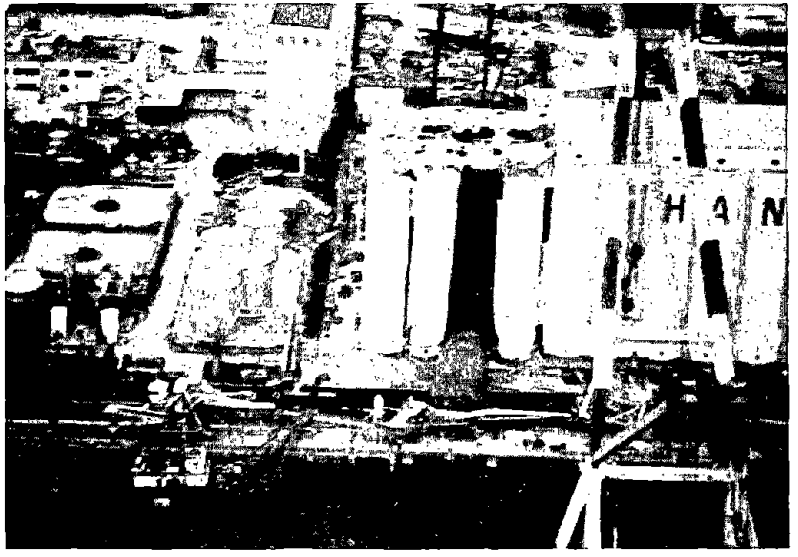

Figure 3.65: Aerial view of the Hanshin silo complex.

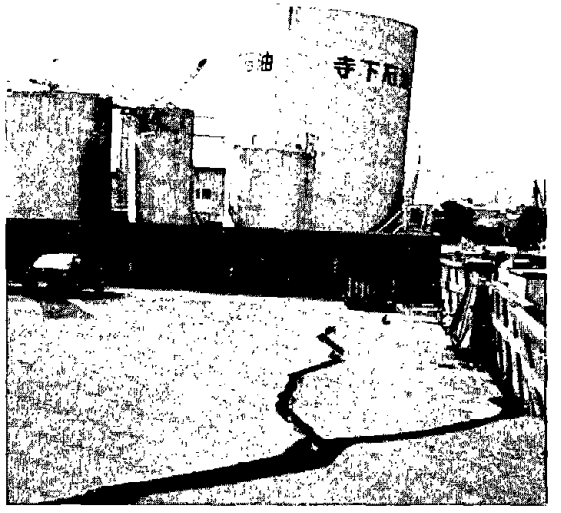

Figure 3.66: Listing tank at the Karumojima tank farm. Note the ground cracking due to lateral spreading in the foreground.

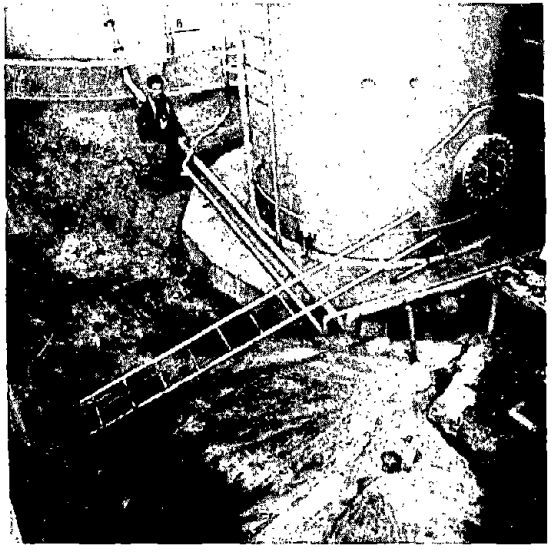

Figure 3.67: Fissures and sand boils within Karumojima tank farm.

Figure 3.68: Displaced collar ring around a large tank in the Karumojima tank farm.

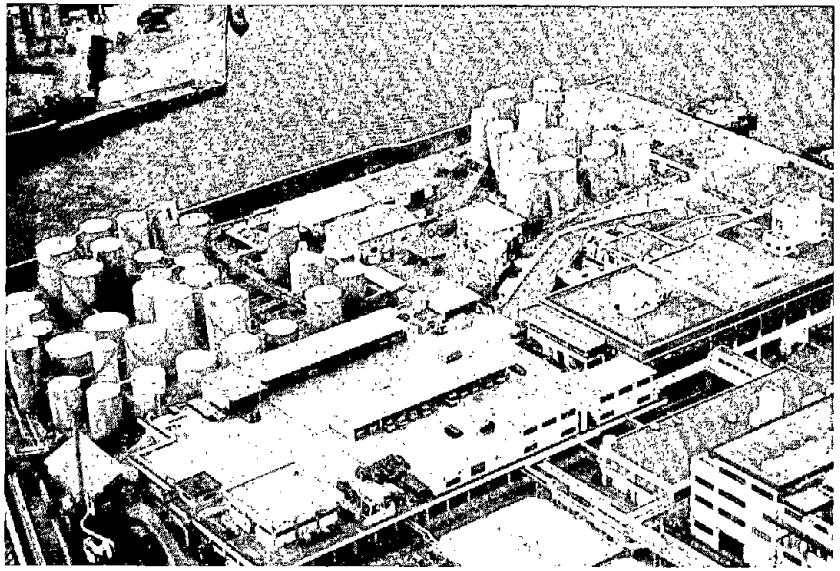

Figure 3.69: Aerial view of the Nippon Gatx tank farm.

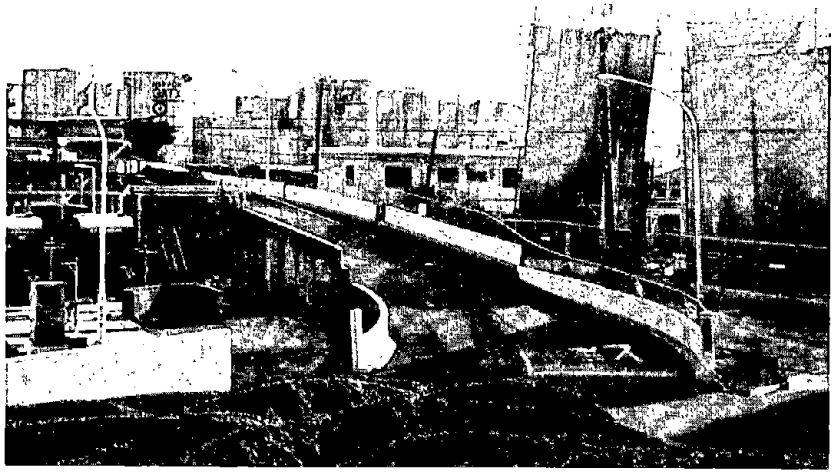

Figure 3.70: Listing tanks in the Nippon Gatx complex.

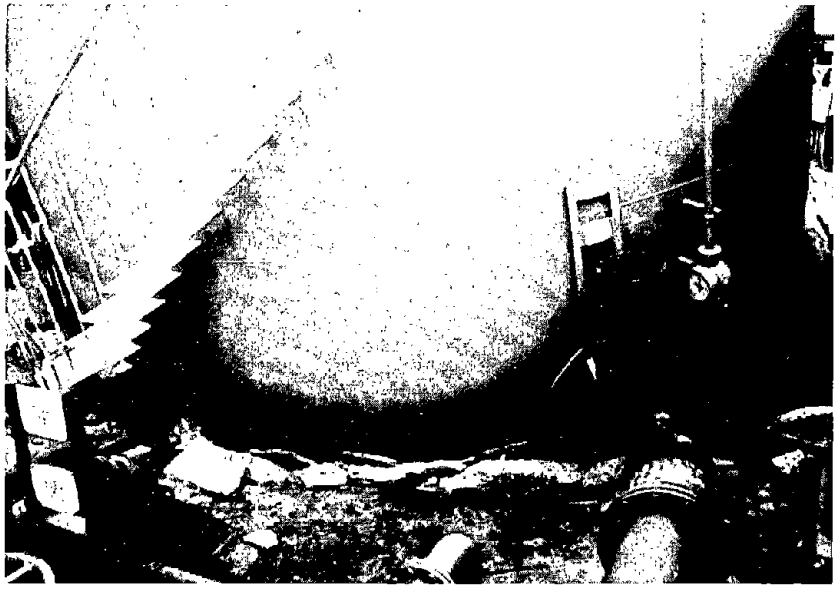

Figure 3.71: Differential settlement at the base of a water tank in the Nippon Gatx complex.

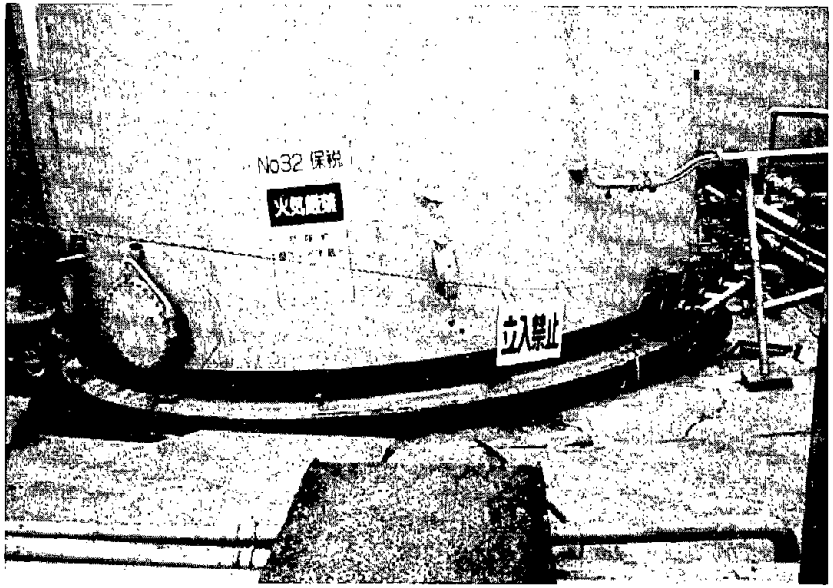

Figure 3.72: Differential settlement at the base of a chemical tank in the Nippon Gatx complex.

most severe liquefaction effects in Tempoyama Park, a hillside park immediately to the east of the ferry building. This park contains an artificial hill, approximately 10 meters high, constructed near the edge of the island. This park was beautified with trees, walkways, and picnic areas. Liquefaction of the fill beneath the man-made hill and adjacent fill caused lateral spreading in several directions, manifested by fissures and sand boils (Figures 3. 73 and Figure 3.74).

3.7 Summary

Deleterious effects of liquefaction were major contributors to the vast amount of damage inflicted by the 1995 Hyogoken-Nanbu earthquake. In particular, port facilities were severely impacted by liquefaction-induced ground displacements. These ground movements pervasively displaced quay walls seaward by an average of 2 m to 3 m and created grabens 2 m to 4 m deep landward from the walls. The damage generated from these ground disturbances effectively shut down the Port of Kobe to shipping; only 6 of about 187 shipping berths were operational after the earthquake. Most of these berths were located around the margins of Port and Rokko islands (filled islands within Osaka Bay) and along filled segments of the Kobe shoreline. Most of the fill in these areas consisted of poorly compacted decomposed granite that was excavated from borrow areas in the Rokko Mountains. This material was transported to the fill sites and loosely dumped in water locations to form the "made-ground." Compaction was generally only applied to materials placed above water level. Liquefaction occurred pervasively within underwater segments of these poorly compacted fills. Around the exteriors of islands and along the Kobe waterfront, liquefaction generated lateral displacements that devastated the port facilities as noted above. This destruction graphically illustrates the vulnerability of waterfront structures constructed on loose, saturated soils to the severe consequences of liquefaction, as well as the need to improve the ground under such important facilities to prevent these deleterious effects.

Within the interiors of the man-made islands, liquefaction led to pervasive eruption of sand boils and to rather uniform ground settlement averaging about 0.5 m. The ground settlement caused surprisingly little damage to high- and low-rise buildings, bridges, tanks and other structures supported on deep foundations. These foundations, including piles and piers, performed very well in supporting superstructures where ground settlement was the principal effect of liquefaction.

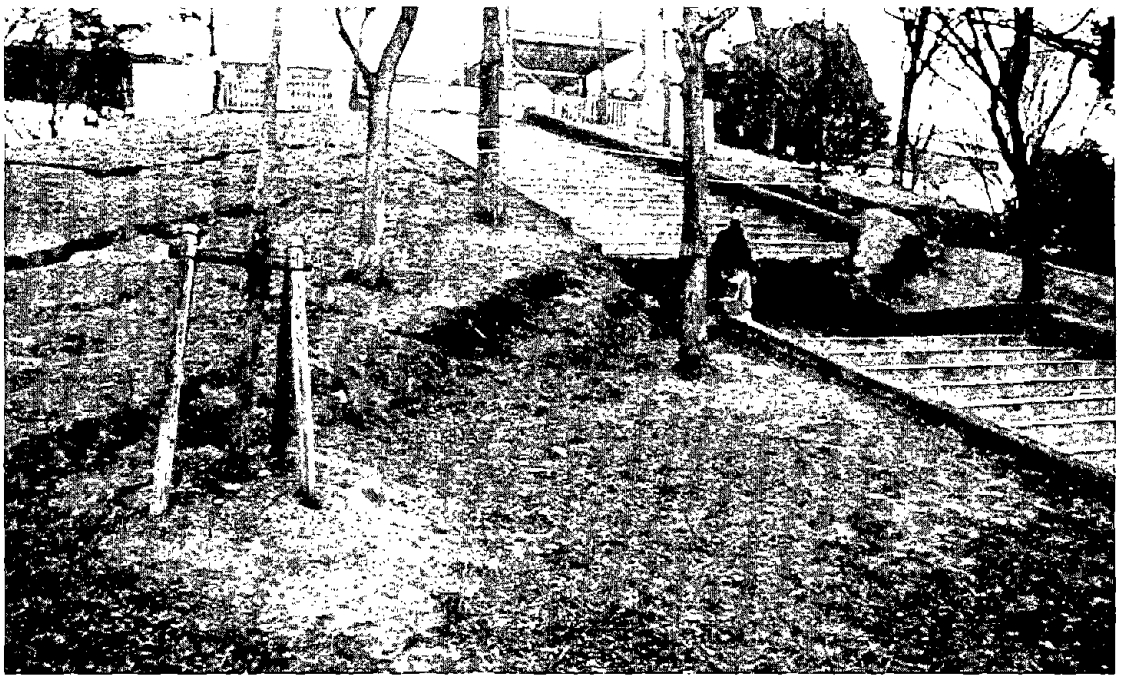

Figure 3.73: Fissure indicative of liquefaction and lateral spread in Osakako park which is located on a small artificial island near the ferry terminal at the port of Osaka.

Figure 3.74: Fissures in Osakako park indicative of liquefaction, differential ground settlement, and lateral spread.

Where liquefaction generated lateral ground displacements, such as near island edges and in other waterfront areas, foundation performance was typically poor. Lateral displacements fractured piles and displaced pile caps, causing structural distress to several bridges, a few of which collapsed. In a few instances, such as the Port Island Ferry Terminal, strong foundations withstood the lateral ground displacement with little damage to the foundation or the superstructure.

Shallow foundations consisting of a grid of interconnected perimeter-wall footings and grade beams performed well in several areas subjected to minor effects of liquefaction, such as eruption of sand boils, ground oscillation, and minor lateral spread. In these instances, the foundation behaved as a diaphragm, preventing differential ground displacements from propagating upward into the superstructure. Most of these structures were small buildings, such as houses and low-rise commercial and industrial facilities. Where foundation elements were not well tied together, differential ground displacements pulled apart overlying structures at points of weakness, such as joints and doorways.

Although hidden from view, and thus not widely examined during this reconnaissance, damage to pipelines and other buried utilities was apparently widespread in areas affected by liquefaction, both in areas of pronounced lateral ground displacement and in areas of ground settlement, ground oscillation and minor lateral spreading. The information collected in this study is insufficient to delineate the extent of damage or the performance of various types of pipe and embedment conditions. These topics, along with more quantitative evaluation of ground and structural response, provide an extraordinary opportunity to evaluate the performance of modern urban and industrial infrastructure in areas subjected to moderate to severe effects of liquefaction.

CHAPTER FOUR: PERFORMANCE OF IMPROVED GROUND SITES

Ground improvement has been used at several filled sites in the Kobe area, primarily on Port and Rokko Islands. Both islands consist of hydraulic fills overlying soft alluvial clays. Information about the setting, soil conditions and ground motions is given in Section 3.2. A typical soil profile for Port Island with relevant soil properties, as given by Nakakita and Watanabe (1981), is shown in Fig. 3.6. As the intensity of ground motions at some of the improved sites was higher than has been experienced in past earthquakes, examination of their behavior provides valuable data concerning the effectiveness of ground improvement methods for mitigation of liquefaction and ground failure.

4.1 Ground Improvement Methods

Sand drains in the young alluvial clay layer and preloading were used at a number of locations on Port and Rokko Islands for settlement control, and most of the high-rise structures, elevated rail lines, bridges, and many of the other buildings were founded on piles. In general the pile supported structures performed well. The installation of the sand drains was reported to give an increase in the SPT N-value of the sand hydraulic fill of the order of 2 to 3 blows per 30 cm. Additional densification of the hydraulic fill was undertaken only at a few locations. It is the response of this densified ground that is of particular interest here.

Most of the densification was done using either the vibro-rod method developed by Saito (1977) or the sand compaction pile method developed by Murayama (1958). Both of these methods are described by Mitchell (1981). In the vibro-rod method a vibratory pile hammer is used to penetrate the ground repeatedly by a specially designed probe. In the sand compaction pile method a casing pipe is driven to the desired depth using a vibrator at the top. A sand charge is introduced into the pipe, and the pipe is withdrawn part way while compressed air is blown into the casing to hold the sand in place. The casing is then vibrated down to compact the sand pile and enlarge its diameter. The process is repeated until the pipe reaches the ground surface. For both the vibro-rod and sand compaction pile methods the spacing between columns is ordinarily 1.5 to 3.0 m depending on the loading conditions and fines content of the soil being

treated. For construction on land a sand compaction pile diameter of 700 mm is used, and the pile diameter by the vibro-rod method is about 600 mm.

4.2 Amusement Park on Port Island

4.2.1 Location and Treatment

The Kobe Portopialand Amusement Park is located along the southern boundary of Port Island Phase I, as shown in Figure 3.4 and 3.11. The ground surface, which is about 1 m higher than the surrounding area, is typically about 3 to 6.5 m above the Mean Water Level, and thus the fill is largely submerged. Within the amusement park area the fill was treated in 1979 by the vibro-rod method over its full 19 m thickness using a 2.6 m square pattern. Post-treatment SPT blow counts typically ranged between about 20 and 30, with averages of 21 and 23 at the rod locations and between rod locations, respectively. Figure 4.1 shows typical SPT blow count data with depth corresponding to the pre-treatment (one set) and post-treatment (two sets - one at the center of a rod location and the other between rod locations) conditions. It was reported that the ground surface settled of the order of 30 to 40 cm during treatment.

4.2.2 Observations Around the Park Perimeter

A narrow parking lot is located along the south side of the park, between a retaining wall for the park to the north at an elevation about 2 to 3 m higher than the parking lot, and the original Port Island Phase I sea wall that parallels the park wall to the south. The concrete pavement slabs separated along the long axis of the parking lot and soil ejecta (predominantly sand) covered the entire parking lot, as may be seen in Figure 4.2. Water marks on the entrance kiosk showed that the parking area filled to a depth of roughly 1 m (Figure 4.3).

The east side of the park is separated from the adjacent road by a strip of unpaved, fenced-off ground. At the southern edge of the east side there is a small water supply building that is fenced on all sides. Liquefaction ejecta covered much of the enclosed area around this building, and differential settlements and ground cracking occurred around the building. At the northern end of the east side there was a large sand boil within the fenced off area. No other evidence of liquefaction was observed in the fenced-off area along the east side. The adjacent street

surface had a hummocky appearance, and on the other side of the street differential settlements of 10 to 50 cm were observed between a building and its adjacent sidewalk and fence.

The north side of the park is next to a road and elevated railway. Differential settlements of 20 to 50 cm occurred between the supporting piers for the railway and the adjacent ground surface. Sand boils were also observed in this area.

The west side of the park is next to the grassy area of a public park. Large sand boils and many ground cracks were seen in the grassy area near the amusement park (Figure 4.4). A differential settlement of roughly 30 cm was observed between a ramp to the elevated railway and the surrounding ground near the northwest corner of the amusement park (Figure 4.5).

4.2.3 Observations Inside the Amusement Park

The amusement park contains a large number of buildings and elevated supports for rides. All structures inside the park reportedly were constructed on shallow foundations. The large Ferris wheel, perhaps the largest structure in the park, was reported to be founded on spread footings tied together by grade beams. At the time of the reconnaissance, no specific survey data about the park was yet available.

Clear evidence of liquefaction inside the amusement park was limited to a small area near the southwest corner, where ground cracking and sand boils were observed as shown in Figure 4.6. Additional cracking and ejecta were observed along most of the southern boundary of the park (Figure 4.7), although some of this may have been the result of a broken water line. Over the remainder of the park the only apparent damage consisted of occasional cracks and separations in pavement materials that were generally less than 5 mm wide, but up to 25 mm wide in some spots, with Figure 4.8 being an example. Cracks and separations generally were smallest near the northern boundary and became progressively larger toward the south. Many large areas in the park had no visible cracks, separations, or differential settlements, as illustrated in Figure 4.9.

No differential settlements were observed at any of the large footings for the Ferris wheel or roller coaster. The roller coaster was operated during the field reconnaissance and appeared to function satisfactorily. No signs of structural distress were seen in any of the park facilities, and all gas lines were reported to be intact.

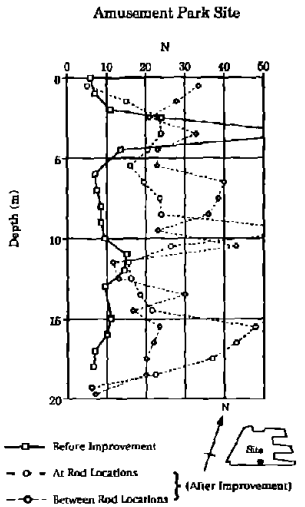

Figure 4.1: Pre- and post-treatment standard penetration resistance values at the Portopialand Amusement Park site on Port Island (after Fudo Construction Co., Ltd., 1995).

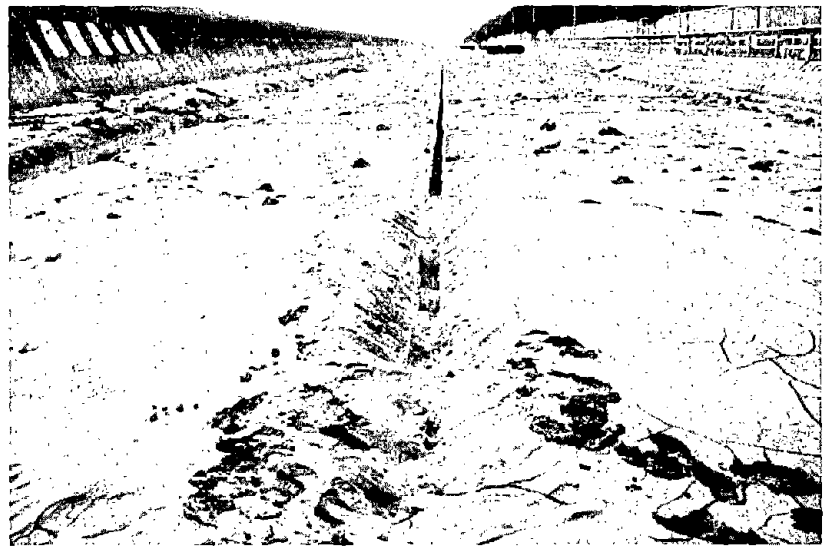

Figure 4.2: Parking lot between the Phase I seawall on the south and the Portopialand Amusement Park on the north.

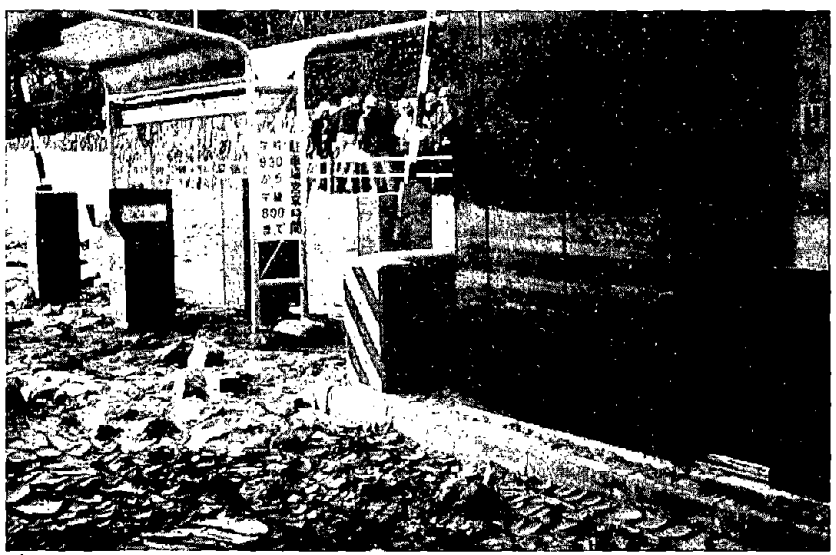

Figure 4.3: Parking lot kiosk showing high water level caused by sand liquefaction.

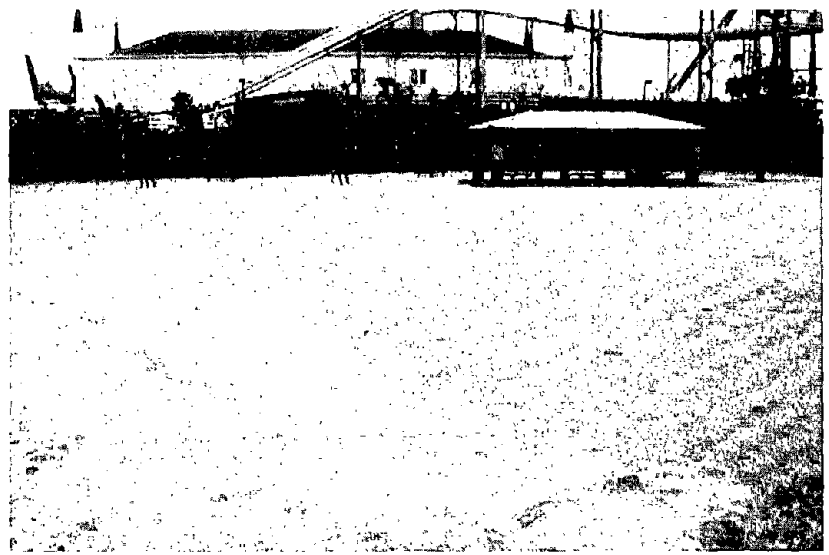

Figure 4.4: Sand boils and ground cracks in the grassy area near the amusement park.

Figure 4.5: Differential settlement and sand boils outside the northwest corner of the amusement park.

Figure 4.6: Sand boil at the southwest corner of the amusement park.

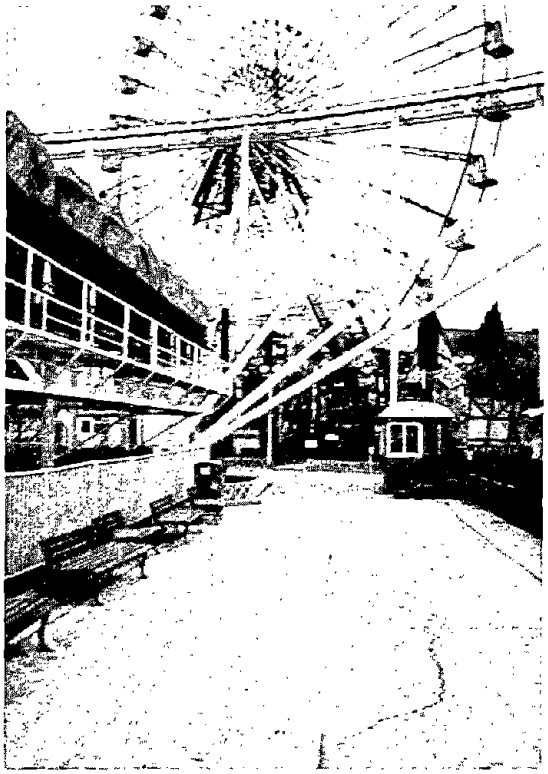

Figure 4.7: Cracks and ejecta along the southern boundary of the amusement park.

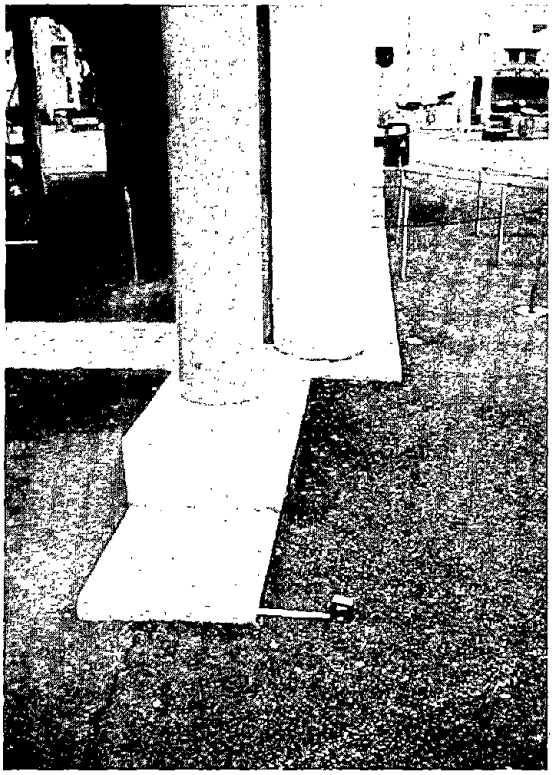

Figure 4.8: Small separation between pavement and concrete in the amusement park.

4.2.4 Discussion

Foundations within the park performed well. Without survey data, however, it is impossible to determine whether the park settled or not. The absence of visible structural damage inside the park does suggest that any areal settlements that may have occurred did not result in unacceptable differential settlements. However, outside the park on many other parts of the island, the liquefaction-induced settlement was remarkably uniform, and many large paved areas away from pile supported structures sustained no visible damage. Differential settlement between the park and the surrounding area was not clearly observed, although only the eastern boundary could be inspected readily.

The significance of the observed liquefaction inside the park along its southern boundary depends on the southern limit of the ground improvement. Liquefaction evidence was mostly within a distance of 10 to 20 m from the southern fence line, which is roughly one half to one times the thickness of the liquefiable fill. Given the extensive liquefaction observed in the parking lot on the south side of the park, ground cracks and soil ejecta could be expected to extend some distance into the treated area. Correlation of the ground performance with level of improvement, together with accurate settlement and lateral displacement data both within the park and in the surrounding areas should provide valuable insights for design of ground improvement projects in the future.

4.3 Warehouse Facility on Port Island

4.3.1 Location and Treatment

Ground improvement was performed at a warehouse facility that includes six main buildings and additional secondary structures covering an entire block near the northwest corner of Port Island, as shown in Figure 3.4. According to office personnel at this site, the "Office" building has deep foundations; whereas, all the other buildings are on shallow foundations. This improved ground site is very close to the seismic monitoring station from which the ground motion data reported in Table 3.1 were obtained. A site map showing the locations of the different

buildings is shown in Figure 4.10, and an aerial view is shown in Figure 4.11. The thickness of the dumped fill, which reportedly has a fines content ranging from 15 to 30 percent in this area, is up to 16 m.

The vibro-rod method was used to improve the site in 1977, with treatment extending a distance of 2 to 5 m laterally beyond the building footprints. Although it is customary to extend the treatment zone beyond building footprints a distance of half the depth of treatment, this was not possible around all the buildings at this site because of space limitations. The vibro-rod reached depths ranging from about 12 to 16 m, corresponding to the full thickness of the fill in this area. A triangular pattern with 2.4 m spacings was used. The areas between the buildings apparently were not treated.

A two-column wide strip of about 18 m long gravel compaction piles, with the 0.6m diameter piles spaced at 2 m on centers, was installed around the perimeter of the treated site. These compaction piles were constructed using the same procedure as used for sand compaction piles. Ground surface subsidence of 20 to 30 cm as a result of treatment was observed. The average SPT penetration resistance was reported to be 14 blows per ft prior to treatment and 27 blows per ft after treatment. SPT N-value profiles before and after treatment are shown in Figure 4.12, and it may be seen that the level of improvement was substantial.

4.3.2 Observations Outside Improved Areas

The aerial photo in Figure 4.11 taken shortly after the earthquake shows extensive soil ejecta around the perimeter of the facility and some ejecta on the open areas between the warehouses. Warehouses in the surrounding areas are on untreated ground.

Ground settlement, cracking, and sand ejecta were widespread on all four roads bounding the facility, with Figure 4.13 showing the road on the north side being a good example. Two warehouses, both apparently on untreated ground, designated #2 and #3 in Figure 4.10 are located north of the facility. The concrete floor slab inside warehouse #2 was badly damaged by differential settlement and ground cracking. Warehouse #3 was not entered. A warehouse across the street to the west had its concrete slab crack away from the apparently pile-supported column footings and the slab then settled uniformly about 50 cm relative to the footings. Sand ejecta

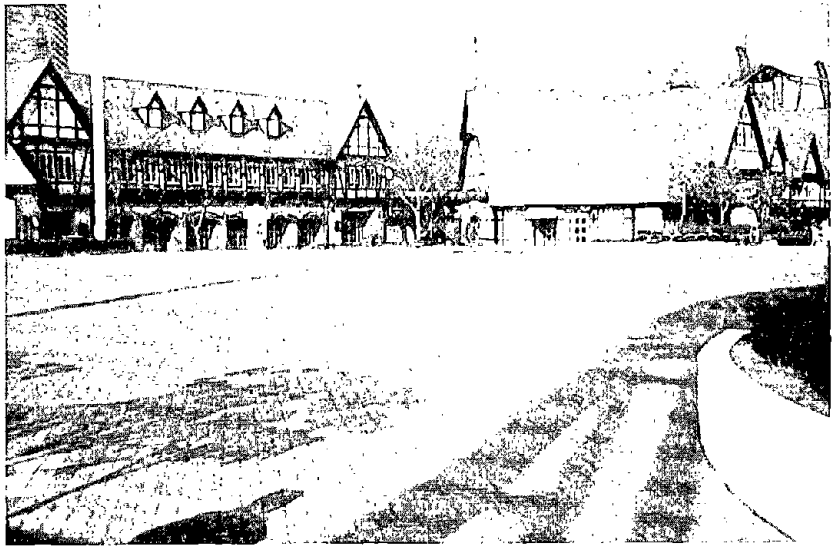

Figure 4.9: Undamaged area in the central portion of the Portopialand amusement park.

Figure 4.11: Aerial view of the Port Island warehouse facility.

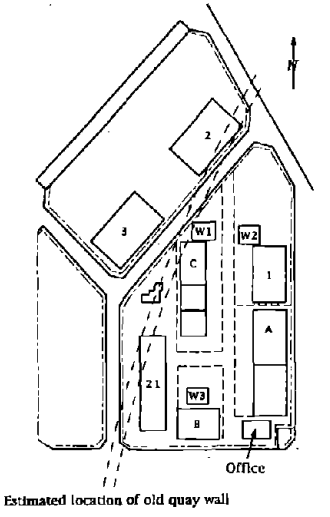

Figure 4.10: Site plan of the warehouse facility on Port Island where ground improvement was used.

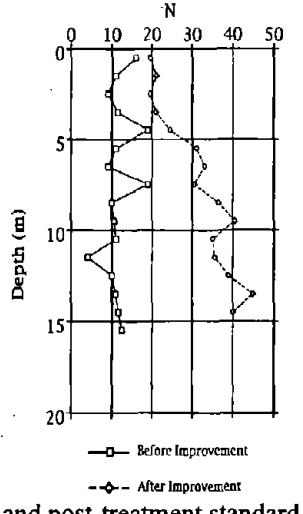

Figure 4.12: Pre- and post-treatment standard penetration resistance profiles at the warehouse site (after Fudo Construction Co., Ltd., 1995)

covered the concrete slab. There were large settlements and large differential settlements adjacent to a pile supported warehouse on untreated ground across the street to the south of the treated site, as may be seen in Figure 4.14.

4.3.3 Observations Within the Treated Area

The untreated open areas between the warehouses within the ground treatment area had several cracks in the asphalt pavement, some up to 2 to 10 cm wide, with the largest cracks observed outside Warehouse C. Sand ejecta were observed along some of the larger cracks. Two secondary structures, labeled W1 and W2 in Figure 4.10, along the north side of the facility, had damage to their concrete slabs. Inside W1 the slabs had cracks up to 3 cm wide, vertical offsets of up to 5 cm, and sand ejecta along some of the cracks. Structure W2 was closed, but severe cracking was visible inside. The northwest corner of W2 was undermined by large ground displacements toward the road.

The "Office", which is the only pile-supported structure within the warehouse complex, was not entered; however, no structural damage was observed from the exterior. Some settlement and cracked glass were observed at the entrance, as seen in Figure 4.15. There was about 30 cm of differential ground settlement at the southeast corner of this building.

Warehouses A, B, and 1 were found to have minor cracks and separations of up to 1 cm in their interior concrete floor slabs, with most separations occurring along joints. No visible differential settlements were observed between column footings and the adjacent concrete slabs. These warehouses were in operation with no disruption to the steady stream of fork-lift traffic in and out of the warehouses. Figure 4.16 is a view along the back of Warehouse A. Figure 4.17 is a view within Warehouse B.

Warehouse #21 had the worst damage observed within the treated area. Concrete slabs had been removed from the northern portion of #21 as a result of excessive cracking. In the southern portion the concrete slabs had cracks up to 5 cm wide and differential settlements up to 5 cm relative to the column footings. A large ground crack, 0.3 m wide and 1 m deep was found in the outside unpaved area near the southwest corner of Warehouse #21 (Figure 4.18).

Warehouse C, Figure 4.10, had more damage in its northern half than in its southern half. The southern half had cracks and separations up to 2 to 10 cm wide in its concrete slabs, with

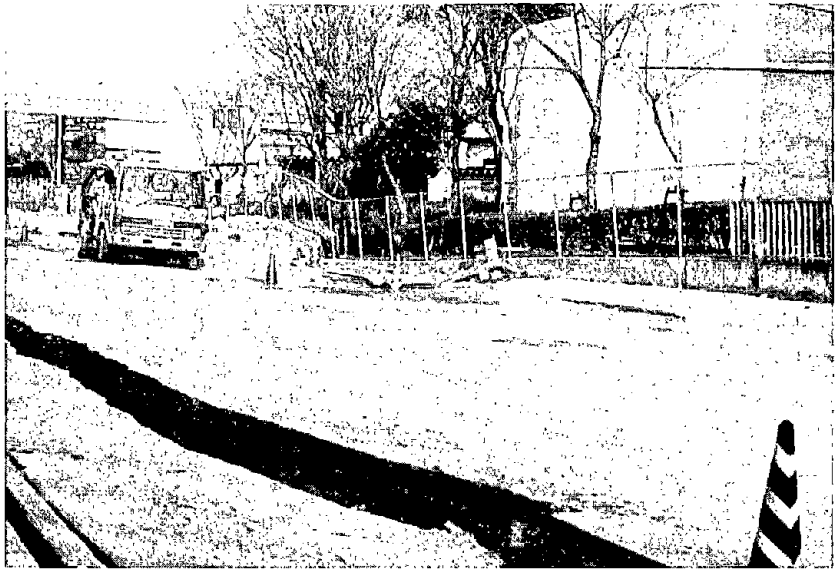

Figure 4.13: Cracking, settlement and ejecta along the road north of the facility.

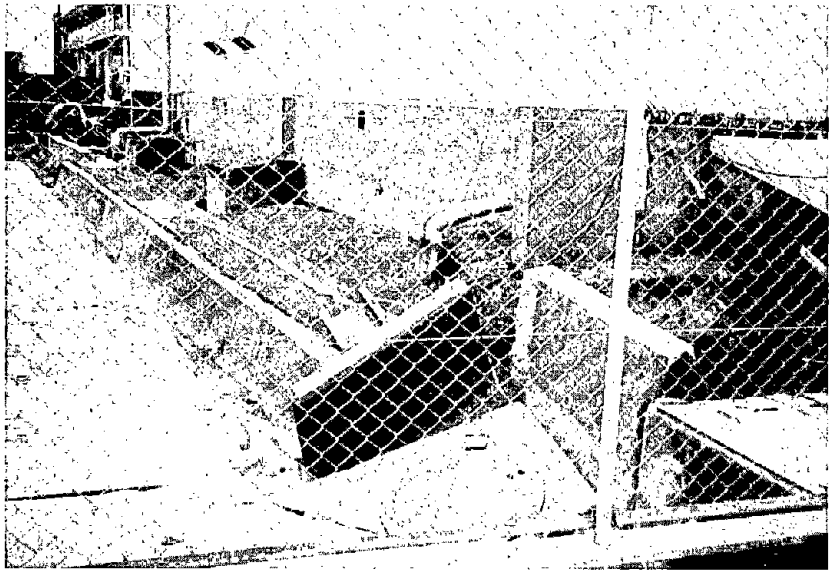

Figure 4.14: Settlement of untreated ground at building across the street to the south of the warehouse facility.

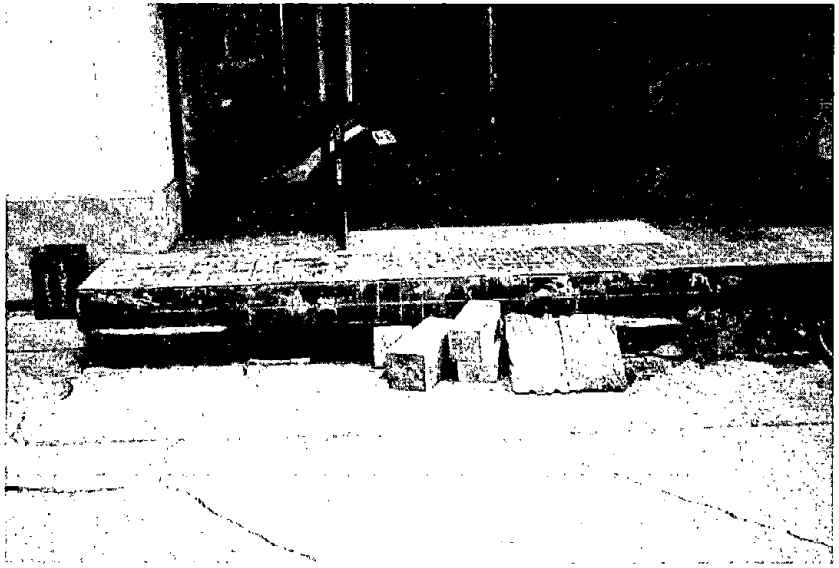

Figure 4.15: Cracked glass and settlement at the entrance to the pile-supported office building at the farehouse facility.

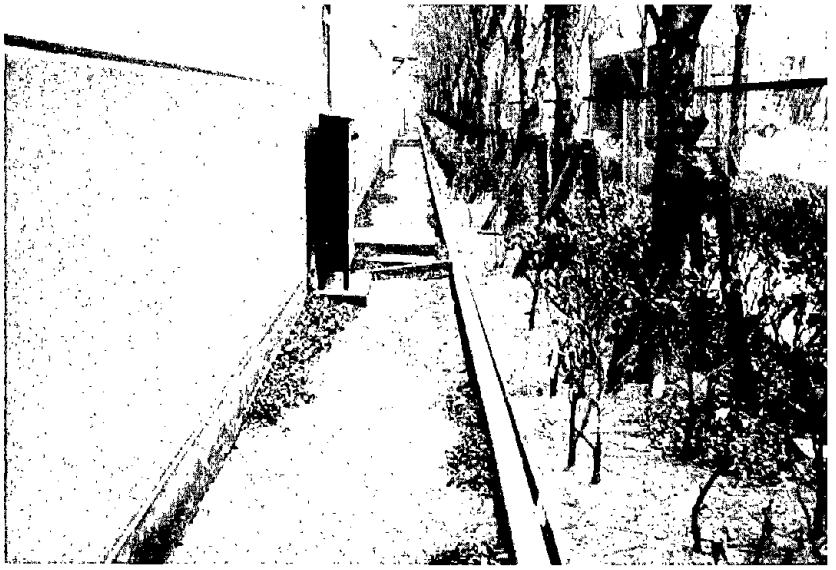

Figure 4.16: Exterior of the back of Warehouse A on the east side of the site.

most separations occurring along the joints. The northern half had cracks and separations up to 20 to 10 cm wide in the concrete slabs and differential settlements between slabs and footings that were nearly as large. The offsets in the white lines in Figure 4.19 are illustrative of these movements. Sand ejecta were also observed in the northern half.

According to personnel at the site and an earlier map of Port Island, an old quay wall, now buried, traverses the site area. An approximate location of this old quay wall, estimated from the earlier map and information from personnel at the site, is shown in Figure 4.10 by the pair of dashed lines. Further details concerning this wall could not be obtained. Damaged portions of Warehouse #21 and Warehouse C appear to correspond roughly to the general area along and outside this old quay wall. Information about how this old wall might have affected the ground improvement was not available.

4.3.4 Discussion

In the absence of survey data it is not possible to determine whether the individual warehouses settled or not. The absence of structural damage to the above ground portions of the structures means that differential settlements were not excessive for the types of structures on the site. There was no apparent superstructure damage to Warehouses #21 and C despite the significant cracking of their concrete slabs. Cracks and separations in the concrete slabs in Warehouses A, B, and 1 were generally insignificant. By contrast, nearby warehouses on untreated ground experienced relatively major damage compared to the warehouses on treated ground.

There is, however, a clear difference between the performance of ground improvement for Warehouses #21 and C, portions of which were underlain by the old quay wall, and Warehouses A, B, and 1. This difference corresponds roughly to the location of the old buried quay wall. It is possible that the presence of this wall may have hampered the ground improvement in these areas.

Another important point is that the observed ground cracks and sand ejecta within the warehouses on improved ground indicate that the level and/or area of improvement achieved were evidently unable to prevent liquefaction totally. However, the reported 2 to 5 m of treatment beyond the building perimeter is only 1/8 to 1/3 the potential depth of liquefiable soil; whereas, 1/2 is often considered the desirable minimum. Thus the buildings could be expected to

be somewhat adversely affected by liquefaction of the surrounding soils. Overall, the warehouses on treated soil suffered less foundation slab damage than nearby warehouses on untreated ground. Thus, the effect of treatment may have been to reduce the consequences of liquefaction rather than to preclude its development completely. Given the proximity of this site to the seismic array for which detailed ground motion data are available, the available soil profile data, and specific information about the gravel compaction piles and vibro-rod treatment, this site would appear to warrant detailed further study.

4.4 Small Building Site on Port Island

4.4.1 Location and Treatment

The ground at the site of a small pile-supported building at the southeast corner of Port Island Phase I, Figure 3.4, was improved by the vibro-rod method in 1981. The building is across the street which parallels, and is directly adjacent to, the sea wall that bounds Phase I on the south. The vibro-rod treatment extended a distance of 10 m around the building.

4.4.2 Observations Outside the Treated Area

The sea wall across the street displaced to the south a distance of 20 to 30 cm, accompanied by settlement and the development of a large parallel crack in the pavement, as shown in Figure 4.20. The building in the left background of Figure 4.20 is located directly across the street to the east of the treated area. A close-up view of that pile-supported building is shown in Figure 4.21. The settlement of the adjacent untreated ground is large.

4.4.3 Observations Within the Treated Area

The post-earthquake conditions at the treated site are shown in Figure 4.22. The building itself appeared undamaged, and the settlements around it were considerably smaller than observed in the untreated areas.

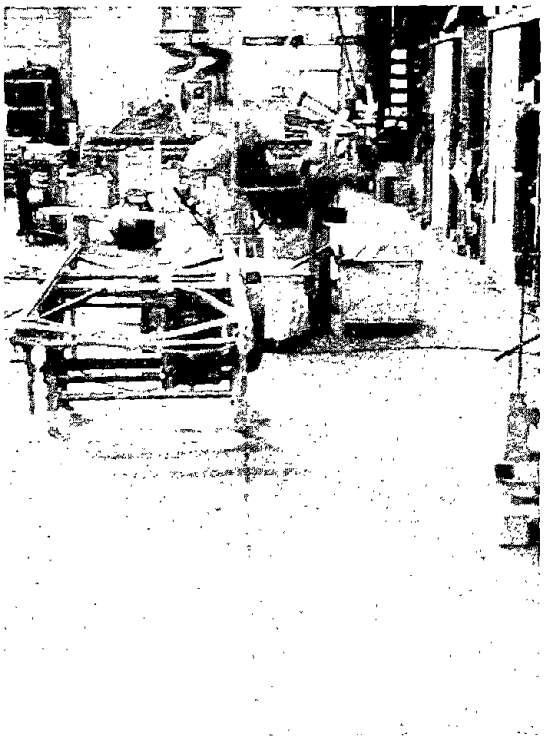

Figure 4.17: View inside Warehouse B showing little damage.

Figure 4.18: Large ground crack outside the southwest corner of Warehouse #21.

Figure 4.19: View inside Warehouse C near the northern end.

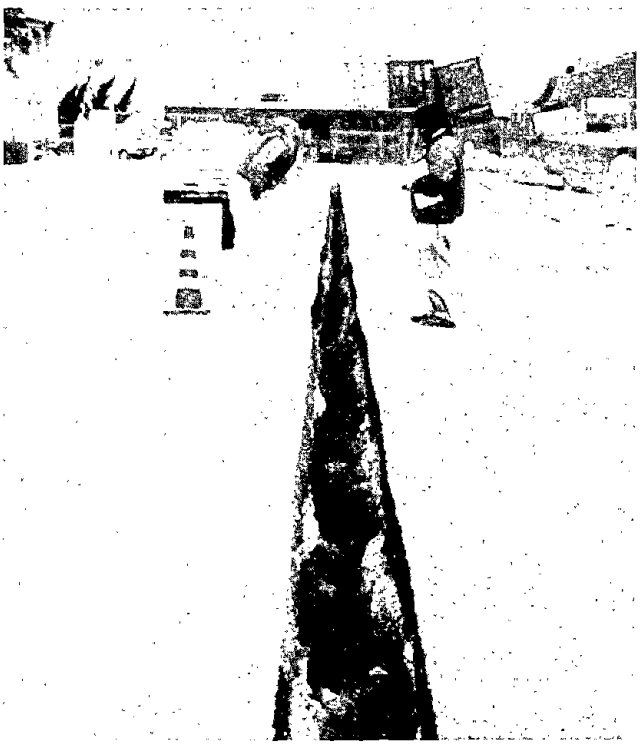

Figure 4.20: Displaced sea wall and cracked pavement at the southeast corner of Port Island Phase I.

4.5 Treated Site on Rokko Island

According to personnel from Fudo Construction Co., Ltd., a small area behind the sea wall at the southeast corner of Rokko Island was treated 2 to 3 years ago using sand drains in the alluvial clay and sand compaction piles in the overlying fill. A target post-treatment N-value for the fill of 15 blows per ft was established; however, a value of 20 to 25 blows per ft was actually achieved. Ground failure at this site developed, probably because of the large movements of the sea wall.

4.6 Rubble Mound Breakwater in the Nishinomiya Area

4.6.1 Location and Treatment.

A rubble mound breakwater was located just offshore to the south of the filled area at the Nishinomiya side of the new Nishinomiya-Osaka bridge which suffered collapse of one span (see Section 3.4, Figure 3.60). A 2 to 3 m thick sand layer was placed over the soft alluvial clay, which had a thickness of 10 m at this location. Sand compaction piles were placed through both the sand and clay layers at 2.1 m on center. For offshore construction Fudo Construction Co., Ltd. used special equipment for installation of 2.0 m diameter sand compaction piles. The rubble mound embankment was placed directly on the treated ground, and the base of the embankment extended to the outer edge of the treated area. A rough approximation of the cross section of the breakwater and the treated ground, based on the information provided at the time of the reconnaissance, is shown in Figure 4.23.

4.6.2 Performance

The breakwater settled from 1 to 2 m as a result of the earthquake. Divers reported evidence of sand boils at the toe of the rubble mound embankment. At the time of the reconnaissance, the failure mechanism had not yet been determined. Possibilities would appear to include (1) liquefaction of the sand adjacent to the treated zone with concurrent loss of lateral support, (2) liquefaction of the treated zone, (3) stability failure within the soft clay, and (4) combinations of all of these. Investigations of the observed behavior are continuing.

Figure 4.21: Large settlements of untreated ground adjacent to pile-supported building, southeast corner of Port Island Phase I.

Figure 4.22: Limited settlement of treated ground adjacent to pile-supported building, southeast corner of Port Island Phase I.

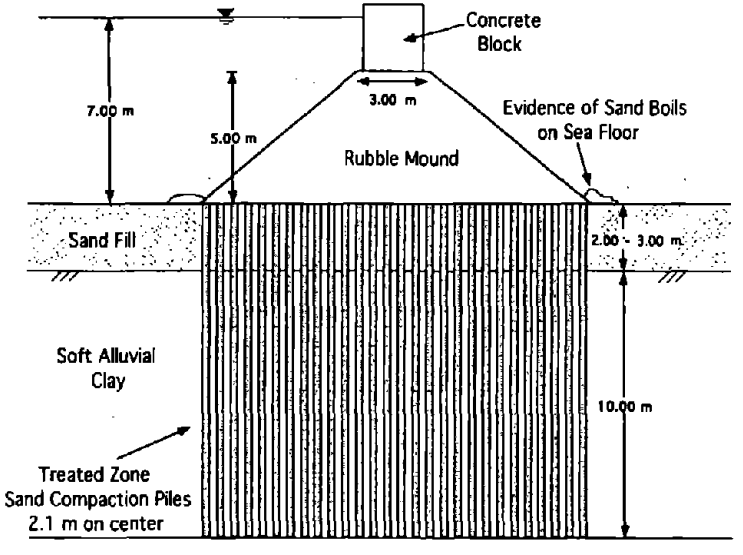

Figure 4.23: Inferred approximate cross section of the treated ground and rubble mound breakwater near Nishinomiya.

4.7 Conclusions

The earthquake provided a severe test for several improved ground sites in the Kobe area. In all cases the site stratigraphy included dumped hydraulic fill placed over soft alluvial clay. The treatment method was to construct sand compaction piles using either the decomposed granite fill itself densified by vibro-rod probes or the casing method with introduction of additional material from above ground. The post-treatment SPT N-values were typically 20 to 25 blows per ft as opposed to about 10 to 15 blows per ft before treatment. The treatment itself resulted in ground surface settlements of 20 to as much as 40 cm, with the largest values being reported for the Portopialand Park area. It may be noted that the surface settlements of untreated ground caused by the earthquake were of the order of 50 cm.

Overall, the observations show that improved ground sites on land sustained significantly less deformation and damage than did the adjacent untreated ground. The offshore Nishinomiya breakwater failed for reasons that have not yet been determined. The amount of differential settlement and the damage to pavements, floor slabs, utilities, and other facilities was variable, ranging from very little over the major part of the amusement park, to substantial within parts of the warehouse area. The larger settlements in the warehouse area appear attributable to the presence of an old buried quay wall which restricted the ground improvement beneath some of the structures.

Further analyses are needed to better correlate the amounts of settlement that were observed to (1) the level of ground improvement, (2) the extent of the treatment zone beyond the structure or facility to be protected, (3) the liquefaction and lateral spreading of the ground adjacent to the treated zone, and (4) the input ground motions.

CHAPTER FIVE: PERFORMANCE OF DAMS AND LEVEES

5.1 Performance of Dams

Aerial reconnaissance and available maps show that there are numerous small dams and reservoirs both on Awaji Island and in the Kobe Area. These dams appear to be typically 10- to 20-meter-high earth embankments and serve to store water for presumably agricultural use on Awaji Island and urban use in the Kobe area. The dams in the Kobe area also appear to provide recreation and flood protection benefits. In addition to the small embankment dams, there are at least two moderately-sized concrete gravity dams: Karasuhara and Nunobiki Dams. Both dams were identified by aerial reconnaissance and appear to store the largest reservoirs in the immediate Kobe area (see Figure 3.1 for locations).

The reservoirs for most of the dams surveyed two weeks after the earthquake seemed substantially below maximum reservoir elevation. In many cases, the reservoir surface elevations appeared to be less than half their maximum heights. In general, preliminary reports indicate that most dams performed well with little or no damage noted. The principal exception to this was the failure of the relatively small Upper and Middle Niteko Dams, together with significant damage sustained at the Lower Niteko Dam.

5.1.1 Upper, Middle, and Lower Niteko Dams

The Upper, Middle, and Lower Niteko Dams are located approximately 4 kilometers north of Nishinomiya in an urban portion of the eastern Kobe region (Figure 3.1). The earthquake was estimated to have induced peak ground accelerations of approximately 0.3 to 0.5g in this area. All three dams are reported to have been constructed over 100 years ago with minor additions and modifications made to them in more recent times. Their current use is to retain small reservoirs or ponds, presumably for water supply and recreation uses. At the time of the earthquake, all three reservoirs were reported to be relatively low, impinging only on the lower third of each dam. All three dams had large trees and/or brush growing in their downstream slopes. Figure 5.1 presents a schematic diagram illustrating the general arrangement of the dams together with a general picture

of the performance of the structures. Figure 5.2 shows an aerial photograph of the three dams and reservoirs.

The Lower Niteko Dam is the largest of the three dams with a maximum height of approximately 12 meters and a crest length of about 120 meters. It has an estimated crest width of about 8 meters and was estimated to have 2:1 to 2.5:1 (horizontal:vertical) upstream and downstream slopes. It also has a 1.5-meter-high retaining wall at its downstream toe. Of the three dams, the Lower Niteko Dam performed the best. This relatively good performance may be due to the fact that some reports indicate that this reservoir was kept nearly empty to alleviate seepage problems being experienced at residences downstream. Nevertheless, the dam sustained major cracking and slumping in the middle of the embankment, losing as much as 2 meters of height (Figure 5.3). Although the slumping appeared to be more towards the upstream direction, there were also significant cracks (10 centimeter widths) observed on the downstream slope near the left abutment. A portion of the downstream retaining wall was also cracked.

The Middle Niteko Dam had a maximum height of approximately 10 meters and a crest length of about 80 meters prior to the earthquake. It had a crest width of about 2 1/2 meters and was estimated to have had 2:1 to 2.5:1 upstream and downstream slopes. As a result of the earthquake, the dam experienced a flow failure reminiscent of the 1925 Sheffield Dam failure in California (Seed et al., 1969). The upper two-thirds of the dam in the central portion appeared to have flowed as much as 70 meters downstream of the dam's centerline (Figure 5.4). At the time of the earthquake, the reservoir was reported to be only slightly higher than the level shown in the photographs. In addition, a small flow of reservoir water was still passing through the breach at the time of the field reconnaissance, 17 days after the earthquake.

The flow movement of the Middle dam appeared to be almost entirely in the downstream direction, although examination of the remaining portions of upstream slope near the abutments indicated minor slumping towards the reservoir. The small outlet structure at the upstream toe near the center of the dam appeared to be nearly vertical with a possible slight upstream tilt, although the catwalk to the structure had collapsed (Figure 5.5). Exposures of the upper portion of the dam near the abutments indicated a layered fill composed of sandy silt and silty sand with gravel. However, the slide debris seemed composed mostly of sandy silt. All of the fill soils were believed to originate from decomposed granite.

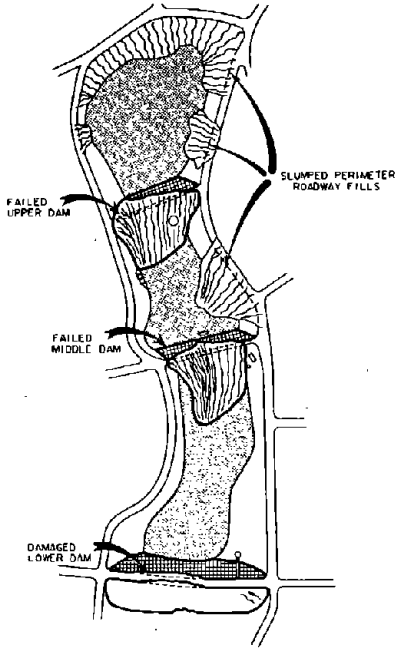

Figure 5.1: Schematic plan of Niteko Dam Complex.

Figure 5.2: Aerial photograph of Niteko Dam Complex.

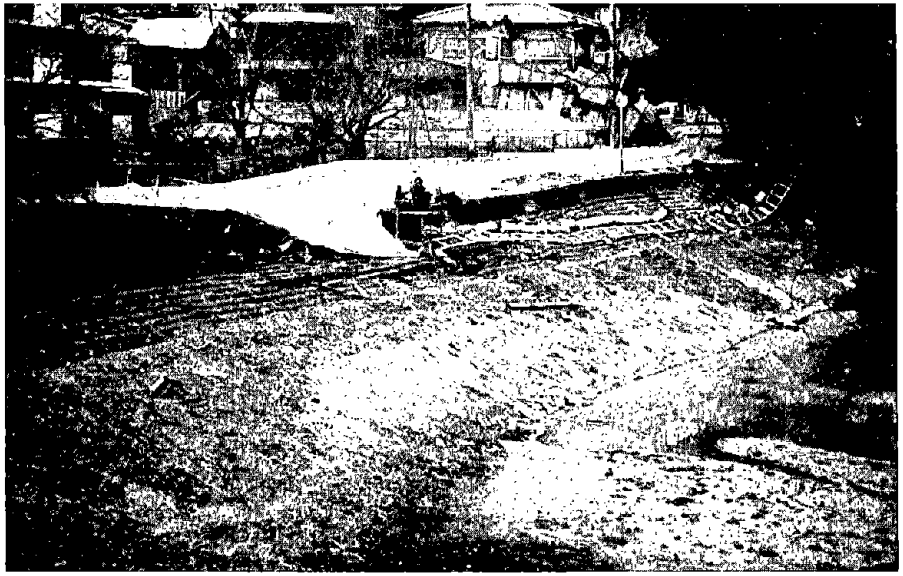

Figure 5.3: Upstream slope of Lower Niteko Dam.

The Upper Niteko Dam also had a maximum height of approximately 10 meters and a crest length of about 80 meters prior to the earthquake. Its crest width had also been 2 1/2 meters and it was also estimated to have had 2:1 to 2.5:1 upstream and downstream slopes. The Upper dam sustained a flow failure very similar to the failure observed at the Middle Dam. The upper two-thirds of the central Upper dam appeared to have also flowed as much as 60 to 70 meters downstream of the dam's centerline (Figure 5.4). Portions of the flow passed around a downstream outlet tower. This tower appeared to have remained stable, together with a possible slight downstream tilt, with little exterior damage observable. The exception to this was the damage sustained as a result of its catwalk being jammed through its doorway into the tower interior by the flowing ground (Figure 5.6). As at the Middle dam, the flow failure observed at the Upper dam seemed to be almost entirely in the downstream direction. However, there was somewhat more slumping of the remaining upstream slope than that observed at the Middle dam (Figure 5.7).

The perimeter roadway fills along the margins of the Upper and Middle Niteko reservoirs also sustained flow failures following the earthquake (Figure 5.1). These perimeter fills were reported to have initially failed either during or shortly after the main shock. Some were then quickly rebuilt and resurfaced with new asphalt concrete only to fail again following the occurrence of a strong aftershock a few days later (Figure 5.8).

The flow failures of the Upper and Middle Niteko Dams, along with the extensive failures of the perimeter fills, strongly suggest that liquefaction was responsible, despite the fact that sediment boils were not observed within the reservoirs during the reconnaissance. However, in the residential neighborhood to the west there was ample evidence of liquefaction in the form of sand ejecta and sand boils. Shortly after the earthquake, a borehole was drilled into each dam embankment to obtain SPT data (see drill rig in Figure 5.3). Reports indicate that the blowcounts within the dam embankments generally ranged between 2 and 10 blows per 30 cm, with mean values around 5 to 6 blows per 30 cm. Blowcounts in the foundation soils beneath the embankments were generally greater than 25 blows per 30 cm. These results suggest that the saturated lower portions of the embankments would have been more likely to liquefy than the foundation soils. Good performance of the foundation soils is also indicated by the good performance of the outlet towers at the Middle and Upper Niteko Dams. The perimeter road fills may also have failed due to liquefaction of the saturated fill or due to liquefaction of less competent

Figure 5.4: Aerial photograph of flow failures at Upper and Middle Niteko Dams.

Figure 5.5: Crest alignment of failed Middle Niteko Dam.

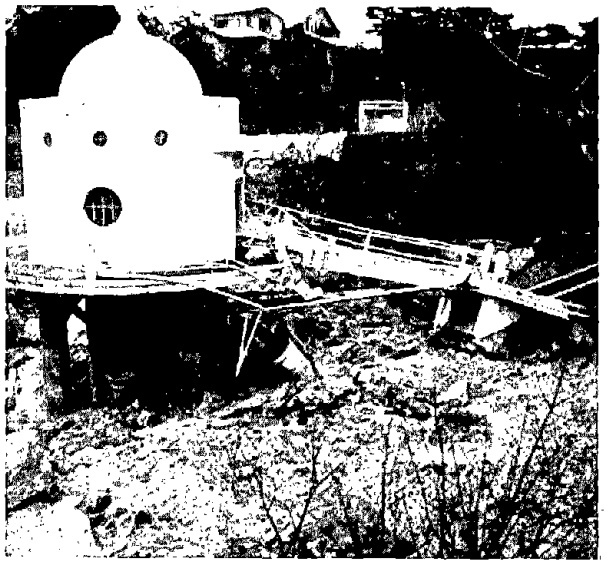

Figure 5.6: Downstream outlet tower at Upper Niteko Dam.

Figure 5.7: Upstream slope of Upper Niteko Dam.

Figure 5.8: Failed perimeter roadway fill along Upper Niteko Reservoir.

foundation material. Overall, it was not possible to discern the relative contributions of possible reservoir releases or aftershocks on the development of the flow slides.

5.1.2 Kitayama Dam

Kitayama Reservoir is one of the larger reservoirs in the eastern Kobe region and is located approximately 6 kilometers north of Nishinomiya (see Figure 3.1). The earthquake was estimated to have induced peak ground accelerations between 0.2 and 0.4g in this area. The reservoir is situated at the top of a hill and is retained by five embankment dams (Figure 5.9). The largest embankment is located on the south side and is estimated to have a maximum height of approximately 25 meters (Figure 5.10). This embankment is reported to have a homogeneous cross section with an internal chimney/blanket drain and was completed in 1962. The field reconnaissance consisted of aerial reconnaissance and limited ground inspections of the embankment crests. No damage was observed during the ground inspections of the crests and the embankments appeared to have generally performed well. However, the aerial reconnaissance discovered what appeared to be significant longitudinal cracking along approximately 100 m of the upstream slope of the main embankment just above the water line (Figures 5.10 and 5.11). There also appeared to be a scarp approximately one meter high associated with this crack. The cracking was indicative of possible upstream slumping of the slope, but no other distress was observed on the slopes above the cracks. It is not known if the apparent cracking is significant or if it involves only surface slope protection materials. Additional investigation is needed to clarify the performance of the dam.

5.1.3 Karasuhara Dam

Karasuhara Reservoir appears to be the largest reservoir in the immediate Kobe area and is located approximately 4 kilometers northwest of the Port Island Bridge (Figure 3.1). The dam appears to be a cemented masonry gravity dam constructed to have a horizontal curve. The dam was estimated to have a maximum height of approximately 35 to 45 meters and incorporates an outlet tower on the upstream center of the dam (Figures 5.12 and 5.13). A monument on the crest of the dam indicates that the dam was originally completed in 1904 and had a 3-meter raise in 1914.

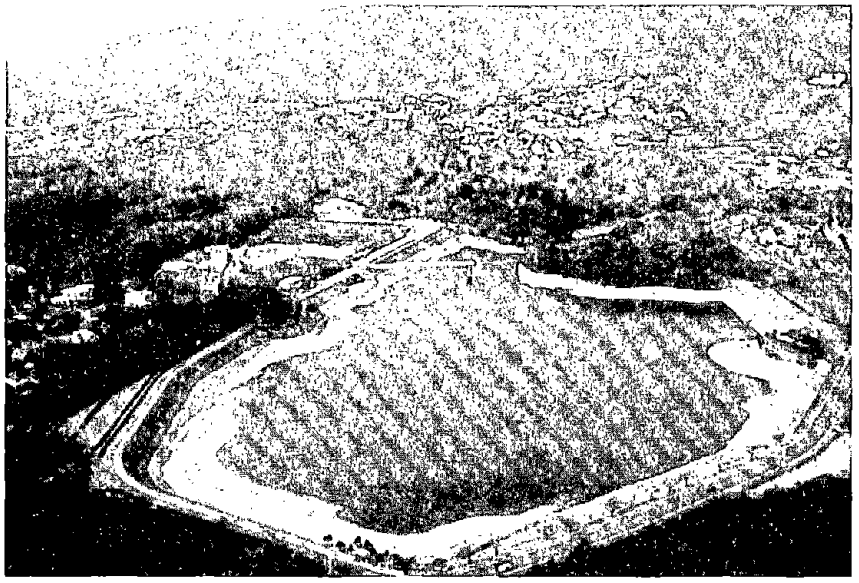

Figure 5.9: Aerial photograph of Kitayama Reservoir.

Figure 5.11: Aerial photograph of cracking on upstream slope of Kitayama South Dam.

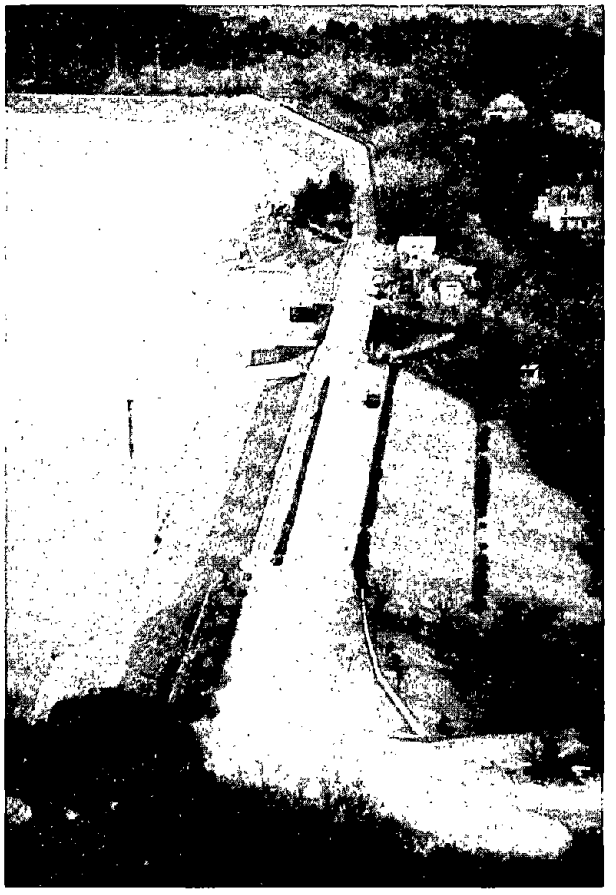

Figure 5.10: Aerial photograph of Kitayama South Dam.

The earthquake was estimated to have induced peak ground accelerations between 0.4 and 0.6g in this area. Karasuhara Dam was surveyed by both aerial and limited ground inspection of the dam crest. The reservoir surface appeared to be approximately 14 meters below the crest of the dam during the field reconnaissance. Overall, the dam appeared to have performed well. No offsets were observed on the crest, and no seepage could be seen on the downstream face of the dam (Figure 5.14). Only one crack was observed in the dam crest. The crack was oriented approximately perpendicular to the dam axis, had a width of about 1-2 millimeters, and appeared to be very old (Figure 5.15).

5.1.4 Nunobiki Dam

Nunobiki Reservoir appears to be the second-largest reservoir in the immediate Kobe area and is located approximately 3 kilometers north of the Port Island Bridge (Figure 3.1). The dam appears to be a concrete gravity dam constructed with a straight axis (Figure 5.16). As with Karasuhara Dam, Nunobiki Dam incorporates an outlet tower within the upstream center of the dam (Figure 5.17). Nunobiki Dam was estimated to have a maximum height of approximately 35 to 45 meters.

The earthquake was estimated to have induced peak ground accelerations between 0.4 and 0.6g in this area. The reservoir surface appeared to be approximately 10 to 15 meters below the crest of the dam during the field reconnaissance. Nunobiki Dam was surveyed only by aerial reconnaissance and no damage was observed.

5.1.5 Summary

The results of the field reconnaissance, together with reports supplied by Japanese colleagues, indicate that modern dams in the Kobe area generally performed well. This behavior matches the good behavior of modern dams in North America following the recent Loma Prieta and Northridge Earthquakes. The only dams known to have sustained major damage were the old, presumably non-engineered Niteko Dams. This latter behavior also matches the experience in North America (e.g. Sheffield Dam, Upper and Lower San Fernando Dams).

Figure 5.12: Aerial photograph of Karasuhara Dam.

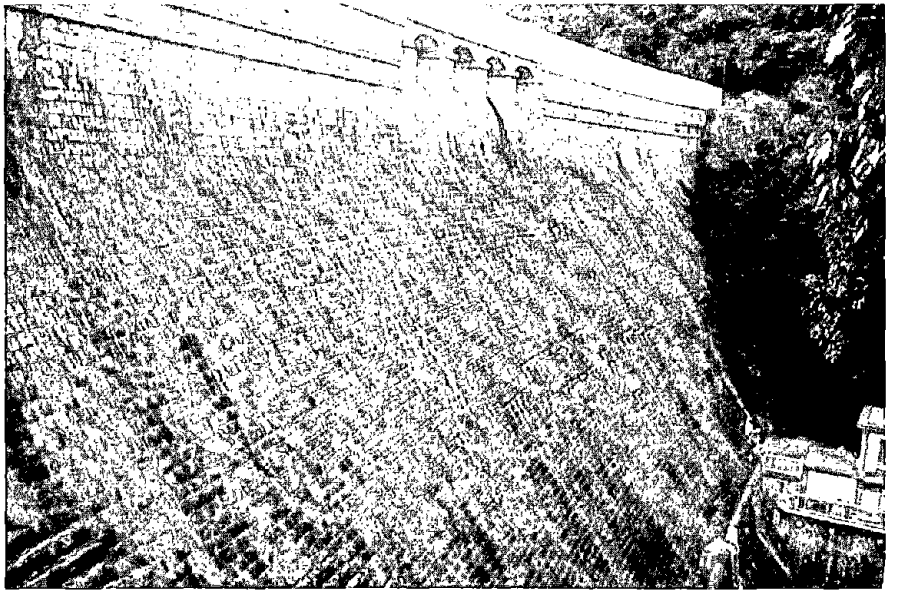

Figure 5.14: Downstream face of Karasuhara Dam.

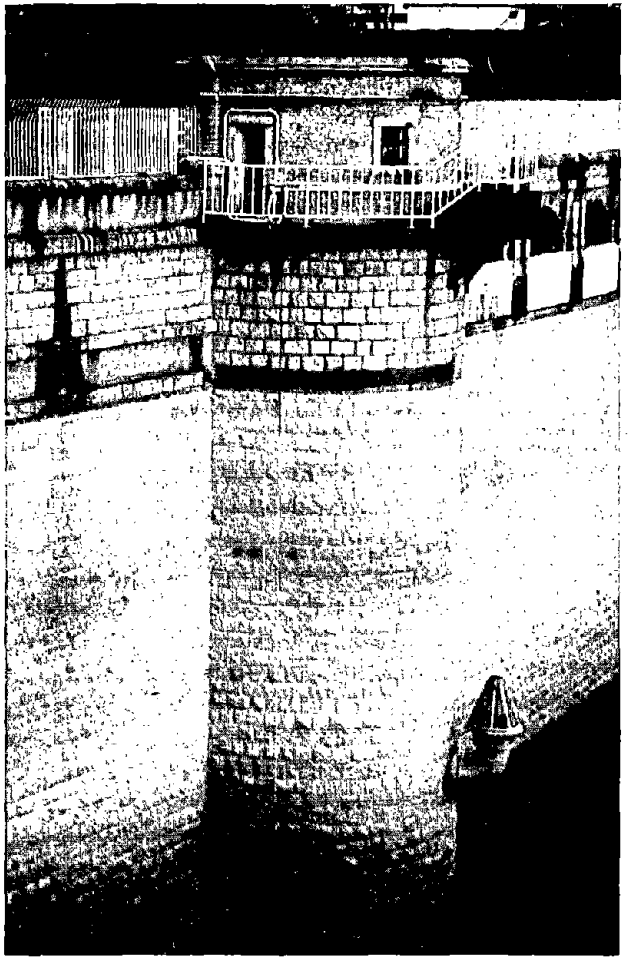

Figure 5.13: Outlet tower on Karasuhara Dam.

Figure 5.15: Old crack observed on crest of Karasuhara Dam.

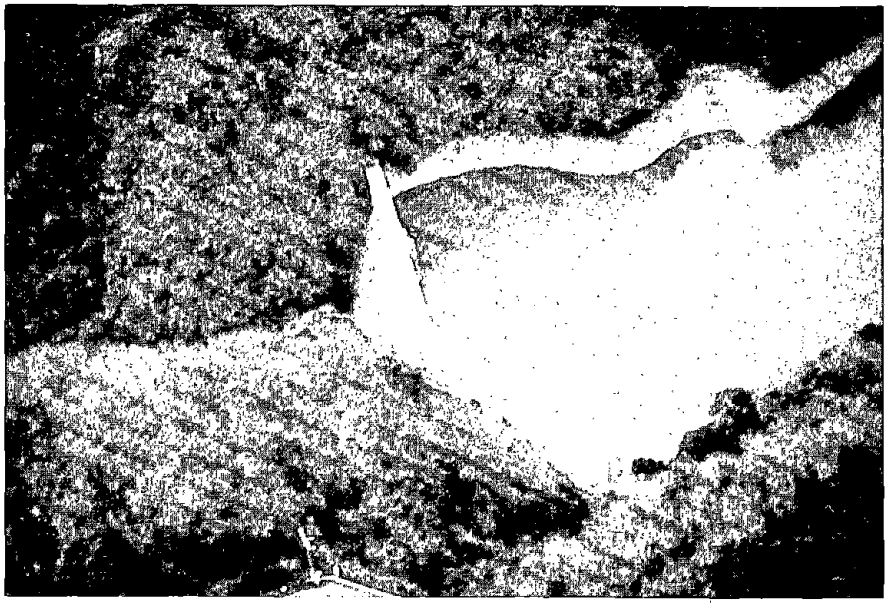

Figure 5.16: Aerial photograph of downstream face of Nunobiki Dam.

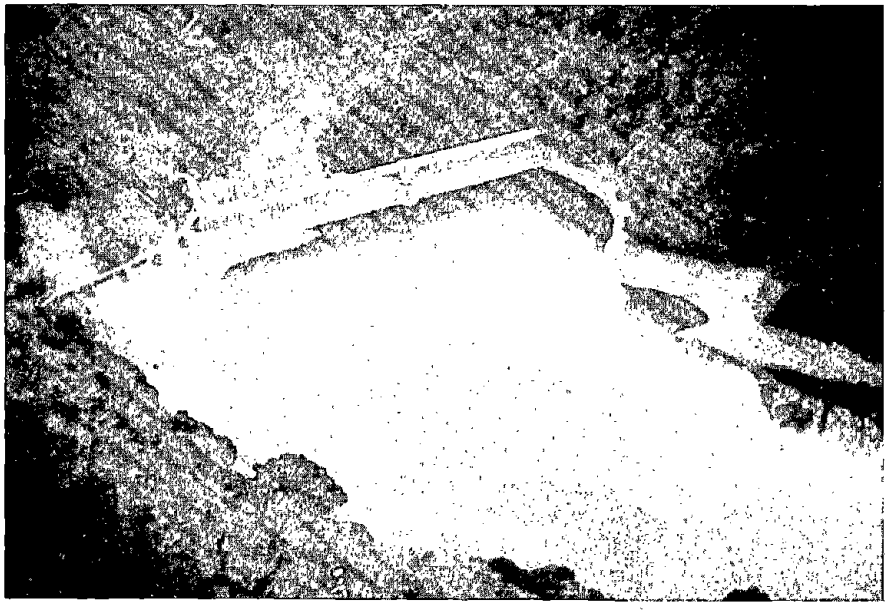

Figure 5.17: Aerial photograph of upstream face of Nunobiki Dam.

5.2 Performance of Levees

There are several small rivers which flow past Kobe and Osaka to Osaka Bay. Most of these rivers have been channelized as they pass through the urban areas to reach the bay. This means that the river is commonly confined by gravity and cantilever retaining walls similar to those which channelize the Los Angeles River. In some places, armored earth embankments are also used as levees. In general, aerial reconnaissance indicated that most of these water retention facilities performed well. The exceptions to this was cracking and slumping observed along the Yodo River Levee and distress observed on a levee along a tributary of the Mukogawa.

5.2.1 Yodo River Levee

The Yodo River is the principal river in the region (see Figure 3.1). The earthquake was estimated to have induced peak ground accelerations of approximately 0.2 to 0.3g in this area. Approximately 1.5 to 2 kilometers of levee on the south, or Osaka, side of the river experienced major damage in the form of extensive cracking and slumping. The levee along this portion of the river is an earth embankment commonly 6 to 8 meters in height. The levee is generally about 7 meters in width and incorporates a 1.5-meter-high concrete parapet wall on the waterside edge of the crown . Both the waterside and the landside slopes of the levee are covered by concrete slabs to prevent erosion failure from overtopping by flood waters. The levee crown has generally been paved with asphalt concrete.

The mode of damage appeared to consist of the levee embankment breaking up into blocks and sinking into and spreading out over a liquefied foundation. At the time of the earthquake, the river stage was relatively low and apparently saturated only about the bottom meter or two of the levee embankment. As a result of the earthquake, the foundation and/or bottom portions of the levee presumably liquefied, resulting in the failure of the levee. At several locations, the levee embankment settled over 3 meters, almost half its total height. Figures 5.18 and 5.19 show the seriously damaged levee. At the time of the reconnaissance, the levee had received initial repairs consisting mainly of adding fill to restore freeboard. To prevent erosion due to rainfall or seepage, the unarmored repaired areas were covered with blue, plastic sheets.

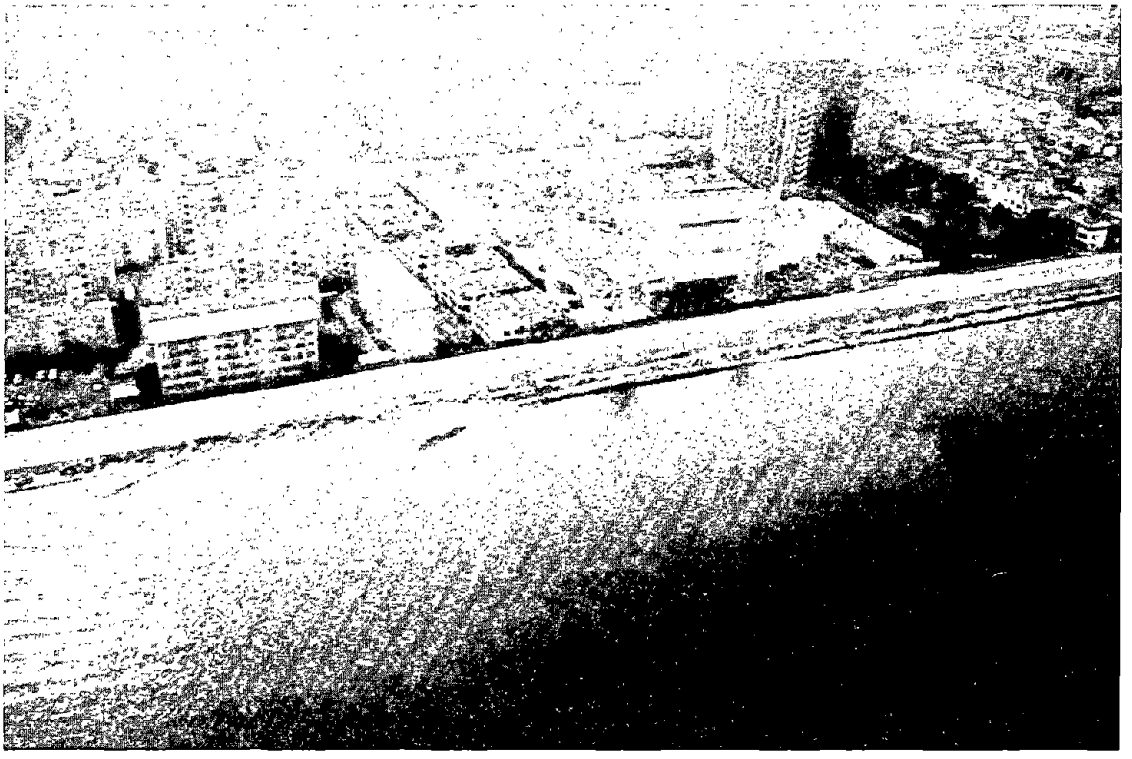

Figure 5.18: Aerial photograph of failed Yodo River levee after initial repairs.

Figure 5.19: Upstream slope of failed Yodo River levee after initial repairs (note horizontal stairway).

Support for the theory that foundation liquefaction was responsible for the serious damage was obtained by examining levee reaches approximately a kilometer east, or upstream, of the seriously damaged levee area. In this eastern area, the levee performed generally well with only isolated reaches sustaining moderate damage in the form of cracking and settlements of up to a meter. In this area, the foundation soils are slightly above the river level and are exposed on the waterside of the levee. As shown in Figure 5.20, several sand boils could be observed in the foundation opposite an area of moderate damage. The improved performance further east may be because the foundation becomes denser as one moves upstream, or perhaps the effect of the relatively lower water level reduced the total amount of foundation or levee materials that liquefied. Reports in the Japanese media also indicated that reaches of the north levee on the Yodo River and some reaches of levees on the Kansaki River sustained similar levels of minor to moderate damage.

5.2.2 Mukogawa Tributary Levee

Figure 5.21 presents an aerial photograph of levees confining a tributary of the Mukogawa. This site is located approximately 8 kilometers north of Amagasaki in the eastern Kobe area (Figure 3.1). The photograph shows the levee crowns on both sides of the channel to be covered with blue, plastic sheeting. This was presumably because the levees had sustained cracking, and perhaps slumping, and the plastic sheets were placed to prevent rainfall from infiltrating into the cracks. Portions of the levee beneath the plastic sheets appear to be significantly distorted and may be indicative of serious damage. The earthquake was estimated to have induced peak ground accelerations of approximately 0.3 to 0.4g in this area. No field reconnaissance was performed on the ground at this site.

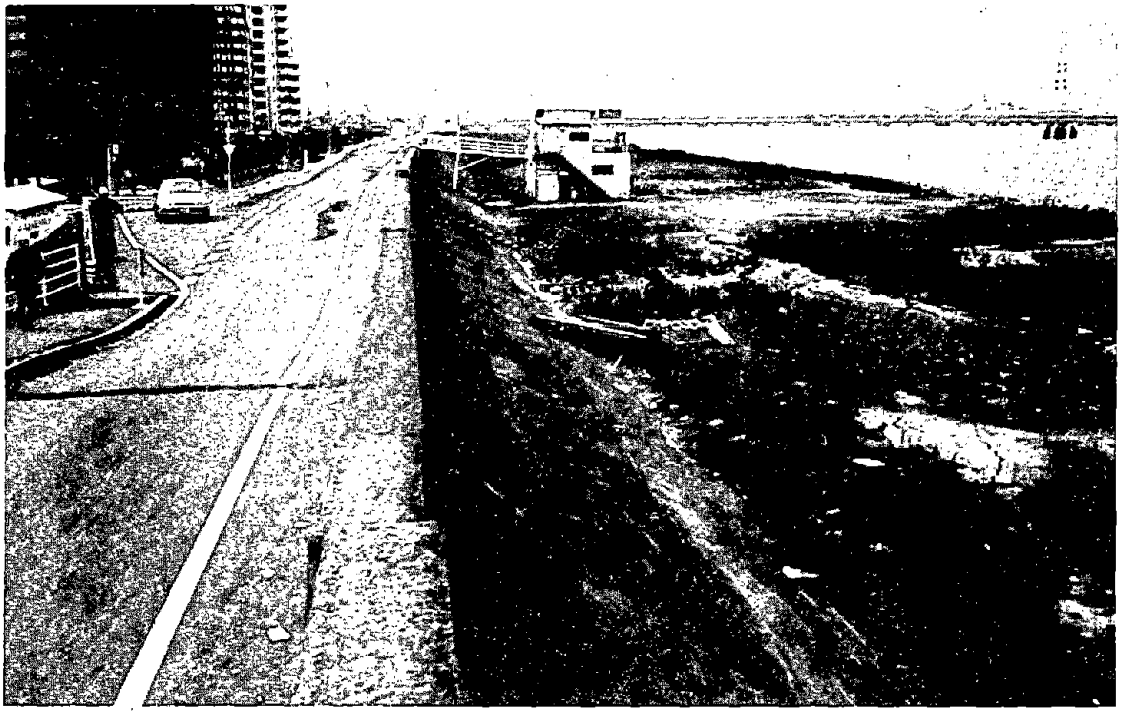

Figure 5.20: Moderately damaged Yodo River levee (note sand boils on exposed waterside foundation).

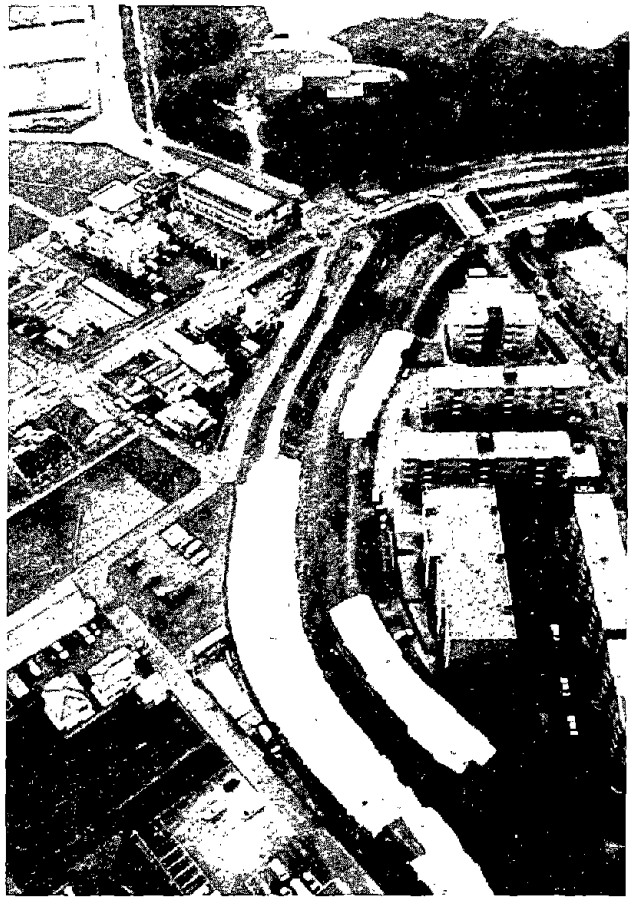

Figure 5.21: Aerial photograph of distressed levees on tributary to Mukogawa.

CHAPTER SIX: LIFELINE SYSTEMS

6.1 Introduction

Extensive damage to lifeline systems occurred throughout the epicentral area of the earthquake. Some of the damage and failures appeared to be primarily structural in nature, such as the failures of elevated sections of freeways, railroads, and bridges, most notably the collapse of the Hanshin Expressway and the collapse of elevated sections of a number of railroad lines, including Tokaido-Sanyo Shinkansen. Other damage seemed to have been caused principally by ground failure, such as the liquefaction induced damage to port facilities, underground transit, and underground utilities. In many instances, the connection between the structural failures and ground deformation could not be evaluated in the course of a reconnaissance visit, and further studies will be needed. The damage to the Port of Kobe has already been described in considerable detail in Chapter 3, and, therefore, the emphasis here is on transit and major utilities.

6.2 Kobe Underground Rapid Transit System

The City of Kobe is serviced by two underground rapid transit systems, as shown in Figure 6.1. The Kobe Rapid Transit Railway, or Kobe Kosoku Tetsudo, is 7.6 km long, with about 6.6 km of the system constructed underground between 1962 and 1968 by cut-and-cover methods. The Kobe Municipal Subway System is 21.7 km long, with approximately one-third of the system underground. The subsurface portions of the subway were built between 1977 and 1983. Earthquake-induced damage was observed at the Daikai and Nagata Stations of the Kobe Kosoku and at the Shin Nagata, Kamisawa, and Sannomiya Stations of the Municipal Subway. All stations were of cut-and-cover construction, with the most prominent damage concentrated at the center reinforced concrete columns of the stations and running tunnels.

Figure 6.2 shows a plan view of the Kobe Kosoku with descriptions of damage. The Daikai Station collapsed along a section approximately 100 m long. It was a reinforced concrete box structure, 7.2 m high and 17.0 m wide, at a depth of 4.8 m from the street surface to the top

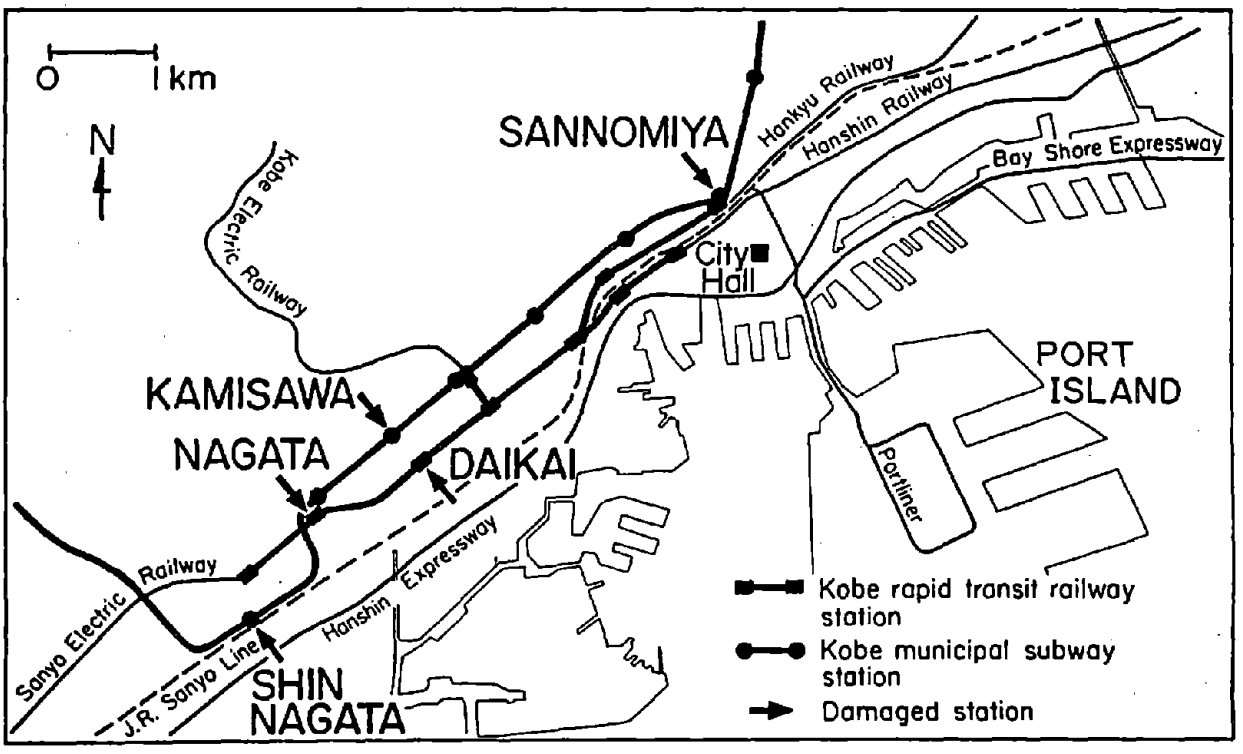

Figure 6.1: Map of underground rapid transit systems in Kobe.

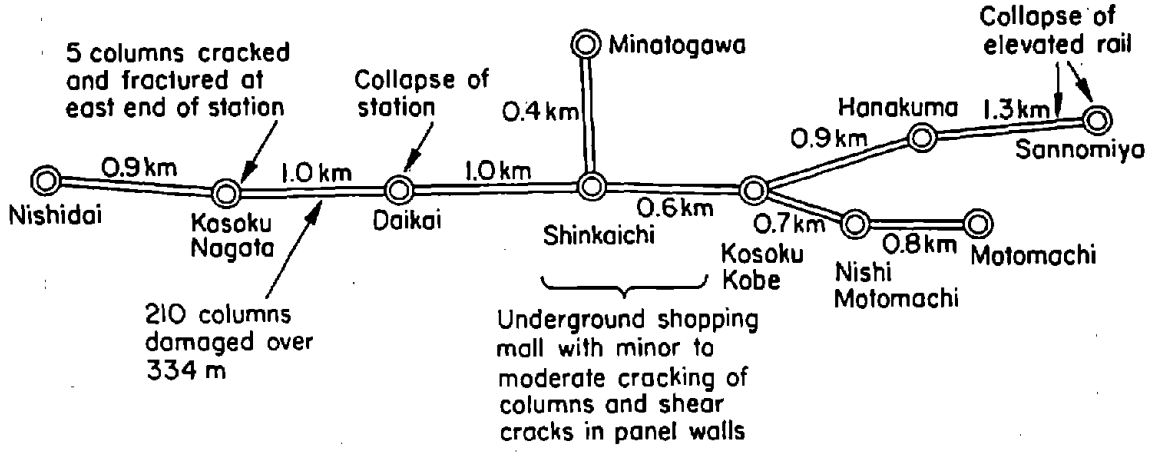

Figure 6.2: Map of Kobe rapid transit railway (Kobe Kosoku) showing locations of earthquake damage.

of the structure. The stratigraphy at the site consists of sands underlain by medium to stiff clay, with the water table at a depth of 3 m. The central reinforced concrete columns of the station failed, apparently by a combination of shear and vertical loading. There was only nominal confining steel (9 mm diameter on 180 mm spacing) for the 20 mm diameter longitudinal rebar on 140 mm centers in the concrete. Collapse of the columns caused subsidence at the street surface of a maximum 2.5 m, with substantial settlement over an area of 100 m by 20 m. Apart from the structural collapse-induced movement, there was no clear evidence of permanent ground deformation at the site induced by other causes, such as liquefaction.

This failure is highly significant because it is the first instance of severe earthquake damage to a modern tunnel for reasons other than fault displacement or instability near the portal. Photographs in Figures 6.3 through 6.5 show the interior portions of the collapsed station. The resulting subsidence at the street surface over the station can be seen in Figure 6.6. In addition to the station collapse, many pipelines and conduits in the street failed. It is noteworthy that two lifelines did not fail. A 400 mm welded steel gas pipeline, although substantially deformed, did not rupture or leak. In addition, an NTT fiber optic cable continued to provide a suitable signal despite severe distortion.

Between the Daikai and Nagata Stations, 210 reinforced concrete columns were cracked and deformed in the running tunnel. The reinforced concrete box structure of the running tunnel was approximately 6.4 m high, 9.0 m wide, and 5.2 m deep. The center columns of the running tunnel were similar to those at the Daikai Station. In addition, minor to moderate cracking of reinforced concrete columns and panel walls was observed in an underground shopping mall located adjacent to the Kobe Kosoku near Shinkaichi Station. Figures 6.7 and 6.8 show the typical damage within the shopping mall.

Damage to the Kobe Municipal Subway was less severe than that to the Kobe Kosoku. Train service in the Subway was restored one month after the earthquake, although Sannomiya Station remained closed because of structural damage to the center columns. Restoration of train service in the Kobe Kosoku is not expected to resume for more than a year after the earthquake.

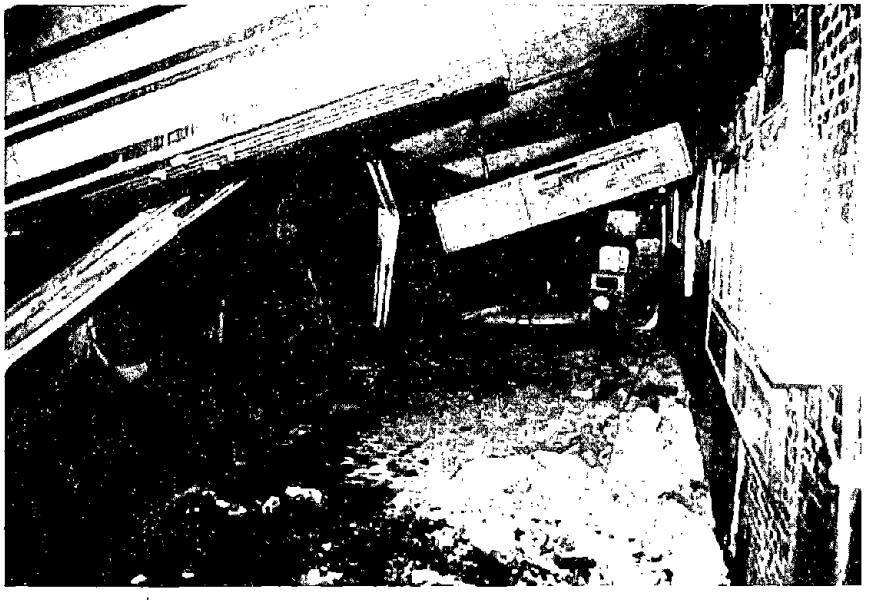

Figure 6.3: Collapsed subway roof at Daikai Station.

Figure 6.4: Collapsed reinforced concrete columns at Daikai Station.

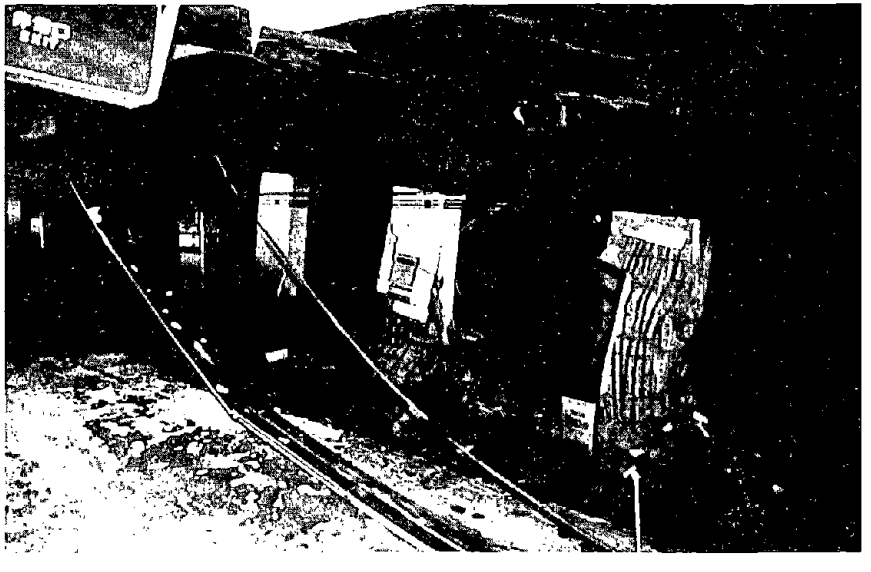

Figure 6.5: Same as Figure 6.4.

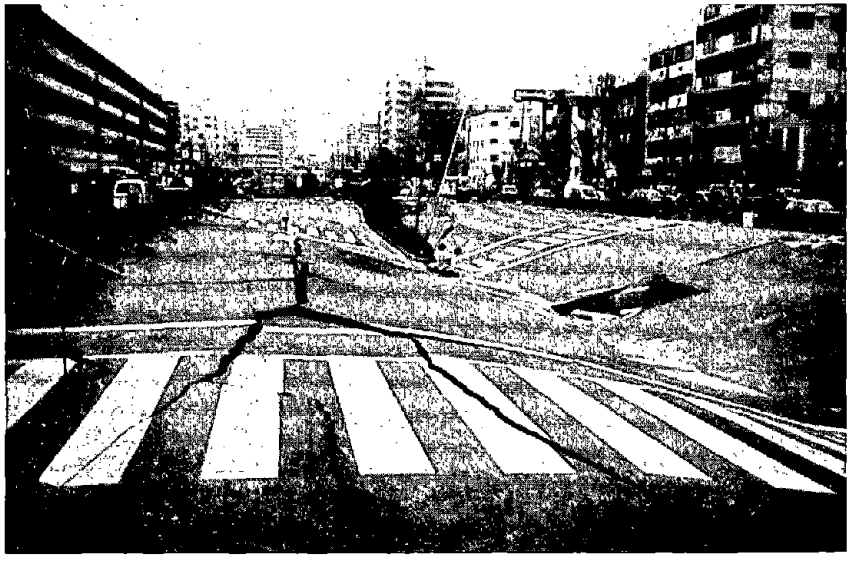

Figure 6.6: Collapsed street surface over Daikai Station.

Figure 6.7: Cracked reinforced concrete column in shopping mall adjacent to Kobe Kosoku.

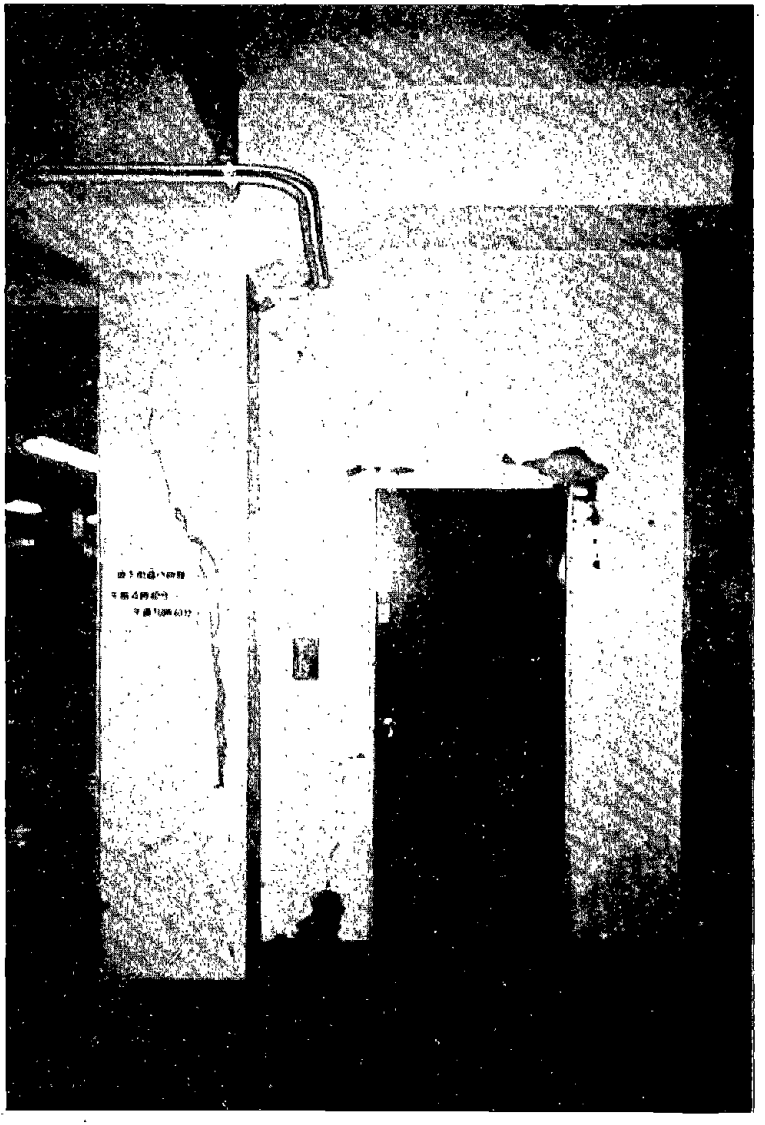

Figure 6.8: Shear cracks in column and partition wall at Kobe Kosoku shopping mall.

6.3 Water Supply

A map of the water distribution system operated by the Kobe Waterworks Bureau is shown in Figure 6.9. Approximately 75% of the water is taken from the Yodo River, and most of the remaining portion is obtained from a half dozen reservoirs throughout the area. Water from the Yodo River is treated at various purification plants and pumped to higher elevations through transmission tunnels and pipelines. There are 8 water purification plants and 57 km of transmission tunnels in the system. Minor to moderate damage was sustained at three purification plants. At the Uegahara Plant, ground deformation behind a retaining wall caused the joints to separate on three 1.5-m-diameter reinforced concrete pipelines which conveyed finished water from the plant. The Hanshin Water Authority purification plant, immediately adjacent to the Uegahara Plant, was affected by the Nigawa landslide which undermined the solids handling building.

Water conveyed to elevations in the hills and mountains north of Kobe is stored in water distribution reservoirs which include cast-in-place concrete, precast concrete, and welded steel construction and have an average capacity of 4,200 m^3. There are 119 distribution reservoir sites operated by the Kobe Waterworks Bureau, of which 86 provide water directly to Kobe City. Water is conveyed by gravity through pipelines to lower elevations. While only one reservoir, the Egeyama Reservoir, was damaged significantly as a result of the earthquake, a substantial amount of water was lost from the reservoirs because of broken and disengaged pipelines. Figure 6.10 is a graph showing the cumulative loss of reservoirs as a function of time after the earthquake. Between 6 and 24 hours after the earthquake, 86 reservoirs had emptied, leaving Kobe without critically needed water for fire fighting purposes.

There are 3,963 km of pipelines in the Kobe water supply and Table 6.1 summarizes the distances and relative percentages of each type of line. Approximately 86.3% of the system is composed of ductile iron pipelines, the great majority of which are equipped with standard mechanical joints that allow for relative rotation, but are not restrained against axial pullout. About 6% of the system is composed of ductile iron pipe with axially restrained mechanical joints. About 11% of the system is composed of cast iron and polyvinyl chloride (PVC).

Welded steel pipelines account for 2.7% of the system, and are used for high pressure trunk and transmission lines. The steel pipelines are constructed with full penetration butt welds, similar to gas and liquid fuel lines, to provide for earthquake resistant strength and ductility.

Table 6.1: Summary of lengths and relative percentages of different pipelines in the Kobe Water Supply.

Pipe Type	Pipe Length (km)	% of Total
Mechanical Joint	3180.2	80.3
Restrained Joint	237.3	6.0
Steel*	103.3	2.7
Cast Iron	315.9	7.9
PVC	126.4	3.1

* With full penetration circular butt welds

As of mid-February, 1995, there had been 778 repairs to distribution mains, and between one and two thousand were anticipated. There had been 3,084 instances of damage to services lines in public roads and 21,458 instances of similar damage on private property. Statistics compiled for a sample of 328 main repairs as of mid-February indicate that 41.5% of the repairs were because of pullout and ramming of pipeline joints, 16.2% associated with broken piping, 21% related to damaged hydrants and air valves, and 21.3% attributed to other causes.

Discussions with waterworks personnel indicate that pipeline damage in many instances was caused by permanent ground deformation related to liquefaction, landslides, and settlement of fill. The large percentage of repairs associated with pullout and ramming of joints implies a degree of axial deformation that the standard mechanical joints were not adequately designed to resist.

Until further investigations it is not possible to evaluate how specific patterns of permanent and transient ground motions influenced the integrity of the system. Nevertheless, it is possible to provide some general observations. Waterworks personnel have noted that bridge crossings of pipelines were especially vulnerable because of differential soil and bridge structure movements at abutments and deformations elsewhere along structural spans. Major trunk lines were damaged at the Port and Rokko Island Bridges. Furthermore, repairs at ductile iron pipelines with axially restrained mechanical joints appear to be low. There were no repairs to such pipelines on Rokko Island. In contrast, there were many repairs in ductile iron pipelines

with conventional mechanical joints on Port Island. Figure 6.11 shows damage to a 700-mm-diameter welded steel trunk line on Port Island. This pipeline was the major trunk line providing all potable water to Port Island. It failed at a welded joint in an area of lateral spread at the north side of the island.

6.4 Sewage Treatment Facilities

There are eight sewage treatment plants for Kobe City, five of which were functioning after the earthquake. Two additional plants were returned to service within one week after the earthquake. Major damage was sustained at the Higashinada Plant, which is located just north of the Kansai Electric Higashinada Power Station (Figure 3.1). The design capacity of the Higashinada Plant was about 225,000 m^3 of raw sewage per day. The oldest portions of the plant are 33 years old. Construction of the plant was started in 1962 shortly after the placement of fill for Uozaki Hama-cho was completed. It is anticipated that the plant will be closed for over a year until repairs are made.

Figure 6.12 is a map of the Higashinada Plant, and soil profiles for the borings shown on the map are presented in Figure 6.13. There was severe liquefaction-induced damage at the plant. Maximum lateral movement of the seawall north of the canal was approximately 1 m. Maximum lateral movement of the seawall south of the canal was roughly 2 m. Lateral displacement and settlement ruptured the inverted siphon at the plant (Figure 6.14) and caused separation of the main sewage treatment conduit through which raw sewage was conveyed (Figure 6.15). Because of the loss of the siphon, sewage was being dumped directly into the canal, which was screened by a temporary cofferdam at its eastern and western ends to create a temporary basin for primary sedimentation.

Lateral deformation caused severe damage to underground structures and facilities founded on spread footings (Figure 6.16). Differential settlement of approximately 600 mm of soil relative to the pile supported sand filter building was observed (see Figure 6.17); and there was cracking and spalling at the tops of reinforced concrete piles which support this structure. Elsewhere, at the digester tanks closest to the canal, cracking at the tops of reinforced concrete piles was visible at several pits excavated to inspect the foundations.

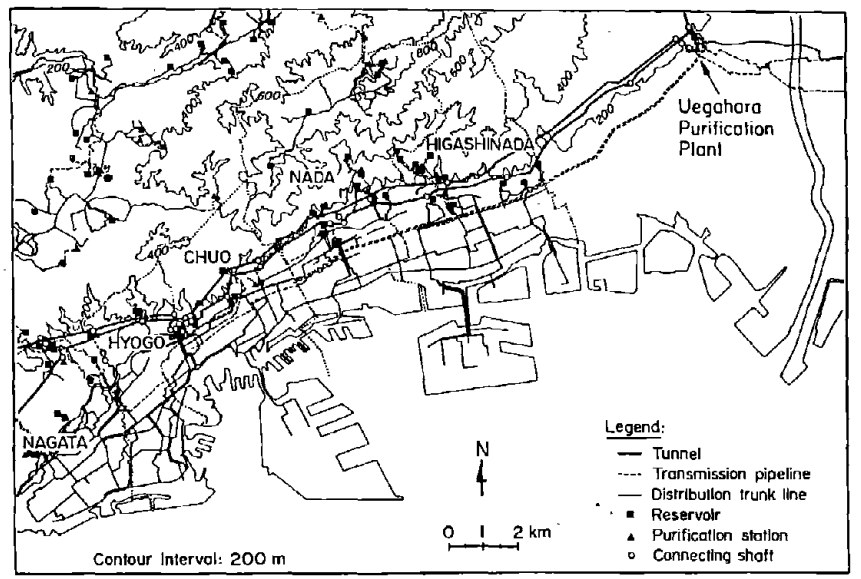

Figure 6.9: Map of Kobe Water Distribution System.

Figure 6.11: Weld rupture of 700-mm-diameter steel water trunk main on Port Island.

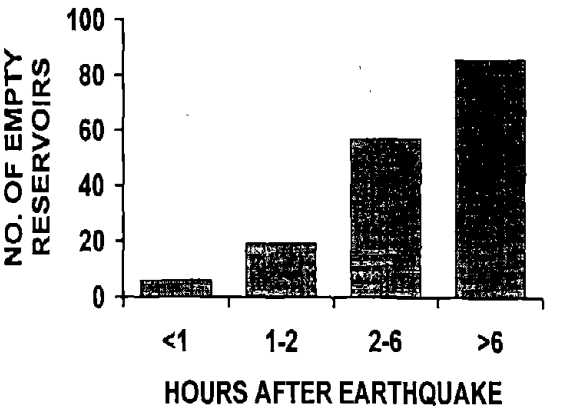

Figure 6.10: Bar graph of cumulative reservoir loss as a function of time after the earthquake.

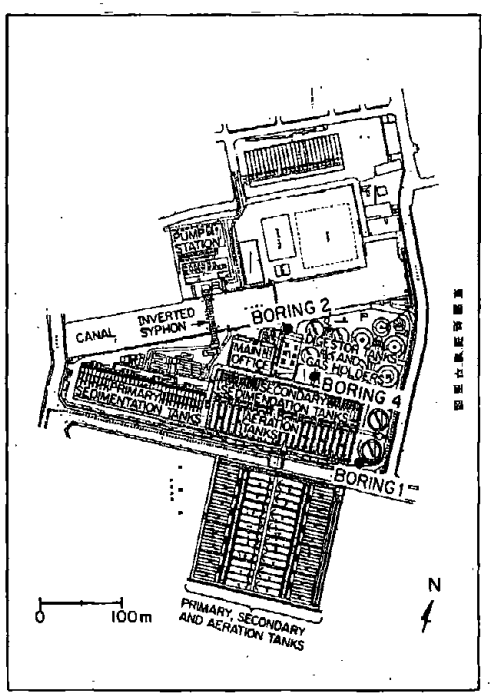

Figure 6.12: Map of Higashinada Sewage Treatment Plant.

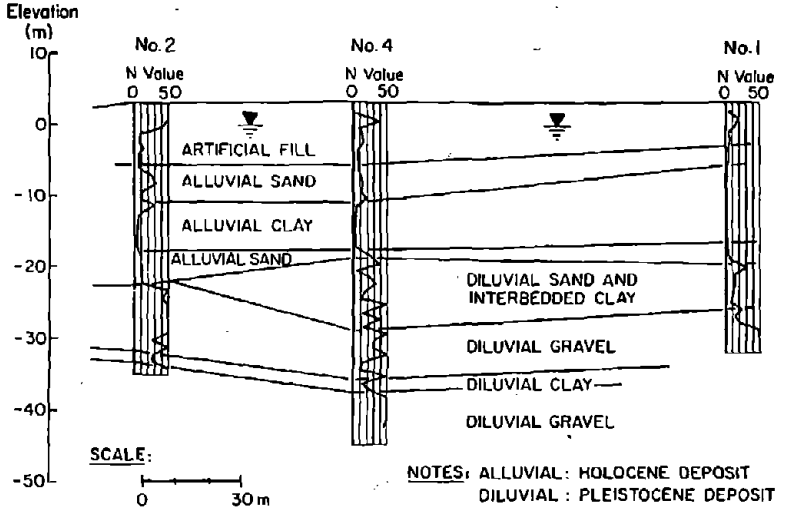

Figure 6.13: Soil profile at Higashinada Sewage Treatment Plant.

Figure 6.14: Severe lateral displacement at the inverted siphon of the plant. The pressurized pipeline siphon carried all sewage treated by the plant.

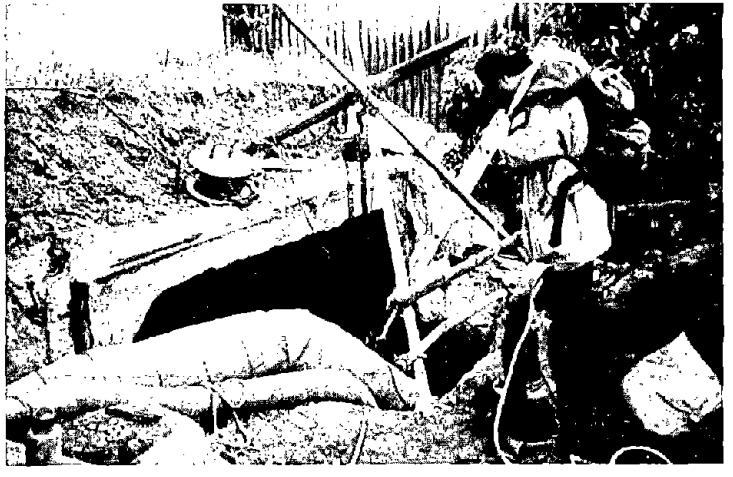

Figure 6.15: Rupture of the main sewage treatment conduit caused by lateral spreading and settlement.

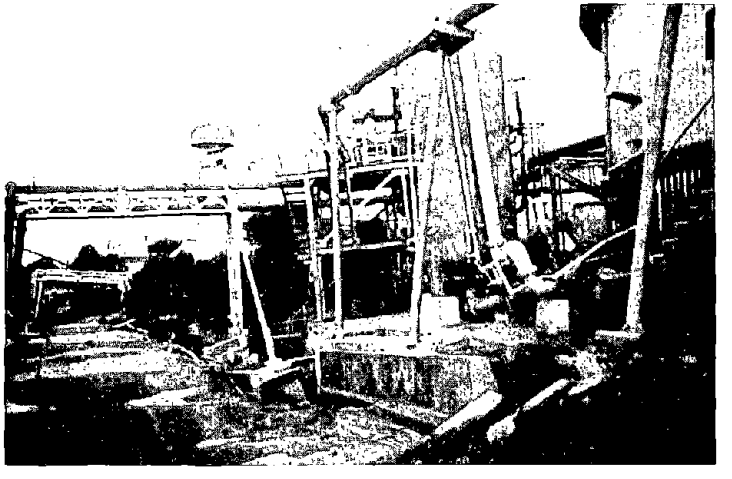

Figure 6.16: Plant facility damage due to lateral ground deformation and settlement.

The primary and secondary sedimentation and aeration tanks closest to the canal were supported on reinforced concrete piles. The primary sedimentation tank was 8 m deep so that the lengths of piles in the liquefied fill were relatively small. Very little damage was observed in this tank. The secondary sedimentation and aeration tanks were approximately 4 m deep, and consequently there were 4 m of additional pile length subject to liquefaction and lateral deformation beneath these facilities and there was significant damage. Figure 6.18 shows the collapse of sludge scrapers in the secondary sedimentation tanks, and Figure 6.19 shows the separations in the reinforced concrete walls of the aeration tanks. These separations have proven to be exceptionally difficult to repair because of flooding of the tanks by infiltrating groundwater. Plans call for the complete replacement of the damaged tanks.

6.5 Gas Delivery System

The gas delivery system for Kobe and surrounding communities is provided by the Osaka Gas Company. The company supplies gas in the Osaka Bay region to 5.7 million metered customers. A map of the Osaka gas pipelines with the highest internal pressures is shown in Figure 6.20. There are approximately 400 km of high pressure pipelines in the system, carrying pressure exceeding 1.95 MPa. There is a similar distance of medium pressure "A" lines with internal pressure between 0.3 and 1.0 MPa, which are also shown in Figure 6.20. Osaka Gas also operates medium pressure "B" lines at 0.1 to 0.3 MPa which are not shown in the figure. The low pressure distribution mains in the system operate at a pressure equivalent to about 20 cm of water column.

The medium pressure A and B lines are composed predominantly of welded steel and ductile iron pipe with mechanical joints. In the Kobe area, the low pressure gas lines were composed predominantly of steel with threaded couplings. The total distance of transmission, trunk, and distribution mains in the Osaka Gas system is 49,430 km. There was no significantdamage reported at the LNG terminals, and no damage reported in the high pressure welded steel pipelines. Minor damage was reported in the medium pressure A lines, and the combined number of repairs in both medium pressure A and B lines was approximately 106.

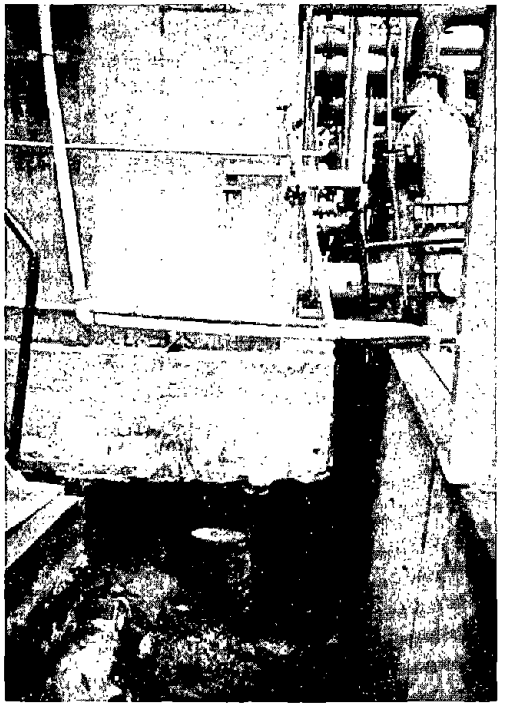

Figure 6.17: Differential settlement of soil relative to pile-supported structure containing sand filters.

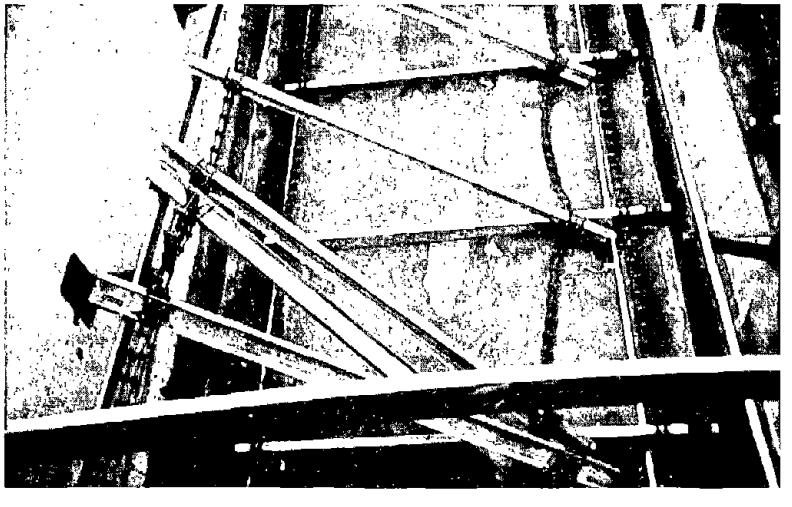

Figure 6.18: Damage to sludge scrapers at the sedimentation tanks.

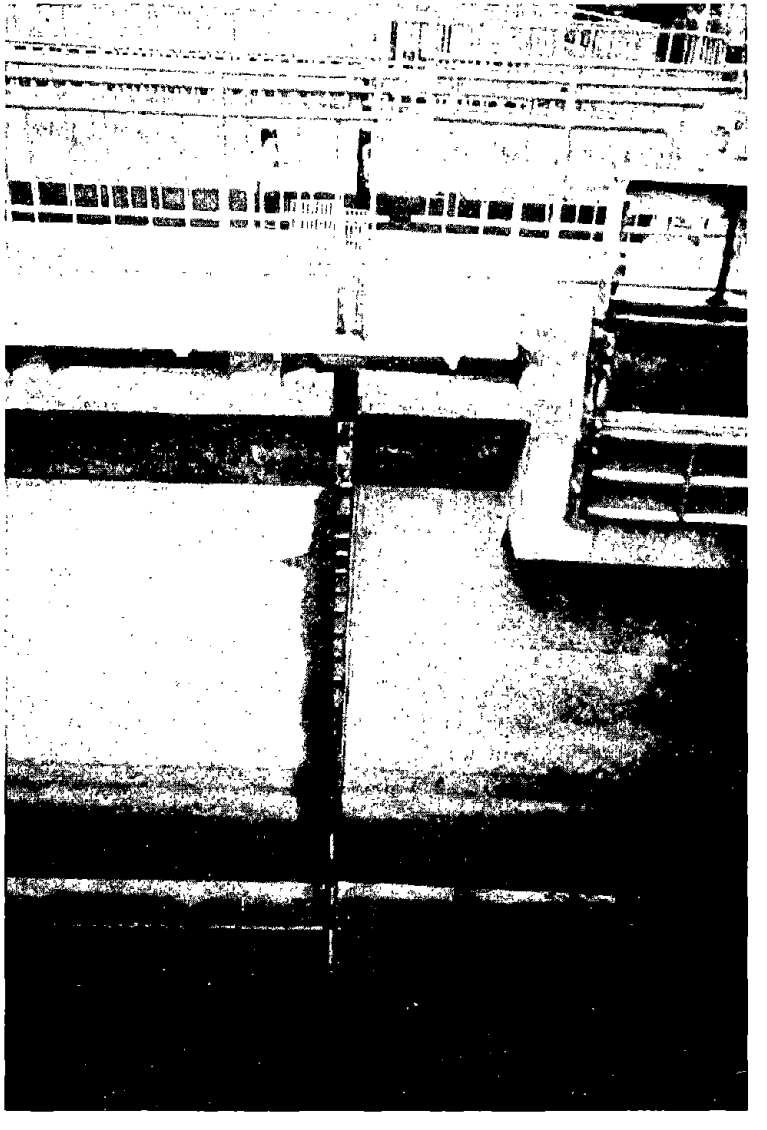

Figure 6.19: Separations in the reinforced concrete walls of the aeration tanks.

The principal source of damage was to threaded steel low pressure pipelines, where thousands of repairs are anticipated. Osaka Gas personnel noted that many of the repairs were at locations of permanent ground deformation caused by soil liquefaction and landslides, as illustrated in Figures 6.21 and 6.22. After the earthquake, the gas supply in the distribution system was shut off for 857,000 customers. Full restoration of service required 3 to 4 months.

6.6 Damage to Electrical Utilities and Phone Lines

Compared to the damage experienced by the water and gas delivery systems, the damage to electrical lines and phone lines had a much lesser impact. While collapsed concrete overhead utility poles were apparent in a number of locations, in general, phone and electricity were restored in a very short period of time to most of the damaged area. Even in the areas of extreme liquefaction and lateral spreading, electricity and phones were generally functioning within a few days of the earthquake, although water, gas, and sewer services were not available. This pattern of damage seems to suggest that underground electrical conduits tend to perform better, although isolated breaks in high voltage conduits did occur, such as shown in Figures 6.23 and 6.24.

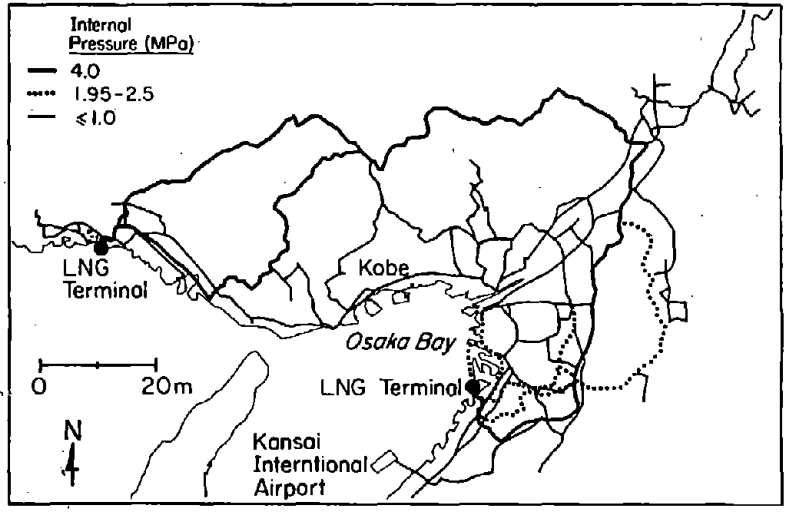

Figure 6.20: Map of high pressure transmission and medium pressure trunk lines operated by the Osaka gas company.

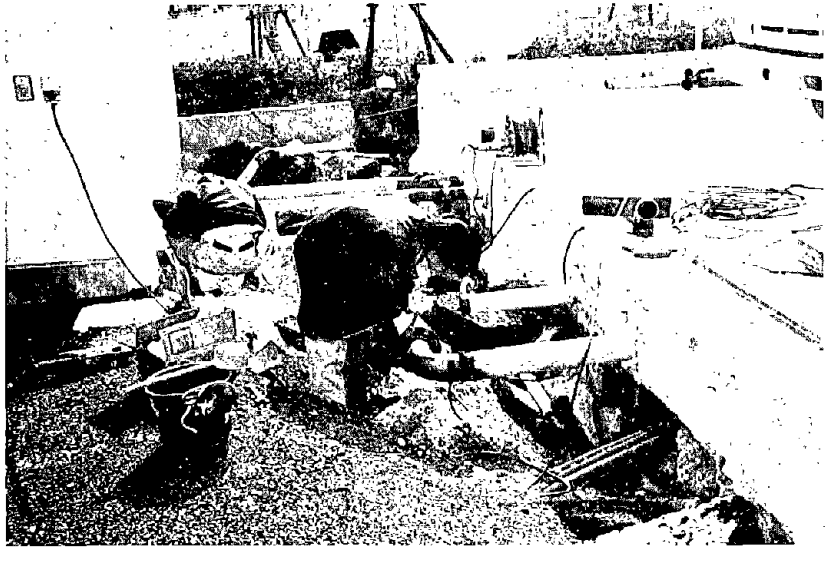

Figure 6.21: Repair of pipes separated by lateral spreading between a building and adjacent concrete slab near Nakahara Wharf, Port Island.

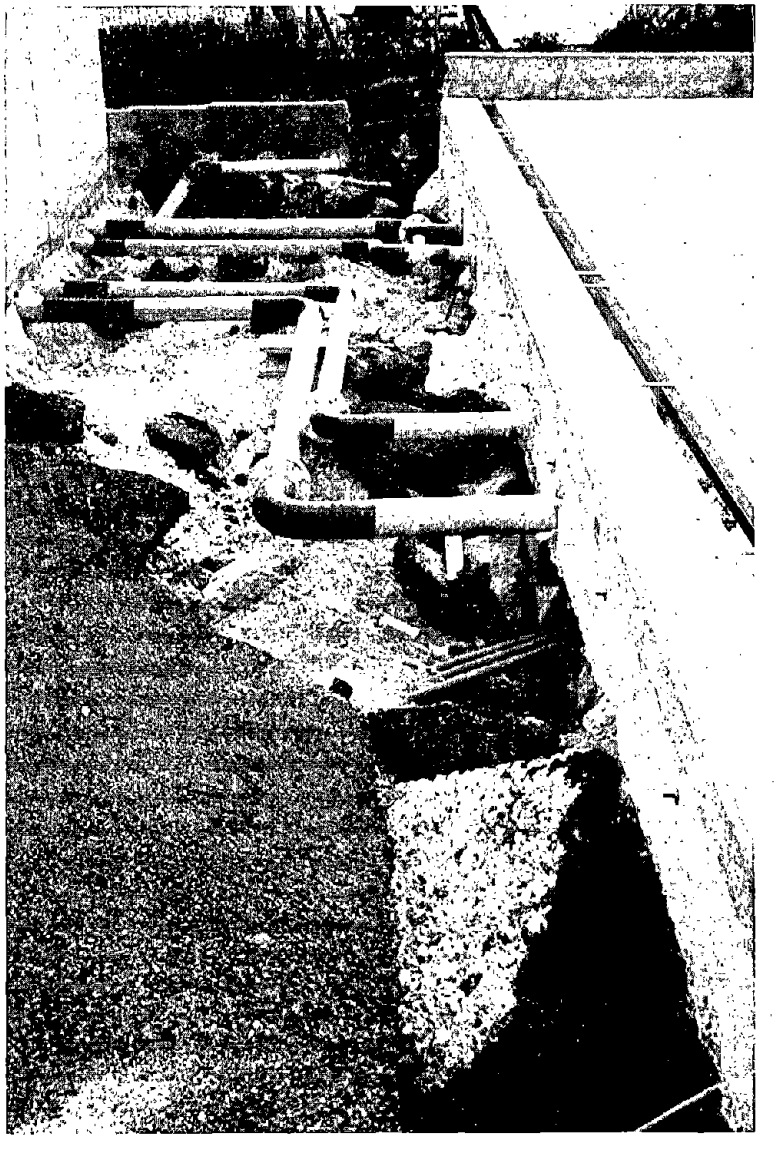

Figure 6.22: Repaired pipes near Nakahara Wharf, Port Island. Prior to earthquake pipes followed a straight path between slabs.

Figure 6.23: Rupture of 6 KV electric cable conduit in Kobe City. (Dr. T. Holzer in photo).

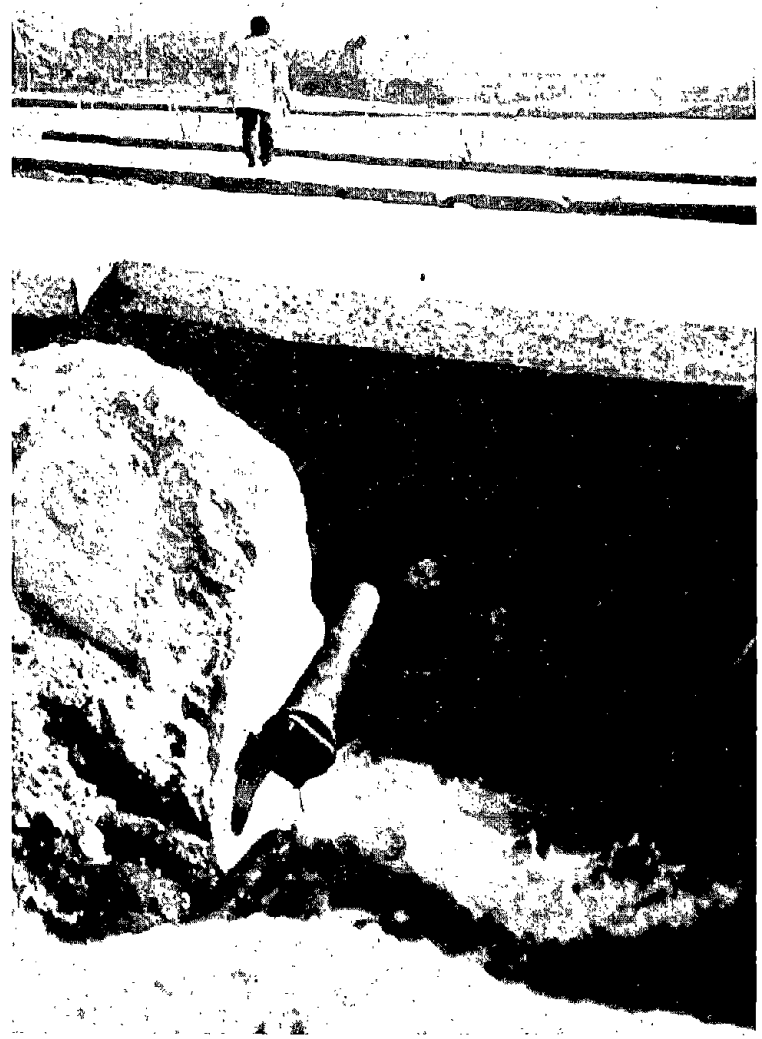

Figure 6.24: Rupture of electric conduit caused by seawall deformation adjacent to north side of Kobe Port Island Bridge.

CHAPTER SEVEN: SLOPES, RETAINING STRUCTURES, AND LANDFILLS

7.1 Landslides and Rockfalls

7.1.1 Introduction

The topography of the region to the north of downtown Kobe, and to the north of the Osaka Bay in general, rises rapidly into the Rokko Mountains, reaching an elevation of 930 m at the highest point. This terrain is generally characterized by relatively steep slopes and short steep valleys. The main rock type in the area is granite, which is deepely weathered and decomposed to saprolite to a considerable depth. The decomposed granite is susceptible to rock falls and debris flows, and the hillslopes show numerous scars from slope failures, as can be seen in the aerial view of the hills shown in Figure 7.1. Most of these scars were apparently caused by rainfall-induced debris flows, and, for the most part, only minor ravelling and rockfalls were reported as a result of the earthquake. Nevertheless, one large flow slide did occur in the decomposed granite in a residential area in the Nigawa district of Nishinomiya, northeast of Kobe. This slide killed 34 people and caused extensive property damage. In addition, considerable damage also occured due to movement of structural fills in residential areas on hillsides, particularly along the projection of the strike of the earthquake fault, and isolated rockfalls also caused localized damage.

7.1.2 Nigawa Landslide

The Nigawa landslide appears to have been a rapidly moving debris slide in decomposed granite. The slide occurred immediately adjacent to the Uegahara filtration plant, along the edge of a large terrace/bench at an elevation of about 100 m. The aerial view of the site in Figure 7.2 shows the head scarp of the slide and most of the deposition area at the toe. Figure 7.3 shows the evidence of runup of the the debris on a building at the base of the slope (second from the bottom left in Figure 7.2). The length of the head scarp was approximately 100 m and the the distance from the headscarp to the toe of the slide was about 250 m, with a vertical drop on the order of 30 to 40 m.

The failed portion of the terrace appears to have been a part of a cut-and-fill extension of a pre-existing natural ridge and saddle, and the mobilized material seemed to be a combination of decomposed granite fill and intact saprolite. The presence of fill was evident along the headscarp which undermined a building, exposing its pile foundation (Figure 7.4). The upper portion of the slope was heavily wooded, and a housing development was built along a series of terraced slopes starting about 15 to 20 m below the crest of the slope. As can be seen from the photographs, the houses in the path of the slide mass were completely obliterated and buried by the slide debris.

The flow like nature of the slide was evident from well-defined levees as high as 6-8 m along the flanks of the slide mass in the lower part of the slope, and the slide debris flowed down a creek bed at the toe of the slope for some distance. The role of water in the mobilization of the slide could not be immediately ascertained. The landslide debris, decomposed granite composed primarily of sand with some fines and some coarser material, appeared to be relatively dry on the surface immediately following the failure. However, wet seep areas became evident with time, at an elevation approximately equivalent to the base of the wooded slope, and the landslide debris was too soft to walk on in those areas.

7.1.3 Rock Falls

Isolated rock falls occurred from natural and cut slopes in the residential area of Nishinomiya. The natural weathering of the granitic rocks leads to the exposure of isolated, rounded granitic boulders precariously perched on the hillslopes. Once loose, they tend to roll downhill quite easily. A boulder approximately 3 m in diameter descended several tens of meters down a wooded slope, crossed a paved road, and crushed a mid-size car and damaged a wrought iron gate at an entrance to a residence (Figures 7.5 and 7.6). At another location, smaller rocks fell from a cut slope behind a residential building, but did not cause any damage because the slope support system was designed to deflect falling rock (Figures 7.7).

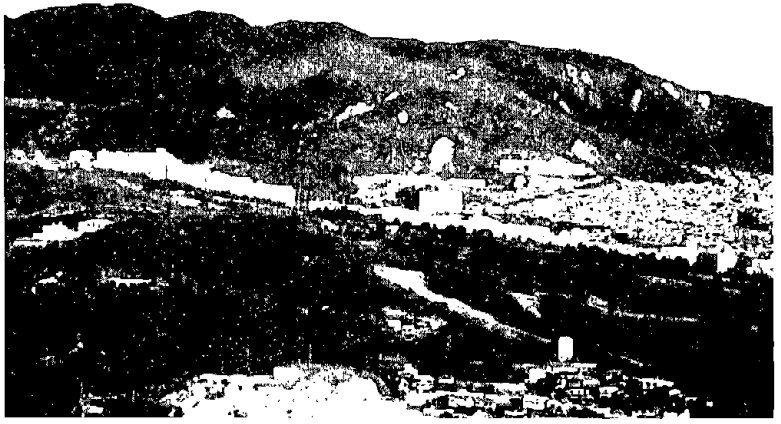

Figure 7.1: Aerial view of the landslide scars in the hills north of Kobe.

Figure 7.2: Aerial view of the Nigawa landslide showing the steep arcuate head scarp and a flatter depositional area at the toe.

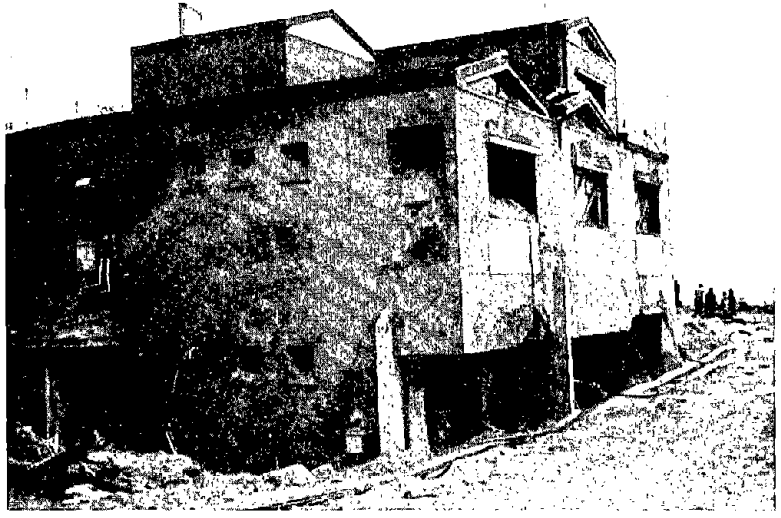

Figure 7.3: Debris stained 3 story building at the toe of the slide (the building is second from the left at the bottom of the photograph in Figure 7.2). Note that the debris invaded the structure without causing extensive structural damage to the exterior walls.

Figure 7.4: Head scarp of the Nigawa landslide. The stratification of soil below the pavement suggests that this upper material is fill. The foundation of the building is pile supported.

7.2 Embankments and Structural Fills

Localized failures of railroad and road embankments occurred throughout the region. In many instances these failures appeared to be directly related to liquefaction of the foundation soil, but more traditional slope failures were also evident. Figure 7.8 shows a typical failure of an embankment above railroad tracks. The slope was initially supported by a low wall, which is now being replaced by a driven steel pile wall. This method of repair was extensively used by the railroads in the wake of the earthquake.

Evidence of downhill extension and displacement of structural fills and stone retaining walls was particularly evident in parts of residential developments extending into the hills. The incidence of these failures seemed to be highest along the extension of the strike of the faulting, and typically involved sidehill fills for roads and residential lots. The fills appeared to be composed of compacted decomposed granite, which is relatively coarse with little apparent cohesion. The deformation of the fills caused displacement and cracking of pavements and retaining walls (Figure 7.9), and in at least one location a road embankment essentially failed leaving the road unservicable (Figure 7.10). The damage to some of the residential lots is illustrated in (Figure 7.11), showing deep extension cracks running parallel to the slope contours. The failures of the fills appeared to be the result of a combination of inadequate compaction and inadequate keying into the bedrock, and the retaining walls lacked adequate capacity to resist seismic loading (Figure 7.12). In addition to structural damage, these failures broke underground utilities, disrupting gas, sewer, and water service to entire neighbourhoods.

In comparison to the residential construction, many large retaining structures for major roads and railways seemed to perform much better. Figures 7.13 and 7.14 show two fairly substantial retaining walls which performed well and showed no apparent signs of distress.

7.3 Reinforced Soil Walls

Three geogrid reinforced soils walls of the type developed by Tatsuoka et al. (1992) were visited; namely, the walls at Tanata, Amagasaki, and Tsukamoto, located as shown on Figure 7.15. Each of these walls was constructed for support of railway lines. The seismic intensities at stations

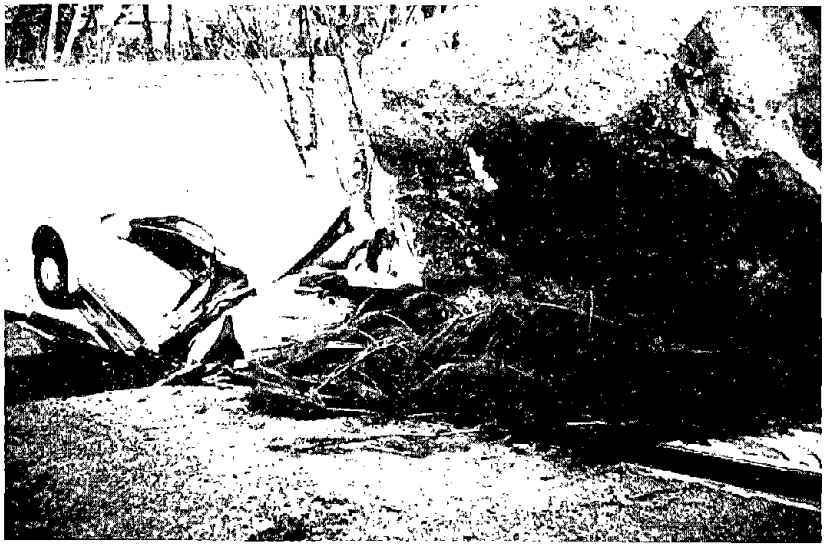

Figure 7.5: A car was flattened by this boulder, approximately 3m in diameter, the largest of several which rolled down the hillslope.

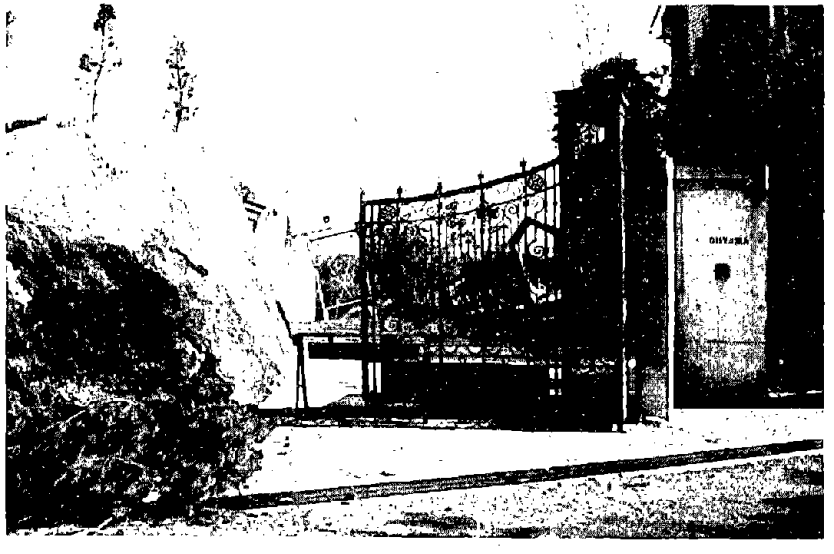

Figure 7.6: A view of the boulder shown in Figure 7.5 resting against the gate at the entrance to a driveway.

Figure 7.7: Freshly fallen rock at the basee of a retaining wall in a residential area.

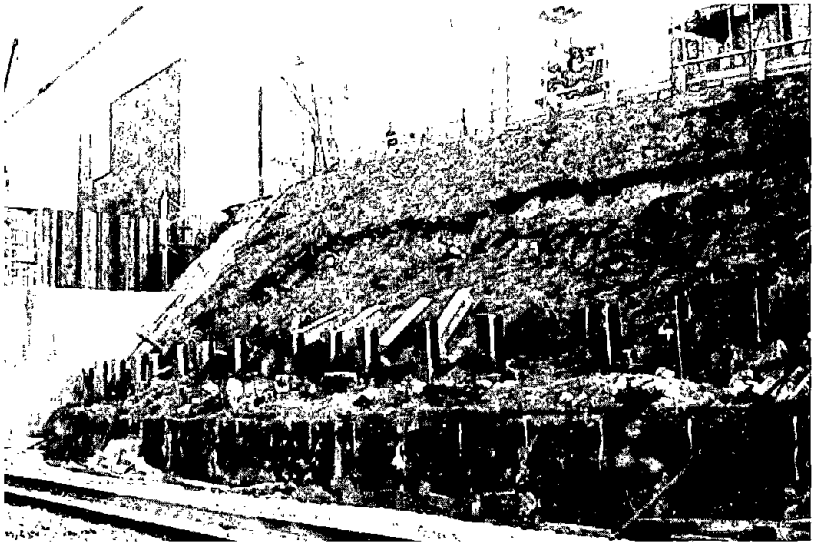

Figure 7.8: Failure of an embankment above railroad tracks in Kobe.

Figure 7.10 A road fill settled and moved laterally several meters.

Figure 7.9: Pavement deformation and damage to rock retaining wall caused by seismically induced deformation of sidehill fill.

Figure 7.11: Deep tension cracks in a sidehill fill on a residential lot. Note the separation in the rock retaining wall in the background. This type of damage was typical in this neighborhood.

close to each of these walls are shown on the figure. A comprehensive report on the performance of these walls is in preparation by Tatsuoka et al. (1995). The Tanata wall was subjected to particularly high ground accelerations; i.e., more than 0.4g in the NS direction, nearly 0.8g in the EW direction, and almost 0.4g in the vertical direction.

A standardized design and construction procedure for permanent geosynthetic-reinforced walls with a full-height rigid facing panels has been developed by the University of Tokyo and the Railway Technical Railway Research Institute of the Japan Railways Group. These walls are referred to as GRS-RW walls. The construction procedure follows the sequence shown in Figure 7.16 and the pseudostatic seismic design is used, assuming a horizontal inertial acceleration of 0.2g.

There was no apparent damage to the walls or measurable displacements at Amagasaki or Tsukamoto, although there was some evidence that there may have been hairline cracking along the surface of the backfill at the Amagasaki wall at a distance about equal to the reinforcement length behind the face of the wall. It should be noted that in both of these areas there was little damage to other structures as well.

The Tanata wall (Figure 7.17) is located between the Ashiya and Setsu-Motoyama JR stations, near the slide shown in Figure 7.8. The wall is somewhat more than 6 m high, with PVC fiber grid reinforcements 2.5 m in length, and cohesionless backfill. A typical cross section is shown in Figure 7.18. The reinforced soil wall is founded directly on the original ground without deep foundation support. Nonetheless, the wall retained its stability, with outward deformations of about 22 cm at the top and 10 cm at the base (Figure 7.19). According to Tatsuoka et al. (1995) several reinforcement layers near the top of the wall could not be extended to the full design length owing to construction limitations, and this may have resulted in the tilting being greater that it might have been otherwise. There was settlement of all four sets of railroad tracks running along the embankment above caused by the dynamic loading; however, the track located above the reinforced backfill settled the least.

Some minor spalling of the concrete facing panels was noted near the top at a construction joint, it appeared that the joint width may have opened to about 2 cm, and some hairline cracking was noted that is suggestive of longitudinal shear in the panels. However, given the extensive

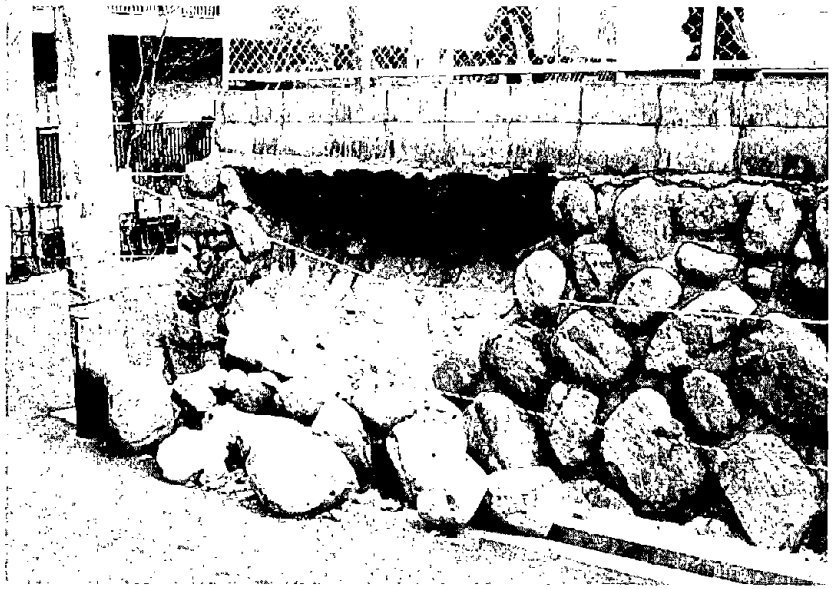

Figure 7.12: Typical failure of a stone retaining wall in a residential area.

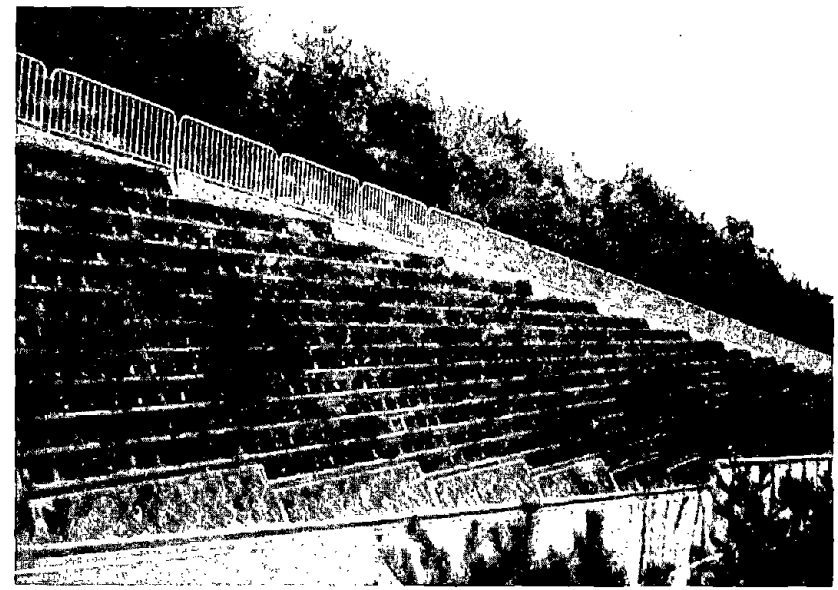

Figure 7.13: Undamaged crib retaining structure in Ashiya.

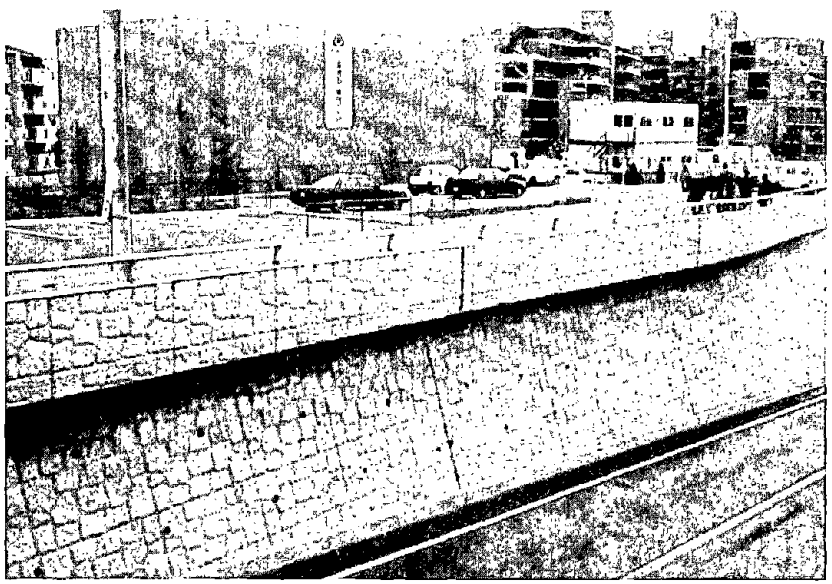

Figure 7.14: Undamaged reinforced earth wall supporting a roadway in Ashiya.

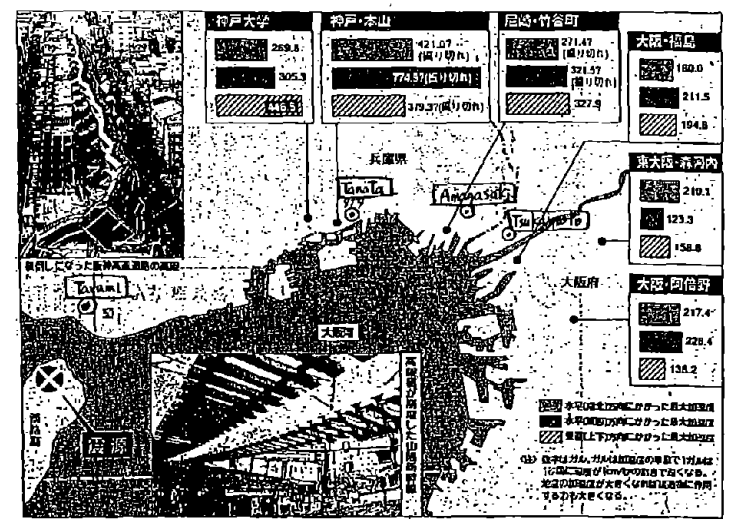

Figure 7.15: Location of Geosynthetic Reinforced Soil Walls (GRS-RW) and nearby seismic intensities (from Tatsuoka et al. 1995).

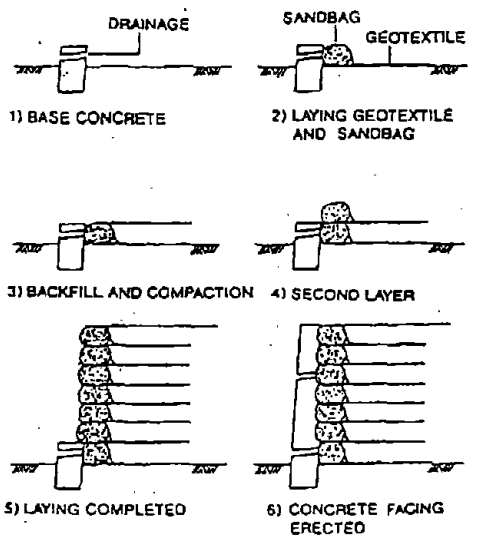

Figure 7.16: Standard construction procedure for GRS-RW wall systems (from Tatsuoka, undated).

Figure 7.17: Post-earthquake view of the Tanata GRS-RW wall.

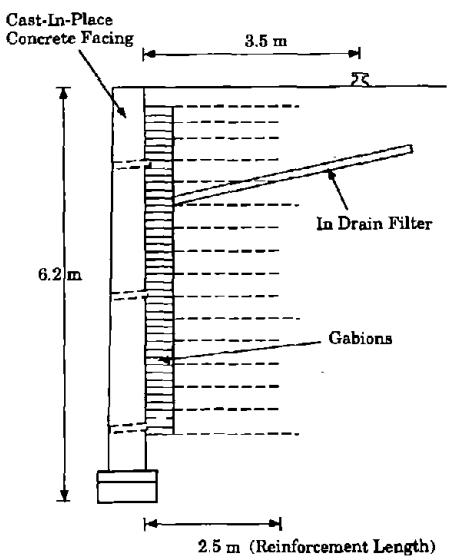

Figure 7.18: Cross-section of the GRS-RW at Tanata (from Tatsuoka et al., 1995).

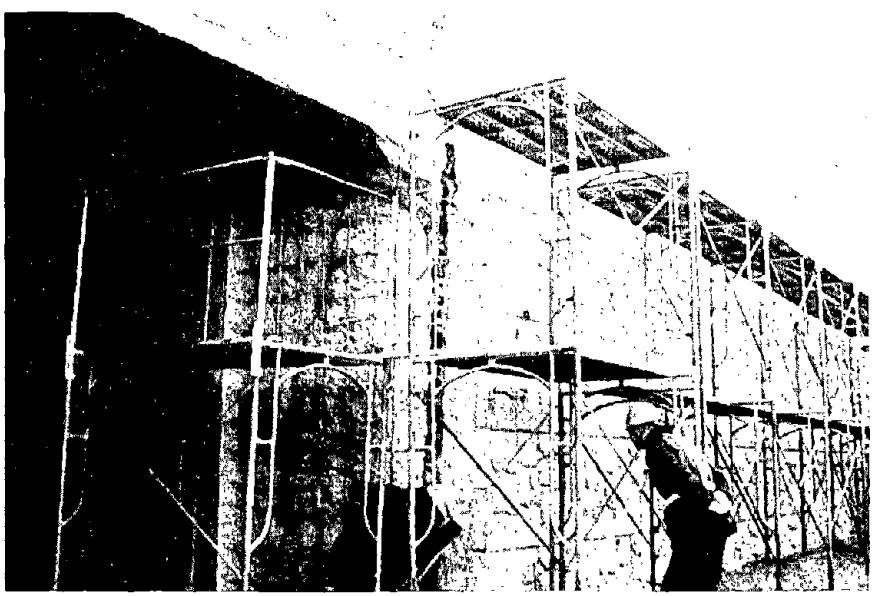

Figure 7.19: Evidence of outward rotation and displacement of the Tanata GRS-RW wall, about 20 cm at the toe and about 10 cm near the base.

damage in the area (most of the buildings directly across the street from the wall had or were heavily damaged collapsed, as seen in Figure 7.17), the GRS-RW demonstrated excellent seismic resistance.

The Tanata GRS-SR wall adjoins a more conventional reinforced concrete cantilever wall which extends to the west (left) of the underpass shown in Figure 7.19. This conventional concrete wall is supported on 6 m deep, 1.2 m diameter cast-in-place reinforced concrete piers. The wall appeared outwardly undamaged, although it displaced laterally on the order of 27 cm at the top and 10 cm at the base (Figure 7.20).

In addition to these walls, which were inspected on foot, two mechanically stabilized walls under construction were seen from the air on Awaji Island at the approaches to the new Akashi Kaikyo Bridge (Figure 7.21). No apparent distress was visible from the air. These walls should provide an excellent opportunity for further study, since they presumably represent the current state-of-the-art.

7.4 Solid Waste Fills

Documenting the seismic performance of solid waste landfills is important to US practice as the Code of Federal Regulations(United States, 1991) requires that landfills located in seismic impact zones be designed to resist earthquake hazards, yet well-documented case histories which could provide insight are lacking. Recent earthquakes, such as the 1989 Loma Prieta and 1994 Northridge earthquakes, are providing some useful case records, but additional case records are needed. With this in mind, a few solid waste landfills located in the Kobe/Osaka area were surveyed. Unfortunately, detailed landfill geometry and waste fill characteristics are not currently available, and it appears that these landfills are not similar to US waste fills (i.e. due to aggressive recycling efforts, the Japanese waste is relatively inert compared to US waste, and, consequently, containment and gas collection systems are not designed at current USEPA Subtitle D standards).

There were a number of temporary waste fills located on newly reclaimed land in Osaka Bay just south of Nishinomiya, but these fills appeared to be set up only to burn and to dispose of construction debris being cleared from the damaged areas following the earthquake (Fig. 7.22).

Figure 7.20: Reinforced concrete cantilever wall adjacent to the Tanata GRS-RW wall. Note the outward displacement of about 10 cm.

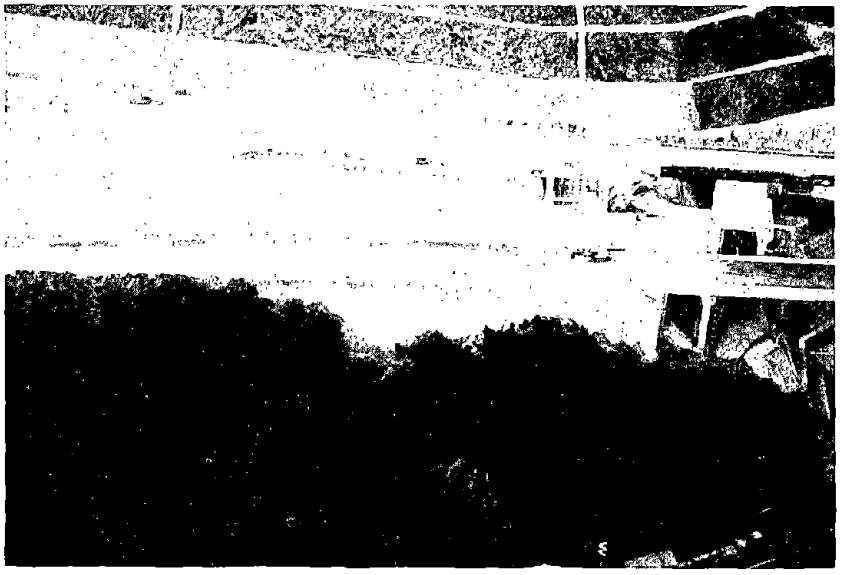

Figure 7.21: Aerial view of mechanically stabilized walls on the approach to the Awaji Island Bridge on Awaji Island.

Figure 7.22: Burning and disposal of debris on reclaimed island south of Nishinomiya.

Two existing large waste fills further to the east were surveyed. The first waste fill (shown in Fig. 7.23) is located west of downtown Osaka on a reclaimed island about 20 km from the zone of energy release. This fill was inspected from the air. Several ground cracks, which were tens of meters long and a few centimeters wide, were identified near the southwest corner of the island. The series of north-south trending cracks appeared to have resulted from ground displacement toward the edges of the island. No evidence of liquefaction was observed, but it would not take much lateral spreading to develop these cracks. Similar ground distress was identified at the second solid waste landfill (shown in Fig. 7.24) which is sited atop a reclaimed island located at the southern tip of the Yodo River, about 12 km from the zone of energy release. A series of ground cracks occurred at the southwest corner of this landfill, which is reportedly lined with a geosynthetic material. One of the larger cracks is shown in Figure 7.25. The width of this crack was roughly 2 to 6 cm with a minor vertical displacement. It cut across the southwest corner of the reclaimed island and appeared to have resulted from lateral movements toward the edges of the island. Other, less continuous, cracks were located to the east of this crack near the southern edge of the island. Surficial evidence of liquefaction in the form of sand boils with ejected garbage was found on this island. Thus, lateral spreading associated with softening of the dumped soil fills could have easily produced the surface cracks noted. However, there was no evidence of any compromise of the waste containment systems at these waste fills.

In summary, waste fill performance was dominated by the sites selected for the surveyed landfills. These sites were reclaimed ground constructed by methods similar to those discussed previously in Chapter 3 which experienced ground cracking resulting from liquefaction-induced lateral spreading. It appears that lateral spreading of the underlying saturated cohesionless fills produced the observed ground cracking. These case records illustrate the potential problems associated with waste fills constructed on ground susceptible to liquefaction.

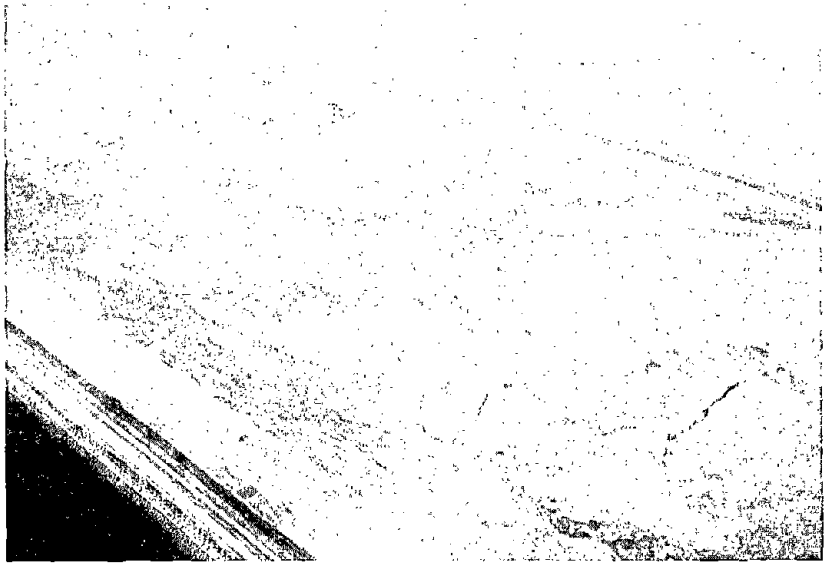

Figure 7.23: Ground cracks (lower right) at waste fill site west of Osaka.

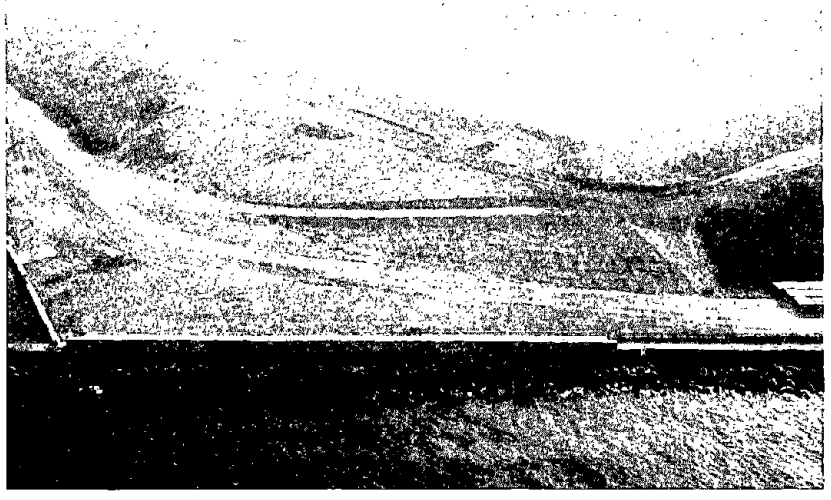

Figure 7.24: Overview of waste fill site at southern tip of the Yodo River.

Figure 7.25: Close-up view of a ground crack in the southwest corner to the right of the site shown in Figure 7.22.

CHAPTER EIGHT: SUMMARY AND CONCLUSIONS

The Hyogoken-Nanbu Earthquake of January 17, 1995, with a JMA magnitude of 7.2 and epicenter about 20 km southwest of downtown Kobe, devastated the city of Kobe, its port, and adjacent areas. As of March 31, 1995, the toll from the earthquake has reached over 5,500 dead and over 26,000 injured. More than 200,000 houses, about 10% of all houses in the Hyogo prefecture, were damaged, including more than 80,000 collapsed, 70,000 severely damaged, and 7,000 consumed by fire (AIJ, 1995). Current estimates of losses in Kobe are about 20 trillion yen (200 billion dollars), one order of magnitude larger than that from the January 17, 1994, Northridge Earthquake.

In addition, the damage to the infrastructure, lifelines, and the port had a large economic impact extending well beyond the immediately affected area. Before the earthquake, Kobe was Japan's busiest and the second largest port after Yokohama. About 39% of the city's gross industrial product was derived from port related industries, accounting for more than 17% of the city work force. The earthquake damage caused essentially total shutdown of all facilities in the port area for several weeks following the earthquake and the full recovery of the port is still in the future.

A combination of factors contributed significantly to the severity of much of the damage: the area had been previously considered to have relatively low seismic risk, the projected location of the release of energy along the earthquake fault was almost immediately below a densely developed urban area, and the geologic setting of the region, on the shores of a large embayment, provided for a substantial thickness and areal distribution of liquefiable sediments and fills. Most importantly, however, the area affected by the 1995 Hyogoken-Nanbu Earthquake has many similarities, in terms of geologic setting and the level of development, to other locations around the world. Therefore, much can be learned about the type and the extent of damage that can occur when a major fault ruptures through an urban environment.

8.1 Geoscience and Strong Motions

The earthquake occurred in a region with a complex system of previously mapped active faults. The focal mechanism of the earthquake indicates right-lateral strike-slip faulting on a nearly vertical fault striking slightly east of northeast, parallel to the strike of the mapped faults. The earthquake produced a surface rupture with an average right-lateral horizontal displacement of 1 to 1.5 m and a maximum recorded horizontal displacement of 1.7 m on the Nojima fault, which runs along the northwest shore of Awaji Island. Vertical displacement across the observed surface rupture of the Nojima fault varied considerably with an average vertical displacement of 0.5 to 1 m (east side up) and a maximum vertical displacement of 1.3 m (east side up). At the southern end of the exposed ground rupture, the observed vertical displacement decreased and was actually in the opposite sense, with the west side moving up slightly (<0.2 m) with respect to the east side. Currently available evidence does not suggest any major differences between the source characteristics of the Kobe earthquake and those of crustal earthquakes that occur in California.

Peak ground accelerations as large as 0.8 g were recorded in the near-fault region on alluvial sites in Kobe and Nishinomiya. The recordings at near-field rock sites typically had significantly lower magnitudes of peak ground acceleration (i.e. around 0.3 g). The vertical peak ground accelerations were generally about two-thirds as large as the horizontal accelerations in the near-field, and significantly lower at more distant alluvial sites. The near-fault ground velocity time histories had large, brief pulses of ground motion which are indicative of rupture directivity effects and are potentially damaging to multi-story buildings and other long-period structures such as bridges. The recorded peak velocities were as large as 175 cm/sec at Takatori in western Kobe, and the largest values occurred in the densely populated urban region. The near-fault horizontal peak velocities were 55 cm/sec on rock at Kobe University and went off scale at soil sites at levels of 40 cm/sec and 100 cm/sec in central Kobe. These values are similar to those recorded close to comparable earthquakes in California.

The recorded peak horizontal accelerations from the Kobe earthquake are comparable to those predicted for a strike-slip earthquake using the Abrahamson and

Silva (1995) empirical attenuation relation for soil based mainly on California data. The recorded peak horizontal velocities are slightly higher (about one standard deviation higher) than those predicted for a similar event using the Campbell (1990) empirical attenuation relation for soil based mainly on California data. Thus, it appears that one important factor contributing to the much larger level of damage that occurred in Kobe, compared with that of recent earthquakes in California, may have been rupture directivity effects.

8.2 Liquefaction and Related Effects

Extensive liquefaction of natural and artificial fill deposits occurred along much of the shoreline on the north side of the Osaka Bay. Probably the most notable were the liquefaction failures of relatively modern fills on the Rokko and Port Islands. On the Kobe mainland, evidence of liquefaction extended along the entire length of the waterfront, east and west of Kobe, for a distance of about 20 km. Overall, liquefaction was a principal factor in the extensive damage experienced by the port facilities in the affected region.

Most of the liquefied fills were constructed of poorly compacted decomposed granite soil. This material was transported to the fill sites and loosely dumped in water. Compaction was generally only applied to materials placed above water level. As a result, liquefaction occurred within the underwater segments of these poorly compacted fills.

Typically, liquefaction led to pervasive eruption of sand boils and, on the islands, to ground settlements on the order of as much as 0.5 m. The ground settlement caused surprisingly little damage to high- and low-rise buildings, bridges, tanks and other structures supported on deep foundations. These foundations, including piles and shafts, performed very well in supporting superstructures where ground settlement was the principal effect of liquefaction. Where liquefaction generated lateral ground displacements, such as near island edges and in other waterfront areas, foundation performance was typically poor. Lateral displacements fractured piles and displaced pile caps, causing structural distress to several bridges. In a few instances, such as the Port Island Ferry

Terminal, strong foundations withstood the lateral ground displacement with little damage to the foundation or the superstructure.

Shallow foundations consisting of a grid of interconnected perimeter-wall footings and grade beams performed well in several areas subjected to liquefaction. Where foundation elements were not well tied together, differential ground displacements pulled apart overlying structures at points of weakness, such as joints and doorways. More importantly, the differential ground movements invariably caused breaks in underground utilities at their entry points into the buildings.

8.3 Performance of Improved Ground Sites

The earthquake provided a severe test for several improved ground sites in the Kobe area. All cases involved loosely dumped hydraulic fill placed over soft alluvial clay. The treatment method was to construct sand compaction piles in-situ by vibro-rod probes or using the casing method with introduction of additional material from above ground. The post-treatment SPT N-values were typically 20 to 25 blows per 30 cm as opposed to about 10 to 15 blows per 30 cm before treatment. The treatment itself resulted in ground surface settlements of 20 to 40 cm, with the largest values being reported for the Portopialand Park area. The liquefaction-induced surface settlements of adjacent untreated ground were on the order of 50 cm. Overall, the observations show that improved ground sites on land sustained significantly less deformation and damage than did the untreated ground.

8.4 Performance of Dams and Levees

In general, most dams performed well with little or no damage noted. The principal exception was the failure of the relatively small Upper and Middle Niteko Dams, together with significant damage sustained at the Lower Niteko Dam. The earthquake was estimated to have induced peak ground accelerations of approximately 0.3 to 0.5g in this area. All three dams are reported to have been constructed over 100 years ago with minor additions

and modifications made to them in more recent times. Of the three dams, the Lower Niteko Dam performed the best. Nevertheless, the dam sustained major cracking and slumping in the middle of the embankment, losing as much as 2 meters of height. The Upper and Middle Niteko Dams experienced flow failures with the material traveling as much as 70 m downstream. This mode of failure strongly suggests that liquefaction was responsible, despite the fact that sediment boils were not observed.

The rivers in the area are commonly confined by gravity and cantilever retaining walls. In some places, armored earth embankments are also used as levees. In several locations major damage to these structures occurred, apparently as a result of liquefaction and associated settlement and lateral spreading. While as much as 3 m of settlement was observed in the most seriously affected area, much of the damage consisted of vertical and lateral deformations in the range of 10 to 20 cm.

8.5 Lifeline Systems

Extensive damage to lifeline systems occurred throughout the epicentral area of the earthquake. Liquefaction appears to have been a major factor involved in the failures of lifeline systems due to geotechnical causes, such as the damage to port facilities, underground transit, and underground utilities. There was pervasive disruption of underground utilities caused by ground deformations. In some locations pipe joints were simply pulled apart due to ground displacement. However, most commonly failures occurred due to differential movements between foundation elements and the surrounding soil at points of entry to buildings and other structures.

Particularly notable was the damage to several underground stations of the Kobe Rapid Transit Railway. These stations were constructed using the cut and cover method of construction and soil-structure interaction appears to have been responsible for the observed failures and distress.

8.6 Slopes, Retaining Structures, and Landfills

Seismically-induced landslides were generally limited to shallow slips and raveling of boulders, with the exception of one large flow slide which killed 34 people. In addition to landsliding on natural slopes, structural fills for roads and house pads experienced cracking and lateral deformations in the hills above Kobe. In many cases, this form of distress caused disruption of underground utilities as well as structural damage to houses and retaining walls. Large retaining structures for roads and railroads generally performed well. In particular, mechanically stabilized walls uniformly performed very well.

Waste fills located on reclaimed land experienced distress which can be directly attributed to the liquefaction of the loosely dumped fill. Liquefaction-induced lateral spreading resulted in cracking in the covers and in lateral displacements of the side slopes. The overall impact of these deformations on the integrity of the containment has yet to be established.

8.7 Conclusions

In conclusion, it is important to note that many of the observed effects of the January 17, 1995, Hyogoken-Nanbu Earthquake are similar to those observed in the most recent urban earthquakes such as the Northridge and Loma Prieta Earthquakes in California. Moreover, while many of the observations will provide an opportunity to further improve and refine our methods of analysis and design, much of the observed phenomena and effects could have been predicted with currently available methodologies. This recognition that seismically-induced damage can be predicted and minimized or even avoided, if appropriate analyses are performed and if appropriate designs are employed, has to be effectively communicated to the profession and to the public. Ultimately, we hope that this knowledge will help shape policies and decision making toward the development and implementation of successful earthquake hazard reduction strategies.

REFERENCES

Abrahamson, N. and W. Silva (1995). A consistent set of ground motion attenuation relations including data from the 1994 Northridge earthquake. Seismological Research Letters, 66, p. 23 (abs).

Architectural Institute of Japan (AIJ) (1995). Preliminary reconnaissance report of the Hyogoken-Nanbu Earthquake. English edition, 216 p.

Campbell, K.W. (1990). Empirical prediction of near-source and soft-rock ground motion for the Diablo Canyon Plant Site, San Luis Obispo County, California. Prepared for the Lawrence Livermore Laboratory.

Fudo Construction Corp., Ltd. (1995). Quick Report on Hyogoken-Nanbujisin of 1995. In japanese, 34 p.

Huzita, K. (1980). Role of the median tectonic line in the Quaternary tectonics of the Japanese islands. Memoirs of the Geological Society of Japan, 18, 129-153.

Iwaski, Y. (1995). Geological and geotechnical characteristics of Kobe Area and Strong Motion Records by 1995 Kobe Earthquake. Tsuchi-to-Kiso, Japanese Society of Soil Mechanics and Foundation Engineering, Ser. No. 449, Vol. 43, No. 6, pp. 15-20.

Kanamori, H. (1973). Mode of strain release associated with major earthquakes in Japan, Ann. Rev. Earth and Planet. Sci. 1, 213-239.

Kanamori, H. (1995). The Kobe(Hyogo-ken) Nanbu), Japan, earthquake of January 16, 1995. Seismological Research Letters 66, 6-10.

Kawase, H., T. Satoh and S. Matsushima (1995). Aftershock measurements and a preliminary analysis of aftershock records in Higashi-Nada Ward in Kobe after the 1995 Hyogo-Ken-Nanbu earthquake, ORI Report 94-04.

Kikuchi, M. (1995). Teleseismic analysis of the Southern Hyogo (Kobe), Japan, earthquake of January 17, 1995, Yokohama City University Seismological Note #38.

Kohketsu, K. (1995). Are predominant period contents of strong-motions the major cause of severe damage by the Kobe earthquake?, Monthly Journal of Science, Kagaku Asahi, No. 652, 11-14.

Matsui, T. (1994). Major onshore and offshore projects in the Osaka Bay area. Proc. 4th Int. offshore and Polar Engr. Conf., Osaka, Japan, Vol. I, 8-17.

Mitchell, J. K. (1981). Soil-improvement - State of the art report, Proc. 10th Int. Conf. Soil Mech. and Foundation Engr., (4), 509-565.

Murayama, S. (1958). Method to install sand compaction piles by vibrating casing pipes, Japanese Patent No. 26680.

Nakakita, Y. and Watanabe, Y. (1981). Soil stabilization by preloading in Kobe Port Island, Proc. of the 9th Int. Conf. Soil Mech. and Foundation Engr., Case History Volume, Japanese Society of Soil Mechanics and Foundation Engineering, 611-622

Pitarka, A., K. Irikura and T. Kagawa (1995). Source complexity of the January 17, 1995 Hyogo-ken-nanbu earthquake from nearfield strong motion modeling: preliminary results. Submitted to Journal of Natural Disaster Science.

Research Group for Active Faults in Japan (1980). Maps of Active Faults in Japan with and Explanatory Text, University of Tokyo Press, Hongo, Bunkyo-ku, Tokyo 113, Japan.

Saito, A. (1977). Characteristics of penetration resistance of a reclaimed sandy deposit and their change through vibratory compaction, Soils and Foundations, (17), No. 4, 34-43.

Seed, H.B., K.L. Lee, and I.M. Idriss (1969). Analysis of Sheffield Dam Failure. J. Soil Mech. Fdn. Div., ASCE, (95), No. 6, 1453-1490.

Seed, H.B. and Idriss, I.M., (1982). Ground Motions and Soil Liquefaction During Earthquakes. Earthquake Engineering Research Institute Monograph, 134 p.

Somerville, P.G. and R..W. Graves (1993). Conditions that give rise to unusually large lang period ground motions. The structural design of tall buildings 2, 211-232.

Somerville, P.G. and R..W. Graves (1995). Ground motion potential of the Los Angeles Region. Proceedings of the 1995 Annual Meeting of the Los Angeles Tall Buildings Structural Design Council, May 5.

Tatsuoka, F., Murata, O., and Tateyama, M. (1992)., Permanent geosynthetic-reinforced soil retaining walls used for railway embankment in Japan, Geosynthetic-Reinforced Soil Retaining Walls, Wu (ed.), Balkema, 101-130.

Tatsuoka, F. (undated). Applications of geosynthetic reinforced embankment for high speed railways, Institute of Industrial Science, University of Tokyo.

Tatsuoka, F., Tateyama, M., Murata, M., and Tarumi, H. (1995). Geogrid-reinforced soil retaining walls performed very well during the Great Hanshin earthquake, January 17, 1995, draft of report in preparation.

Youd, T.L., Chung, R.M., and Harp, E.L., (1995), "Liquefaction and Other Geotechnical Effects," in The July 12, 1993 Hokkaido-Nansei-Oki Earthquake: Earthquake Spectra, EERI.

EARTHQUAKE ENGINEERING RESEARCH CENTER REPORT SERIES

EERC reports are available from the National Information Service for Earthquake Engineering (NISEE) and from the National Technical Information Service (NTIS). Numbers in parentheses are Accession Numbers assigned by the National Technical Information Service; these are followed by a price code. Contact NTIS, 5285 Port Royal Road, Springfield Virginia, 22161 for more information. Reports without Accession Numbers were not available from NTIS at the time of printing. For a current complete list of EERC reports (from EERC 67-1) and availablity information, please contact University of California, EERC, NISEE, 1301 South 46th Street, Richmond, California 94804-4698.

UCB/EERC-84/01 "Pseudodynamic Test Method for Seismic Performance Evaluation: Theory and Implementation," by Shing, P.-S.B. and Mahin, S.A., January 1984, (PB84 190 644)A08.

UCB/EERC-84/02 "Dynamic Response Behavior of Kiang Hong Dian Dam," by Clough, R.W., Chang, K.-T., Chen, H.-Q. and Stephen, R.M., April 1984, (PB84 209 402)A08.

UCB/EERC-84/03 "Refined Modelling of Reinforced Concrete Columns for Seismic Analysis," by Kaba, S.A. and Mahin, S.A., April 1984, (PB84 234 384)A06.

UCB/EERC-84/04 "A New Floor Response Spectrum Method for Seismic Analysis of Multiply Supported Secondary Systems," by Asfura, A. and Der Kiureghian, A., June 1984, (PB84 239 417)A06.

UCB/EERC-84/05 "Earthquake Simulation Tests and Associated Studies of a 1/5th-scale Model of a 7-Story R/C Frame-Wall Test Structure," by Bertero, V.V., Aktan, A.E., Charney, F.A. and Sause, R., June 1984, (PB84 239 409)A09.

UCB/EERC-84/06 "Unassigned," by Unassigned, 1984.

UCB/EERC-84/07 "Behavior of Interior and Exterior Flat-Plate Connections Subjected to Inelastic Load Reversals," by Zee, H.L. and Moehle, J.P., August 1984, (PB86 117 629/AS)A07.

UCB/EERC-84/08 "Experimental Study of the Seismic Behavior of a Two-Story Flat-Plate Structure," by Moehle, J.P. and Diebold, J.W., August 1984, (PB86 122 553/AS)A12.

UCB/EERC-84/09 "Phenomenological Modeling of Steel Braces under Cyclic Loading," by Ikeda, K., Mahin, S.A. and Dermitzakis, S.N., May 1984, (PB86 132 198/AS)A08.

UCB/EERC-84/10 "Earthquake Analysis and Response of Concrete Gravity Dams," by Fenves, G.L. and Chopra, A.K., August 1984, (PB85 193 902/AS)A11.

UCB/EERC-84/11 "EAGD-84: A Computer Program for Earthquake Analysis of Concrete Gravity Dams," by Fenves, G.L. and Chopra, A.K., August 1984, (PB85 193 613/AS)A05.

UCB/EERC-84/12 "A Refined Physical Theory Model for Predicting the Seismic Behavior of Braced Steel Frames," by Ikeda, K. and Mahin, S.A., July 1984, (PB85 191 450/AS)A09.

UCB/EERC-84/13 "Earthquake Engineering Research at Berkeley - 1984," by EERC, August 1984, (PB85 197 341/AS)A10.

UCB/EERC-84/14 "Moduli and Damping Factors for Dynamic Analyses of Cohesionless Soils," by Seed, H.B., Wong, R.T., Idriss, I.M. and Tokimatsu, K., September 1984, (PB85 191 468/AS)A04.

UCB/EERC-84/15 "The Influence of SPT Procedures in Soil Liquefaction Resistance Evaluations," by Seed, H.B., Tokimatsu, K., Harder, L.F. and Chung, R.M., October 1984, (PB85 191 732/AS)A04.

UCB/EERC-84/16 "Simplified Procedures for the Evaluation of Settlements in Sands Due to Earthquake Shaking," by Tokimatsu, K. and Seed, H.B., October 1984, (PB85 197 887/AS)A03.

UCB/EERC-84/17 "Evaluation of Energy Absorption Characteristics of Highway Bridges Under Seismic Conditions - Volume I (PB90 262 627)A16 and Volume II (Appendices) (PB90 262 635)A13," by Imbsen, R.A. and Penzien, J., September 1986.

UCB/EERC-84/18 "Structure-Foundation Interactions under Dynamic Loads," by Liu, W.D. and Penzien, J., November 1984, (PB87 124 889/AS)A11.

UCB/EERC-84/19 "Seismic Modelling of Deep Foundations," by Chen, C.-H. and Penzien, J., November 1984, (PB87 124 798/AS)A07.

UCB/EERC-84/20 "Dynamic Response Behavior of Quan Shui Dam," by Clough, R.W., Chang, K.-T., Chen, H.-Q., Stephen, R.M., Ghanaat, Y. and Qi, J.-H., November 1984, (PB86 115177/AS)A07.

UCB/EERC-85/01 "Simplified Methods of Analysis for Earthquake Resistant Design of Buildings," by Cruz, E.F. and Chopra, A.K., February 1985, (PB86 112299/AS)A12.

UCB/EERC-85/02 "Estimation of Seismic Wave Coherency and Rupture Velocity using the SMART 1 Strong-Motion Array Recordings," by Abrahamson, N.A., March 1985, (PB86 214 343)A07.

UCB/EERC-85/03 "Dynamic Properties of a Thirty Story Condominium Tower Building," by Stephen, R.M., Wilson, E.L. and Stander, N., April 1985, (PB86 118965/AS)A06.

UCB/EERC-85/04 "Development of Substructuring Techniques for On-Line Computer Controlled Seismic Performance Testing," by Dermitzakis, S. and Mahin, S., February 1985, (PB86 132941/AS)A08.

UCB/EERC-85/05 "A Simple Model for Reinforcing Bar Anchorages under Cyclic Excitations," by Filippou, F.C., March 1985, (PB86 112 919/AS)A05.

UCB/EERC-85/06 "Racking Behavior of Wood-framed Gypsum Panels under Dynamic Load," by Oliva, M.G., June 1985, (PB90 262 643)A04.

UCB/EERC-85/07 "Earthquake Analysis and Response of Concrete Arch Dams," by Fok, K.-L. and Chopra, A.K., June 1985, (PB86 139672/AS)A10.

UCB/EERC-85/08 "Effect of Inelastic Behavior on the Analysis and Design of Earthquake Resistant Structures," by Lin, J.P. and Mahin, S.A., June 1985, (PB86 135340/AS)A08.

UCB/EERC-85/09 "Earthquake Simulator Testing of a Base-Isolated Bridge Deck," by Kelly, J.M., Buckle, I.G. and Tsai, H.-C., January 1986, (PB87 124 152/AS)A06.

UCB/EERC-85/10 "Simplified Analysis for Earthquake Resistant Design of Concrete Gravity Dams," by Fenves, G.L. and Chopra, A.K., June 1986, (PB87 124 160/AS)A08.

UCB/EERC-85/11 "Dynamic Interaction Effects in Arch Dams," by Clough, R.W., Chang, K.-T., Chen, H.-Q. and Ghanaat, Y., October 1985, (PB86 135027/AS)A05.

UCB/EERC-85/12 "Dynamic Response of Long Valley Dam in the Mammoth Lake Earthquake Series of May 25-27, 1980," by Lai, S. and Seed, H.B., November 1985, (PB86 142304/AS)A05.

UCB/EERC-85/13 "A Methodology for Computer-Aided Design of Earthquake-Resistant Steel Structures," by Austin, M.A., Pister, K.S. and Mahin, S.A., December 1985, (PB86 159480/AS)A10 .

UCB/EERC-85/14 "Response of Tension-Leg Platforms to Vertical Seismic Excitations," by Liou, G.-S., Penzien, J. and Yeung, R.W., December 1985, (PB87 124 871/AS)A08.

UCB/EERC-85/15 "Cyclic Loading Tests of Masonry Single Piers: Volume 4 - Additional Tests with Height to Width Ratio of 1," by Sveinsson, B., McNiven, H.D. and Sucuoglu, H., December 1985, (PB87 165031/AS)A08.

UCB/EERC-85/16 "An Experimental Program for Studying the Dynamic Response of a Steel Frame with a Variety of Infill Partitions," by Yanev, B. and McNiven, H.D., December 1985, (PB90 262 676)A05.

UCB/EERC-86/01 "A Study of Seismically Resistant Eccentrically Braced Steel Frame Systems," by Kasai, K. and Popov, E.P., January 1986, (PB87 124 178/AS)A14.

UCB/EERC-86/02 "Design Problems in Soil Liquefaction," by Seed, H.B., February 1986, (PB87 124 186/AS)A03.

UCB/EERC-86/03 "Implications of Recent Earthquakes and Research on Earthquake-Resistant Design and Construction of Buildings," by Bertero, V.V., March 1986, (PB87 124 194/AS)A05.

UCB/EERC-86/04 "The Use of Load Dependent Vectors for Dynamic and Earthquake Analyses," by Leger, P., Wilson, E.L. and Clough, R.W., March 1986, (PB87 124 202/AS)A12.

UCB/EERC-86/05 "Two Beam-To-Column Web Connections," by Tsai, K.-C. and Popov, E.P., April 1986, (PB87 124 301/AS)A04.

UCB/EERC-86/06 "Determination of Penetration Resistance for Coarse-Grained Soils using the Becker Hammer Drill," by Harder, L.F. and Seed, H.B., May 1986, (PB87 124 210/AS)A07.

UCB/EERC-86/07 "A Mathematical Model for Predicting the Nonlinear Response of Unreinforced Masonry Walls to In-Plane Earthquake Excitations," by Mengi, Y. and McNiven, H.D., May 1986, (PB87 124 780/AS)A06.

UCB/EERC-86/08 "The 19 September 1985 Mexico Earthquake: Building Behavior," by Bertero, V.V., July 1986.

UCB/EERC-86/09 "EACD-3D: A Computer Program for Three-Dimensional Earthquake Analysis of Concrete Dams," by Fok, K.-L., Hall, J.F. and Chopra, A.K., July 1986, (PB87 124 228/AS)A08.

UCB/EERC-86/10 "Earthquake Simulation Tests and Associated Studies of a 0.3-Scale Model of a Six-Story Concentrically Braced Steel Structure," by Uang, C.-M. and Bertero, V.V., December 1986, (PB87 163 564/AS)A17.

UCB/EERC-86/11 "Mechanical Characteristics of Base Isolation Bearings for a Bridge Deck Model Test," by Kelly, J.M., Buckle, I.G. and Koh, C.-G., November 1987, (PB90 262 668)A04.

UCB/EERC-86/12 "Effects of Axial Load on Elastomeric Isolation Bearings," by Koh, C.-G. and Kelly, J.M., November 1987, PB88-179015(A06).

UCB/EERC-87/01 "The FPS Earthquake Resisting System: Experimental Report," by Zayas, V.A., Low, S.S. and Mahin, S.A., June 1987, (PB88 170 287)A06

UCB/EERC-87/02 "Earthquake Simulator Tests and Associated Studies of a 0.3-Scale Model of a Six-Story Eccentrically Braced Steel Structure," by Whittaker, A., Uang, C.-M. and Bertero, V.V., July 1987, (PB88 166 707/AS)A18.

UCB/EERC-87/03 "A Displacement Control and Uplift Restraint Device for Base-Isolated Structures," by Kelly, J.M., Griffith, M.C. and Aiken, I.D., April 1987, (PB88 169 933)A04.

UCB/EERC-87/04 "Earthquake Simulator Testing of a Combined Sliding Bearing and Rubber Bearing Isolation System," by Kelly, J.M. and Chalhoub, M.S., December 1990, PB92-192962(A09).

UCB/EERC-87/05 "Three-Dimensional Inelastic Analysis of Reinforced Concrete Frame-Wall Structures," by Moazzami, S. and Bertero, V.V., May 1987, (PB88 169 586/AS)A08.

UCB/EERC-87/06 "Experiments on Eccentrically Braced Frames with Composite Floors," by Ricles, J. and Popov, E., June 1987, (PB88 173 067/AS)A14.

UCB/EERC-87/07 "Dynamic Analysis of Seismically Resistant Eccentrically Braced Frames," by Ricles, J. and Popov, E., June 1987, (PB88 173 075/AS)A16.

UCB/EERC-87/08 "Undrained Cyclic Triaxial Testing of Gravels-The Effect of Membrane Compliance," by Evans, M.D. and Seed, H.B., July 1987, (PB88 173 257)A19.

UCB/EERC-87/09 "Hybrid Solution Techniques for Generalized Pseudo-Dynamic Testing," by Thewalt, C. and Mahin, S.A., July 1987, (PB 88 179 007)A07.

UCB/EERC-87/10 "Ultimate Behavior of Butt Welded Splices in Heavy Rolled Steel Sections," by Bruneau, M., Mahin, S.A. and Popov, E.P., September 1987, (PB90 254 285)A07.

UCB/EERC-87/11 "Residual Strength of Sand from Dam Failures in the Chilean Earthquake of March 3, 1985," by De Alba, P., Seed, H.B., Retamal, E. and Seed, R.B., September 1987, (PB88 174 321/AS)A03.

UCB/EERC-87/12 "Inelastic Seismic Response of Structures with Mass or Stiffness Eccentricities in Plan," by Bruneau, M. and Mahin, S.A., September 1987, (PB90 262 650/AS)A14.

UCB/EERC-87/13 "CSTRUCT: An Interactive Computer Environment for the Design and Analysis of Earthquake Resistant Steel Structures," by Austin, M.A., Mahin, S.A. and Pister, K.S., September 1987, (PB88 173 339/AS)A06.

UCB/EERC-87/14 "Experimental Study of Reinforced Concrete Columns Subjected to Multi-Axial Loading," by Low, S.S. and Moehle, J.P., September 1987, (PB88 174 347/AS)A07.

UCB/EERC-87/15 "Relationships between Soil Conditions and Earthquake Ground Motions in Mexico City in the Earthquake of Sept. 19, 1985," by Seed, H.B., Romo, M.P., Sun, J., Jaime, A. and Lysmer, J., October 1987, (PB88 178 991)A06.

UCB/EERC-87/16 "Experimental Study of Seismic Response of R. C. Setback Buildings," by Shahrooz, B.M. and Moehle, J.P., October 1987, (PB88 176 359)A16.

UCB/EERC-87/17 "The Effect of Slabs on the Flexural Behavior of Beams," by Pantazopoulou, S.J. and Moehle, J.P., October 1987, (PB90 262 700)A07.

UCB/EERC-87/18 "Design Procedure for R-FBI Bearings," by Mostaghel, N. and Kelly, J.M., November 1987, (PB90 262 718)A04.

UCB/EERC-87/19 "Analytical Models for Predicting the Lateral Response of R C Shear Walls: Evaluation of their Reliability," by Vulcano, A. and Bertero, V.V., November 1987, (PB88 178 983)A05.

UCB/EERC-87/20 "Earthquake Response of Torsionally-Coupled Buildings," by Hejal, R. and Chopra, A.K., December 1987, PB90-208638(A15).

UCB/EERC-87/21 "Dynamic Reservoir Interaction with Monticello Dam," by Clough, R.W., Ghanaat, Y. and Qiu, X-F., December 1987, (PB88 179 023)A07.

UCB/EERC-87/22 "Strength Evaluation of Coarse-Grained Soils," by Siddiqi, F.H., Seed, R.B., Chan, C.K., Seed, H.B. and Pyke, R.M., December 1987, (PB88 179 031)A04.

UCB/EERC-88/01 "Seismic Behavior of Concentrically Braced Steel Frames," by Khatib, I., Mahin, S.A. and Pister, K.S., January 1988, (PB91 210 898/AS)A11.

UCB/EERC-88/02 "Experimental Evaluation of Seismic Isolation of Medium-Rise Structures Subject to Uplift," by Griffith, M.C., Kelly, J.M., Coveney, V.A. and Koh, C.G., January 1988, (PB91 217 950/AS)A09.

UCB/EERC-88/03 "Cyclic Behavior of Steel Double Angle Connections," by Astaneh-Asl, A. and Nader, M.N., January 1988, (PB91 210 872)A05.

UCB/EERC-88/04 "Re-evaluation of the Slide in the Lower San Fernando Dam in the Earthquake of Feb. 9, 1971," by Seed, H.B., Seed, R.B., Harder, L.F. and Jong, H.-L., April 1988, (PB91 212 456/AS)A07.

UCB/EERC-88/05 "Experimental Evaluation of Seismic Isolation of a Nine-Story Braced Steel Frame Subject to Uplift," by Griffith, M.C., Kelly, J.M. and Aiken, I.D., May 1988, (PB91 217 968/AS)A07.

UCB/EERC-88/06 "DRAIN-2DX User Guide.," by Allahabadi, R. and Powell, G.H., March 1988, (PB91 212 530)A12.

UCB/EERC-88/07 "Theoretical and Experimental Studies of Cylindrical Water Tanks in Base-Isolated Structures," by Chalhoub, M.S. and Kelly, J.M., April 1988, (PB91 217 976/AS)A05.

UCB/EERC-88/08 "Analysis of Near-Source Waves: Separation of Wave Types Using Strong Motion Array Recording," by Darragh, R.B., June 1988, (PB91 212 621)A08.

UCB/EERC-88/09 "Alternatives to Standard Mode Superposition for Analysis of Non-Classically Damped Systems," by Kusainov, A.A. and Clough, R.W., June 1988, (PB91 217 992/AS)A04.

UCB/EERC-88/10 "The Landslide at the Port of Nice on October 16, 1979," by Seed, H.B., Seed, R.B., Schlosser, F., Blondeau, F. and Juran, I., June 1988, (PB91 210 914)A05.

UCB/EERC-88/11 "Liquefaction Potential of Sand Deposits Under Low Levels of Excitation," by Carter, D.P. and Seed, H.B., August 1988, (PB91 210 880)A15.

UCB/EERC-88/12 "Nonlinear Analysis of Reinforced Concrete Frames Under Cyclic Load Reversals," by Filippou, F.C. and Issa, A., September 1988, (PB91 212 589)A07.

UCB/EERC-88/13 "Implications of Recorded Earthquake Ground Motions on Seismic Design of Building Structures," by Uang, C.-M. and Bertero, V.V., November 1988, (PB91 212 548)A06.

UCB/EERC-88/14 "An Experimental Study of the Behavior of Dual Steel Systems," by Whittaker, A.S. , Uang, C.-M. and Bertero, V.V., September 1988, (PB91 212 712)A16.

UCB/EERC-88/15 "Dynamic Moduli and Damping Ratios for Cohesive Soils," by Sun, J.I., Golesorkhi, R. and Seed, H.B., August 1988, (PB91 210 922)A04.

UCB/EERC-88/16 "Reinforced Concrete Flat Plates Under Lateral Load: An Experimental Study Including Biaxial Effects," by Pan, A. and Moehle, J.P., October 1988, (PB91 210 856)A13.

UCB/EERC-88/17 "Earthquake Engineering Research at Berkeley - 1988," by EERC, November 1988, (PB91 210 864)A10.

UCB/EERC-88/18 "Use of Energy as a Design Criterion in Earthquake-Resistant Design," by Uang, C.-M. and Bertero, V.V., November 1988, (PB91 210 906/AS)A04.

UCB/EERC-88/19 "Steel Beam-Column Joints in Seismic Moment Resisting Frames," by Tsai, K.-C. and Popov, E.P., November 1988, (PB91 217 984/AS)A20.

UCB/EERC-88/20 "Base Isolation in Japan, 1988," by Kelly, J.M., December 1988, (PB91 212 449)A05.

UCB/EERC-89/01 "Behavior of Long Links in Eccentrically Braced Frames," by Engelhardt, M.D. and Popov, E.P., January 1989, (PB92 143 056)A18.

UCB/EERC-89/02 "Earthquake Simulator Testing of Steel Plate Added Damping and Stiffness Elements," by Whittaker, A., Bertero, V.V., Alonso, J. and Thompson, C., January 1989, (PB91 229 252/AS)A10.

UCB/EERC-89/03 "Implications of Site Effects in the Mexico City Earthquake of Sept. 19, 1985 for Earthquake-Resistant Design Criteria in the San Francisco Bay Area of California," by Seed, H.B. and Sun, J.I., March 1989, (PB91 229 369/AS)A07.

UCB/EERC-89/04 "Earthquake Analysis and Response of Intake-Outlet Towers," by Goyal, A. and Chopra, A.K., July 1989, (PB91 229 286/AS)A19.

UCB/EERC-89/05 "The 1985 Chile Earthquake: An Evaluation of Structural Requirements for Bearing Wall Buildings," by Wallace, J.W. and Moehle, J.P., July 1989, (PB91 218 008/AS)A13.

UCB/EERC-89/06 "Effects of Spatial Variation of Ground Motions on Large Multiply-Supported Structures," by Hao, H., July 1989, (PB91 229 161/AS)A08.

UCB/EERC-89/07 "EADAP - Enhanced Arch Dam Analysis Program: Users's Manual," by Ghanaat, Y. and Clough, R.W., August 1989, (PB91 212 522)A06.

UCB/EERC-89/08 "Seismic Performance of Steel Moment Frames Plastically Designed by Least Squares Stress Fields," by Ohi, K. and Mahin, S.A., August 1989, (PB91 212 597)A05.

UCB/EERC-89/09 "Feasibility and Performance Studies on Improving the Earthquake Resistance of New and Existing Buildings Using the Friction Pendulum System," by Zayas, V., Low, S., Mahin, S.A. and Bozzo, L., July 1989, (PB92 143 064)A14.

UCB/EERC-89/10 "Measurement and Elimination of Membrane Compliance Effects in Undrained Triaxial Testing," by Nicholson, P.G., Seed, R.B. and Anwar, H., September 1989, (PB92 139 641/AS)A13.

UCB/EERC-89/11 "Static Tilt Behavior of Unanchored Cylindrical Tanks," by Lau, D.T. and Clough, R.W., September 1989, (PB92 143 049)A10.

UCB/EERC-89/12 "ADAP-88: A Computer Program for Nonlinear Earthquake Analysis of Concrete Arch Dams," by Fenves, G.L., Mojtahedi, S. and Reimer, R.B., September 1989, (PB92 139 674/AS)A07.

UCB/EERC-89/13 "Mechanics of Low Shape Factor Elastomeric Seismic Isolation Bearings," by Aiken, I.D., Kelly, J.M. and Tajirian, F.F., November 1989, (PB92 139 732/AS)A09.

UCB/EERC-89/14 "Preliminary Report on the Seismological and Engineering Aspects of the October 17, 1989 Santa Cruz (Loma Prieta) Earthquake," by EERC, October 1989, (PB92 139 682/AS)A04.

UCB/EERC-89/15 "Experimental Studies of a Single Story Steel Structure Tested with Fixed, Semi-Rigid and Flexible Connections," by Nader, M.N. and Astaneh-Asl, A., August 1989, (PB91 229 211/AS)A10.

UCB/EERC-89/16 "Collapse of the Cypress Street Viaduct as a Result of the Loma Prieta Earthquake," by Nims, D.K., Miranda, E., Aiken, I.D., Whittaker, A.S. and Bertero, V.V., November 1989, (PB91 217 935/AS)A05.

UCB/EERC-90/01 "Mechanics of High-Shape Factor Elastomeric Seismic Isolation Bearings," by Kelly, J.M., Aiken, I.D. and Tajirian, F.F., March 1990.

UCB/EERC-90/02 "Javid's Paradox: The Influence of Preform on the Modes of Vibrating Beams," by Kelly, J.M., Sackman, J.L. and Javid, A., May 1990, (PB91 217 943/AS)A03.

UCB/EERC-90/03 "Earthquake Simulator Testing and Analytical Studies of Two Energy-Absorbing Systems for Multistory Structures," by Aiken, I.D. and Kelly, J.M., October 1990, (PB92 192 988)A13.

UCB/EERC-90/04 "Unassigned," by Unassigned, 1990.

UCB/EERC-90/05 "Preliminary Report on the Principal Geotechnical Aspects of the October 17, 1989 Loma Prieta Earthquake," by Seed, R.B., Dickenson, S.E., Riemer, M.F., Bray, J.D., Sitar, N., Mitchell, J.K., Idriss, I.M., Kayen, R.E., Kropp, A., Harder, L.F., Jr. and Power, M.S., April 1990, (PB 192 970)A08.

UCB/EERC-90/06 "Models of Critical Regions in Reinforced Concrete Frames Under Seismic Excitations," by Zulfiqar, N. and Filippou, F.C., May 1990.

UCB/EERC-90/07 "A Unified Earthquake-Resistant Design Method for Steel Frames Using ARMA Models," by Takewaki, I., Conte, J.P., Mahin, S.A. and Pister, K.S., June 1990, PB92-192947(A06).

UCB/EERC-90/08 "Soil Conditions and Earthquake Hazard Mitigation in the Marina District of San Francisco," by Mitchell, J.K., Masood, T., Kayen, R.E and Seed, R.B., May 1990, (PB 193 267/AS)A04.

UCB/EERC-90/09 "Influence of the Earthquake Ground Motion Process and Structural Properties on Response Characteristics of Simple Structures," by Conte, J.P., Pister, K.S. and Mahin, S.A., July 1990, (PB92 143 064)A15.

UCB/EERC-90/10 "Experimental Testing of the Resilient-Friction Base Isolation System," by Clark, P.W. and Kelly, J.M., July 1990, (PB92 143 072)A08.

UCB/EERC-90/11 "Seismic Hazard Analysis: Improved Models, Uncertainties and Sensitivities," by Araya, R. and Der Kiureghian, A., March 1988, PB92-193010(A08).

UCB/EERC-90/12 "Effects of Torsion on the Linear and Nonlinear Seismic Response of Structures," by Sedarat, H. and Bertero, V.V., September 1989, (PB92 193 002/AS)A15.

UCB/EERC-90/13 "The Effects of Tectonic Movements on Stresses and Deformations in Earth Embankments," by Bray, J. D., Seed, R. B. and Seed, H. B., September 1989, PB92-192996(A18).

UCB/EERC-90/14 "Inelastic Seismic Response of One-Story, Asymmetric-Plan Systems," by Goel, R.K. and Chopra, A.K., October 1990, (PB93 114 767)A11.

UCB/EERC-90/15 "Dynamic Crack Propagation: A Model for Near-Field Ground Motion.," by Seyyedian, H. and Kelly, J.M., 1990.

UCB/EERC-90/16 "Sensitivity of Long-Period Response Spectra to System Initial Conditions," by Blasquez, R., Ventura, C. and Kelly, J.M., 1990.

UCB/EERC-90/17 "Behavior of Peak Values and Spectral Ordinates of Near-Source Strong Ground-Motion over a Dense Array," by Niazi, M., June 1990, (PB93 114 833)A07.

UCB/EERC-90/18 "Material Characterization of Elastomers used in Earthquake Base Isolation," by Papoulia, K.D. and Kelly, J.M., 1990, PB94-190063(A08).

UCB/EERC-90/19 "Cyclic Behavior of Steel Top-and-Bottom Plate Moment Connections," by Harriott, J.D. and Astaneh-Asl, A., August 1990, (PB91 229 260/AS)A05.

UCB/EERC-90/20 "Seismic Response Evaluation of an Instrumented Six Story Steel Building," by Shen, J.-H. and Astaneh-Asl, A., December 1990, (PB91 229 294/AS)A04.

UCB/EERC-90/21 "Observations and Implications of Tests on the Cypress Street Viaduct Test Structure," by Bollo, M., Mahin, S.A., Moehle, J.P., Stephen, R.M. and Qi, X., December 1990, (PB93 114 775)A13.

UCB/EERC-91/01 "Experimental Evaluation of Nitinol for Energy Dissipation in Structures," by Nims, D.K., Sasaki, K.K. and Kelly, J.M., 1991.

UCB/EERC-91/02 "Displacement Design Approach for Reinforced Concrete Structures Subjected to Earthquakes," by Qi, X. and Moehle, J.P., January 1991, (PB93 114 569/AS)A09.

UCB/EERC-91/03 "A Long-Period Isolation System Using Low-Modulus High-Damping Isolators for Nuclear Facilities at Soft-Soil Sites," by Kelly, J.M., March 1991, (PB93 114 577/AS)A10.

UCB/EERC-91/04 "Dynamic and Failure Characteristics of Bridgestone Isolation Bearings," by Kelly, J.M., April 1991, (PB93 114 528)A05.

UCB/EERC-91/05 "Base Sliding Response of Concrete Gravity Dams to Earthquakes," by Chopra, A.K. and Zhang, L., May 1991, (PB93 114 544/AS)A05.

UCB/EERC-91/06 "Computation of Spatially Varying Ground Motion and Foundation-Rock Impedance Matrices for Seismic Analysis of Arch Dams," by Zhang, L. and Chopra, A.K., May 1991, (PB93 114 825)A07.

UCB/EERC-91/07 "Estimation of Seismic Source Processes Using Strong Motion Array Data," by Chiou, S.-J., July 1991, (PB93 114 551/AS)A08.

UCB/EERC-91/08 "A Response Spectrum Method for Multiple-Support Seismic Excitations," by Der Kiureghian, A. and Neuenhofer, A., August 1991, (PB93 114 536)A04.

UCB/EERC-91/09 "A Preliminary Study on Energy Dissipating Cladding-to-Frame Connection," by Cohen, J.M. and Powell, G.H., September 1991, (PB93 114 510)A05.

UCB/EERC-91/10 "Evaluation of Seismic Performance of a Ten-Story RC Building During the Whittier Narrows Earthquake," by Miranda, E. and Bertero, V.V., October 1991, (PB93 114 783)A06.

UCB/EERC-91/11 "Seismic Performance of an Instrumented Six-Story Steel Building," by Anderson, J.C. and Bertero, V.V., November 1991, (PB93 114 809)A07.

UCB/EERC-91/12 "Performance of Improved Ground During the Loma Prieta Earthquake," by Mitchell, J.K. and Wentz, Jr., F.J., October 1991, (PB93 114 791)A06.

UCB/EERC-91/13 "Shaking Table - Structure Interaction," by Rinawi, A.M. and Clough, R.W., October 1991, (PB93 114 917)A13.

UCB/EERC-91/14 "Cyclic Response of RC Beam-Column Knee Joints: Test and Retrofit," by Mazzoni, S., Moehle, J.P. and Thewalt, C.R., October 1991, (PB93 120 277)A03.

UCB/EERC-91/15 "Design Guidelines for Ductility and Drift Limits: Review of State-of-the-Practice and State-of-the-Art in Ductility and Drift-Based Earthquake-Resistant Design of Buildings," by Bertero, V.V., Anderson, J.C., Krawinkler, H., Miranda, E. and The CUREe and The Kajima Research Teams, July 1991, (PB93 120 269)A08.

UCB/EERC-91/16 "Evaluation of the Seismic Performance of a Thirty-Story RC Building," by Anderson, J.C., Miranda, E., Bertero, V.V. and The Kajima Project Research Team, July 1991, (PB93 114 841)A12.

UCB/EERC-91/17 "A Fiber Beam-Column Element for Seismic Response Analysis of Reinforced Concrete Structures," by Taucer, F., Spacone, E. and Filippou, F.C., December 1991, (PB94 117 629AS)A07.

UCB/EERC-91/18 "Investigation of the Seismic Response of a Lightly-Damped Torsionally-Coupled Building," by Boroschek, R. and Mahin, S.A., December 1991, (PB93 120 335)A13.

UCB/EERC-92/01 "Studies of a 49-Story Instrumented Steel Structure Shaken During the Loma Prieta Earthquake," by Chen, C.-C., Bonowitz, D. and Astaneh-Asl, A., February 1992, (PB93 221 778)A08.

UCB/EERC-92/02 "Response of the Dumbarton Bridge in the Loma Prieta Earthquake," by Fenves, G.L., Filippou, F.C. and Sze, D.T., January 1992, (PB93 120 319)A09.

UCB/EERC-92/03 "Models for Nonlinear Earthquake Analysis of Brick Masonry Buildings," by Mengi, Y., McNiven, H.D. and Tanrikulu, A.K., March 1992, (PB93 120 293)A08.

UCB/EERC-92/04 "Shear Strength and Deformability of RC Bridge Columns Subjected to Inelastic Cyclic Displacements," by Aschheim, M. and Moehle, J.P., March 1992, (PB93 120 327)A06.

UCB/EERC-92/05 "Parameter Study of Joint Opening Effects on Earthquake Response of Arch Dams," by Fenves, G.L., Mojtahedi, S. and Reimer, R.B., April 1992, (PB93 120 301)A04.

UCB/EERC-92/06 "Seismic Behavior and Design of Semi-Rigid Steel Frames," by Nader, M.N. and Astaneh-Asl, A., May 1992, PB93-221760(A17).

UCB/EERC-92/07 "A Beam Element for Seismic Damage Analysis," by Spacone, E., Ciampi, V. and Filippou, F.C., August 1992, (PB95-192126)A06.

UCB/EERC-92/08 "Nonlinear Static and Dynamic Analysis of Reinforced Concrete Subassemblages," by Filippou, F.C., D'Ambrisi, A. and Issa, A., August 1992, PB95-192175(A09).

UCB/EERC-92/09 "Evaluation of Code Accidental-Torsion Provisions Using Earthquake Records from Three Nominally Symmetric-Plan Buildings," by De la Llera, J.C. and Chopra, A.K., September 1992, (PB94 117 611)A08.

UCB/EERC-92/10 "Slotted Bolted Connection Energy Dissipators," by Grigorian, C.E., Yang, T.-S. and Popov, E.P., July 1992, (PB92 120 285)A03.

UCB/EERC-92/11 "Mechanical Characteristics of Neoprene Isolation Bearings," by Kelly, J.M. and Quiroz, E., August 1992, (PB93 221 729)A07.

UCB/EERC-92/12 "Application of a Mass Damping System to Bridge Structures," by Hasegawa, K. and Kelly, J.M., August 1992, (PB93 221 786)A06.

UCB/EERC-92/13 "Earthquake Engineering Research at Berkeley - 1992," by EERC, October 1992, PB93-223709(A10).

UCB/EERC-92/14 "Earthquake Risk and Insurance," by Brillinger, D.R., October 1992, (PB93 223 352)A03.

UCB/EERC-92/15 "A Friction Mass Damper for Vibration Control," by Inaudi, J.A. and Kelly, J.M., October 1992, (PB93 221 745)A04.

UCB/EERC-92/16 "Tall Reinforced Concrete Buildings: Conceptual Earthquake-Resistant Design Methology," by Bertero, R.D. and Bertero, V.V., December 1992, (PB93 221 695)A12.

UCB/EERC-92/17 "Performance of Tall Buildings During the 1985 Mexico Earthquakes," by Terán-Gilmore, A. and Bertero, V.V., December 1992, (PB93 221 737)A11.

UCB/EERC-92/18 "Dynamic Analysis of Nonlinear Structures using State-Space Formulation and Partitioned Integration Schemes," by Inaudi, J.A. and De la Llera, J.C., December 1992, (PB94 117 702/AS/A05.

UCB/EERC-93/01 "Seismic Performance of an Instrumented Six-Story Reinforced-Concrete Building," by Anderson, J.C. and Bertero, V.V., 1993.

UCB/EERC-93/02 "Evaluation of an Active Variable-Damping-Structure," by Polak, E., Meeker, G., Yamada, K. and Kurata, N., 1993, (PB93 221 711)A05.

UCB/EERC-93/03 "An Experimental Study of Flat-Plate Structures under Vertical and Lateral Loads," by Hwang, S.-H. and Moehle, J.P., February 1993, (PB94 157 690/AS)A13.

UCB/EERC-93/04 "Seismic Performance of a 30-Story Building Located on Soft Soil and Designed According to UBC 1991," by Terán-Gilmore, A. and Bertero, V.V., 1993, (PB93 221 703)A17.

UCB/EERC-93/05 "Multiple-Support Response Spectrum Analysis of the Golden Gate Bridge," by Nakamura, Y., Der Kiureghian, A. and Liu, D., May 1993, (PB93 221 752)A05.

UCB/EERC-93/06 "On the Analysis of Structures with Viscoelastic Dampers," by Inaudi, J.A., Zambrano, A. and Kelly, J.M., August 1993, PB94-165867(A06).

UCB/EERC-93/07 "Earthquake Analysis and Response of Concrete Gravity Dams Including Base Sliding," by Chávez, J.W. and Fenves, G.L., December 1993, (PB94 157 658/AS)A10.

UCB/EERC-93/08 "Model for Anchored Reinforcing Bars under Seismic Excitations," by Monti, G., Spacone, E. and Filippou, F.C., December 1993, PB95-192183(A05).

UCB/EERC-93/09 "A Methodology for Design of Viscoelastic Dampers in Earthquake-Resistant Structures," by Abbas, H. and Kelly, J.M., November 1993, PB94-190071(A10).

UCB/EERC-93/10 "Tuned Mass Dampers Using Viscoelastic Dampers," by Inaudi, J.A., Lopez-Almansa, F. and Kelly, J.M., December 1993.

UCB/EERC-93/11 "Nonlinear Homogeneous Dynamical Systems," by Inaudi, J.A. and Kelly, J.M., December 1993.

UCB/EERC-93/12 "Synthesized Strong Ground Motions for the Seismic Condition Assessment of the Eastern Portion of the San Francisco Bay Bridge," by Bolt, B.A. and Gregor, N.J., December 1993, PB94-165842(A10).

UCB/EERC-93/13 "On the Analysis of Structures with Energy Dissipating Restraints," by Inaudi, J.A., Nims, D.K. and Kelly, J.M., December 1993, PB94-203619(A07).

UCB/EERC-94/01 "Preliminary Report on the Seismological and Engineering Aspects of the January 17, 1994 Northridge Earthquake," by EERC, January 1994, (PB94 157 666/AS)A05.

UCB/EERC-94/02 "Energy Dissipation with Slotted Bolted Connections," by Grigorian, C.E. and Popov, E.P., February 1994, PB94-164605.

UCB/EERC-94/03 "The Influence of Plate Flexibility on the Buckling Load of Elastomeric Isolators," by Kelly, J.M., March 1994, PB95-192134(A04).

UCB/EERC-94/04 "Insitu Test Results from Four Loma Prieta Earthquake Liquefaction Sites: SPT, CPT, DMT and Shear Wave Velocity," by Mitchell, J.K., Lodge, A.L., Coutinho, R.Q., Kayen, R.E., Seed, R.B., Nishio, S. and Stokoe II, K.H., April 1994, PB94-190089(A09).

UCB/EERC-94/05 "Seismic Response of Steep Natural Slopes," by Sitar, N. and Ashford, S.A., May 1994, PB94-203643(A10).

UCB/EERC-94/06 "Small-Scale Testing of a Self-Centering Friction Energy Dissipator for Structures," by Nims, D.K. and Kelly, J.M., August 1994.

UCB/EERC-94/07 "Accidental and Natural Torsion in Earthquake Response and Design of Buildings," by De la Llera, J.C. and Chopra, A.K., June 1994, PB94-203627(A14).

UCB/EERC-94/08 "Preliminary Report on the Principal Geotechnical Aspects of the January 17, 1994 Northridge Earthquake," by Stewart, J.P., Bray, J.D., Seed, R.B. and Sitar, N., June 1994, PB94203635(A12).

UCB/EERC-94/09 "Performance of Steel Building Structures During the Northridge Earthquake," by Bertero, V.V., Anderson, J.C. and Krawinkler, H., August 1994, PB95-112025(A10).

UCB/EERC-94/10 "Manual for Menshin Design of Highway Bridges: Ministry of Construction, Japan," by Sugita, H. and Mahin, S., August 1994, PB95-192100(A08).

UCB/EERC-94/11 "Earthquake Analysis and Response of Two-Level Viaducts," by Singh, S.P. and Fenves, G.L., October 1994, (A09).

UCB/EERC-94/12 "Response of the Northwest Connector in the Landers and Big Bear Earthquakes," by Fenves, G.L. and Desroches, R., December 1994, PB95-192001(A08).

UCB/EERC-95/01 "Geotechnical Reconnaissance of the Effects of the January 17, 1995, Hyogoken-Nanbu Earthquake, Japan," August 1995.

UCB/EERC-95/02 "The Attenuation of Strong Ground Motion Displacement," by Gregor, N.J., June 1995.

UCB/EERC-95/03 "Upgrading Bridge Outrigger Knee Joint Systems," by Stojadinovic, B. and Thewalt, C.R., June 1995.

UCB/EERC-95/04 "Earthquake Hazard Reduction in Historical Buildings Using Seismic Isolation," by Garevski, M., June 1995.

UCB/EERC-95/05 "Final Report on the International Workshop on the Use of Rubber-Based Bearings for the Earthquake Protection of Building," by Kelly, J.M., May 1995.

UCB/EERC-95/06 "Seismic Rehabilitation of Framed Buildings Infilled with Unreinforced Masonry Walls Using Post-Tensioned Steel Braces," by Terán-Gilmore, A., Bertero, V.V. and Youssef, N., June 1995.